The synthesis and evaluation of tetralone derivatives as inhibitors of monoamine oxidase

SJ Cloete

orcid.org/ 0000-0002-3770-8403

Dissertation submitted in partial fulfilment of the requirements for the degree *Master of Science* in *Pharmaceutical Chemistry* at the

North-West University

Supervisor: Prof JP Petzer

Co-supervisor: Prof A Petzer

Co-supervisor: Prof LJ Legoabe

Graduation May 2018

Student number: 23496959

NWU®

NORTH-WEST UNIVERSITY
NOORDWES-UNIVERSITEIT
UNIBESITI YA BOKONE-BOPHIRIMA

The financial assistance of the National Research Foundation (NRF) towards this research is hereby acknowledged. Opinions expressed and conclusions arrived at, are those of the author and are not necessarily to be attributed to the NRF.

ACKNOWLEDGEMENTS

Jesus: Heel eerste wil ek rêrig net dankie sê aan God. Van kleins af het U vir my die wil gegee om goed te ondersoek, en sonder U sou ek nie gedink het ek kon wees vandag waar ek is nie. Jesus, Jy het my so baie gehelp deur die twee jaar en die guns wat ek op my lewe het is alles te danke aan U. Alle eer aan U. U is awesome, en mag my lewe en M dit wys. Jesus wen. ALTYD.

Pa en Ma: Dankie dat julle my ondersteun in my lewe, met alles wat ek aanpak. Julle motiveer my altyd om beter te word want julle weet tot wat ek in staat is. Daar is nie beter ouers in die wêreld nie, en soos Orkney Snork Nie sê: “Vir ryker kon ek vra, maar nie vir beter nie.”. Ek is rêrig lief vir julle, en dankie dat julle ALTYD daar is.

Abri, Theunis en Anke: Die twee legendariese broers en my suster. So baie dankie vir alles wat julle vir my beteken, julle sal nooit ooit weet hoe diep julle in my hart lê nie. Julle ondersteun my in alles wat ek aanpak en lewer altyd goeie inspraak waarvoor ek so dankbaar is. Julle wysheid en liefde word ontsettend baie waardeer. Dankie vir al julle tyd en liefde, dankie dat ons so naby aan mekaar kan wees en weet dit gaan lewens-lank hou. Baie lief vir julle.

Cherie Eleanor Sierra Smith: 2 jaar terug toe ek my M begin het, het ek nie geweet jou naam gaan voor in hom staan nie, maar Jesus het beter geweet. Eleanor, dankie vir al jou motivering en die feit dat jy die goud in my uittrek. In ons kort tydjie saam het jy baie diep in my hart ingekruip. Nou gaan jy vir die volgende 3 jaar my PhD saam my aanpak. Na dit gaan jy vir almal kan sê jou ou se naam word met ’n PhD gespel ;) Die toekoms saam jou lyk blink en ek sien baie uit. Baie lief vir jou x33

Prof Jacques en Prof Anel Petzer: Toe ek moes gekies het waar in ek my M gaan doen het ek goeie raad gekry dat mens eerste jou studie leiers moet kies, en Prof-hulle het kop en skouers bo almal uitgestaan en ek kon sien hoekom. Prof-hulle het my so mooi ondersteun en my altyd reg gehelp. Dankie dat Prof-hulle se deure altyd oopgestaan het en dat ek altyd “dom” vrae kon vra. Sonder Prof-hulle se leiding en baie motivering sou die nie moontlik gewees het nie, Prof-hulle het vir altyd ‘n goeie impak op my navorsings loopbaan gemaak.

Elani, Cornel, Pieter, Lianie, Heleen, De-nice en Ida: Lab-werk, kantoor-tyd en kla oor wanneer ons gaan ingee of hoe sleg die Aptekers-raad kan wees was altyd lekker saam julle.

Gabriel en Michelle: Dankie dat julle vriende is wat familie geword het. Hoeveel julle vir my beteken sal julle nooit kan weet nie. Dankie vir al die harte deel sessies en harde tye waardeur

ons saam is. Dankie dat julle saam my met bid vir alles en julle ondersteuning vir wat God mee besig is in my lewe. Baie lief vir julle en geniet Hawaii.

Wikus, Jaco Heyns, Jaco Diederiks en Hanjo (van Namibië): Dankie vir al julle hulp en ondersteuning en dat ons die lewe kan saam doen. Julle vier is rêrig broers waarmee ek die res van my lewe gaan stap, deur dik en dun. Dankie vir al die Mugg & Bean saam werk sessies. Oor drie jaar noem julle my Stefan met ’n PhD.

Marlene en Cristo: Dankie. Woorde kan nie beskryf hoe dankbaar ek vir julle is in my lewe nie. Sonder julle sou my lewe nie dieselfde gelyk het nie, en tien-teen-een “gesuck” het. Julle is altyd daar vir my en ek weet ons paaie gaan nooit van mekaar af skei nie. Julle is werklik-waar lewens-lange beste vriende vir my hart. Ek kan nie wag vir daardie eiland vakansie sodra Marlene ’n “partner” is nie. Phileos liefde.

UITTREKSEL

Monoamienoksidase (MAO)-inhibeerders word gebruik vir die behandeling van toestande wat veroorsaak word deur verlaagde vlakke van neuro-oordragstowwe soos dopamien, noradrenalien en serotonien. MAO-inhibeerders is aanvanklik vir die behandeling van depressie gebruik, maar verdere kliniese gebruik is beperk deur 'n potensieel-ernstige hipertensiewe krisis wat ontstaan indien dié middels saam met tiramien-bevattende kossoorte gebruik word. Dit staan bekend as die "kaasreaksie". Met die ontdekking van middels wat die MAO-B-isoform meer spesifiek inhibeer of MAO omkeerbaar inhibeer, is die waarskynlikheid vir die kaasreaksie drasties verlaag en word hierdie inhibeerders dus as veilig beskou.

Inhibeerders wat spesifiek MAO-B inhibeer word vir die behandeling van Parkinson se siekte gebruik, wat gekarakteriseer word deur die afsterwing van die dopaminergiese neurone wat vanuit die substansia nigra pars compacta in die brein na die striatum projekteer. Dopamien word deur MAO-B in die brein gemetaboliseer en dus word MAO-B-inhibeerders gebruik om dopaminergiese neurotransmissie te verbeter en op dié manier verskaf dit simptomatiese verligting van die motoriese simptome van Parkinson se siekte. Die primêre behandeling vir Parkinson se siekte is orale toediening van *L*-dopa, die metaboliese voorloper vir dopamien. MAO-B-inhibeerders word dikwels in kombinasie met *L*-dopa gebruik sodat die dosis vir *L*-dopa verlaag kan word. Dit verlaag ook die newe-effekte soos diskinesie, wat met die langtermyngebruik van *L*-dopa geassosieer word.

Vir die doel van hierdie studie is nuwe middels gesintetiseer, wat moontlik MAO-B omkeerbeer sal inhibeer, deur gebruik te maak van 1-tetraloon as leidraad. Dit is voorheen bewys dat derivate van 1-tetraloon hoogs potente en baie spesifieke inhibeerders van MAO-B is. Om die 1-tetraloonderivate te sintetiseer is substitusie op die C5, C6 en C7 posisies van 1-tetraloon uitgevoer met bensieloksi, 4-chloorbensieloksi en 2-fenoksietoksi as substituente. Die belangrikste doel van hierdie studie was egter om die 1-tetraloonderivate na die ooreenstemmende 1-tetralolderivate te reduseer, wat nog nie voorheen as potensiële MAO-inhibeerders geëvalueer is nie. Hierdie studie gaan dus die inhibisie-eienskappe van die 1-tetraloonderivate vergelyk met die van die 1-tetralolderivate.

Die 1-tetraloonderivate is gesintetiseer deur 5-, 6- en 7-hidroksie-1-tetraloon te laat reageer met die gepaste gesubstitueerde alkielbromied in die teenwoordigheid van aluminiumchloried en tolueen. Hierdie reaksies het die 1-tetraloonderivate **1a-h** gelewer. Die 1-tetraloonderivate is in die teenwoordigheid van etanol en natriumboorhidried gereduseer na die ooreenstemmende 1-tetralol (1,2,3,4-tetrahidro-1-naftol)-derivate **1i-p**. Al die strukture is met behulp van

kernmagnetieseresonans (KMR)-spektroskopie en massaspektrometrie (MS) opgeklaar. Die suiwerhede is deur hoë-prestasie vloeistofchromatografie (HPVC) bepaal.

Die 1-tetraloonderivate is as moontlike inhibeerders van menslike rekombinante MAO-A en MAO-B geëvalueer en die potensies is as die IC_{50}-waarde uitgedruk. Daar is gevind dat beide die 1-tetraloon- en 1-tetralolderivate potente inhibeerders van MAO-B is, en ook dat sekere verbindings potente inhibeerders van MAO-A is. Tetraloonderivaat **1h** het die mees potente MAO-A- en MAO-B-inhibisie getoon met IC_{50}-waardes van 0.036 μM en 0.0011 μM, onderskeidelik. Tussen die 1-tetralolderivate was **1p** (IC_{50} = 0.785 μM) en **1o** (IC_{50} = 0.0075 μM) die mees potente inhibeerders van MAO-A en MAO-B, onderskeidelik. Hierdie derivate is gekies om die omkeerbaarheid van MAO-inhibisie te evalueer omdat die omkeerbaarheid van MAO-inhibisie nog nie voorheen vir 1-tetralolderivate geëvalueer is nie. Die resultate toon dat hierdie verbindings omkeerbare inhibeerders van MAO is omdat die ensiemaktiwiteit herwin kon word nadat die inhibeerder deur dialise verwyder is. Lineweaver-Burk grafieke is opgestel en het getoon dat **1p** en **1o** kompeterende inhibeerders van MAO-A en MAO-B is met K_i-waardes van 0.0065 μM en 1.0 μM, onderskeidelik.

Sommige 1-tetraloon- en 1-tetralolderivate toon hoë potensies vir inhibisie van MAO-B maar lae potensies vir die inhibisie van MAO-A. 'n Voorbeeld hiervan is die alkoholderivaat **1m** wat 'n IC_{50}-waarde van 0.068 μM toon vir MAO-B, maar geen merkbare inhibisie van MAO-A by die maksimum getoetste konsentrasie besit nie. Molekulêre modulering is met verbindings **1m** en **1e** uitgevoer om die moontlike bindingsoriëntasies in MAO te voorspel en sodoende 'n moontlike verduideliking vir hierdie verskynsel te bied. Die resultate toon dat beide verbindings in die aktiewe setel van MAO-A bind en interaksies ondergaan. Molekulêre modulering bied dus nie 'n verduideliking vir die afwesigheid van MAO-A-inhibisie deur verbinding **1m** nie, maar dit is wel bekend dat groter molekules nie in die aktiewe setel van MAO-A pas nie, terwyl dit wel in die aktiewe setel van MAO-B bind. Die bevinding dat **1e** beter MAO-B-inhibisie as verbinding **1m** besit kan moontlik toegeskryf word aan die feit dat **1m** 'n rasemiese mengsel van 2 enantiomere is, naamlik (R)-**1m** en (S)-**1m**. Dit kan gepostuleer word dat **1e** deur beide pi-pi en waterstofbindingsinteraksies gestabiliseer word, terwyl die enantiomere van **1m** deur of pi-pi óf waterstofbindingsinteraksies gestabiliseer word.

Hierdie studie het bevind dat beide 1-tetraloon- en 1-tetralolderivate potente inhibeerders van MAO-A en MAO-B is. Sommige verbindings het selfs hoër potensies getoon as geneesmiddels wat tans as MAO-inhibeerders gebruik word. Sulke verbindings mag as voorlopers gebruik word vir die verdere ontwerp van MAO-inhibeerders vir die behandeling van Parkinson se siekte.

Sleutelwoorde: Monoamienoksidase, Inhibeerder, Parkinson se siekte, MAO-A, MAO-B

ABSTRACT

Monoamine oxidase (MAO) inhibitors are used for the treatment of disorders that are caused by deficient levels of neurotransmitters such as dopamine, noradrenaline and serotonin. MAO inhibitors were first used for the treatment of depression, but their clinical use was limited due to a potentially fatal hypertensive crisis that may occur when these drugs are combined with tyramine containing foods. This adverse effect is known as the cheese reaction. With the discovery of inhibitors that are specific for the MAO-B isoform as well as reversible inhibitors of the MAOs, the liability of the cheese reaction was greatly decreased and such MAO inhibitors are considered to be relatively safe drugs.

MAO-B specific inhibitors are used for the treatment of Parkinson's disease, which is characterised by the loss of the dopaminergic neurons projecting from the substantia nigra pars compacta of the brain to the striatum. Since MAO-B metabolises dopamine in the brain, MAO inhibitors are used to enhance dopaminergic neurotransmission and thus provide symptomatic relief of the motor symptoms of Parkinson's disease. The primary treatment for Parkinson's disease is *L*-dopa, the metabolic precursor of dopamine. MAO-B inhibitors are frequently used in conjunction with *L*-dopa and may allow for a lower dose of *L*-dopa to be administered. This, in turn, reduces adverse effects such as dyskinesia associated with long-term *L*-dopa treatment.

The current study set out to discover novel drugs that inhibit MAO-B reversibly by using 1-tetralone as lead compound. It was previously shown that 1-tetralone derivatives are high potency and specific inhibitors of MAO-B. To synthesise the series of 1-tetralone derivatives, substitution on C5, C6 and C7 with the benzyloxy, 4-chlorobenzyloxy and 2-phenoxyethoxy substituents was carried out. A key objective of this study was to reduce the 1-tetralone derivatives to the corresponding 1-tetralol derivatives, which have not previously been investigated as MAO inhibitors. This study will therefore compare the MAO inhibition properties of 1-tetralone derivatives to the corresponding 1-tetralol compounds.

The 1-tetralone derivatives were synthesised by reacting 5-, 6- and 7-hydroxy-1-tetralone with an appropriate substituted alkyl bromide in the presence of aluminium chloride and toluene. This yielded 1-tetralone derivatives **1a-h**. The 1-tetralone derivatives were subsequently reduced in the presence of ethanol and sodium borohydride to the corresponding 1-tetralol (1,2,3,4-tetrahydro-1-naphthol) derivatives **1i-p**. All compounds were characterised by nuclear magnetic resonance (NMR) spectroscopy and mass spectrometry (MS). Purities were assessed by high-performance liquid chromatography (HPLC).

The 1-tetralone derivatives were subsequently evaluated as potential inhibitors of recombinant human MAO-A and MAO-B, and the inhibition potencies were expressed as IC_{50} values. Both

the 1-tetralone and 1-tetralol derivatives were found to be potent inhibitors of MAO-B, while some compounds also acted as MAO-A inhibitors. 1-Tetralone derivative **1h** exhibited the most potent inhibition of MAO-A and MAO-B with IC_{50} values of 0.036 µM and 0.0011 µM, respectively. Among the 1-tetralol derivatives, **1p** (IC_{50} = 0.785 µM) and **1o** (IC_{50} = 0.0075 µM) were the most potent inhibitors of MAO-A and MAO-B, respectively. These derivatives were selected to evaluate the reversibility of MAO inhibition since the reversibility of MAO inhibition by 1-tetralol derivatives has not yet been evaluated. The results showed that these compounds are reversible MAO inhibitors since most of the enzyme activity could be recovered by removal of the inhibitor by dialysis. Lineweaver-Burk plots were subsequently constructed and showed that **1p** and **1o** are competitive inhibitors of MAO-A and MAO-B with K_i values of 0.0065 µM and 1.0 µM, respectively.

Some of the 1-tetralone and 1-tetralol derivatives exhibit high potency inhibition towards MAO-B but low potency inhibition towards MAO-A, such as the alcohol derivative **1m** which possesses an IC_{50} value of 0.068 µM for the inhibition of MAO-B but no measureable inhibition towards MAO-A at the maximum tested concentration. Molecular modelling was performed with compounds **1m** and **1e** to explore their possible binding orientations in MAO and to provide a possible explanation for this phenomenon. The results show that both inhibitors are able to bind and interact with the active site of MAO-A. A molecular explanation for the lack of inhibition towards MAO-A by compound **1m** is therefore not apparent, but it is well-known that larger molecules fit poorly in the active site of MAO-A compared to the active site of MAO-B. The slightly higher inhibition towards MAO-B by **1e** compared to **1m** can possibly be explained by the fact that **1m** is the racemic mixture of two enantiomers, (R)-**1m** and (S)-**1m**. It may be postulated that **1e** is stabilised by both pi-pi and hydrogen bond interactions while either enantiomer of **1m** is stabilised only by pi-pi or hydrogen bond interactions.

This study found that both 1-tetralone and 1-tetralol derivatives are potent inhibitors of MAO-A and MAO-B, with some compounds exhibiting higher potencies than clinically used MAO inhibitors. Such compounds may act as leads for the design of future MAO inhibitors for the treatment of Parkinson's disease.

Keywords: Monoamine oxidase inhibitors, Parkinson's disease, MAO-A, MAO-B

TABLE OF CONTENTS

LIST OF ABBREVITATIONS

ALS - Amyotrophic lateral sclerosis

ANP - Atrial natriuretic peptide

APCI - Atmospheric-pressure chemical ionisation

ASN - Asparagine

Bcl-2 - B-cell lymphoma 2

BDNF - Brain-derived neurotrophic factor

COMT - Catechol-O-methyl transferase

Cys - Cysteine

DFO - Deferoxamine

DMSO - Dimethyl sulfoxide

FAD - Flavin adenine dinucleotide

FDA - Food and drug administration

HPLC - High-performance liquid chromatography

HRMS - High resolution mass spectra

Ile - Isoleucine

***L*-dopa** - Levodopa

Leu - Leucine

MAO - Monoamine oxidase

MPP^+ - 1-Methyl-4-phenylpyridinium

MPTP - 1-methyl-4-phenyl-1,2,3,6-tetrahydropyridine

mRNA – Messenger ribonucleic acid

MS - Mass spectrometry

NMR - Nuclear magnetic resonance

Phe - Phenylalanine

ppm - Parts per million

PMT - Photomultiplier

Tyr - Tyrosine

UPDRS - Unified Parkinson’s disease rating scale

UV - Ultraviolet

RIMAS - Reversible MAO-A inhibitors

RMSD – Root-mean-square deviation

RNA - Ribonucleic acid

ROS - Reactive oxygen species

SARs - Structure-activity relationships

SSRI - Serotonin selective reuptake inhibitor

TLC - Thin layer chromatography

LIST OF TABLES

LIST OF FIGURES

LIST OF EQUATIONS

CHAPTER 1

INTRODUCTION

1.1 Introduction and overview

The monoamine oxidases (MAO) are enzymes located on the outer membrane of the mitochondria which are responsible for the metabolism of neurotransmitters and amine compounds derived from the diet. Since the MAOs metabolise neurotransmitters in the brain, they are involved in certain neurological diseases such as Parkinson's disease, Alzheimer's disease and depression (Binda *et al.,* 2007; Edmondson *et al*., 2009). There are two isoforms of the MAO enzyme, namely MAO-A and MAO-B (Borštnar *et al.*, 2011). The two isoforms are drug targets for different disease states with MAO-A inhibitors being used in the treatment of depression while MAO-B inhibitors are used for the treatment of Parkinson's disease (Borštnar *et al.*, 2011; Youdim & Bakhle, 2006).

James Parkinson wrote a monograph in 1817 titled: "An essay on shaking palsy". In it he described what he believed was an unrecognised and not yet known disease which he observed in six subjects that he examined in his own practice and on walks in his neighbourhood. Later on a neurologist from France named Jean Martin Charcot, also known as the father of neurology, acknowledged James Parkinson's work, and named the disease after him (Lees *et al*., 2009).

Studies done on Parkinson's disease have not yet found the primary cause of this disease. A number of probable causes have been investigated such as environmental, pathological and genetically driven causes. None of them have yet been identified as the main cause of Parkinson's disease (Lees *et al*., 2009). It is, however, known that the primary characteristic of Parkinson's disease is the degeneration of the dopaminergic neurons in the substantia nigra pars compacta of the brain, which leads to the depletion of dopamine that is required for normal functions within the brain. To date, the most important treatments of Parkinson's disease are focused on replenishing the central dopamine levels. *L*-Dopa, the metabolic precursor of dopamine, is the most effective treatment of Parkinson's disease. Long-term treatment with *L*-dopa, however, results in debilitating adverse effects such as dyskinesia (Dauer & Przedborski, 2003).

Since MAO metabolises dopamine in the brain, inhibitors of MAO are used in the treatment of Parkinson's disease. In this respect, MAO inhibitors conserve the dopamine supply in the brain and enhance dopaminergic neurotransmission. This leads to an improvement of the motor symptoms of Parkinson's disease (Foley *et al*., 2000). With ageing, the levels and activity of

MAO-B increases in the brain, which further depletes central dopamine levels in Parkinson's disease. MAO catalytic activity is also associated with the production of hydrogen peroxide, and an increase in MAO-B activity in Parkinson's disease may contribute to the degeneration of the dopaminergic cells (Fowler *et al*., 1997; LeWitt & Taylor, 2008). Thus the inhibition of MAO-B not only leads to enhanced dopamine levels and an improvement of the motor symptoms of Parkinson's disease, but also may prevent further degeneration of neurons due to oxidative damage initiated by hydrogen peroxide. MAO-B specific inhibitors such as rasagiline and selegiline have shown to possess good safety profiles, and are considered valuable drugs for the treatment of Parkinson's disease.

When designing MAO inhibitors, the published X-ray structures of the MAOs are valuable tools. The active sites of MAO-A and MAO-B are highly similar and both contain the flavin adenine dinucleotide (FAD) cofactor in their substrate cavities. The active sites of the MAO enzymes, however, display structural differences which are responsible for the differences in substrate and inhibitor specificities between the MAO isoforms. The cavity of MAO-B is bipartite and is made up of two separate spaces, the substrate cavity (~400 $Å^3$) and the entrance cavity (~300 $Å^3$). The cavity of MAO-A is more compact and, in humans, consists of a single cavity with a volume of ~400 $Å^3$. Human MAO-B can bind to substrates and inhibitors of different sizes since the MAO-B active site has a high degree of plasticity. This plasticity creates the opportunity for both small inhibitors and cavity-filling inhibitors to bind to MAO-B (Edmondson *et al*., 2009). This represents an opportunity to design inhibitors with specificity for MAO-B over the MAO-A isoform.

1.2 Rationale for the design of MAO inhibitors for Parkinson's disease

MAO-B inhibitors are considered useful agents for the treatment of Parkinson's disease. Currently two MAO-B inhibitors, selegiline and rasagiline, are used in the clinic for this purpose. Although these drugs are irreversible inhibitors, they exhibit good safety profiles with very few adverse effects (Ives *et al*., 2004; Rascol *et al*., 2000; Holloway *et al*., 2004). MAO-A inhibitors, in turn, are used for the treatment of depression, but their use is limited due to a serious adverse effect associated with MAO-A inhibition termed the "cheese reaction". The cheese reaction occurs when MAO-A inhibitors are combined with tyramine-containing food such as cheese and wine, and is more likely with irreversible acting compounds. Newer MAO-A inhibitors with reversible modes of action, however, are not associated with the cheese reaction (Youdim *et al*., 2006). MAO-A inhibitors may also be of value in Parkinson's disease since 40-60% of patients with Parkinson's disease show signs of depression (Youdim & Bakhle, 2006). Thus compounds that inhibit both MAO-A and MAO-B may be of enhanced value in the treatment of Parkinson's disease by slowing the depletion of central dopamine stores and by treating symptoms of depression.

1.3 Hypothesis of the study

This study will attempt to discover novel MAO-B inhibitors by using 1-tetralone as lead compound. It was previously shown that 1-tetralone derivatives are high potency and specific inhibitors of MAO-B (Legoabe *et al*., 2014; 2015). The X-ray crystal structure of rasagiline in complex with MAO-B shows that rasagiline binds in the substrate cavity of the enzyme, leaving the entrance cavity unoccupied (Hubálek *et al*., 2004). It has thus been suggested that substitution of rasagiline could yield compounds that bind to both the substrate cavity and entrance cavity. In this instance, the C5, C6 and C7 substituents will extend into the entrance cavity. Cavity spanning inhibitors often possess a high degree of selectivity for MAO-B and do not bind to MAO-A. This greatly reduces the potential for causing the cheese reaction. A second objective of this study is to reduce the 1-tetralone derivatives to the corresponding 1-tetralol (1,2,3,4-tetrahydro-1-naphthol) derivatives, which have not previously been investigated as MAO inhibitors. This study will therefore compare the MAO inhibition properties of 1-tetralone derivatives to the corresponding 1-tetralol compounds. The structures that will be synthesised and investigated in this study are shown below in table 1.1.

This study therefore hypothesises that the 1-tetralone and 1-tetralol derivatives that will be investigated in this study will act as highly potent and specific MAO-B inhibitors.

Table 1.1 The structures that will be synthesised and investigated in this study.

1-Tetralone	1-Tetralol	R =
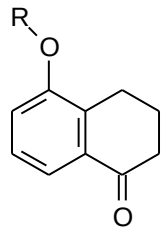	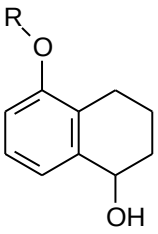	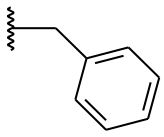
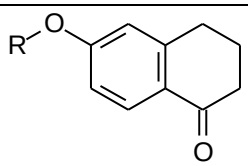	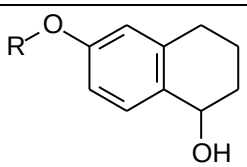	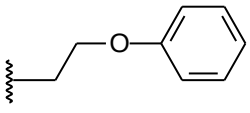
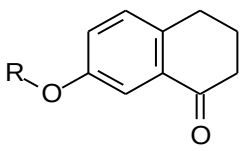	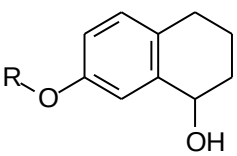	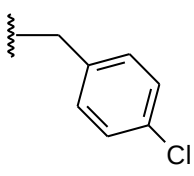

1.4 Objectives of the study

The objectives of this study are as follows:

- To synthesise a series of 1-tetralone derivatives substituted on C5, C6 and C7 with the benzyloxy, 4-chlorobenzyloxy and 2-phenoxyethoxy substituents.
- To reduce the 1-tetralone derivatives to the corresponding 1-tetralol compounds.
- To evaluate the synthesised derivatives as inhibitors of the human MAOs, MAO-A and MAO-B, by measuring IC_{50} values.
- To determine the reversibility of the inhibition of selected 1-tetralol derivatives by dialysis. Since the reversibility of inhibition of 1-tetralones has been established, this study selected two 1-tetralol compounds.
- To determine the mode of inhibition (e.g. competitive) of the selected 1-tetralol derivatives and to measure their K_i values for the reversible inhibition of MAO. Since the mode of MAO inhibition of 1-tetralones has been investigated, this study selected 1-tetralol compounds.
- To determine the possible binding orientations of the 1-tetralone and 1-tetralol derivatives in the active sites of MAO-A and MAO-B by molecular modelling studies.

CHAPTER 2

LITERATURE BACKGROUND

2.1 Monoamine oxidase

2.1.1 General background

Monoamine oxidases are FAD dependent enzymes which metabolise monoamine neurotransmitters such as adrenaline, serotonin, dopamine and noradrenaline (Johnston, 1968). The MAOs are membrane-associated enzymes, specifically located on the outer membranes of mitochondria (Edmondson *et al*., 2009). There are two isoforms of this enzyme, MAO-A and MAO-B (Borštnar *et al*., 2011). The two isoforms are targeted for different disease states. MAO-A inhibitors are used in the treatment of depression since these drugs increase the levels of noradrenaline and serotonin in the brain. Both noradrenaline and serotonin are substrates for MAO-A (Kalgutkar *et al*., 2001; Youdim & Bakhle, 2006). MAO-B inhibitors, in turn, are used for the treatment of Parkinson's disease, a disorder characterised by progressive death of dopaminergic neurons in the pars compacta of the substantia nigra (Borštnar *et al*., 2011). MAO-A inhibition may also be relevant in Parkinson's disease since 40-60% of patients with Parkinson's disease show signs of depression (Youdim & Bakhle, 2006).

The two MAO isozymes are coded by separate genes located on the X chromosome. The amino acid sequences of MAO-A and MAO-B are very similar (Kochersperger *et al*., 1986), with the active sites displaying a 93.9% sequence identity. The substrate specificity of MAO is determined by differences in key amino acid residues in the catalytic sites of MAO-A and MAO-B (Grimsby *et al*., 1991; Fowler *et al*., 1980; Kalir *et al*., 1981; Shih *et al*., 1998). Experiments have shown that there are differences in the cellular and regional distribution of the two MAO isoforms in human and rodent brains. The substrate specificity and sensitivity of the MAO forms also differ in human and rodent brains. In the human brain, MAO-B is much more prevalent than MAO-A, whereas in the rodent brain MAO-A is more prevalent. This is of great importance considering that rodents are often used in preclinical studies, thus results generated with rodents must be extrapolated to humans with great caution (Squires, 1972; Oreland *et al*., 1983; Azzaro *et al*., 1985; Ross, 1987; Saura *et al*., 1996).

MAO catalytic activity generates hydrogen peroxide (H_2O_2) as a by-product. Hydrogen peroxide can damage the cellular components after reacting with ferrous ion in the Fenton reaction to produce the highly destructive hydroxyl radical. The hydroxyl radical is associated with single-strand breaks in mitochondrial DNA and lipid peroxidation (Hauptmann *et al*., 1996). To illustrate the involvement of the MAOs in cellular damage, the inhibition of MAO-A with clorgyline, or

MAO-B with rasagiline in the rat brain decreases lipid peroxidation by half (Aluf *et al*., 2013). Besides reducing the MAO-B catalysed formation of hydrogen peroxide, defences against oxidative stress is also increased with chronic rasagiline treatment because of the up-regulated expression of BDNF (brain-derived neurotrophic factor), Bcl-2 (B-cell lymphoma 2) and catalase in the brain (Weinreb *et al*., 2015). MAO has also been reported to be a source of oxidative stress in diabetes. This may provide a rationale for the application of MAO inhibitors in the treatment of heart diseases and vascular damage (Sturza *et al*., 2015; Deftereos *et al*., 2012)

2.1.2 Tissue distribution of MAO

MAO-A and MAO-B can be found in different parts of the body. The distribution of the different forms varies between tissues. Within the human body, the gastrointestinal tract mainly expresses MAO-A while in the liver MAO-B is the predominant isoform. The placenta in turn contains 98% MAO-A and only 2% MAO-B. Lymphocytes and platelets have been found to contain exclusively MAO-B (Von Korff, 1979).

The oxidation of dopamine in the brain is catalysed by both MAO-A and MAO-B. MAO-B is, however, more prevalent than MAO-A in the human brain with 70-75% of brain MAO being in the MAO-B isoform (Foley *et al*., 2000). The MAO isoforms, however, differ in their regional distribution in the brain with MAO-A being more localised in the pars compacta of the substantia nigra, and MAO-B being more localised to the pars reticulata (Saura Marti *et al*., 1990). In the brain, the highest concentration of MAO-A is found in the catecholaminergic neurons in the locus ceruleus. The highest concentration of MAO-B is found in the histaminergic and serotonergic neurons of the raphe and posterior hypothalamus. High concentrations of both isoforms can be found in the basal ganglia (Oreland *et al*., 1983; Saura *et al*., 1996; Westlund *et al*., 1985; 1988). As mentioned, the MAO catalytic cycle produces toxic by-products such as hydrogen peroxide, which promotes apoptotic signalling events that may result in the destruction of dopamine-producing cells (Edmondson *et al*., 2009; LeWitt & Taylor, 2008). Of note are reports that MAO-B levels increase in the brain as a person ages (Fowler *et al*., 1997). It has also been reported that in older rats, the activity of MAO-B in the brain increases remarkably by 21% whereas MAO-A activity exhibits a decrease by 4% (Cao Danh *et al*., 1984). It has therefore been proposed that hydrogen peroxide produced by MAO-B in the aged Parkinsonian brain may contribute to the degenerative process. MAO-B inhibitors may thus reduce hydrogen peroxide production and protect against further neurodegeneration (LeWitt & Taylor, 2008).

Ladostigil and a novel drug which is still being evaluated, M30, are both irreversible inhibitors of MAO-A and MAO-B. These compounds are unique since they only inhibit MAO in the brain and not the peripheral tissues. The advantage of this mode of inhibition is that MAO-A is not

inhibited in the gut and liver, which reduces the potential for the cheese effect, a potentially fatal adverse effect of MAO-A inhibition. Dopamine metabolism in the brain is not completely inhibited by selective inhibition of MAO-B because dopamine is a substrate for MAO-A as well. MAO-A will compensate and metabolise a portion of dopamine even when MAO-B activity is completely abolished. Non-selective MAO inhibitors such as ladostigil and M30 thus have the advantage over selective MAO-B inhibitors by inhibiting both forms of MAO in the brain, which may dramatically increase nigrostriatal dopaminergic transmission. Such compounds may also possess a promising antidepressant effect (Youdim *et al*., 2014).

M30 is also a multifunctional brain permeable iron chelator which possesses neuroprotective activities *in vivo* and *in vitro*. Such compounds prevent the accumulation of iron at sites of neurodegeneration and thus prevent the exacerbation of oxidative stress by iron-mediated pathways. Youdim *et al*. (2014) evaluated M30 and ladostigil in the MPTP (1-methyl-4-phenyl-1,2,3,6-tetrahydropyridine) mouse model of Parkinson's disease, and found that a daily dose of M30 or ladostigil inhibited MAO-A and MAO-B by more than 70% and prevented neurotoxicity of MPTP and the depletion of striatal dopamine. MPTP is oxidised by MAO-B to the active neurotoxin, MPP^+ (1-Methyl-4-phenylpyridinium), which inhibits mitochondrial respiration and subsequently causes death of nigrostriatal dopaminergic neurons (Jenner & Marsden, 1988). These properties together with a high degree of selectivity for the brain, suggest that these compounds could be candidates for neuroprotective treatment of Parkinson's disease by preventing key cellular events implicated in the pathogenesis of Parkinson's disease.

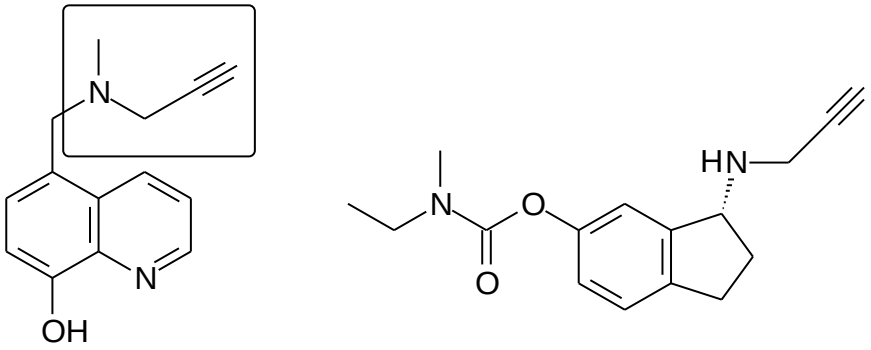

Figure 2.1 The structure of M30 showing the propargylamine moiety on the left, and on the right is the structure of ladostigil.

2.1.3 Structures of MAO-A and MAO-B

MAO-A and MAO-B are membrane-associated enzymes. They are more specifically located on the outer mitochondrial membrane. When examining human MAO-A and MAO-B, as well as rat MAO-A, it may be concluded that all three of these enzymes have structures with similar folds. Human MAO-A is comprised of 527 amino acids and MAO-B is comprised of 520 amino acids.

Their amino acid sequences are approximately 70% identical (Arai *et al*., 1998; Bach *et al*., 1988; Fitzgerald *et al*., 1990). The identities of the Cα-coordinates in three-dimensional space also have a high level of similarity. The X-ray crystal structures of MAO-A and MAO-B show that residues 35-40 at the C-terminal are the motifs that bind to the outer membrane of the mitochondria. The human MAO-B structure has an α-helix trans-membrane region that protrudes perpendicularly out of the protein. With human MAO-B the last 20 residues of the binding motifs are too disordered to provide precise electron density (Hubálek *et al*., 2003). With human MAO-A the C-terminal has a very similar topology to that of rat MAO-A. Thus the electron density can be defined accurately enough to provide a view of the trans-membrane α-helix of MAO-A. The X-ray crystal structure of MAO-A thus supports previous studies (Mitoma & Ito, 1992) where it was suggested that the C-terminal is responsible for the binding of MAO-A and MAO-B to the outer membrane of the mitochondria. It has been shown that “swapping” the C-terminals of MAO-A and MAO-B with each other results in inactive enzymes which suggests that there are differences in the architecture of the two enzymes’ binding motifs (Chen *et al*., 1996; Gottowik *et al*., 1995).

The structures of MAO-A and MAO-B reveal that the active sites of these enzymes are very similar with only 6 residues differing among the 16 residues that line the active sites. The structures further show that the FAD cofactors are covalently bound to the MAO enzymes. The FAD cofactor within the enzyme is highly conserved while the substrate binding sites are elongated cavities. The flavin rings are found to be “bent”, rather than planar, which is more commonly found in flavoproteins. In MAO-A the FAD is bound to the MAO protein with an 8α thioether linkage to Cys406 (Son *et al*., 2008), whereas in MAO-B the FAD is bound to the MAO protein also with an 8α thioether linkage, in this case to Cys397 (Binda *et al*., 2003). An important structural difference between human MAO-A and MAO-B is their oligomeric states. Human MAO-A is known to be a monomer whereas MAO-B is a dimer.

In human MAO-A and MAO-B the cavities are found to be hydrophobic, but the details of the active site architectures show differences in their structures which is the reason for differences in inhibitor and substrate specificities between the two isoforms.

2.1.3.1 MAO-B

Substrate binding in MAO-B takes place within an elongated cavity which spans from the flavin binding site to the surface of the protein. The cavity of the MAO-B enzyme is bipartite and consists of two separate spaces. The first cavity is the entrance cavity with a volume of 300 $Å^3$ and faces the solvent after movement of loop 99-110. The second cavity is the substrate cavity which has a volume of 400 $Å^3$. The two cavities are separated by the side chain of Ile199, and when combined they form a large cavity with a volume of 700 $Å^3$. Ile199 is known as a “gating”

residue, which means that it can change conformation to an “open” or “closed” state, determined by the nature of the bound ligand. This gives the MAO-B cavity a high level of plasticity. Because of this plasticity, MAO-B can bind various types of inhibitors, from small inhibitors (e.g. isatin and tranylcypromine) to cavity-filling inhibitors (e.g. safinamide). There are smaller inhibitors, such as rasagiline and selegiline, that induces a mid-span type of binding by being just big enough to push open the gating residue Ile199 (De Colibus *et al*., 2005; Hubálek *et al*., 2004). This versatility of binding to inhibitors of different sizes has great implications because smaller inhibitors show almost similar binding affinities towards MAO-A and MAO-B, whereas the larger inhibitors (e.g. cavity-filling ligands) show specificity for MAO-B.

Figure 2.2 The structure of human MAO-B. The FAD is shown in magenta while the co-crystallised ligand, safinamide, is shown in yellow. The C-terminal α-helix is at the bottom of the structure (Binda *et al*., 2007).

2.1.3.2 MAO-A

The MAO-A enzyme, as with the MAO-B enzyme, has an elongated cavity spanning from the flavin site to the surface of the protein. MAO-A, unlike MAO-B, only has a single cavity which has a volume of 400 Å^3 and is much more compact. It thus has a much smaller cavity compared to the combined entrance and substrate cavities (700 Å^3) of MAO-B (Son *et al*., 2008). MAO-B has a high level of plasticity and can fuse its two cavities by conformational change of Ile199, which acts as a “gating” residue. The corresponding residue to Ile199 in MAO-A is Phe208. Phe208 does not act as a “gating” residue since it is much more bulky than Ile199. Since

Phe208 fills up more space in the MAO-A active site, larger cavity spanning MAO-B inhibitors cannot bind to MAO-A due to structural overlap with Phe208. There are other key residues that may also determine substrate and inhibitor specificity. The active site of MAO-B possesses the Tyr326 residue which is not directly involved in dividing the entrance and substrate cavity, but it does produce a restriction between the two cavities. This restriction is less pronounced by the homologous residue in MAO-A, Ile335. Other key residues in the active site include Asn181 and Ile180 in MAO-A, and their counter-parts in MAO-B, Cys172 and Leu171. They however do not affect the shape of the active sites significantly. The differences between Phe208 and Ile335 in MAO-A compared to Ile199 and Tyr326 in MAO-B appear to be a major cause for the differences in substrate and inhibitor specificities between the two MAO isoforms (Son *et al*., 2008).

Figure 2.3 The structure of human MAO-A. The FAD is shown in magenta while the co-crystallised ligand, harmine, is shown in yellow. The C-terminal α-helix is at the bottom of the structure (Son *et al*., 2008).

2.1.4 The biological function of the MAOs

*Metabolism of neurotransmitter*s: Neurotransmitters such as dopamine, noradrenaline and serotonin must be maintained at appropriate levels by degradation by the MAOs so that synaptic neurotransmission occurs normally. These neurotransmitters, to a large extent, determine mood and emotions. They also control motoric and cognitive functions. MAO-A and MAO-B metabolise neurotransmitters in the peripheral tissues as well as in the brain. The direct

metabolic product of the oxidation of an amine substrate by MAO is the corresponding aldehyde. Aldehyde dehydrogenase is responsible for the oxidation of the aldehyde to the corresponding acid. Alternatively, the aldehyde may be metabolised to an alcohol or a glycol by aldehyde reductase. The MAO catalytic cycle also produces hydrogen peroxide as by-product. Hydrogen peroxide in turn can be converted to reactive oxygen species (ROS) which damages cells and causes apoptosis. MAO-A and MAO-B inhibitors are used to increase the levels of neurotransmitter substrates at their sites of action by blocking their metabolism. An example of this is the inhibition of serotonin metabolism by MAO-A in the brain, which leads to an increase in central serotonin levels and an antidepressant effect (Lum & Stahl, 2012). In turn, MAO-B is the predominant enzyme that metabolises dopamine within the human brain and MAO-B inhibitors are thus used for the treatment of Parkinson's disease (Youdim & Bakhle, 2006). Dopamine is formed by the conversion of dietary tyrosine to *L*-dopa in neurons. *L*-Dopa is subsequently decarboxylated to yield dopamine in the dopaminergic and noradrenergic neurons. As soon as dopamine is released from the synaptic vesicles it is metabolised by MAO-B, which is localised in the mitochondria of the glial cells surrounding the synaptic cleft (Kaakkola *et al*., 1987).

In peripheral tissue such as the lungs, placenta, intestine and the liver, MAO has a protective role by metabolising amines in the blood, or by preventing dietary amines from entering into the systemic circulation. At the blood-brain barrier MAO-B seems to also have a protective effect by limiting the entry of amine compounds into the brain, thus forming a metabolic barrier. It has been suggested that the function of MAO in the brain is to protect the neurons from exogenous bioactive amines, regulate the amine stores intracellularly and stop the action of amine neurotransmitters (Shih *et al*., 1999).

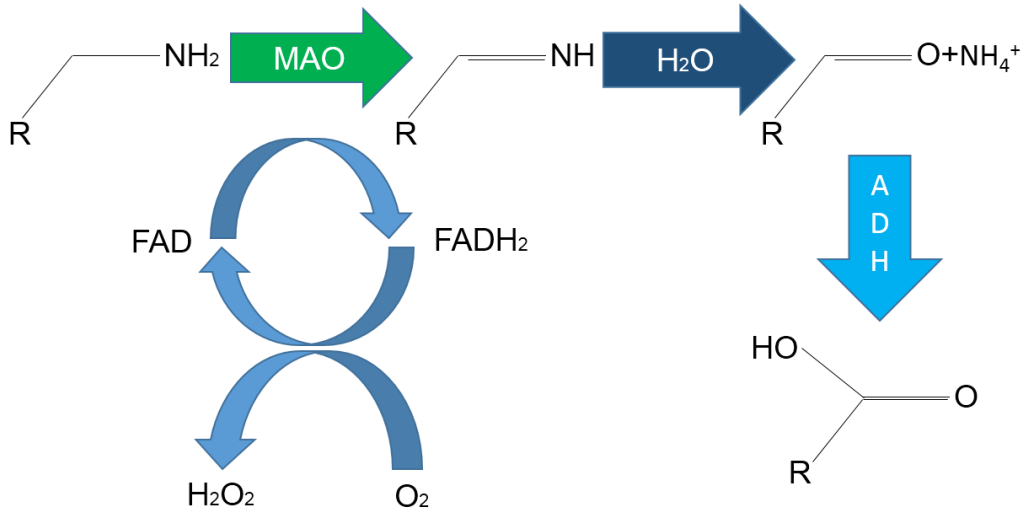

Figure 2.4 The metabolic pathway for the metabolism of neurotransmitters.

Metabolism of tyramine and the cheese reaction: Tyramine is an amine found in many foods, such as beer, wine and cheese. Tyramine is metabolised by MAO-A in the gut which limits its entry into the systemic circulation (Foley *et al*., 2000). If tyramine is not metabolised sufficiently it will enter into the systemic circulation in large amounts, which may subsequently trigger the excessive release of noradrenaline from the medulla. This will then activate the sympathetic system and result in a hypertensive response which may be fatal. This is known as the "cheese reaction" and causes cerebral haemorrhages and an increase in blood pressure (Youdim & Bakhle, 2006). The potential for the cheese reaction severely limits the clinical use of MAO-A inhibitors, particularly irreversible inhibitors (which most of the first known MAO inhibitors was). The cheese reaction can however be overcome by inhibiting MAO-A reversibly instead of irreversibly. Reversible MAO-A inhibitors (RIMAS) as well as MAO-B inhibitors do not cause the cheese reaction since reversible inhibitors can be displaced from the MAO enzyme by increasing levels of tyramine while MAO-B is found in very small amounts within the gastrointestinal tract (Foley *et al*., 2000; Youdim & Bakhle, 2006).

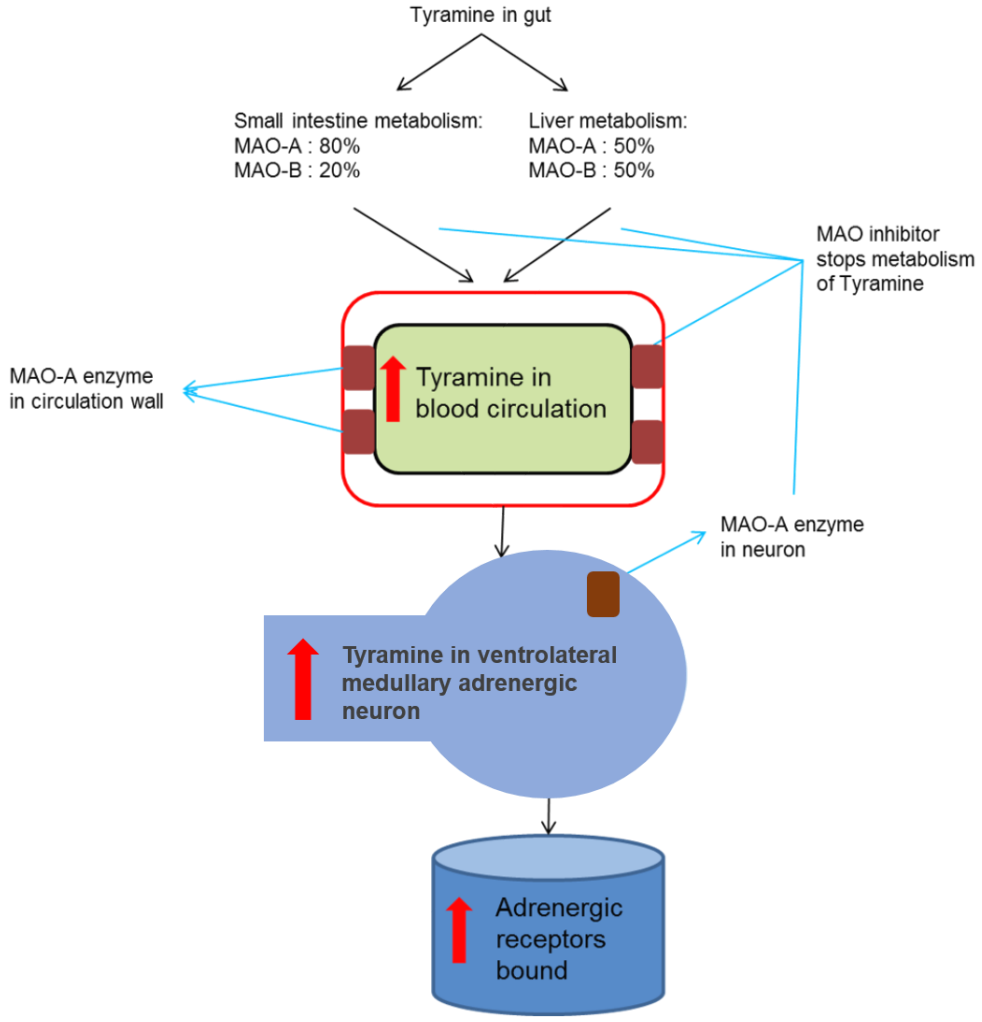

Figure 2.5 Metabolism of tyramine and the cheese reaction (Youdim *et al*., 2006).

Metabolism of serotonin and the serotonin syndrome: Serotonin is primarily metabolised by MAO-A in the human brain. Combining MAO-A inhibitors with other antidepressants that elevate serotonin levels have been found to cause serotonin toxicity. Serotonin toxicity presents as tremors, seizures, restlessness, diaphoresis, headaches and dizziness. This is mainly due to excessive levels of serotonin in the central nervous system and usually occurs when a serotonin selective reuptake inhibitor (SSRI), such as fluoxetine, is administered in combination with a MAO-A inhibitor. This has led to the contraindication of SSRIs and MAO inhibitors, especially irreversible MAO inhibitors (Neuvonen *et al*., 1993). There have been several fatalities reported after a high dose of moclobemide was used with a serotoninergic antidepressant, such as fluoxetine, citalopram or clomipramine. If this syndrome presents itself in a person, it is mainly treated by supportive care such as intravenous hydration. Before switching between antidepressant medications, it is suggested to allow for a wash-out period for the first drug before administering the new therapy (Sternbach, 1991).

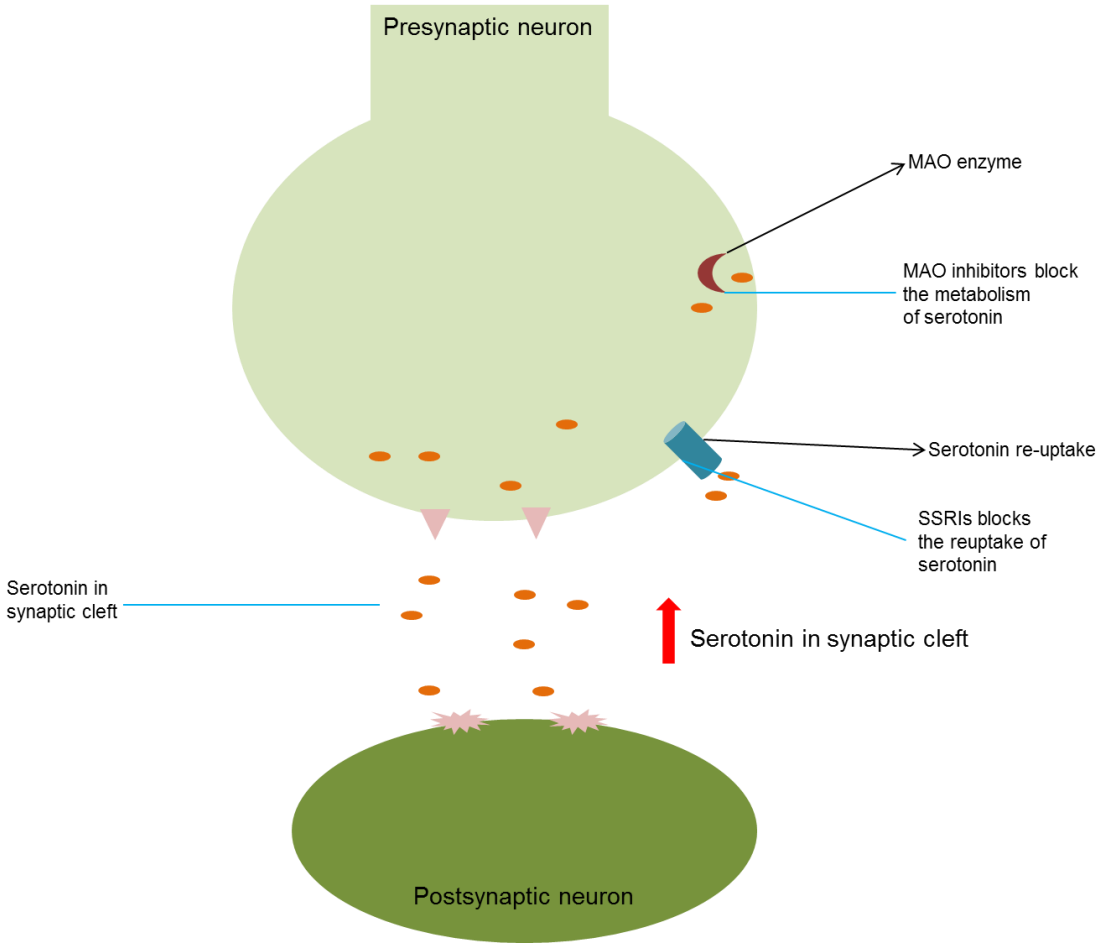

Figure 2.6 Metabolism of serotonin and serotonin syndrome (Steinberg & Morin, 2007).

2.1.5 The role of MAO-B in Parkinson's disease

Parkinson's disease is a neurodegenerative disease characterised by the degeneration of the melanin-containing dopaminergic neurons which is located in the substantia nigra pars compacta. This results in the depletion of dopamine in the nigrostriatal pathway. While Alzheimer's disease is the most common neurodegenerative disease, Parkinson's disease is the second most prevalent with 1-2% of people older than 65 years being affected (Alves *et al*., 2008). The main goal for using MAO-B inhibitors in the treatment of Parkinson's disease is to elevate striatal dopaminergic activity and thus to improve the motor deficit (Samii *et al*., 2004; Riederer *et al*., 1978). This is accomplished by reducing the MAO-B-catalysed metabolism of dopamine in the brain.

The first reports of using MAO-B inhibitors in Parkinson's disease were by Sano (2000). These researchers used iproniazid and pheniprazine as monotherapy or in combination with *L*-dopa. Degkwitz *et al*. (1960), who also used iproniazid, used it in conjunction with *L*-dopa. Although the results of these studies were modest at best, it was concluded that MAO inhibitors enhance the effects of *L*-dopa. In modern times, it has been found that the early treatment of Parkinson's disease is greatly beneficial for patients, since untreated patients show a rapid deterioration of health and quality of life, especially when compared to those people who has received early treatment (Grosset *et al*., 2007). Research done on the simultaneous treatment of *L*-dopa and a MAO-B inhibitor (in this case selegiline) has shown that a MAO-B inhibitor decreases the dose of *L*-dopa needed by 30-40% (Lees, 1995).

Studies done with the MAO-B inhibitor, rasagiline, have shown an improvement of 3 points on the UPDRS scale (unified Parkinson's disease rating scale) in 3 months of usage (Parkinson Study Group, 2002). Researchers use the UPDRS scale to measure the progression of Parkinson's disease, especially the motor section in the scale, which is a good indication of the disease progression. A similar study was also done with selegiline treatment which showed a slower progression of Parkinson's disease when compared to the placebo counterparts (Pålhagen *et al*., 2006). These studies, however, show that the symptomatic relief provided by MAO-B inhibitors is modest compared to that of the traditionally used therapy of dopamine agonists or *L*-dopa. MAO-B inhibitors do however show less adverse effects than the other treatments and are thus appropriate for treatment in early Parkinson's disease since they can control milder motor symptoms without significant adverse effects. Other dopaminergic agents such as *L*-dopa may thus be reserved for the later stages of the disease (Stowe *et al*., 2011; Caslake *et al*., 2009). It has been found that using MAO-B inhibitors in the early stages of Parkinson's disease delays the need to start therapy with *L*-dopa or dopamine agonists (Parkinson Study Group, 1993; Pålhagen *et al*., 1998). This is a significant advantage since long-term usage of *L*-dopa causes severe motor complications. Other dopamine agonists also

have been found to produce adverse effects such as hallucinations, dizziness, nausea and oedema with long-term use, which leads to drop-out rates as high as 30-40%. Thus delaying *L*-dopa and dopamine agonist treatment for as long as possible is a valid approach and may be accomplished by treatment with a MAO-B inhibitor, which is better tolerated and do not cause substantial adverse effects (Ives *et al*., 2004; Rascol *et al*., 2000; Holloway *et al*., 2004).

Currently, two MAO-B inhibitors, selegiline and rasagiline, are established therapy for Parkinson's disease. While selegiline has been proven to be useful for treating the motor symptoms of Parkinson's disease, rasagiline may be superior to selegiline in this regard (Birkmayer *et al*., 1975; Olanow *et al*., 2008; 2009; Parkinson Study Group, 2002; 2004; 2005). Rasagiline was compared to dopamine agonists, ropinirole and pramipexole, as monotherapy in Parkinson's disease. The study concluded that, in the early stages of Parkinson's disease, rasagiline is the better choice since it has much less adverse effects compared to the dopamine agonists. Rasagiline is also better tolerated by patients while the dopamine agonists were found to produce more adverse effects such as gastrointestinal issues and sleep fatigue. Pramipexole particularly had more cognitive adverse effects than ropinirole (Zagmutt & Tarrants, 2012). In all of these studies rasagiline has proven its value in the treatment of Parkinson's disease by being effective as monotherapy as well as in combination therapy with *L*-dopa and COMT (catechol-O-methyl transferase) inhibitors, showing its exceptionally good safety profile and benefits on the patient's quality of life (Rascol *et al*., 2005).

MAO-B selective inhibitors as a class are very well tolerated and have very few drug-drug interactions. A more serious complication of MAO inhibition is the cheese reaction, which as mentioned is generally not associated with MAO-B inhibitors because these drugs do not inhibit the metabolism of tyramine in the gut. Higher doses of certain MAO-B inhibitors than required can, however, inhibit MAO-A as well. In the doses required for the treatment of Parkinson's disease, MAO-B selective inhibitors do not inhibit MAO-A (Finberg, 2014; Finberg & Tenne, 1982; Mann *et al*., 1989; Chen & Wilkinson, 2012). As mentioned, serotonin syndrome is another serious adverse reaction which may occur when MAO inhibitors and serotonergic agents are combined. It causes an accumulation of serotonin, which could result in fever, hallucinations, tachycardia and gastrointestinal symptoms. The high selectivity of the MAO-B inhibitors used in the clinic, however, makes this a very rare occurrence. This was confirmed in a study where selegiline and a SSRI were co-administered. The results showed that only 0.24% of the patients developed symptoms consistent with serotonin syndrome. Only 0.04% experienced a serious reaction and there were no fatalities (Panisset *et al*., 2014). This is of importance because Parkinson's disease patients often also present with depression, which increases the probability that a SSRI will be required at some point of the treatment (Reijnders *et al*., 2008; Richard *et al*., 2012; Weintraub *et al*., 2003).

2.1.6 The role of MAO-A in Depression

In medium to high income countries, major depressive disorder is reported to be the leading cause of death and disability according to the World Health Organization (2008). One of the major causes for this statistic is the fact that when initially treated, less than 40% of all major depressive episodes show an optimal response (Trivedi *et al*., 2006). There also exist a variety of biological abnormalities which may lead to major depressive episodes, including reduced monoamine levels, increased apoptosis, an increase in oxidative stress, greater glucocorticoid secretion, reduced hippocampal volume, elevated cytokine levels, deficient neurogenesis, deficient signal transduction and a reduction in glial cell density. Identifying the underlying pathological cause for the disorder in each case is anticipated to improve the treatment response drastically. This can be done by applying biomarkers or clinical measures (Meyer, 2012; Rajkowska & Stockmeier, 2013; Schmidt *et al*., 2011).

MAO-A is responsible for the metabolism of serotonin, dopamine as well as norepinephrine. In the process of metabolising these monoamines, MAO-A produces hydrogen peroxide. Hydrogen peroxide may enhance apoptosis within the brain (Youdim *et al.,* 2006). The level of MAO-A in the brain correlates with the activity of MAO-A (Saura *et al*., 1992). In three studies done to investigate the most common cause for early onset of major depressive disorder, it was found that MAO-A levels in the prefrontal cortex as well as the anterior cingulate cortex of depressed patients is increased by 25-40% (Johnson *et al*., 2011; Meyer *et al*., 2006; 2009). Chiuccariello *et al*. (2014) recently concluded that MAO-A levels in the brain, specifically the prefrontal cortex and the anterior cingulate cortex, was notably higher in people with moderate to severe major depressive episodes. These higher levels of MAO-A in the brain have the potential of influencing the neural systems in such a way as to influence the severity of the illness. Major depressive episodes are associated with high stress, and in response to this the human brain produces glucocorticoids. Glucocorticoid administration has been found to increase the transcription rate of MAO-A as well as the activity of the enzyme in neuroblastoma and glioblastoma cell lines. This combination of higher levels of glucocorticoids and increased stress levels also seem to increase MAO-A mRNA (messenger ribonucleic acid) as well as the enzyme protein levels in the prefrontal cortex of rodents. During a major depressive episode in humans, the turnover rate of serotonin within the whole brain has been found to be elevated. This turnover of serotonin is consistent with an increase in MAO-A activity and levels, since MAO-A is the principal enzyme for the metabolism of serotonin in the brain (Ou *et al*., 2006; Filipenko *et al*., 2002; Slotkin *et al*., 1998; Barton *et al*., 2008).

When using MAO-A inhibitors in depression, the potential for the cheese reaction should always be considered. When MAO-A inhibitors are used, dietary restrictions should be imposed. In this respect, foods rich in tyramine should be avoided. When using a reversible MAO-A inhibitor

however, the potential for the cheese reaction is reduced drastically and dietary restrictions are normally not required (Youdim *et al*., 2006).

A study was done by Chiuccariello *et al*. (2014) to determine the density of MAO-A enzymes in the brain, focusing on the prefrontal cortex and the anterior cingulate cortex, and also taking the two subtypes of major depressive episodes into account (severity – moderate to severe vs. mild and reversed neurovegetative symptoms). They measured these two regions of the brain specifically because they are associated with the induction of sadness as well as the anticipation of something bad happening (Liotti *et al*., 2002; Ressler & Mayberg, 2007). This is done by measuring the MAO-A V_T, which is an index of the level of the enzyme in a particular region. The subjects with moderate to severe major depressive episodes (compared to the control groups) was found to have a remarkably higher MAO-A V_T in the prefrontal cortex, anterior cingulate cortex as well as the rest of the brain. Comparing this with subjects who only had mild to moderate major depressive episode, it was found that this group displayed no increase in MAO-A V_T compared to the control groups. The reversed neurovegetative group of subjects was also found to have a remarkably higher MAO-A V_T compared to the control groups. Chiuccariello *et al*. (2014) concluded that MAO-A levels in the brain, specifically the prefrontal cortex and the anterior cingulate cortex, were notably higher in people with moderate to severe major depressive episodes, as well as with people who has reversed neurovegetative symptoms. These higher levels of MAO-A in the brain have the potential of influencing the neural systems in such a way as to influence the severity of the illness.

2.1.7 Additional therapeutic roles of the MAOs

When amine substrates are metabolised by the MAO enzymes, hydrogen peroxide is formed as by-product. MAO inhibitors thus reduce the levels of hydrogen peroxide. While hydrogen peroxide is not a reactive molecule, it serves as substrate in the Fenton reaction and is converted to the highly reactive hydroxyl radical that causes oxidative damage to the surrounding tissue. MAO inhibitors thus reduce oxidative stress indirectly by reducing the formation of the hydroxyl radical. Because of this, it has been suggested that the MAO-B inhibitors, rasagiline and selegiline, may have a neuroprotective effect in Parkinson's disease by reducing oxidative stress (Youdim & Bakhle, 2006; Riederer & Müller, 2017; Bar-Am *et al*., 2016). Studies with selegiline suggested that treatment with this inhibitor prolongs the life-span of Parkinson's disease patients by potentially slowing the degeneration of the dopaminergic neurons in the brain. Further support for the neuroprotective effect of selegiline was provided by the observation that MPTP is metabolised by MAO-B to the active neurotoxin, MPP^+. This neurotoxin is responsible for inducing a Parkinsonian syndrome in humans as well as non-human primates (Birkmayer *et al*., 1985). As a MAO-B inhibitor, selegiline protects against the activation and toxicity of MPTP.

The catalytic activity of MAO-A is one of the main sources of hydrogen peroxide within the heart. In previous studies it has been found that MAO-A levels increase in the heart of rats with age, which suggests that hydrogen peroxide produced by MAO-A may contribute to cardiac cellular degeneration in human subjects as well (Maurel *et al*., 2003). The inhibition of MAO-A will thus lower the levels of the hydrogen peroxide that is formed and, in turn, decrease oxidative stress on the heart. This will lead to a reduction in necrosis and apoptosis of cardiac tissue. Inhibitors of MAO-A may have future application in heart diseases, specifically heart failure (Umbarkar *et al*., 2015; Kaludercic *et al*., 2014).

In patients suffering from Alzheimer's disease, it has been found that MAO-B levels are increased in the brain, which may enhance oxidative stress levels. Selegiline has been evaluated in Alzheimer's disease patients, but there has been no concrete results that support an improvement in the symptoms (Kennedy *et al*., 2003). It was suggested that combining a MAO-B inhibitor with a cholinesterase inhibitor (such as physostigmine) may lead to an improved response in Alzheimer's disease. Another way to counter this disease is to combine the inhibition of both these enzymes in one single compound. In this regard ladostigil is a compound that inhibits both MAO-B and cholinesterase, and may thus be particularly useful for the treatment of Alzheimer's disease. Ladostigil has been found to augment cognition in older primates and has been reported to have anxiolytic and antidepressant activities (Marin *et al*., 1995; Youdim & Weinstock, 2001; Weinstock *et al*., 2003; Buccafusco *et al*., 2003; Poltyrev *et al*., 2005).

Selegiline has also shown to decrease the damage done to tissue in the brain caused by cerebral ischaemia in animal models. This may be attributed to a reduction in hydrogen peroxide produced by MAO-B during ischaemia-reperfusion (Kunduzova *et al*., 2002; Vondriska *et al*., 2001; Weinreb *et al*., 2004). Another study showed that selegiline may enhance the recovery process after a person has suffered a cerebral infarction (Sivenius *et al*., 2001).

Amyotrophic lateral sclerosis (ALS) and Huntington's disease share some of the pathological characteristics of Alzheimer's disease and Parkinson's disease, which include accumulation of iron in the brain, oxidative stress and excitotoxicity. There have been reports that rasagiline may be effective against ALS in mice, while selegiline treatment has not been as successful. In contrast, in Huntington's disease, a study has shown that selegiline in combination with a serotonin reuptake inhibitor, such as fluoxetine, can be successful (Lange *et al*., 1998; Waibel *et al*., 2004; Sagot *et al*., 2000; Patel *et al*., 1996).

MAO-A inhibitors and non-selective MAO inhibitors have been found to be good in treating phobic anxiety as well as atypical depression (those having hysterical traits, tiredness,

hypersomnia, bulimia as well as impressions of rejection) and appear to be better than amine-uptake inhibitors (Zisook, 1985).

The MAO-B inhibitors, lazabemide and selegiline, have both been identified to assist smokers to stop smoking and to continue in abstinence. Moclobemide, a MAO-A inhibitor, has been reported to have the same effect which has been attributed to increased serotonin levels in the brain. The effect on smoking cessation may also be attributed to the fact that smoking inhibits MAO in the brain, thus MAO inhibition mimics this effect of compounds that inhibit the MAOs in cigarette smoke (Houtsmuller *et al*., 2002; Berlin *et al*., 1995; 2002; Fowler *et al*., 1996; 2003; Herraiz & Chaparro, 2005).

Some MAO-A selective inhibitors are currently being evaluated for their potential effects against prostate cancer (Flamand *et al*., 2010). This is based on the finding that MAO-A activity is increased in certain cancer tissues. MAO-A inhibition may, in synergism with survivin suppressants, inhibit cancer cell growth, migration and invasion (Xu *et al*., 2015; Wu *et al*., 2014).

Table 2.1 MAO inhibitors and their indicated usage.

Compound	MAO selectivity	Inhibition type	Application
Befloxatone 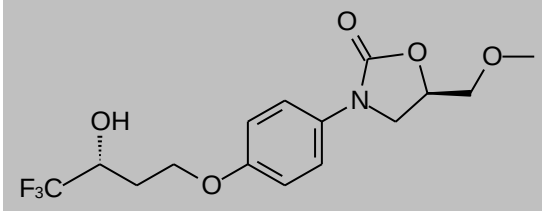	A	Reversible	Depression
Brofaromine 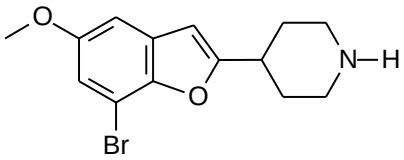	A	Reversible	Depression

Clorgyline 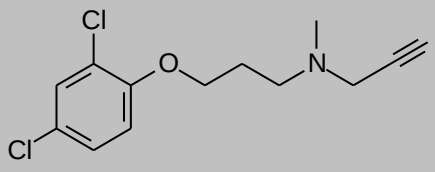	A	Irreversible	Depression
Selegiline 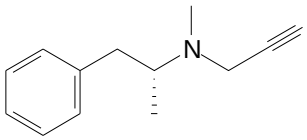	B	Irreversible	Parkinson's disease
Iproniazid 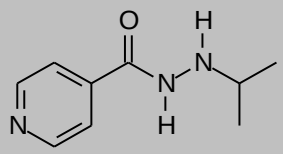	A & B	Irreversible	Depression
Ladostigil 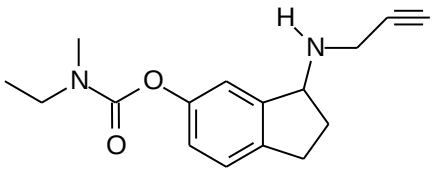	A & B (brain selective)	Irreversible	Antidepressant, Parkinson's & Alzheimer's diseases
Lazabemide 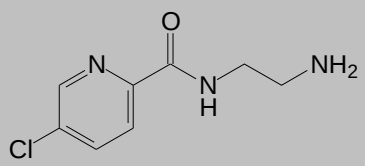	B	Reversible	Parkinson's disease
M30 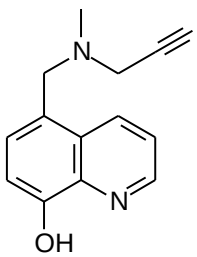	A & B (brain selective)	Irreversible	Depression, Parkinson's & Alzheimer disease

Moclobemide 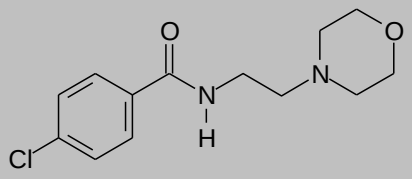	A	Reversible	Depression
Nialamide 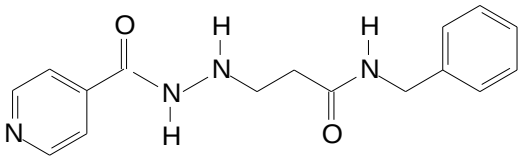	A & B	Irreversible	Depression
Phenelzine 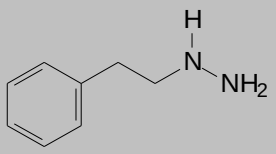	A & B	Irreversible	Depression
Rasagiline 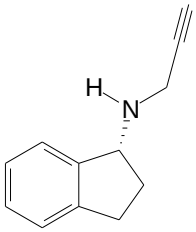	B	Irreversible	Parkinson's disease
Safinamide 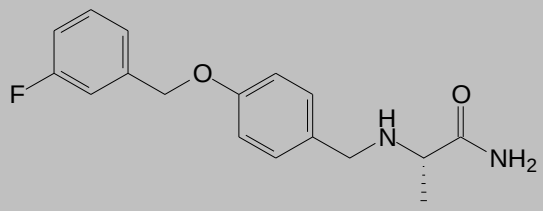	B	Reversible	Parkinson's disease

Toloxatone 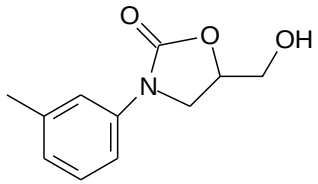	A	Reversible	Depression
Tranylcypromine 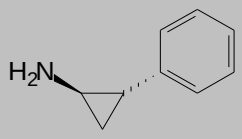	A & B	Irreversible	Depression
Isocarboxazid 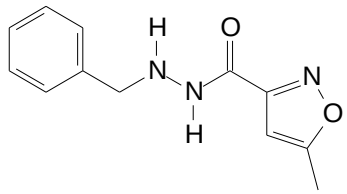	A & B	Irreversible	Depression
Pirlindole 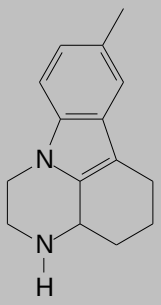	A	Reversible	Depression

2.1.8 Inhibitors of MAO-B

Two selective irreversible MAO-B inhibitors are currently approved for Parkinson's disease treatment, selegiline and rasagiline. Both of these drugs are used in the early stages of Parkinson's disease as monotherapy or in later stages as adjunctive therapy to *L*-dopa and dopamine agonists.

2.1.8.1 Selegiline

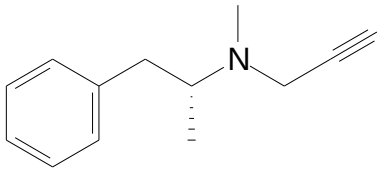

Figure 2.7 The structure of selegiline.

Selegiline was first synthesised by Zoltan Ecsery in Hungary's capital city, Budapest, 1962. In 1965 it was patented as an antidepressant. Selegiline is the *R*-optical enantiomer of deprenyl. This compound is a selective inhibitor of MAO-B with an affinity 500-fold greater for MAO-B than MAO-A, and an IC_{50} value of 20 nM for the inhibition of MAO-B (Magyar, 1993). Selegiline was the first MAO-B inhibitor to be approved for the treatment of Parkinson's disease by the Food and Drug Administration (FDA) of the USA. It is still used as monotherapy but also as an add-on to other anti-Parkinson's disease drugs. In Parkinson's disease, selegiline increases dopamine concentrations in the central nervous system and provide some symptomatic benefit (Hornykiewicz, 2001; 2002). Treatment with selegiline may also reduce hydrogen peroxide production by MAO-B, thus decreasing oxidative stress in the brain (Tipton *et al*., 2004). By reducing the formation of potentially harmful metabolic by-products of MAO-B catalysis, selegiline may also possess neuroprotective properties in Parkinson's disease (Knoll, 1988).

2.1.8.2 Rasagiline

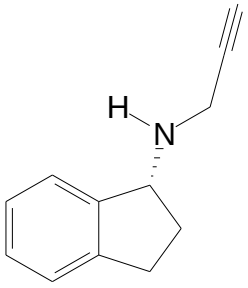

Figure 2.8 The structure of rasagiline.

Rasagiline was developed by Professor Moussa Youdim from Haifa, Israel in the Rappaport Faculty of Medicine, Technion. Rasagiline is a selective and irreversible (second generation) inhibitor of MAO-B and was approved by the FDA for the treatment of Parkinson's disease in 2006. It is approved for the treatment of Parkinson's disease in the European Union as well. Rasagiline is used as monotherapy and as adjunctive to *L*-dopa in the later stages of the disease. Rasagiline is selective for the inhibition of MAO-B when used at therapeutic dosages (0.5 – 1 mg/day) and does not potentiate the cheese reaction when combined with tyramine. At

high doses (10 mg/kg) rasagiline may inhibit both MAO-A and MAO-B. Rasagiline has IC_{50} values of 4.43 nM for MAO-B and 412 nM for MAO-A (Youdim *et al*., 2001). The inhibitor is known to bind covalently to the N5 nitrogen of the flavin cofactor of MAO, which results in irreversible inhibition. Rasagline has been shown to be neuroprotective in a series of *in vivo* and *in vitro* tests, and it has been suggested that the propargyl moiety of rasagiline is important for this neuroprotective effect. While the inhibition of MAO-B may contribute to the neuroprotective properties of rasagiline, some aspects of its neuroprotective mechanism may be independent of the inhibition of MAO-B, because another compound, AGN1135 which is not a MAO-B inhibitor, also possesses neuroprotective effects. Regarding its neuroprotective effects, rasagiline reduces oxidative stress, prevents apoptosis and stabilises the membranes of mitochondria (Hoy & Keating, 2012; Weinreb *et al*., 2011; Naoi *et al*., 2013). This drug has been one of the most used antiparkinsonian drugs during the past couple of years because of its good safety profile.

2.1.8.3 Safinamide

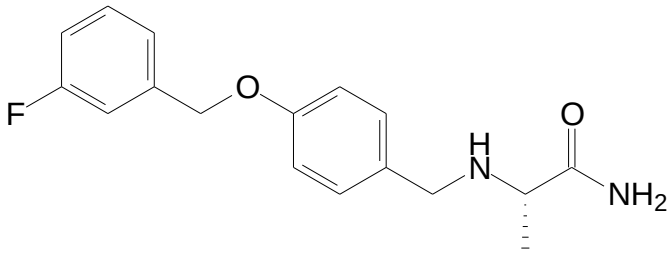

Figure 2.9 The structure of safinamide.

Safinamide was recently approved by the European Commission as an add-on to *L*-dopa and other antiparkinsonian drugs. It is currently under review by the FDA. Safinamide was found to have a novel mechanism of action since it is a reversible and a selective inhibitor of MAO-B but it also blocks the reuptake of dopamine. It was discovered that safinamide also has an effect on the glutamate pathway. Safinamide has been shown to be a very potent MAO-B inhibitor with an IC_{50} value of 0.08 µM. It binds to human MAO-B with a K_i value of 0.5 µM, which is 700-fold more potent than its inhibition potency towards human MAO-A (Caccia *et al*., 2006). When safinamide is bound to the enzyme it spans over both the entrance and substrate cavities which contributes to the specificity of this inhibitor for MAO-B. MAO-A has a much smaller single cavity compared to MAO-B and does not accommodate larger inhibitors such as safinamide well. Safinamide is a reversible MAO-B inhibitor and does not form a covalent adduct with the FAD cofactor. Since safinamide is selective it may be administered at a higher dose than therapeutic doses (10 mg/kg) and will not produce any MAO-A inhibition (Cattaneo *et al*., 2003). Safinamide has a bioavailability of 80-92%, is very quickly absorbed and has a half-life of 3 hours in mice, 7

hours in rats and 13 hours in monkeys. After administration, the concentration of safinamide is higher in the brain compared to the plasma, which is where antiparkinsonian drugs act. In a placebo-controlled study, safinamide demonstrated no issues regarding tolerability and adverse effects were much lower than that of the placebo group (Stocchi *et al*., 2004).

2.1.8.4 Lazabemide

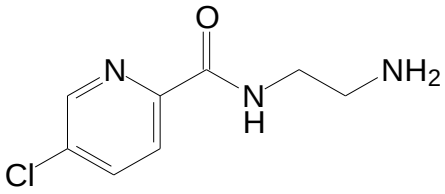

Figure 2.10 The structure of lazabemide.

Lazabemide is known for being a very potent inhibitor of especially MAO-B compared to MAO-A. It is 100-fold more potent than selegiline and also protects experimental animals against the neurotoxic action of MPTP. Although lazabemide is an irreversible inhibitor *in vitro*, *in vivo* MAO-B activity in platelets is recovered shortly after drug withdrawal (Cesura *et al.,* 1989; Haefely *et al*., 1990). Complete enzyme recovery has been found 24 hours after drug withdrawal in humans. In contrast to selegiline, lazabemide does not potentiate the cheese reaction when administered in high doses (Cesura *et al*., 1999). Lazabemide was tested as a potential aid to smoking cessation on the basis that it facilitates dopaminergic neurotransmission which will substitute the effect that nicotine has. This study had promising prospects, but the development of lazabemide was terminated by its sponsors (Berlin *et al*., 2002).

2.1.8.5 Isatin

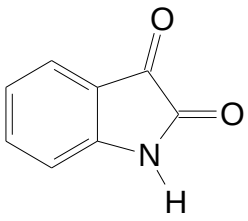

Figure 2.11 The structure of isatin.

Isatin was discovered in the 1800's as a product of the oxidation of indigo. It is bright orange coloured and has a very wide range of pharmacological actions. Isatin is an endogenous indole and has a peculiar distribution in the body, ranging from the brain to peripheral tissues. Within the brain it is most concentrated in the hippocampus and cerebellum, with the frontal cortex having lower concentrations (Watkins *et al*., 1990; Glover *et al*., 1991). *In vitro* studies have

shown that isatin's most potent action is the inhibition of MAO-B with an IC_{50} value of 3 µM. It was also found to bind the receptors of atrial natriuretic peptide (ANP) and inhibit the formation of ANP-induced guanylate cyclase with an IC_{50} value of 0.4 µM. *In vivo* studies have shown that administering isatin to experimental animals causes an increase in brain monoamine neurotransmitter levels, which may be attributed to the inhibition of MAO-B. Research has shown isatin to be a reversible, competitive and selective inhibitor of MAO-B with K_i values of 3-20 µM towards rat MAO-B. MAO-A inhibition does occur at higher concentrations in rats with a K_i value of 60-70 µM (Glover *et al*., 1988; Medvedev *et al*., 1992; 1995). Isatin was found to be an anticonvulsant at high doses, but also induced sedation (Sareen *et al*., 1962; Bhattacharya *et al*., 1991). Although isatin is a MAO-B selective inhibitor, it has been seen that at high doses it can inhibit MAO-A as well. Studies have also found that isatin increased vigilance and induced anxiety in rodents (Seidel & Wenzel, 1979).

2.1.9 Inhibitors of MAO-A

Inhibitors of MAO-A have been of value since the discovery of MAO and the enzyme's role in depression. Since the earliest MAO-A inhibitors had the tendency to cause the cheese reaction which was fatal in some instances, the clinical use of MAO-A inhibitors has declined. With the discovery and development of reversible MAO-A inhibitors, the cheese reaction is of lesser concern and MAO-A inhibitors are again frequently prescribed as antidepressants (Youdim *et al*., 2006).

2.1.9.1 Moclobemide

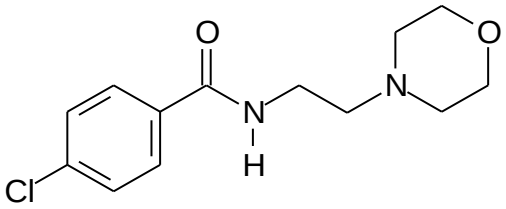

Figure 2.12 The structure of moclobemide.

Moclobemide was launched in December of 1989 in Sweden. It is a reversible inhibitor of MAO-A. MAO inhibitors may be divided in to three classes based on the reversibility and specificity of inhibition. The first generation of MAO inhibitors is the irreversible and non-selective inhibitors. The second generation is irreversible but selective towards either MAO-A or MAO-B. Moclobemide is a third generation MAO inhibitor, and is reversible and selective. As a MAO-A inhibitor, moclobemide is used for the treatment of major depression, and is nearly devoid of hepatotoxicity, hypotension and the potential for causing the cheese reaction. To test this, healthy subjects were treated with high doses of moclobemide in combination with tyramine.

There was no drastic increase in systolic blood pressure found showing that moclobemide has a low risk of causing the cheese reaction (Dingemanse *et al*., 1998). Moclobemide is a benzamide derivative and contains the morpholine ring. Interestingly other benzamide derivatives do not inhibit MAO-A or increase monoamines (Da Prada *et al*., 1989). Moclobemide has an IC_{50} value towards MAO-A of 6 μM and >1000 μM towards MAO-B. This shows a very selective but relatively weak inhibition of MAO-A (Kettler *et al*., 1990). Moclobemide was found to increase the levels of cerebral dopamine, norepinephrine as well as serotonin (Da Prada *et al*., 1994).

2.1.9.2 Toloxatone

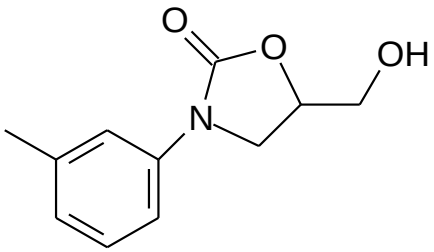

Figure 2.13 The structure of toloxatone.

Toloxatone has been marketed in France since 1985 and is used as an antidepressant. Toloxatone is a selective and reversible inhibitor of human MAO-A with an IC_{50} value of 6.71 μM and a K_i value of 1.34 μM (Benedetti *et al*., 1983; Herraiz & Brandt, 2014). Because it is a reversible inhibitor, it displays no interaction with tyramine and thus does not cause the cheese reaction. Even at higher doses it is safe with a very low risk for causing a hypertensive reaction (Berlin *et al*., 1989; Bieck *et al*., 1989; Mann *et al*., 1984). By inhibition of MAO-A, toloxatone drastically inhibits the deamination of dopamine as well as noradrenaline. Toloxatone is very rapidly absorbed and has a peak plasma concentration between 0.5 and 1 hour after oral administration. Toloxatone is metabolised in the liver and is mainly excreted in the urine. Toloxatone also reaches the central nervous system quickly, whilst 70% of the total drug plasma concentration reaches the cerebrospinal fluid (Benedetti *et al*., 1982; Malnoë & Benedetti, 1979; Vistelle *et al*., 1992).

2.1.9.3 Befloxatone

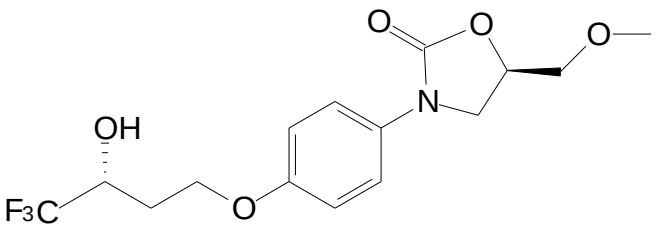

Figure 2.14 The structure of befloxatone.

Befloxatone is an oxazolidinone derivative and is a reversible and selective inhibitor of MAO-A with an IC_{50} value of 4 nM, and an *in vitro* K_i value of 1.9-3.6 nM. After administration to rats, befloxatone increased monoamine levels in the brain (Curet *et al*., 1996). Befloxatone is considered to be safe with a low risk of the cheese reaction. Studies done on the interaction between befloxatone and tyramine showed that dietary restrictions are not required for patients treated with this drug. Befloxatone is 276-fold more specific towards MAO-A than MAO-B, and after administration to rats, befloxatone inhibited more than 90% of brain MAO-A. Befloxatone is absorbed rapidly and has a short half-life. In animal studies it was shown that the inhibition of MAO-A in the brain is very efficient, even at low doses of befloxatone. This showed that befloxatone can be used as an antidepressant (Caille *et al*., 1996).

2.2 Parkinson's disease

As mentioned earlier, Parkinson's disease was first described by James Parkinson, who wrote a monograph on his observations called "An essay on the shaking palsy". He examined six patients in his private practice and in his neighbourhood and wrote the monograph hoping to describe what he thought was a previously unknown disorder. Later on, Jean Martin Charcot read James' monograph and proposed that this disease be named "maladie de Parkinson", in English – Parkinson's disease (Parkinson, 2002; Kempster *et al*., 2007). The rate at which the disease occurs has been found to increase with age. For people between the age of 50-59, the occurrence is 17.4 people in every 100 000. Between the ages of 70-79 it rises to 93.1 people in every 100 000. The average age at which Parkinson's disease is diagnosed is 60, with an average life duration of 15 years after diagnoses. As the average age in the western world rises, the incidence of Parkinson's disease is also expected to rise even as research continues (Bower *et al*., 1999; De Rijk *et al*., 1995). The most documented cause of death in Parkinson's disease patients is pneumonia. It has been shown that Parkinson's disease does not distinguish between different races and cultures, however some studies have shown that men has a 1.5-fold greater chance of developing Parkinson's disease than women (Katzenschlager *et al*., 2008; Twelves *et al*., 2003).

The pathological cause or trigger of Parkinson's disease has not yet been discovered, although age does seem to play a major role, even though 10% of Parkinson's disease patients are under the age of 45. It has also been discovered that the incidence decreases within the ninth decade of life (Tanner, 2003; Taylor *et al*., 2005). People who have never smoked before also have a twofold greater chance of developing the disease (Hernán *et al*., 2001). Postmenopausal women and men who do not take hormone replacements and on average consumes no caffeine or a small amount each day, has a much higher probability to develop Parkinson's disease (25% increased risk) (Ascherio *et al*., 2003; 2004). This occurrence may be due to dopamine release in the "reward pathway" of the brain. Caffeine and nicotine are known to release

dopamine in the striatum of the brain, and smoking is known to inhibit MAO in the brain as well (Fowler *et al*., 1996). Caffeine is also a known adenosine A2 receptor antagonist, and because of this trait it has shown some potential as a therapeutic agent in Parkinson's disease (Jankovic, 2008). There has also been some association between Parkinson's disease and the following: obesity in middle age, not enough exercise, head injuries, living in rural areas, indigestion of water from an unclean water source as well as herbicides and insecticides (Elbaz & Tranchant, 2007; Thacker *et al*., 2008).

The ubiquitin proteasome pathway is known as one of the primary mechanisms by which the human body maintains the homeostasis of proteins within cells. If this system is defective, it may lead to the aggregation of cytotoxic proteins as well as mutations in other proteins such as α-synuclein and parkin. α-Synuclein is involved in the apoptosis process, and elevated levels of α-synuclein promote apoptosis. These protein imbalances can result in unwanted proteins exceeding their natural levels and the capacity of the proteasomes to clear them. This will in turn lead to proteolytic stress which can result in neuronal damage and Parkinson's disease. Ubiquitin ligase parkin protein is involved in the metabolism of any dysfunctional mitochondria via autophagosomes. Failing to clear these dysfunctional mitochondria may be an important pathogenic factor in Parkinson's disease (Olanow & McNaught, 2006; Narendra *et al*., 2008).

In Parkinson's disease, pathogenic mutations can cause the disease in two ways: directly by causing the abnormal formation of certain proteins which can be toxic, or indirectly by hampering the process that usually recognises and eliminates unwanted and misfolded proteins and thus prevent them from aggregating and possibly becoming toxic (Bussell & Eliezer, 2001). One of the possible triggers for the dysfunction of the protein metabolism system may be oxidative stress. Oxidative stress is postulated to be one of the pathogenic causes of Parkinson's disease since it causes cell damage via ROS. It was found, that with an increase in age the amount of abnormally oxidised proteins, which has the ability to misfold and be toxic, also increases. This may cause human cells to lose its ability to clear these misfolded proteins over time (Beckman & Ames, 1998; Sherman & Goldberg, 2001). Usually healthy cells respond to misfolded proteins by sending chaperones to refold the protein to its normal conformation, but if the protein cannot be refolded it is degraded by polyubiquitination. Cells subjected to oxidative stress also lose the ability to induce a variety of chaperone proteins with aging. The proteasomal activity also becomes dysfunctional and thus misfolded proteins aggregate and become toxic. α-Synuclein is a good example as it has been observed to aggregate easier as soon as it is oxidatively modified (Giasson *et al*., 2000).

The accumulation of proteins in the brain has been found to be involved in the pathogenesis of a variety of neurodegenerative disorders. It differs from one disease to another and whether the accumulation is intracellularly or extracellularly, but it can be postulated that the accumulation of

excess proteins in the brain leads to neuronal damage. The aggregation of misfolded proteins has been found to be very neurotoxic and leads to cell death by deformation of the cell itself or interference with intracellular traffic neurons. In the case of α-synuclein, the accumulation of aggregated forms of this protein leads to oxidative damage (Giasson *et al*., 2000).

The possibility that defective mitochondrial respiration could play a role in causing Parkinson's disease became a possibility when it was discovered that MPTP inhibits complex I of the electron transport chain (Nicklas *et al*., 1987). Complex I is an enzyme system within the mitochondrial respiratory chain and is the first and largest enzyme in this system. It plays a major role in the transfer of electrons and moving of protons which maintains the electrochemical gradient over the inner mitochondrial membrane. It is also the most prevalent mitochondrial deficiency in children (30%) (Fassone & Rahman, 2012). Studies done *in vitro* has shown that a defect in complex I leads to oxidative stress within cells, and it has been seen that these abnormalities in complex I is present in Parkinson's disease patients. A defect in mitochondrial complex I has been found to be inherited by the mitochondrial genome, but it can also be caused by systemic toxicity which may cause mutations in the mitochondrial genome (Greenamyre *et al*., 2001).

Almost all molecular oxygen is used in the mitochondria for respiration purposes, which forms oxidants such as hydrogen peroxide as well as superoxide radicals as by-products. The inhibition of complex I will elevate the levels of superoxide, which in turn can lead to toxic hydroxyl radicals being formed. Superoxide may also react with nitric oxide and form peroxynitrite. These molecules are known to damage cells and cause cell death by reacting with lipids, nucleic acids or proteins. The hydroxyl radical and peroxynitrite may also cause damage to the electron transport chain that will bring about damage to the mitochondria as well as further elevating the levels of ROS (Cohen, 2000). When ROS levels are increased, the levels of misfolded proteins will also increase which will demand more from the ubiquitin proteasome system to remove the misfolded proteins. When dopamine is metabolised by MAO, the reaction produces hydrogen peroxide. Auto-oxidation of dopamine has been found to produce dopamine quinone, a molecule that may react with cysteine residues and cause damage to proteins. This takes place mainly within the dopaminergic neurons, which leads to neuronal death in Parkinson's disease (Graham, 1978).

Iron is a very important trace element in the human body, often used to help with oxygen transport, neurotransmitter synthesis and nerve myelination (van Gelder *et al*., 1998; Mounsey & Teismann, 2012). Iron also plays a role in the pathogenesis of Parkinson's disease, which is characterised by the loss of dopaminergic neurons in the substantia nigra pars compacta and severe motor dysfunction. It has been shown that iron accumulates in the brain of Parkinson's disease patients, especially in the substantia nigra, the affected area (Dexter *et al*., 1987; Sofic

et al., 1988; Jenner & Olanow, 1998). When iron is deposited in excess, it generates ROS. Iron catalyses the Fenton reaction which increases the levels of oxidative stress. ROS will damage cell membranes, nucleic acids and proteins, and thereby cause apoptosis and necrosis of the dopaminergic neurons. This suggests that iron is a key factor in dopaminergic neuronal death in the brain of Parkinson's patients (You *et al*., 2015). Iron also increases in the brain as a person ages. Studies with post-mortem Parkinson's disease patients reveal an increase in non-heme iron in the substantia nigra (Dexter et al., 1987; Shi *et al*., 2010). You *et al*. (2015) also found that an increase in iron aggravates dopaminergic cell death and motor dysfunction in animals treated with MPTP. Treatment with an iron chelator such as deferoxamine (DFO), however, attenuates the damage. Previous research has similarly shown that an iron chelator and genetically low levels of brain iron protect mice against the effects of MPTP (Kaur *et al*., 2003). You *et al*. (2015) also found that an increase in oxidative stress leads to the activation of apoptotic pathways and plays a role in the onset and progression of Parkinson's disease.

As literature has shown, the precise mechanism of pathogenesis in Parkinson's disease is still not known. Further research is required to gain insight into potential causes of Parkinson's disease, which will lead to the design of treatment strategies.

2.3 Conclusion

This chapter provides background on the MAO enzymes with the focus on their roles in depression and Parkinson's disease. It is shown that MAO inhibitors are useful therapeutic agents with MAO-A inhibitors being used as antidepressants while MAO-B inhibitors are used in the treatment of Parkinson's disease. MAO-B inhibitors may also possess neuroprotective properties by reducing the potentially harmful metabolic products of the MAO catalytic cycle. When using MAO inhibitors in the clinic, their potential for causing tyramine-induced hypertension should always be considered. Reversible MAO-A inhibitors and highly specific MAO-B inhibitors possess a much lower risk of causing tyramine-induced hypertension compared to irreversible MAO-A inhibitors. This dissertation will attempt to discover reversible and highly specific inhibitors of MAO-B by synthesising a series of 1-tetralone and 1-tetralol derivatives. The syntheses and biological evaluation of these derivatives will be presented in the following chapters.

CHAPTER 3

SYNTHESIS

3.1 Introduction

In this study a series of 1-tetralone derivatives were synthesised and evaluated as inhibitors of MAO-A and MAO-B. In this chapter the syntheses of the derivatives are described. 1-Tetralone derivatives have previously been shown to act as potent MAO inhibitors and this observation formed the basis of this study (Legoabe *et al*., 2014; 2015). This study will thus expand on the structure-activity relationships (SARs) of MAO inhibition by the 1-tetralone class of compounds. In particular, the effect on MAO inhibition of the reduction of the 1-tetralone carbonyl to the corresponding alcohol will be determined. For this purpose, this study therefore synthesises the 1-tetralone derivatives shown in table 3.1. The chemical modifications that were made to 1-tetralone included (1) substitution on C5, C6 and C7 and (2) reduction of the carbonyl to the corresponding alcohol. The substituents considered were the benzyloxy, 4-chlorobenzyloxy and 2-phenoxyethoxy moieties. All of these substituents have been shown to enhance the MAO inhibition potencies of caffeine derivatives, while the benzyloxy side chain has also been shown to yield good MAO inhibition when substituted on C6 and C7 of 1-tetralone (Strydom *et al*., 2010; 2012; Legoabe *et al*., 2014; 2015).

Table 3.1 The structures of the 1-tetralone derivatives (1a-p) synthesised in this study. The shaded entries are the 1-tetralones while the unshaded entries are the alcohol derivatives.

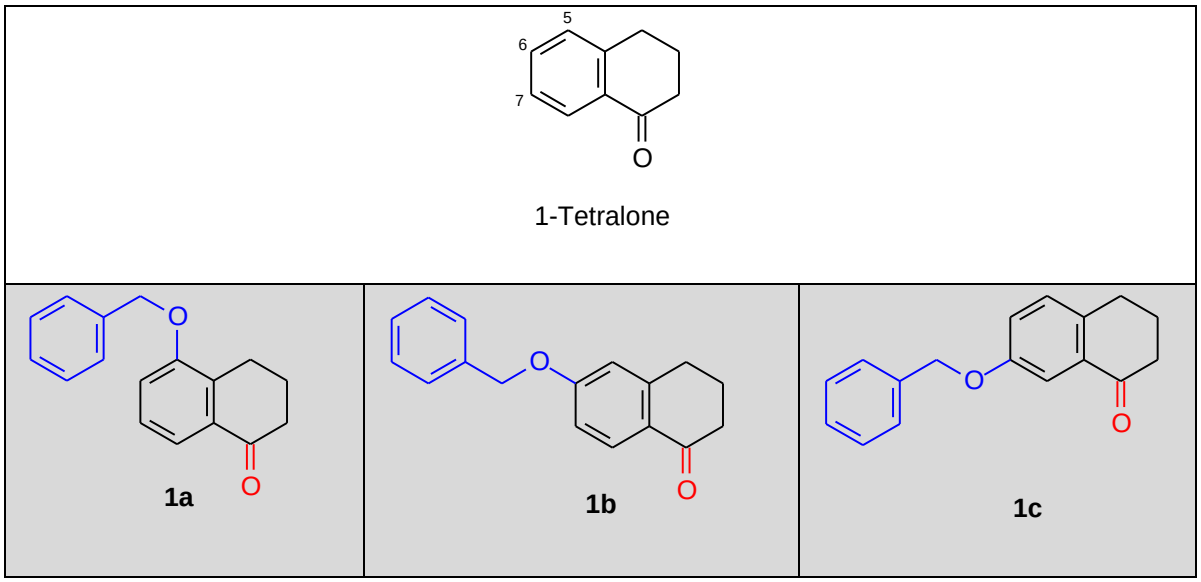

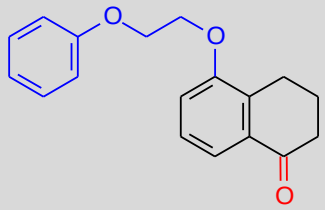 **1d**	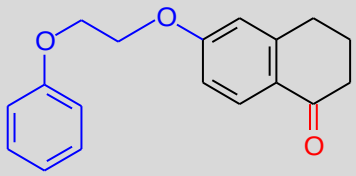 **1e**	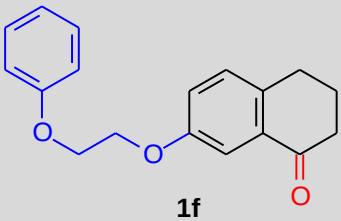 **1f**
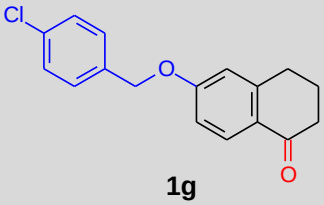 **1g**	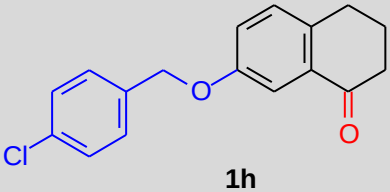 **1h**	
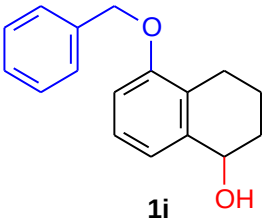 **1i**	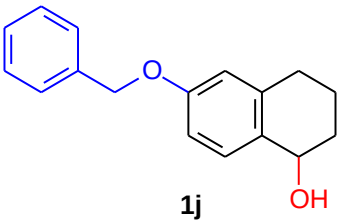 **1j**	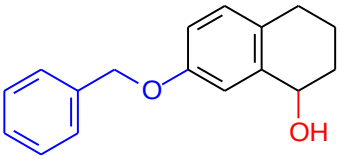 **1k**
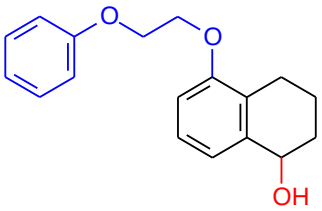 **1l**	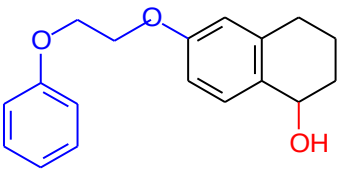 **1m**	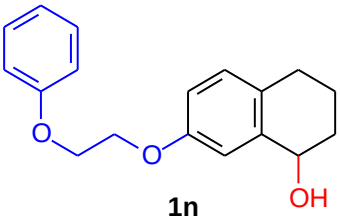 **1n**
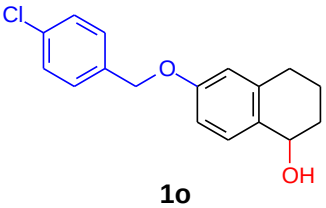 **1o**	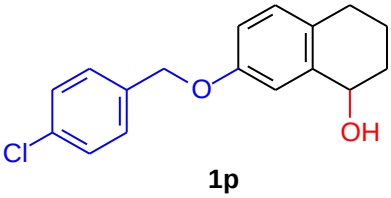 **1p**	

3.2 Materials and instrumentation

3.2.1 Materials:

All the reagents and solvents used in this study were obtained from Sigma-Aldrich and were used without further purification.

3.2.2 Thin layer chromatography (TLC):

Silica gel TLC sheets with a UV_{254} fluorescent indicator was used to determine the progression of the reactions. Compounds were spotted on the TLC plate and eluted with a mobile phase consisting of ethyl acetate and petroleum ether. The TLC sheets were examined under a UV (ultraviolet) light at a wavelength of 254 nm in order to determine if the reactions proceeded to completion. The *Rf* values of the 1-tetralone derivatives were calculated and are given in the results section.

3.2.3 Melting points:

All melting points were determined on a Büchi B-545 melting point apparatus. Melting points are uncorrected.

3.2.4 Mass spectra (MS):

A Bruker micrOTOF-Q II mass spectrometer functioning in atmospheric-pressure chemical ionisation (APCI) mode was used to record the high resolution mass spectra (HRMS) as well as nominal mass spectra (MS).

3.2.5 Nuclear magnetic resonance (NMR):

Proton (^{1}H) and carbon (^{13}C) NMR spectra were determined using a Bruker Avance III 600 spectrometer at 600 MHz (for ^{1}H) and 150 MHz (for ^{13}C). Choloform-D1 was used a solvent.

3.2.6 High pressure liquid chromatography (HPLC):

The purity of the synthesised compounds was determined by HPLC. The apparatus used was an Agilent 1100 HPLC system equipped with a quaternary pump and a diode array detector. HPLC grade acetonitrile (Merc) and Milli-Q water (Millipore) were used for the chromatography. A Venusil XBP C18 column (4.60 x 150 mm, 5 µm) was used for separation and the mobile phase consisted at the start of each run of acetonitrile 30% and Milli-Q water 70%, and the flow rate was set at 1 ml/min. After each run was started, a solvent gradient program was initiated. The composition of acetonitrile in the mobile phase was increased linearly to 80% over a period of 5 min. Each run lasted 15 min, with a 5 min equilibration time between runs. 20 µl of each test compound dissolved in acetonitrile (1 mM) was injected into the HPLC system and the eluent was monitored at a wavelength of 254 nm.

3.3 Method for the synthesis of 1-tetralone derivatives

In the first step of the synthesis, the key starting materials, 5-, 6- and 7-hydroxy-1-tetralone (**2a-c**) were synthesised from the corresponding methoxy-1-tetralone derivatives by reaction with

aluminium chloride ($AlCl_3$). In the subsequent step, the hydroxy derivatives were alkylated with benzyl bromide, 4-chlorobenzyl bromide or 2-phenoxyethyl bromide to yield the substituted 1-tetralone derivatives **1a**-**h**. Reduction with sodium borohydride ($NaBH_4$) yielded the alcohol derivatrives **1i**-**p**.

3.3.1 The synthesis of 5-, 6- and 7-hydroxy-1-tetralone (2a-c).

The key starting materials, 5-, 6- and 7-hydroxy-1-tetralone (**2a**-**c**), were synthesised by the method described by Legoabe *et al*. (2014). The corresponding methoxy-1-tetralone derivatives **3a**-**c** (10 mmol) were added to aluminium chloride ($AlCl_3$) (25 mmol) and toluene (50 ml) in a round bottom flask. The reaction was heated under reflux for 1 h. Silica gel TLC was used to determine if the reaction has proceeded to completion. The reaction was placed on ice for 30 min and water (75 ml) was cautiously added to the reaction. The mixture was subsequently extracted to ethyl acetate (3 x 75 ml). The combined organic phases were dried over anhydrous $MgSO_4$ at room temperature for at least 20 min. The $MgSO_4$ was removed by filtration, the organic phase evaporated under reduced pressure and the crude product was purified by recrystallisation from ethyl acetate.

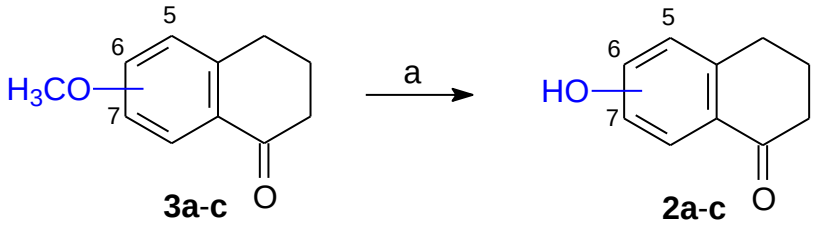

a: 5-substituted
b: 6-substituted
c: 7-substituted

Figure 3.1 Reaction pathway for the synthesis of 5-, 6- and 7-hydroxy-1-tetralone (2a-c). Key: (a) $AlCl_3$, toluene, reflux, 1 h.

3.3.2 The synthesis of substituted 1-tetralone derivatives (1a-h).

5-, 6- or 7-Hydroxy-1-tetralone (**2a**-**c**) (10 mmol) was added to a round bottom flask containing 100 ml acetone. Anhydrous potassium carbonate (K_2CO_3) (20 mmol) and the appropriate substituted alkyl bromide (11.2 mmol) were added. The alkyl bromides were manipulated with a syringe within a fume cupboard. The reaction was heated under reflux for 24 h. Silica gel TLC was used to determine if the reactants have been consumed indicating completion of the reaction. The remaining K_2CO_3 was removed from the reaction by filtration. The organic phase was evaporated under reduced pressure and the residue was recrystallised from cyclohexane. The products were the substituted 1-tetralone derivatives **1a**-**h**.

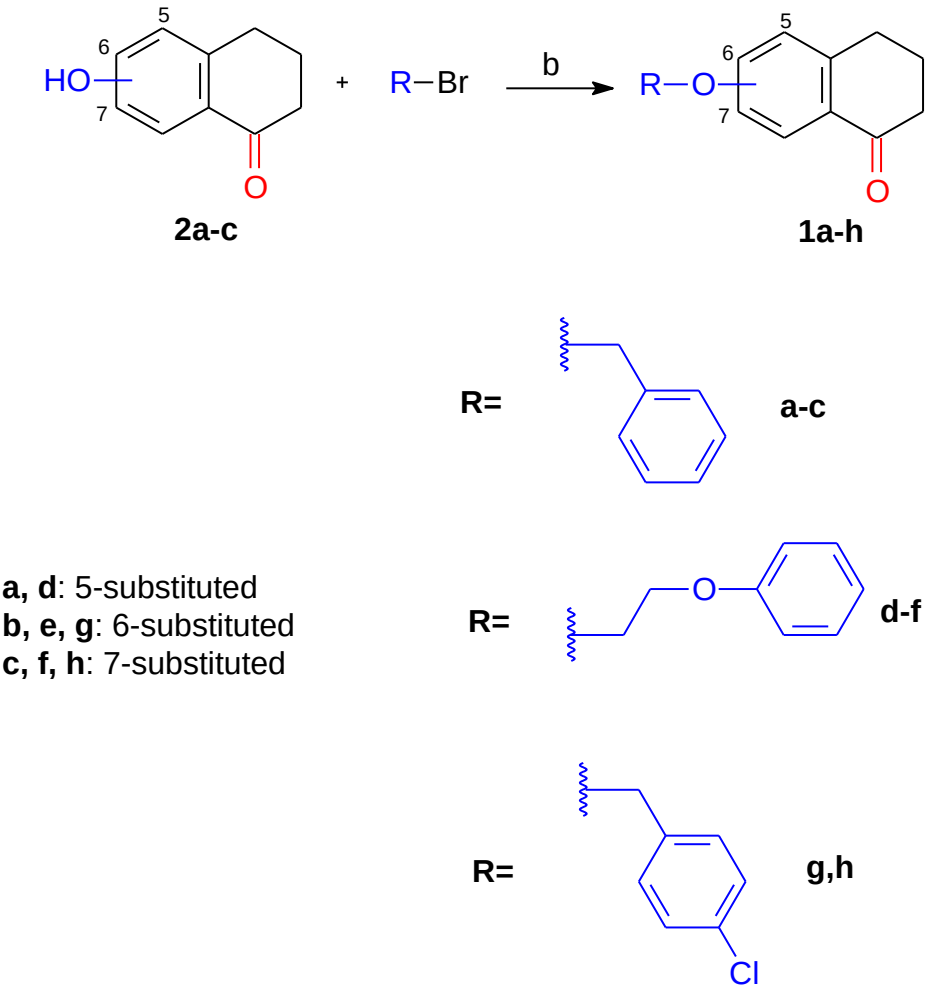

Figure 3.2 Reaction pathway for the synthesis of substituted 1-tetralone derivatives (1a-h). Key: (b) K_2CO_3, acetone, reflux, 24 h.

3.3.3 The synthesis of alcohol derivatives (1i-p).

In a round bottom flask, 1-tetralone derivatives **1a**-**h** (10 mmol) were dissolved in 100 ml ethanol. Sodium borohydride (20 mmol) was added, and the reaction mixtures were heated under reflux for 24 h. Silica gel TLC was used to determine if the reactants have been consumed indicating completion of the reaction. The solvent was removed under reduced pressure and water (100 ml) was cautiously added to the reaction. The resulting mixture was extracted to dichloromethane (3 x 75 ml) and the organic phase was dried by stirring with anhydrous $MgSO_4$ for at least 20 min at room temperature. The $MgSO_4$ was removed by filtration and the organic phase was evaporated under reduced pressure. The residue was subsequently purified by recrystallisation with cyclohexane to yield the target alcohols **1i**-**p**.

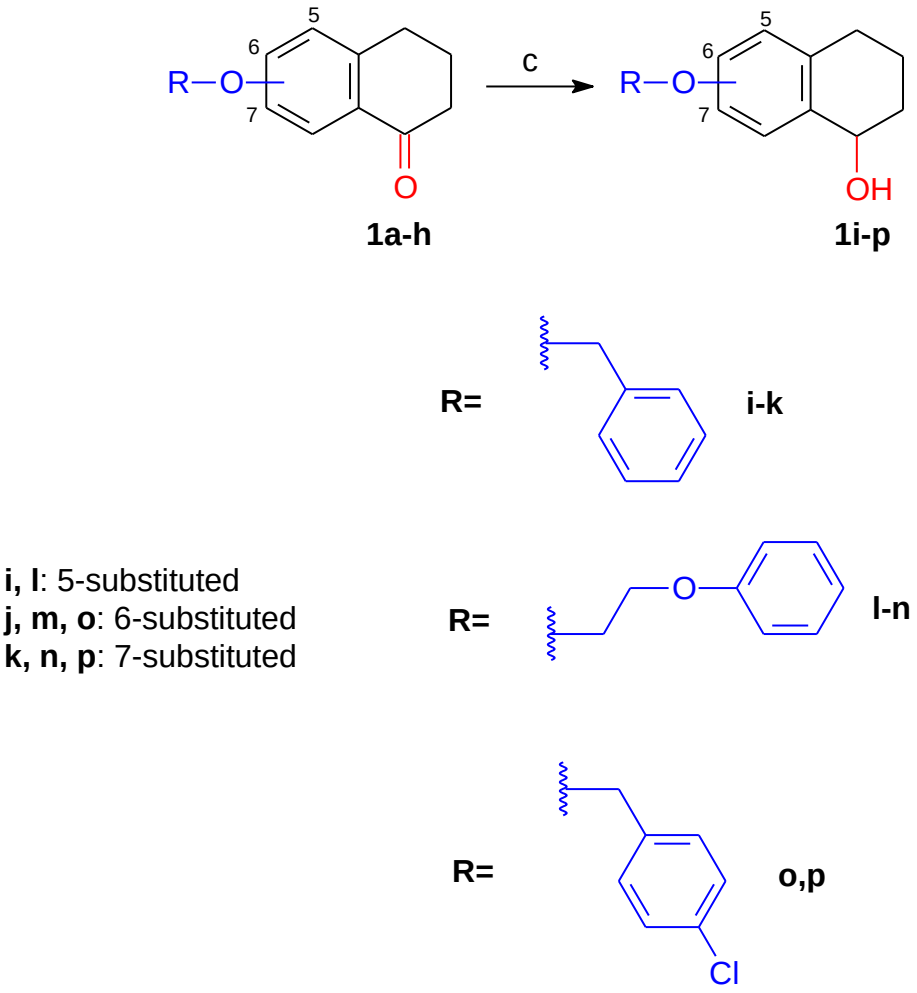

Figure 3.3 Reaction pathway for the synthesis of alcohol derivatives (1i-p). Key: (c) $NaBH_4$, ethanol, reflux, 24 h.

3.4 Physical characterisation

This section provides the characterisation of the synthesised 1-tetralone derivatives. These are the proton and carbon NMR notations as well as the high resolution masses recorded by MS. Also given are the melting points (where applicable), purities as determined by HPLC and the retention factor (R*f*) recorded by TLC analysis. For all compounds synthesised, the NMR spectra corresponded well with the proposed structures with respect to the number of signals observed, the chemical shifts and multiplicity.

3.4.1 Interpretation of NMR spectra

As an example, the NMR spectra of compound **1k** will be discussed. On the ^{13}C NMR spectra, ten signals are observed in the aromatic region (δ>110 ppm) which corresponds to the ten aromatic C atoms of this compound. In the aliphatic region (δ<75 ppm), five signals are observed, which corresponds to the five aliphatic carbons of this compound, including the

secondary alcohol carbon. For the carbonyl containing compounds, the carbonyl carbon corresponds to the signal at 198 ppm, which is absent in the alcohol containing 1-tetralone derivatives. On the ^{1}H NMR spectra of **1k**, the aromatic protons integrate for eight protons as expected for this compound. Among these is a doublet of doublets (6.77 ppm) which corresponds to the CH on the 1-tetralone C6. This proton couples *ortho* and *meta* with the other protons of the aromatic ring-system. For certain compounds (e.g. **1j**) the CH on the 1-tetralone C8 was observed as a doublet with a small coupling constant (J = 2.7 Hz) indicating *meta* coupling with a ring CH. The benzyloxy CH_2 was observed as a singlet at 4.97 ppm, while the aliphatic proton at C1 of the ring corresponds to the triplet at 4.65 ppm (1H). As anticipated, for the carbonyl-containing 1-tetralone derivatives, the signal at 4.65 ppm is absent. The multiplicity of this signal is the result of coupling with two protons on C2. The remaining aliphatic protons (6H) are represented by signals at 1.63-2.67 ppm (6H in total). Since this compound is chiral and represents two enantiomers, the multiplicities of the aliphatic signals are rather complex, indicating non-equivalence of protons attached to the same carbons and complex splitting patterns.

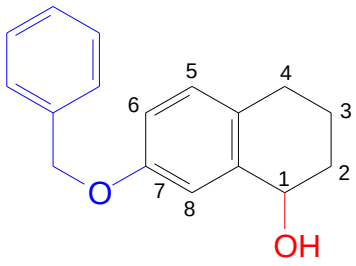

Figure 3.4 The atom numbering scheme for **1k**.

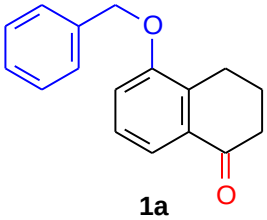 **1a**	Melting point: Oil Purity: 98.5% R*f*: 0.72 (Ethyl acetate 3:7 Petroleum ether) Yield (final step): 38.3%
^{1}H NMR:	^{13}C NMR:
^{1}H NMR (600 MHz, Chloroform-*d*) δ 7.60 (dd, *J* = 7.9, 1.1 Hz, 1H), 7.39 – 7.30 (m, 4H), 7.31 – 7.24 (m, 1H), 7.21 – 7.15 (m, 1H), 7.01 (dd, *J* = 8.1, 1.1 Hz, 1H), 5.03 (s, 2H), 2.90 (t, *J* = 6.2 Hz, 2H), 2.59 – 2.53 (m, 2H), 2.08 – 2.01 (m, 2H).	^{13}C NMR (151 MHz, Chloroform-*d*) δ 198.65, 155.90, 136.81, 133.95, 133.79, 128.63, 128.04, 127.20, 126.73, 119.11, 115.76, 70.33, 38.86, 23.04, 22.54.

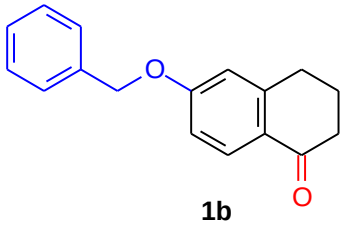 **1b**	Melting point: 100.6 - 106.2 °C Purity: 99.8% R*f*: 0.45 (Ethyl acetate 1:3 Petroleum ether) Yield (final step): 76.3%
^{1}H NMR:	^{13}C NMR:
^{1}H NMR (600 MHz, Chloroform-*d*) δ 7.93 (d, *J* = 8.8 Hz, 1H), 7.37 – 7.27 (m, 4H), 7.30 – 7.24 (m, 1H), 6.82 (dd, *J* = 8.7, 2.6 Hz, 1H), 6.71 (d, *J* = 2.4 Hz, 1H), 5.03 (s, 2H), 2.84 (t, *J* = 6.1 Hz, 2H), 2.53 (dd, *J* = 7.2, 5.8 Hz, 2H), 2.07 – 1.99 (m, 2H).	^{13}C NMR (151 MHz, Chloroform-*d*) δ 197.18, 162.69, 146.96, 136.23, 129.68, 128.70, 128.23, 127.48, 126.53, 113.70, 113.59, 70.06, 38.92, 30.17, 23.37.

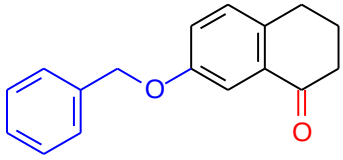 **1c**	Melting point: 87.6 - 88.3 °C Purity: 99.7% R*f*: 0.5 (Ethyl acetate 3:7 Petroleum ether) Yield (final step): 77.2%
^{1}H NMR:	^{13}C NMR:
^{1}H NMR (600 MHz, Chloroform-*d*) δ 7.54 (d, *J* = 2.8 Hz, 1H), 7.39 – 7.34 (m, 2H), 7.31 (dd, *J* = 8.4, 6.8 Hz, 2H), 7.28 – 7.23 (m, 1H), 7.12 – 7.02 (m, 2H), 5.01 (s, 2H), 2.82 (t, *J* = 6.1 Hz, 2H), 2.56 (dd, *J* = 7.3, 5.8 Hz, 2H), 2.07 – 2.00 (m, 2H).	^{13}C NMR (151 MHz, Chloroform-*d*) δ 198.31, 157.48, 137.41, 136.68, 133.39, 130.07, 128.60, 128.04, 127.58, 122.36, 110.27, 70.17, 39.01, 28.92, 23.49.

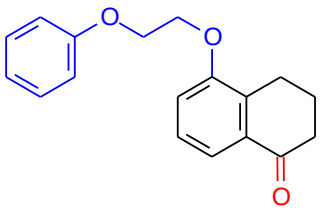 **1d**	Melting point: 135.6 - 144.0 °C Purity: 99.8% R*f*: 0.51 (Ethyl acetate 3:7 Petroleum ether) Yield (final step): 66.6%
^{1}H NMR:	^{13}C NMR:
^{1}H NMR (600 MHz, Chloroform-*d*) δ 7.60 (d, *J* = 7.9 Hz, 1H), 7.27 – 7.16 (m, 3H), 6.99 (d, *J* = 8.0 Hz, 1H), 6.94 – 6.86 (m, 3H), 4.28 (s, 4H), 2.82 (t, *J* = 6.2 Hz, 2H), 2.54 (dd, *J* = 7.3, 5.8 Hz, 2H), 2.05 – 1.98 (m, 2H).	^{13}C NMR (151 MHz, Chloroform-*d*) δ 198.64, 158.63, 155.91, 134.05, 133.79, 129.57, 126.71, 121.21, 119.32, 115.68, 114.69, 67.29, 66.46, 38.85, 22.90, 22.50.

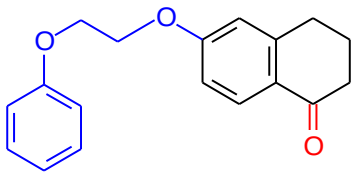 **1e**	Melting point: 107.0 - 128.1 °C Purity: 98.2% R*f*: 0.57 (Ethyl acetate 7:8 Petroleum ether) Yield (final step): 60.2%
^{1}H NMR:	^{13}C NMR:
^{1}H NMR (600 MHz, Chloroform-*d*) δ 7.94 (d, *J* = 8.7 Hz, 1H), 7.27 – 7.20 (m, 2H), 6.96 – 6.85 (m, 3H), 6.80 (dd, *J* = 8.7, 2.6 Hz, 1H), 6.69 (d, *J* = 2.5 Hz, 1H), 4.33 – 4.24 (m, 4H), 2.85 (t, *J* = 6.1 Hz, 2H), 2.57 – 2.51 (m, 2H), 2.08 – 2.00 (m, 2H).	^{13}C NMR (151 MHz, Chloroform-*d*) δ 197.20, 162.56, 158.46, 146.96, 129.68, 129.55, 126.62, 121.25, 114.66, 113.47, 113.42, 66.61, 66.20, 38.92, 30.15, 23.37.

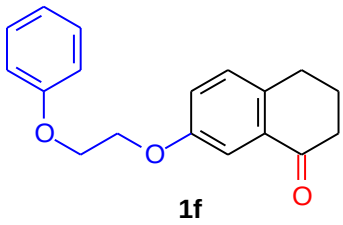 **1f**	Melting point: 115.6 - 118.4 °C Purity: 99.7% R*f*: 0.63 (Ethyl acetate 7:8 Petroleum ether) Yield (final step): 83.7%
^{1}H NMR:	^{13}C NMR:
^{1}H NMR (600 MHz, Chloroform-*d*) δ 7.49 (d, *J* = 2.8 Hz, 1H), 7.25 – 7.18 (m, 2H), 7.10 (d, *J* = 8.4 Hz, 1H), 7.04 (dd, *J* = 8.4, 2.8 Hz, 1H), 6.92 – 6.85 (m, 3H), 4.31 – 4.22 (m, 4H), 2.83 (t, *J* = 6.1 Hz, 2H), 2.59 – 2.54 (m, 2H), 2.11 – 2.00 (m, 2H).	^{13}C NMR (151 MHz, Chloroform-*d*) δ 198.31, 158.57, 157.37, 137.57, 133.35, 130.11, 129.51, 122.48, 121.13, 114.70, 109.84, 66.79, 66.37, 39.00, 28.91, 23.49.

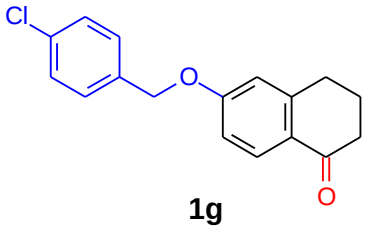 **1g**	Melting point: 96.1 - 98.2 °C Purity: 99.7% R*f*: 0.55 (Ethyl acetate 3:7 Petroleum ether) Yield (final step): 48.2%
^{1}H NMR:	^{13}C NMR:
^{1}H NMR (600 MHz, Chloroform-*d*) δ 7.94 (d, *J* = 8.7 Hz, 1H), 7.32 – 7.26 (m, 4H), 6.80 (dd, *J* = 8.7, 2.6 Hz, 1H), 6.69 (d, 1H), 5.00 (s, 2H), 2.84 (t, *J* = 6.1 Hz, 2H), 2.56 – 2.51 (m, 2H), 2.08 – 2.00 (m, 2H).	^{13}C NMR (151 MHz, Chloroform-*d*) δ 197.13, 162.38, 146.98, 134.73, 134.05, 129.72, 128.88, 128.76, 126.69, 113.63, 113.59, 69.24, 38.90, 30.15, 23.34.

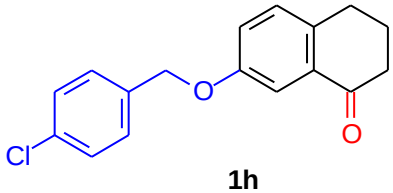 **1h**	Melting point: 93.6 - 95.8 °C Purity: 99.8% R*f*: 0.47 (Ethyl acetate 3:7 Petroleum ether) Yield (final step): 73.4%
^{1}H NMR:	^{13}C NMR:
^{1}H NMR (600 MHz, Chloroform-*d*) δ 7.51 (d, *J* = 2.8 Hz, 1H), 7.32 – 7.25 (m, 4H), 7.13 – 7.08 (m, 1H), 7.03 (dd, *J* = 8.4, 2.8 Hz, 1H), 4.98 (s, 2H), 2.83 (t, *J* = 6.1 Hz, 2H), 2.59 – 2.53 (m, 2H), 2.08 – 2.00 (m, 2H).	^{13}C NMR (151 MHz, Chloroform-*d*) δ 198.24, 157.19, 137.60, 135.20, 133.82, 133.40, 130.15, 128.85, 128.77, 122.32, 110.24, 69.34, 38.98, 28.91, 23.46.

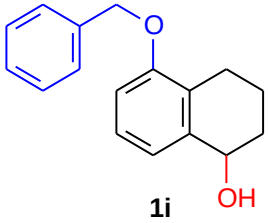 **1i**	Melting point: 86.1 - 89.9 °C Purity: 99.6% R*f*: 0.36 (Ethyl acetate 3:7 Petroleum ether) Yield (final step): 43.8%
^{1}H NMR:	^{13}C NMR:
^{1}H NMR (600 MHz, Chloroform-*d*) δ 7.35 (d, *J* = 7.2 Hz, 2H), 7.33 – 7.28 (m, 2H), 7.28 – 7.20 (m, 1H), 7.09 (t, *J* = 7.9 Hz, 1H), 7.00 (d, *J* = 7.7 Hz, 1H), 6.73 (dd, *J* = 8.0, 1.1 Hz, 1H), 4.99 (s, 2H), 4.69 (s, 1H), 2.81 – 2.73 (m, 1H), 2.60 – 2.51 (m, 1H), 1.93 – 1.82 (m, 2H), 1.75 – 1.66 (m, 2H).	^{13}C NMR (151 MHz, Chloroform-*d*) δ 156.15, 140.20, 137.38, 128.54, 127.79, 127.08, 126.53, 126.51, 120.84, 110.08, 69.82, 68.20, 31.76, 23.24, 18.08.

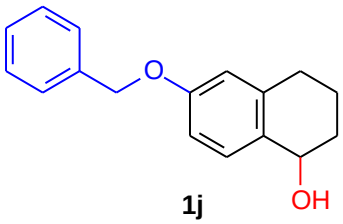 **1j**	Melting point: 59.5 - 93.5 °C Purity: 98.9% R*f*: 0.28 (Ethyl acetate 1:4 Petroleum ether) Yield (final step): 70.5%
^{1}H NMR:	^{13}C NMR:
^{1}H NMR (600 MHz, Chloroform-*d*) δ 7.36 – 7.31 (m, 2H), 7.34 – 7.25 (m, 2H), 7.23 (t, *J* = 7.5 Hz, 2H), 6.75 (dd, *J* = 8.5, 2.7 Hz, 1H), 6.62 (d, *J* = 2.7 Hz, 1H), 4.95 (s, 2H), 4.64 (t, *J* = 4.3 Hz, 1H), 2.70 (dt, *J* = 17.3, 4.9 Hz, 1H), 2.65 – 2.55 (m, 1H), 1.91 – 1.77 (m, 2H), 1.73 – 1.61 (m, 2H).	^{13}C NMR (151 MHz, Chloroform-*d*) δ 158.10, 138.68, 137.08, 131.55, 130.13, 128.60, 127.95, 127.45, 114.45, 113.26, 69.95, 67.65, 32.40, 29.63, 18.61.

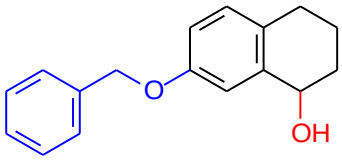 **1k**	Melting point: 57.2 - 59.9 °C Purity: 99.9% R*f*: 0.33 (Ethyl acetate 1:4 Petroleum ether) Yield (final step): 79.9%
^{1}H NMR:	^{13}C NMR:
^{1}H NMR (600 MHz, Chloroform-*d*) δ 7.38 – 7.33 (m, 2H), 7.33 – 7.27 (m, 2H), 7.27 – 7.20 (m, 1H), 7.00 (d, *J* = 2.7 Hz, 1H), 6.96 – 6.91 (m, 1H), 6.77 (dd, *J* = 8.4, 2.7 Hz, 1H), 4.97 (d, *J* = 1.8 Hz, 2H), 4.65 (t, *J* = 5.3 Hz, 1H), 2.67 (dt, *J* = 16.4, 5.9 Hz, 1H), 2.58 (ddd, *J* = 16.4, 7.8, 5.5 Hz, 1H), 1.96 – 1.81 (m, 2H), 1.82 – 1.74 (m, 1H), 1.72 – 1.63 (m, 1H).	^{13}C NMR (151 MHz, Chloroform-*d*) δ 157.20, 139.89, 137.15, 129.99, 129.44, 128.57, 127.91, 127.50, 115.11, 113.80, 70.08, 68.48.

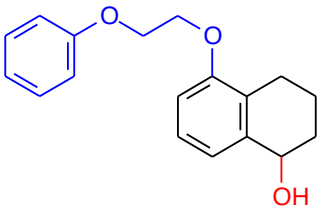 **1l**	Melting point: 102.3 - 103.4 °C Purity: 99.6% R*f*: 0.36 (Ethyl acetate 3:7 Petroleum ether) Yield (final step): 90.8%
^{1}H NMR:	^{13}C NMR:
^{1}H NMR (600 MHz, Chloroform-*d*) δ 7.26 – 7.16 (m, 2H), 7.11 (t, *J* = 7.9 Hz, 1H), 7.01 (d, *J* = 7.7 Hz, 1H), 6.93 – 6.85 (m, 3H), 6.72 (dd, *J* = 8.1, 1.1 Hz, 1H), 4.72 – 4.66 (m, 1H), 4.29 – 4.20 (m, 4H), 2.70 (dt, *J* = 17.4, 5.4 Hz, 1H), 2.53 – 2.44 (m, 1H), 1.91 – 1.74 (m, 3H), 1.74 – 1.65 (m, 1H).	^{13}C NMR (151 MHz, Chloroform-*d*) δ 158.72, 156.09, 140.24, 129.52, 126.64, 126.50, 121.08, 121.02, 114.73, 109.98, 68.19, 66.80, 66.54, 31.74, 23.06, 18.03.

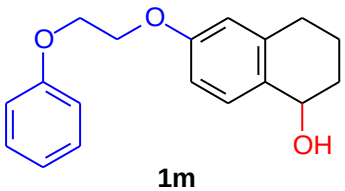 **1m**	Melting point: 116.8 - 117.7 °C Purity: 98.3% R*f*: 0.46 (Ethyl acetate 7:8 Petroleum ether) Yield (final step): 44.9%
^{1}H NMR:	^{13}C NMR:
^{1}H NMR (600 MHz, Chloroform-*d*) δ 7.26 (d, *J* = 8.5 Hz, 1H), 7.26 – 7.18 (m, 2H), 6.92 – 6.84 (m, 3H), 6.74 (dd, *J* = 8.5, 2.7 Hz, 1H), 6.60 (d, *J* = 2.5 Hz, 1H), 4.69 – 4.64 (m, 1H), 4.23 (s, 4H), 2.71 (dt, *J* = 17.3, 4.3 Hz, 1H), 2.66 – 2.57 (m, 1H), 1.93 – 1.79 (m, 2H), 1.73 – 1.64 (m, 1H), 1.61 (s, 1H).	^{13}C NMR (151 MHz, Chloroform-*d*) δ 158.60, 157.94, 138.69, 131.70, 130.12, 129.51, 121.10, 114.70, 114.31, 113.15, 67.65, 66.51, 66.42, 32.40, 29.61, 18.59.

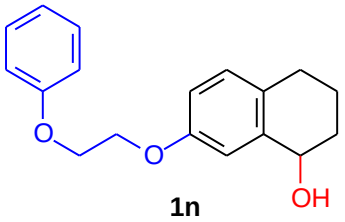 **1n**	Melting point: 103.4 - 106.5 °C Purity: 98.6% R*f*: 0.55 (Ethyl acetate 7:8 Petroleum ether) Yield (final step): 50.5%
^{1}H NMR:	^{13}C NMR:
^{1}H NMR (600 MHz, Chloroform-*d*) δ 7.27 – 7.19 (m, 2H), 6.99 – 6.92 (m, 2H), 6.92 – 6.83 (m, 3H), 6.75 (dd, *J* = 8.4, 2.7 Hz, 1H), 4.65 (q, *J* = 5.5 Hz, 1H), 4.24 (d, *J* = 2.2 Hz, 4H), 2.68 (dt, *J* = 16.4, 5.9 Hz, 1H), 2.58 (ddd, *J* = 16.4, 7.7, 5.5 Hz, 1H), 1.99 – 1.82 (m, 2H), 1.82 – 1.73 (m, 1H), 1.72 – 1.62 (m, 1H).	^{13}C NMR (151 MHz, Chloroform-*d*) δ 158.63, 157.04, 139.91, 130.01, 129.60, 129.50, 121.07, 115.08, 114.71, 113.63, 68.48, 66.67, 66.48, 32.42, 28.46, 19.20.

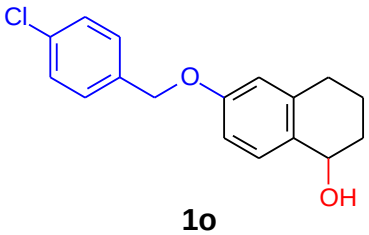 **1o**	Melting point 91.6 - 97.0 °C Purity: 99.5% R*f*: 0.18 (Ethyl acetate 1:4 Petroleum ether) Yield (final step): 30.4%
^{1}H NMR:	^{13}C NMR:
^{1}H NMR (600 MHz, Chloroform-*d*) δ 7.27 (s, 5H), 6.74 (dd, *J* = 8.5, 2.7 Hz, 1H), 6.61 (d, *J* = 2.5 Hz, 1H), 4.93 (s, 2H), 4.70 – 4.64 (m, 1H), 2.71 (dt, *J* = 17.2, 5.3 Hz, 1H), 2.65 – 2.57 (m, 1H), 1.91 – 1.85 (m, 1H), 1.88 – 1.79 (m, 1H), 1.73 – 1.64 (m, 1H), 1.57 (d, *J* = 5.7 Hz, 1H).	^{13}C NMR (151 MHz, Chloroform-*d*) δ 157.82, 138.74, 135.58, 133.70, 131.75, 130.14, 128.75, 128.71, 114.45, 113.21, 69.15, 67.64, 32.39, 29.61, 18.58.

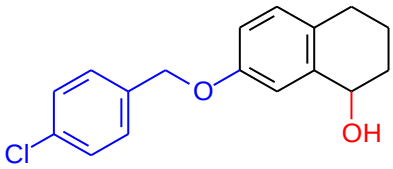 **1p**	Melting point: 95.4 - 98.2 °C Purity: 99.6% R*f*: 0.35 (Ethyl acetate 1:4 Petroleum ether) Yield (final step): 54.7%
^{1}H NMR:	^{13}C NMR:
^{1}H NMR (600 MHz, Chloroform-*d*) δ 7.31 – 7.24 (m, 4H), 6.98 (d, *J* = 2.7 Hz, 1H), 6.94 (d, *J* = 8.4 Hz, 1H), 6.74 (dd, *J* = 8.4, 2.8 Hz, 1H), 4.94 (d, *J* = 2.0 Hz, 2H), 4.68 – 4.61 (m, 1H), 2.67 (dt, *J* = 16.5, 6.0 Hz, 1H), 2.62 – 2.54 (m, 1H), 1.97 – 1.89 (m, 1H), 1.91 – 1.81 (m, 1H), 1.81 – 1.73 (m, 1H), 1.67 (d, *J* = 6.3 Hz, 1H).	^{13}C NMR (151 MHz, Chloroform-*d*) δ 156.92, 139.97, 135.68, 133.66, 130.03, 129.66, 128.76, 128.73, 115.05, 113.77, 69.27, 68.48, 32.44, 28.46, 19.21.

3.4.2 Interpretation of the TLC

TLC was used to determine whether a reaction was completed or not. TLC was carried out using silica gel 60 with UV_{254} fluorescent indicator. TLC sheets were observed under a UV light (254 nm wavelength). The mobile phase used consisted of petroleum ether and ethyl acetate. Fig. 3.5 provides examples of TLC sheets for the syntheses of compounds **1a** and **1d**. Using equation 3.1, the *Rf* value of each 1-tetralone derivative was calculated and tabulated in Table 3.2. Since only one spot is visible for each 1-tetralone derivative it may be concluded that the reaction was completed and that the compounds may be pure. This will be confirmed by the absence of signals of impurities in the NMR spectra and additional peaks in HPLC traces.

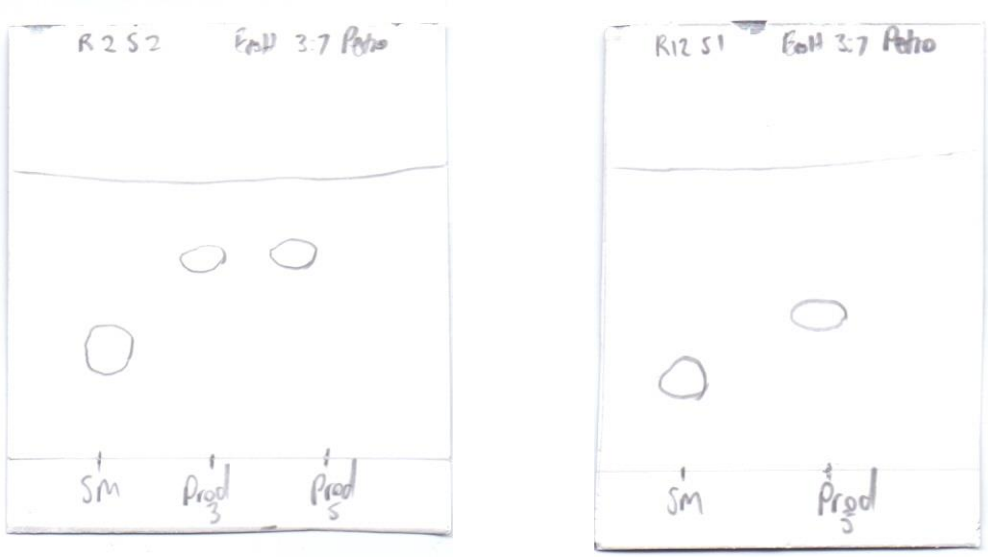

Figure 3.5 The developed TLC sheets for the syntheses of compounds **1a** (left) and **1d** (right). sm, starting material; prod, product.

$$Rf = \frac{[Analyte]_{Distance\ of\ migration}}{[Solvent]_{Distance\ of\ migration}}$$

Equation 3.1 The equation for the calculation of R*f* values.

Table 3.2 The R*f* values of the 1-tetralone derivatives.

Compound	**R*f* values**	**Compound**	**R*f* values**
1a	0.72	**1i**	0.36
1b	0.45	**1j**	0.28
1c	0.5	**1k**	0.33
1d	0.51	**1l**	0.36
1e	0.57	**1m**	0.46
1f	0.63	**1n**	0.55
1g	0.55	**1o**	0.18
1h	0.47	**1p**	0.35

3.4.3 Interpretation of mass spectra

The 1-tetralone derivatives were characterised by high resolution mass spectrometry. The calculated and experimentally determined molecular weights of the derivatives are given in table 3.3 and show that, for all analogues, the calculated and experimental values correspond well. The differences between the calculated and experimentally determined molecular weights may be evaluated by calculating the difference in parts per million (ppm) according to equation 3.2. In general, a ppm difference smaller than 5 is considered to indicate good agreement between the calculated and experimental values.

$$ppm = \frac{[Found\ -Calculated]}{[Calculated]} \times 10^6$$

Equation 3.2 The equation for the calculation of ppm values as an indication of the difference between calculated and experimentally determined molecular weights.

Table 3.3 The calculated and experimentally determined high resolution masses of the 1-tetralone derivatives.

	Calculated	**Found**	**Formula**	**Ppm**
1a	253.1223	253.1216	$C_{17}H_{17}O_2$ (MH^+)	-2.7655
1b	253.1223	253.1202	$C_{17}H_{17}O_2$ (MH^+)	-8.2964
1c	253.1223	253.1243	$C_{17}H_{17}O_2$ ($MH^{+)}$	7.9013
1d	283.1329	283.1349	$C_{18}H_{19}O_3$ (MH^+)	7.0638
1e	283.1329	283.1313	$C_{18}H_{19}O_3$ (MH^+)	-5.6511
1f	283.1329	283.1339	$C_{18}H_{19}O_3$ (MH^+)	3.5319
1g	287.0833	287.0857	$C_{17}H_{16}ClO_2$ (MH^+)	8.3599
1h	287.0833	287.0839	$C_{17}H_{16}ClO_2$ (MH^+)	2.09
1i	254.1307	254.1295	$C_{17}H_{18}O_2$ (M^+)	-4.7220
1j	254.1307	254.1277	$C_{17}H_{18}O_2$ (M^+)	-11.8049
1k	254.1307	254.1305	$C_{17}H_{18}O_2$ (M^+)	-0.7870
1l	284.1412	284.1416	$C_{18}H_{20}O_3$ (M^+)	1.4078
1m	284.1412	284.1384	$C_{18}H_{20}O_3$ (M^+)	-9.8543
1n	284.1412	284.1410	$C_{18}H_{20}O_3$ (M^+)	-0.7039
1o	288.0917	288.0925	$C_{17}H_{17}ClO_2$ (M^+)	2.7769
1p	288.0917	288.0938	$C_{17}H_{17}ClO_2$ (M^+)	7.2893

3.4.4 Purity by HPLC

The purities of the 1-tetralone derivatives were estimated by HPLC analyses. For this purpose, the 1-tetralone derivatives were dissolved in acetonitrile (1 mM), injected into the HPLC system and the eluent was monitored at a wavelength of 254 nm. The results are tabulated in Table 3.4 and show that the purities, as estimated by HPLC, are in excess of 98.2%. For the purpose of this dissertation a purity of >97% is acceptable and the compounds may thus be evaluated as potential MAO inhibitors. It should be noted that the purity determination by HPLC is only an estimate of purity since different organic compounds (e.g. 1-tetralone derivatives and impurities) will possess different molar extinction coefficients at 254 nm, and thus yield peaks of different sizes (areas and heights) even when present in the exact same molar concentration.

Table 3.4 The purity of each 1-tetralone derivative as determined by HPLC.

	Purity		**Purity**
1a	98.5%	**1i**	99.6%
1b	99.8%	**1j**	98.9%
1c	99.7%	**1k**	99.9%
1d	99.8%	**1l**	99.6%
1e	98.2%	**1m**	98.3%
1f	99.7%	**1n**	98.6%
1g	99.7%	**1o**	99.5%
1h	99.8%	**1p**	99.6%

3.5 Conclusion

We used the methods reported by Legoabe *et al*. (2014; 2015) to synthesise eight new 1-tetralone derivatives. These tetralones were reduced to the corresponding alcohol derivatives. The tetralones and their alcohol derivatives will be evaluated as potential inhibitors of MAO in the next chapter. NMR and MS were used to determine whether the synthesised compounds corresponded with the proposed structures. On the NMR spectra the integration values, multiplicities, chemical shifts and number of signals recorded corresponded with the proposed structures. The calculated high resolution molecular weights also corresponded well with the experimentally determined values. The yields at which the compounds were synthesised were moderate, and the purities of the synthesised products were acceptable as determined by HPLC. It can be concluded that the 1-tetralones and their alcohol derivatives proposed in table 3.1 have been successfully synthesised and may be evaluated as potential MAO inhibitors in the next chapter.

CHAPTER 4

BIOLOGY

4.1 Introduction

According to Palmer & Bonner (2007), an enzyme is a biological catalyst which increases the rate at which chemical reactions take place within living cells. The enzyme does not suffer any damage or change during this reaction. Enzymes react with substrates to form products. In each of these cases enzymes are highly specific towards the substrates they can react with, and produce particular products.

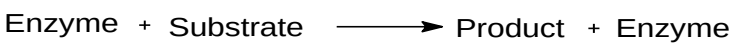

Figure 4.1 The reaction pathway for enzymes.

In this chapter the series of 1-tetralone derivatives that were synthesised in chapter 3, compounds **1a-p**, will be evaluated as potential inhibitors of human MAO-A and MAO-B. The mode of inhibition for **1h** (e.g. competitive) and its reversibility of MAO inhibition will also be evaluated. To test whether the synthesised compounds inhibited the target MAO enzymes, the IC_{50} values will be determined by a spectrofluorometric assay.

4.2 General background

To measure the inhibition potencies of the synthesised compounds towards human MAO-A and MAO-B, an *in vitro* protocol will be followed in which kynuramine is used as a substrate in a fluorometric assay. Kynuramine is oxidised by MAO-A and MAO-B to produce 4-hydroxyquinoline as shown in fig. 4.2. Using a fluorescence spectrophotometer, the concentration of 4-hydroxyquinoline will be determined since this compound fluoresces in alkaline media. The fluorescence measurements will be carried out at an excitation wavelength of 310 nm and an emission wavelength of 400 nm. As inhibition of the enzyme increases, the formation of 4-hydroxyquinoline (as product) decreases. With a lower degree of inhibition, relatively larger concentrations of 4-hydroxyquinoline is formed in the *in vitro* enzyme reactions. The inhibition potency of each compound will be expressed as the IC_{50} value, which indicates the concentration at which the enzyme activity is reduced to 50% by an inhibitor.

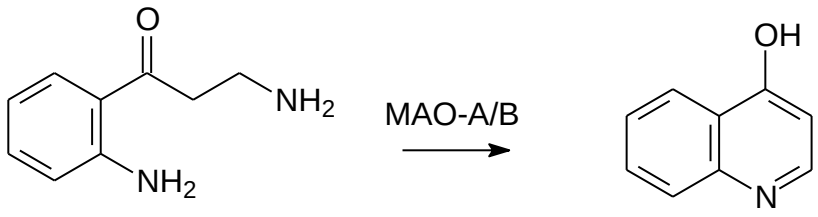

Kynuramine 4-Hydroxyquinoline

Figure 4.2 Oxidation of kynuramine by MAO-A or MAO-B to yield 4-hydroxyquinoline.

The inhibition potency of each of the synthesised compounds was evaluated using recombinant human MAO-A and MAO-B as enzyme sources. By constructing a sigmoidal dose-response curve of enzyme catalytic rate versus the logarithm of inhibitor concentration, the IC_{50} value for the inhibition of a MAO isoform may be calculated. Inhibitors that have lower IC_{50} values are more potent inhibitors since a lower concentration of the inhibitor produces 50% inhibition compared to an inhibitor with a higher IC_{50} value.

4.3 Materials and instrumentation

Kynuramine dihydrobromide, 4-hydroxyquinoline, selegiline and insect cell microsomes containing recombinant human MAO-A and MAO-B (5 mg/ml) were obtained from Sigma-Aldrich.

Potassium phosphate (K_2HPO_4/KH_2PO_4), sodium hydroxide (NaOH), dimethyl sulfoxide (DMSO), sucrose and white polypropylene 96-well microtiter plates were obtained from Merck.

Fluorescence measurements were carried out with a Varian Cary Eclipse fluorescence spectrophotometer.

The IC_{50} values were estimated by constructing sigmoidal dose-response curves of enzyme catalytic rate versus the logarithm of inhibitor concentration. For this purpose, the Graphpad Prism 5 software package was used.

Slide-A-Lyzer dialysis cassettes with a sample volume capacity of 0.5-3 ml and a molecular weight cut-off of 10 000 were obtained from Thermo Scientific.

4.4 Determining the IC_{50} values of the synthesised compounds

4.4.1 Experimental method

Recombinant human MAO-A and MAO-B (both 5 mg protein/ml) were stored at -70 °C until the day of the experiment. All enzyme reactions were carried out in white 96-well microtiter plates.

Each plate was allocated either for MAO-A or MAO-B. And to each well the following was added:

- 92 µl potassium phosphate buffer (K_2HPO_4/KH_2PO_4), pH 7.4, 100 mM, made isotonic with KCl.
- 50 µl kynuramine to yield a final concentration of 50 µM in the wells.
- 8 µl of the test inhibitor prepared in DMSO to yield a concentration range of 0.003 to 100 µM. Each inhibitor was tested at eight different concentrations: 0.003, 0.01, 0.03, 0.1, 0.3, 1, 10 and 100 µM. As negative control, 8 µL of DMSO was added instead of test inhibitor to yield a concentration of 0 µM.
- Each reaction was carried out in triplicate.

The plates were then pre-incubated for 30 min at 37 °C in a convection oven. 50 µl of the MAO enzyme was subsequently added to the reactions to yield a concentration of 0.0075 mg/ml for MAO-A, and a concentration of 0.0015 mg/ml for MAO-B. The plates were incubated for 20 min at 37 °C during which the enzyme catalysed oxidation of kynuramine occurred. Following the incubation, the reactions were terminated with the addition of 80 µl NaOH (2 N) to each well.

The concentration of 4-hydroxyquinoline formed by MAO catalysis was measured by fluorescence spectroscopy employing a Varian Cary Eclipse fluorescence spectrophotometer. The excitation wavelength was set to 310 nm and the emission wavelength to 400 nm. The PMT (photomultiplier) voltage was set to medium with an excitation slit width of 5 nm and emission slit width of 10 nm. The spectrofluorometer measures the fluorescence intensity of 4-hydroxyquinoline, from which the concentration of 4-hydroxyquinoline can be calculated with the aid of a calibration curve.

To construct the calibration curve, known amounts of 4-hydroxyquinoline were dissolved to a volume of 200 µl in potassium phosphate buffer (K_2HPO_4/KH_2PO_4), after which 80 µl NaOH was added. The concentrations of the calibration standards were 0.047, 0.094, 0.188, 0.375, 0.75 and 1.5 µM. The fluorescence intensities of these calibration standards were measured and a linear calibration curve was constructed. This curve was used to make quantitative estimations of the 4-hydroxyquinoline formed in the enzyme reactions. The linearity of the calibration curves was routinely found to be 0.99.

Control samples were also added to the assay to confirm whether or not the test inhibitors quench the fluorescence of 4-hydroxyquinoline. These samples contained 4-hydroxyquinoline (1.50 µM), test inhibitor (100 µM) and NaOH (80 µl).

Preparation of the inhibitors:

- Prepare 10 mM concentrations of each inhibitor in DMSO.
- Dilute each inhibitor to yield stock solutions of various concentrations in DMSO.
- The concentrations of the stock solutions were selected such that when added to the enzyme reaction at a dilution of 25-fold, the DMSO concentration is 4%.

Preparation of microtiter plates:

To each well plate add the following:

- 92 µl of the buffer, potassium phosphate (100 mM, pH 7.4, made isotonic with KCl 20.2 mM).
- 50 µl kynuramine as substrate.
- 8 ul of each inhibitor dilution.

Incubation:

- Pre-incubate the microtiter plates at 37 °C for at least 20 min.
- Add 50 µl MAO-A (0.0075 mg/ml) and MAO-B (0.0015 mg/ml) to the wells.
- Incubate the well plates for 20 min each at 37 °C.
- After 20 min terminate the reactions by adding 80 µl NaOH (2 N).

Measuring fluorescence:

- Determine the amount of 4-hydroxyquinoline formed by MAO by measuring the fluorescence at an excitation wavelength of 310 nm and an emission wavelength 400

Linear calibration curve:

- Construct a calibration curve with 0.047-1.50 µM 4-hydroxyquinoline.

Calculating IC_{50} values:

- Plot the rate at which the enzyme initially oxidises the substrate against the logarithm of the concentration of the inhibitor.
- Use Prism 5 to construct sigmoidal rate-concentration curves.
- Determine the IC_{50} values in triplicate and express as mean ± SD.

Figure 4.3 A flow diagram illustrating the protocol for the measurement of IC_{50} values for the inhibition of MAO-A and MAO-B.

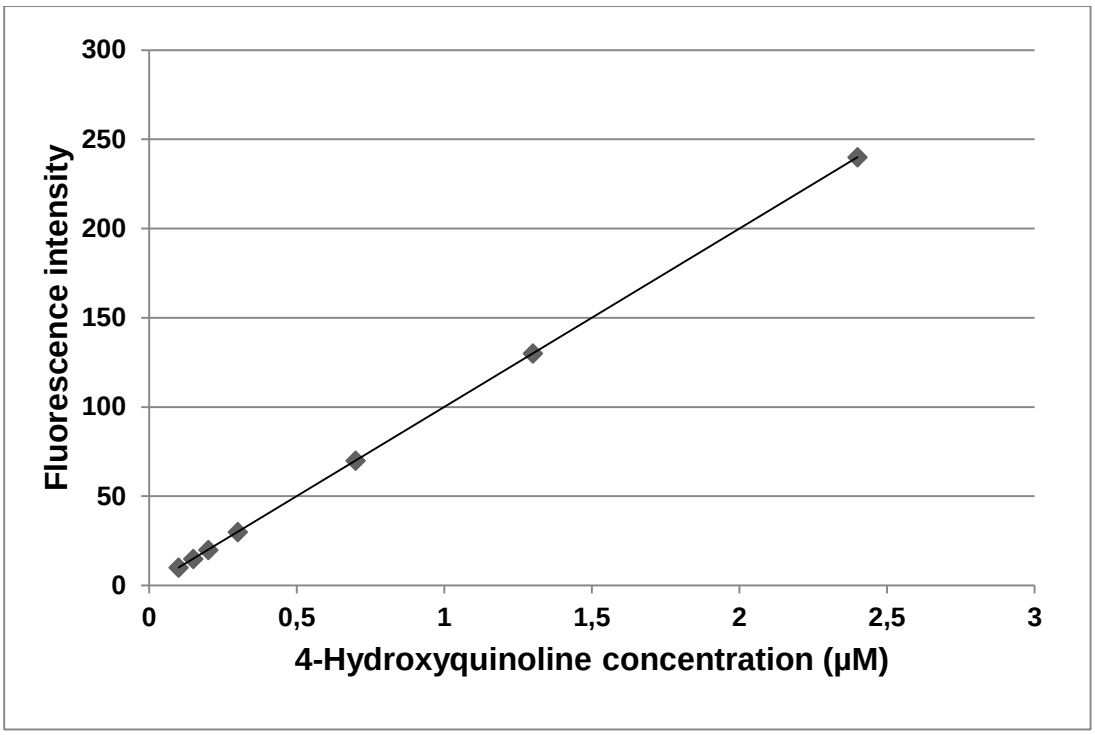

Figure 4.4 An example of a linear calibration curve constructed to make quantitative estimations of the 4-hydroxyquinoline**.**

4.4.2 Results

Table 4.1 The IC_{50} values for the inhibition of recombinant human MAO-A and MAO-B by compounds **1a-h**.

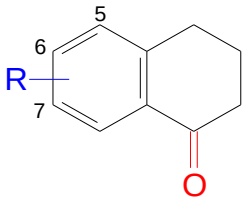

			IC_{50} (µM)	**IC_{50} (µM)**	
Compd.	**R**	**Posit-ion**	**MAO-A**	**MAO-B**	**SI**
1a	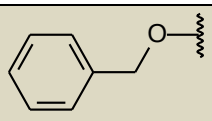	5	53.9 ± 7.02	3.62 ± 0.34	14.9
1b	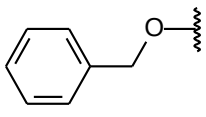	6	1.39 ± 0.30	0.025 ± 0.0029	55.6

1c	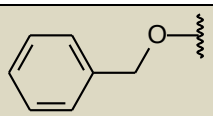	7	0.623 ± 0.021	0.0024 ± 0.0004	260
1d	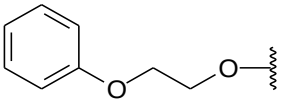	5	No inhibition	3.26 ± 1.86	>30.7
1e	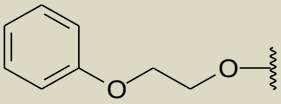	6	2.58 ± 0.30	0.033 ± 0.0053	78.2
1f	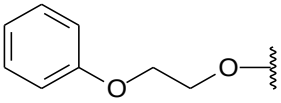	7	1.91 ± 0.37	0.0012 ± 0.0003	1591.7
1g	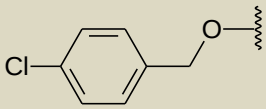	6	0.575 ± 0.018	0.0055 ± 0.0006	104.5
1h	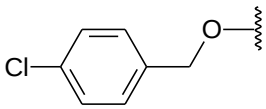	7	0.036 ± 0.0059	0.0011 ± 0.0002	32.7

Table 4.2 The IC_{50} values for the inhibition of recombinant human MAO-A and MAO-B by compounds **1i-p**.

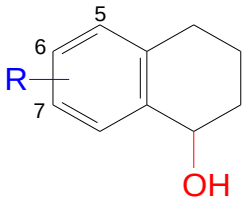

			IC_{50} (μM)	**IC_{50} (μM)**	
Compd.	**R**	**Posit-ion**	**MAO-A**	**MAO-B**	**SI**
1i	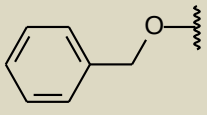	5	9.27 ± 0.83	5.05 ± 0.42	1.8

1j	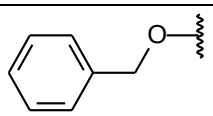	6	35.5 ± 5.60	0.079 ± 0.012	449.4
1k	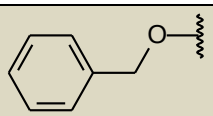	7	34.6 ± 3.80	0.249 ± 0.061	139
1l	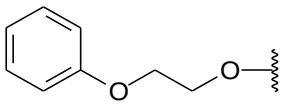	5	No inhibition	1.66 ± 0.14	>60.2
1m	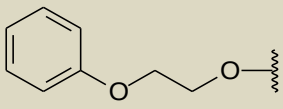	6	No inhibition	0.068 ± 0.0034	>1470.6
1n	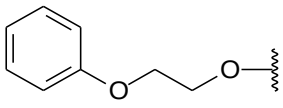	7	No inhibition	0.189 ± 0.013	>529.1
1o	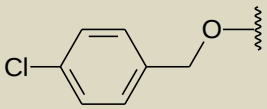	6	1.086 ± 0.12	0.0075 ± 0.0011	146.3
1p	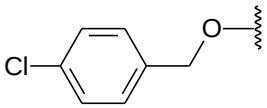	7	0.785 ± 0.047	0.039 ± 0.013	20.1

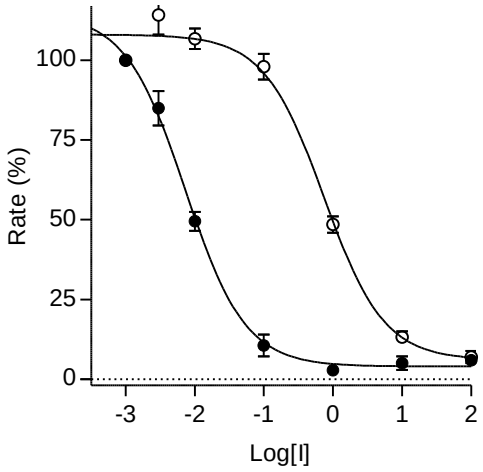

Figure 4.5 Examples of sigmoidal plots obtained in this study for the inhibition of MAO-A (by **1p**; open circles) and MAO-B (by **1o**; filled circles) by selected inhibitors.

The results of the MAO inhibition studies are given in tables 4.1 and 4.2. The inhibition potencies are expressed as the corresponding IC_{50} values. As mentioned, a lower IC_{50} indicates that an inhibitor exerts more potent inhibition at a specific concentration. From the inhibition data, the following conclusions may be made:

1. It is clear that both the 1-tetralone (**1a**–**h**) and alcohol (**1i**–**p**) derivatives are selective inhibitors of MAO-B over the MAO-A isoform. In this respect, the SI values were >1.8, indicating selectivity for MAO-B in all cases. Among the compounds evaluated, **1d** and **1l**-**n** are particularly selective and do not display any inhibition of MAO-A at a maximal tested concentration of 100 µM.
2. Although the 1-tetralone and alcohol derivatives are MAO-B selective, some compounds were found to be good potency MAO-A inhibitors. Compound **1h**, in particular is a high potency MAO-A inhibitor with an IC_{50} value of 0.036 µM. This is 89-fold more potent than the reference MAO-A inhibitor, toloxatone (IC_{50} = 3.92 µM), which was evaluated under identical experimental conditions (Petzer *et al*., 2013). This study also identifies three other compounds with submicromolar MAO-A inhibition potencies, compounds **1c** (IC_{50} = 0.623 µM), **1g** (IC_{50} = 0.575 µM) and **1p** (IC_{50} = 0.785 µM).
3. As mentioned the 1-tetralone and alcohol derivatives are MAO-B selective inhibitors. This study discovered several high potency MAO-B inhibitors. Among the 16 compounds evaluated, 10 compounds display IC_{50} <0.1 µM, while 5 compounds display IC_{50} <0.01 µM. The most potent MAO-B inhibitors are compounds **1f** and **1h** with IC_{50} values of 0.0012 and 0.0011 µM, respectively. These compounds are 76-fold more potent than the reference MAO-B inhibitor, lazabemide (IC_{50} = 0.091 µM), which was evaluated under identical experimental conditions (Petzer *et al*., 2013).

4. From the MAO-A inhibition data the following structure-activity relationships (SARs) may be derived. Among the 1-tetralone derivatives, the position of the substituent on the 1-tetralone moiety has a pronounced effect on the inhibition potency with substitution on C7 yielding more potent inhibition than substitution on C6 (e.g. **1c** versus **1b**). Substitution on C6 in turn lead to more potent inhibition than substitution on C5 (e.g. **1b** versus **1a**). This trend is observed for all the 1-tetralone derivatives evaluated. For the alcohol derivatives, a clear trend with regards to the position of the substituent was not observed. It is, however, noteworthy that the C7-substituted derivative **1p** is more potent than the corresponding C6-substituted derivative **1o**. It is also noteworthy that the derivatives containing chlorine are more potent MAO-A inhibitors compared to the corresponding unsubstituted homologues (e.g. **1h** versus **1c**). This trend is observed for all compounds evaluated, including the alcohol derivatives (e.g. **1p** versus **1k**).
5. From the MAO-B inhibition data the following SARs may be derived. As for MAO-A, substitution on C7 yields more potent inhibition than substitution on C6 (e.g. **1c** versus **1b**). Substitution on C6 in turn leads to more potent inhibition than substitution on C5 (e.g. **1b** versus **1a**). This trend is observed for all the 1-tetralone derivatives evaluated. For the alcohol derivatives, a clear trend with regards to the position of the substituent was not observed. Interestingly, among the alcohol derivatives, a C6-substituted derivative, **1o** (IC_{50} = 0.0075 µM) is the most potent MAO-B inhibitor. For MAO-B inhibition, the chlorine containing compounds are also more potent MAO-B inhibitors compared to the unsubstituted derivatives (e.g. **1g** versus **1b**, and **1o** versus **1j**). This trend is observed for both the 1-tetralone and alcohol derivatives.
6. A further SAR is that, among the 1-tetralone derivatives, the 2-phenoxyethoxy substituted derivatives are weaker MAO-A and MAO-B inhibitors than the corresponding benzyloxy substituted derivatives (e.g. **1d**-**f** versus **1a**-**c**). The exception here is that **1f** is a higher potency MAO-B inhibitor than **1c**. Among the alcohol derivatives, this trend is also observed for MAO-A, but not for MAO-B inhibition (e.g. **1l**-**n** versus **1i**-**k**). It is noteworthy that the alcohol derivatives substituted with the 2-phenoxyethoxy are not MAO-A inhibitors with IC_{50} values >100 µM. This group of compounds are thus highly selective for MAO-B with **1m** representing a particularly potent MAO-B inhibitor.
7. Finally, it should be kept in mind that the alcohol derivatives are the racemic mixtures of two enantiomers. Considering that two enantiomers may exhibit different inhibition potencies, the IC_{50} values given in table 4.2 are the means of the individual enantiomeric potencies. The higher potency enantiomer may thus exhibit a much higher degree of inhibition than that given in the results table. For this reason, clear SARs and trends are not as readily observed for the alcohol derivatives compared to the 1-tetralone derivatives. Considering this, it is not surprising that with the exception of **1a** versus **1i**

(MAO-A) and **1d** versus **1l** (MAO-B), the 1-tetralone derivatives are in all instances more potent MAO inhibitors than the corresponding alcohol derivatives.

4.5 Determination of the reversibility of MAO-A and MAO-B inhibition by dialysis

For reversibility studies, the most potent MAO-B inhibitor among the alcohol derivatives was selected as representative inhibitor. An alcohol derivative was selected since the reversibility of inhibition of tetralones has been investigated before (Legoabe *et al*., 2015).

Reversibility of MAO inhibition is an important consideration since compounds which are reversible inhibitors, especially of MAO-A, have a reduced risk for causing the cheese reaction compared to irreversible inhibitors. Furthermore, for reversible inhibition, enzyme activity is quickly recovered after drug withdrawal. Reversibility is thus a desired property of MAO inhibitors.

Reversibility is often evaluated by measuring the recovery of enzyme activity after it has been exposed to the test compound and subsequently dialysed. In this study, compounds **1p** and **1o** were selected as representative inhibitors for the evaluation of the reversibility of MAO-A and MAO-B inhibition, respectively.

4.5.1 Method for measuring reversibility of synthesised compounds

For the reversibility studies, compounds **1p** and **1o** were selected as representative test inhibitors since these compounds were the most potent MAO-A and MAO-B inhibitors, respectively, among the alcohol derivatives. The reversibility studies were conducted by dialysis with Slide-A-Lyzer dialysis cassettes (Thermo Scientific) which have a sample volume capacity of 0.5 to 3 ml and a molecular weight cut-off of 10 000.

Pre-incubation: Compounds **1p** and **1o**, at concentrations of 4 x IC_{50}, were pre-incubated with recombinant human MAO-A or MAO-B (0.03 mg protein/ml) at 37 ºC for 15 min. The buffer used for the enzyme-inhibitor incubations was potassium phosphate buffer (100 mM, pH 7.4, made isotonic with KCl) containing 5% sucrose. Control incubations were performed in the absence of inhibitor (negative control) and in the presence of the irreversible inhibitors pargyline (IC_{50} = 13 µM for MAO-A) or selegiline (IC_{50} = 0.079 µM for MAO-B) (positive controls).

Dialysis: The dialysis mixtures were prepared to a final volume of 0.8 ml and DMSO (4%) served as co-solvent in all pre-incubations. The dialysis of the enzyme-inhibitor complexes were carried out for 24 h at 4 ºC in 80 ml outer buffer (100 mM potassium phosphate, pH 7.4, 5% sucrose). The sucrose buffer was replaced at 3 and 7 h following the start of dialysis.

Measure residual MAO activity: The residual MAO-A and MAO-B activities were determined after two-fold dilution of the reactions with the addition of kynuramine as the substrate. The final MAO concentration after dilution was 0.015 mg protein/ml and final kynuramine concentration was 50 µM. The reactions were incubated for 20 min and subsequently terminated by addition of 1000 µl deionised water and 400 µl NaOH (2 N). The concentrations of 4-hydroxyquinoline generated by MAO catalysis were measured by fluorescence spectroscopy at an excitation wavelength of 310 nm and an emission wavelength of 400 nm.

Data analysis: The reactions were performed in triplicate and the residual catalytic rates are given as mean ± SD. For comparison, enzyme-inhibitor complexes that did not undergo dialysis were maintained at 4 ºC for the same amount of time and the residual MAO-B activity subsequently measured as above.

Calibration curve: Quantitative estimations of 4-hydroxyquinoline in the enzyme reactions were made by using a linear calibration curve. In order to make these estimations, known quantities of 4-hydroxyquinoline (0.047 – 1.50 µM) were dissolved in potassium phosphate buffer (100 mM, pH 7.4, made isotonic with 20.2 mM KCl) to a final volume of 200 µl. To each calibration standard, 80 µl NaOH (2 N) was added.

Pre-incubation:

Each reaction contains the following:

- 0.8 ml of the buffer, potassium phosphate (100 mM, pH 7.4) containing 5% sucrose.
- 0.03 mg/ml MAO-A or MAO-B.
- Inhibitors **1p** or **1o** at fourfold the IC_{50} value.
- Negative control incubations did not contain inhibitor, while positive controls contained pargyline or selegiline, at fourfold IC_{50}.
- Pre-incubate the reactions at 37 °C for 15 min.

Dialysis:

- The cassettes should be hydrated in the outer buffer for 2 min.
- Samples are then inserted into the cassettes.
- Dialysis takes place at 4 °C in 80 ml of the outer buffer for 24 h.
- After dialysis is started the outer buffer should be replaced after 3 h and 7 h.
- Also keep non-dialysed enzyme-inhibitor samples at 4 °C for 24 h.

Incubations:

- After dialysis, remove 250 µl of each sample and add 250 µl kynuramine (100 µM).
- Incubate samples at 37 °C for 20 min.
- Terminate the reactions by adding 400 µl NaOH (2 N).
- Also add 1000 µl deionised water.

Measuring fluorescence:

- Measure the amount of 4-hydroxyquinoline formed by MAO-A and MAO-B spectrofluorometrically using an excitation wavelength of 310 nm and an emission wavelength of 400 nm.

Quantitative estimations with a linear calibration curve:

The calibration standards were prepared as follows:

- 4-Hydroxyquinoline at 0.047-1.50 µM in potassium phosphate buffer (500 µl).
- 400 µl NaOH and 1000 µl deionised water added to each standard.

Data analysis:

- The measured residual MAO-A and MAO-B activities are plotted on a histogram.
- All incubations are done in triplicate and the residual activities are expressed as mean ± SD.

Figure 4.6 A flow diagram illustrating the experimental method for determining reversibility of inhibition by dialysis.

4.5.2 Results

After dialysis of a mixture of compound **1p** and MAO-A for 24 hours, an almost complete recovery of MAO-A activity could be observed (Fig. 4.7). Inhibition by compound **1p** is therefore reversible with the catalytic activity of MAO-A recovering to 81% of the control value (recorded without the presence of the inhibitor). Contrary to this, in non-dialysed mixtures of MAO-A and the inhibitor the residual MAO-A activity was only 34%. Dialysis of mixtures of MAO-A and pargyline, an irreversible MAO-A inhibitor, resulted in almost no recovery of MAO-A activity with residual enzyme activity of only 1.9% of the control value. The conclusion may be made that compound **1p** is a reversible inhibitor of human MAO-A, and that all the other alcohol derivatives synthesised in this study are likely to also act as reversible inhibitors.

After dialysis of a mixture of compound **1o** and MAO-B for 24 hours, an almost complete recovery of MAO-B activity could be observed (Fig. 4.7). Inhibition by compound **1o** is therefore reversible with the catalytic activity of MAO-B recovering to 76% of the control value (recorded without the presence of the inhibitor). Contrary to this, in non-dialysed mixtures of MAO-B and the inhibitor the residual MAO-B activity was only 48%. Dialysis of mixtures of MAO-A and selegiline, an irreversible MAO-B inhibitor, resulted in almost no recovery of MAO-B activity with residual enzyme activity of only 3.5% of the control value. The conclusion may be made that compound **1o** is a reversible inhibitor of human MAO-B, and that all the other alcohol derivatives synthesised in this study are likely to also act as reversible inhibitors.

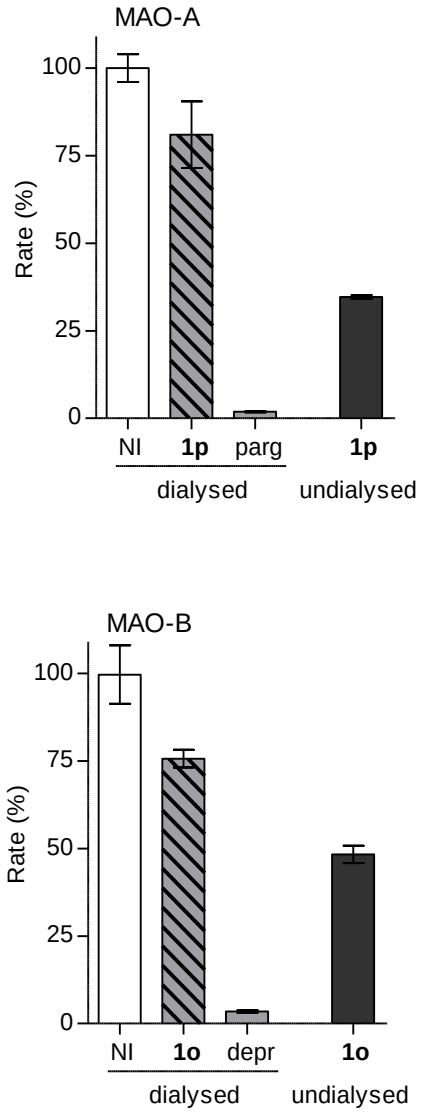

Figure 4.7 Reversibility of inhibition of MAO-A and MAO-B by compounds 1p and 1o, respectively. MAO-A was pre-incubated in the absence of inhibitor and presence of 1p and pargyline (top), and MAO-B was pre-incubated in the absence of inhibitor and presence of 1o and selegiline (depr) (bottom). After dialysis, the residual enzyme activities were measured. For comparison, the MAO activities of undialysed mixtures of the MAOs and the test inhibitors were also measured.

4.6 Construction of Lineweaver-Burk plots for the inhibition of MAO-A and MAO-B

The modes of inhibition of compounds **1p** and **1o** were examined using sets of Lineweaver-Burk plots. The aim of this study was to determine whether inhibition is competitive or non-competitive. Compounds **1p** and **1o** were selected as representative inhibitors since they were the most potent MAO-A and MAO-B inhibitors, respectively, among the alcohol derivatives. The catalytic rates of MAO-A and MAO-B were measured at eight different kynuramine

concentrations (15-250 µM) in the absence and presence of five different concentrations of the test inhibitor. These inhibitor concentrations were: ¼ x IC_{50}, ½ x IC_{50}, ¾ x IC_{50}, 1 x IC_{50} and 1¼ x IC_{50}.

4.6.1 Method

For this experiment recombinant human MAO-A and MAO-B (5 mg protein/ml) was used. The reaction mixtures were made up to a volume of 500 µl in potassium phosphate buffer (100 mM with a pH of 7.4 and made isotonic with KCl 20.2 mM). DMSO at 4% was used as a co-solvent in all reactions. The reactions contained kynuramine as substrate (final concentration of 15-250 µM) and compounds **1p** or **1o** at concentrations of ¼ x IC_{50}; ½ x IC_{50}; ¾ x IC_{50}; 1 x IC_{50} and 1 ¼ x IC_{50}. Reactions in the absence of an inhibitor were also included in this study. The reactions were initiated with the addition of MAO-A or MAO-B (0.015 mg protein/ml) and then incubated at 37 °C for 20 min. The reactions were subsequently terminated by the addition of 400 µl NaOH (2 N) and 1000 µl deionised water. Each reaction was then centrifuged for 10 min at 16 000 g and 4-hydroxyquinoline generated by the MAOs was measured spectrofluorometrically to determine the MAO-A or MAO-B catalytic rates of the reactions. This was done at an excitation wavelength of 310 nm and an emission wavelength of 400 nm. To construct a calibration curve, known amounts (0.047-1.50 µM) of 4-hydroxyquinoline were prepared in 500 µl potassium phosphate buffer (100 mM, pH 7.4). 400 µl NaOH (2 N) and 1000 µl deionised water was subsequently added to each calibration standard and the fluorescence was measured as described above. The data obtained was used to construct Lineweaver-Burk plots in Prism 5.

Preparation for the samples:

Each sample should contain the following:

- 500 µl potassium phosphate buffer (100 mM, pH 7.4, made isotonic with KCl 20.2 mM).
- 0.015 mg/ml MAO-B.
- The test inhibitors at different concentrations of: ¼ x IC_{50}, ½ x IC_{50}, ¾ x IC_{50}, 1 x IC_{50} and 1¼ x IC_{50}.
- Eight different concentrations of kynuramine as substrate (15-250 µM).

Incubation:

- Incubate the samples for 20 min at 37 °C.
- Terminate the reactions by adding 400 µl NaOH (2 N) and 1000 µl deionised water to the samples.

Measuring fluorescence:

- Centrifuge each sample at 16000 g for 10 min each.
- Measure the amount of 4-hydroxyquinoline formed spectrofluorometrically at an excitation wavelength of 310 nm and an emission wavelength of 400 nm.

Calibration curve:

The calibration standards were prepared as follows:

- 4-Hydroxyquinoline at 0.047-1.50 µM in potassium phosphate buffer (500 µl).
- 400 µl NaOH and 1000 µl deionised water added to each standard.

Lineweaver-Burk plot:

- Plot the inverse of the rate of kynuramine oxidation against the inverse of substrate concentration.
- Use GraphPad Prism 5 to perform linear regression analysis.

Figure 4.8 A flow diagram illustrating the experimental method to construct Lineweaver-Burk plots.

4.6.2 Results

To determine whether compounds **1p** and **1o** are competitive inhibitors of MAO-A and MAO-B, respectively, Lineweaver-Burk plots where constructed. Measurement of the catalytic rates of MAO-A and MAO-B were done with eight different concentrations of kynuramine in the presence of five different concentrations of the test inhibitor and also in the absence of an inhibitor. From the MAO activity data, the Lineweaver-Burk plots given in fig. 4.9 were constructed.

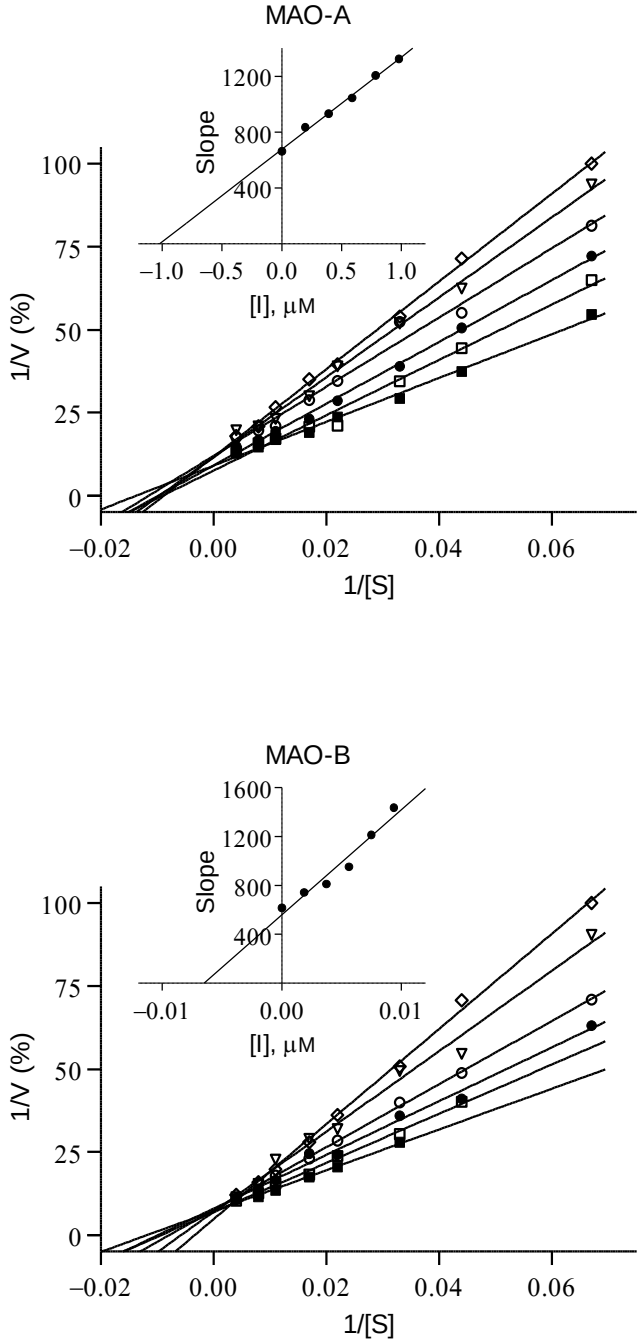

Figure 4.9 Lineweaver-Burk plots for the activities of MAO-A and MAO-B in the absence and presence of 1p and 1o, respectively. The insets are replots of the slopes of the Lineweaver-Burk plots versus inhibitor concentration.

Examination of the Lineweaver-Burk plots shows that for both **1o** and **1p**, the lines are linear and intersect on the y-axis. This is indicative of competitive inhibition and is further support that **1o** and **1p** are reversible inhibitors of MAO-A and MAO-B, respectively. From the replots of the slopes of the Lineweaver-Burk plots versus inhibitor concentration, K_i values of 1.0 μM and 0.0065 μM are estimated for the inhibition of MAO-A and MAO-B by **1o** and **1p**.

4.7 Molecular modelling

This chapter has shown that some of the 1-tetralone and alcohol derivatives have high potency inhibition towards MAO-B while most has low potency inhibition towards MAO-A. This is illustrated by the alcohol derivative **1m** which possesses an IC_{50} value of 0.068 µM for MAO-B and no measureable inhibition for MAO-A at the maximum tested concentration of 100 µM. In this section we will explore possible binding orientations by **1m** in MAO-A and MAO-B using molecular modelling to gather more insight into this phenomenon. Before docking **1m** the co-crystallised ligands, harmine and safinamide (MAO-A and MAO-B, respectively), were redocked into protein models of their respective enzymes. This is done to determine the accuracy of the docking procedure. For comparison, 1-tetralone derivative **1e** was also included in this study.

4.7.1 Materials

- Windows-based Discovery Studio 3.1 software package (Accelrys, San Diego, CA, USA) was used for all of the docking studies. The default values and conditions were applied unless it was otherwise specified.
- Protein models were obtained from the X-ray crystal structures reported by Son *et al.* (2008) and Binda *et al.* (2007) for human MAO-A (PDB code 2Z5X) and human MAO-B (PDB code 2V5Z), respectively. The models were obtained from the Brookhaven Protein Bank. In these structures safinamide served as the co-crystallised ligand for MAO-B while MAO-A was complexed with harmine.
- Discovery Studio 3.1 was used to prepare the illustrations.

4.7.2 Docking procedure

The docking of a structure into a receptor model is carried out in three steps and is illustrated in fig. 4.10 below.

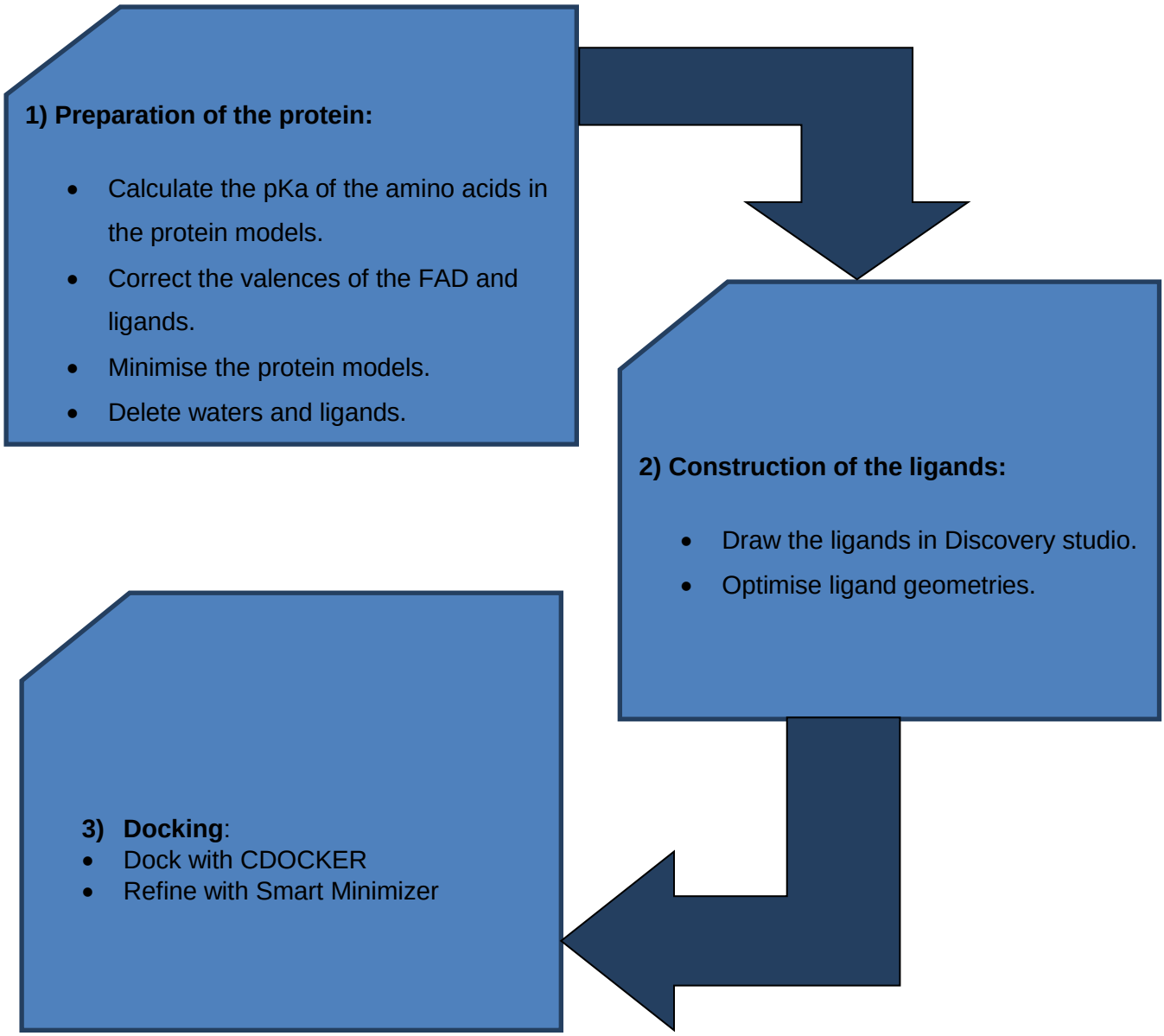

Figure 4.10 An illustration of the protocol followed for the docking study.

Preparation of the protein:

- The models used for docking simulations were prepared by calculating the pKa values and protonation states (pH 7.4) of the ionisable amino acids. Hydrogen atoms were added according to the calculations.
- The FAD cofactors were set to their oxidised states and the valences of both the FAD cofactors and the co-crystallised ligands, safinamide and harmine, were verified. After verification the Momany and Rone CHARMm force field was applied to each model.
- The models were energy minimised after a fixed atom constraint was applied to the backbone of the peptide. The Smart Minimizer algorithm (with maximum steps of 5000) and the implicit generalized Born solvation model (with molecular volume) was employed.

- The co-crystallised ligands and the backbone constraints were removed and, by analysing the cavities that are present in the proteins, the active site cavities were identified.
- All of the waters were removed from the protein models except those waters that are located in the active site of MAO-A and MAO-B, and which are considered to be conserved. The waters that were not removed are HOH 710, 718 and 739 in MAO-A, and HOH 1155, 1170 and 1351 in the A-chain of MAO-B.

Construction of the ligands:

- Discovery Studio was used to draw the structures of the ligands and a Dreiding-like force field (5000 iterations) was used to optimise their geometries. In this step the ligands safinamide, harmine, **1e** and **1m** were constructed.
- The inhibitor structures were submitted to the Prepare Ligands protocol, after which the partial charges and potential types of each atom were assigned with the Momany and Rone CHARMm force field.

Docking:

- The CDOCKER algorithm was used to dock the ligands into the MAO-A and MAO-B models. This algorithm allows for ten random conformations for each inhibitor. For this procedure the heating target temperature was set to 700 K and full potential mode was used.
- *In situ* ligand minimisation with Smart Minimizer algorithm was used to refine the docking orientations.

4.7.3 Results

Harmine docked into MAO-A

As shown in fig. 4.11, harmine docks into the MAO-A active site with a similar orientation to that observed in the X-ray crystal structure. The docked orientation of harmine exhibits a root-mean-square deviation (RMSD) value of 1.20 Å from the orientation of the co-crystallised ligand. Based on the relatively small RMSD, it may be concluded that the docking protocol is suitable for docking ligands into an active site model of MAO-A.

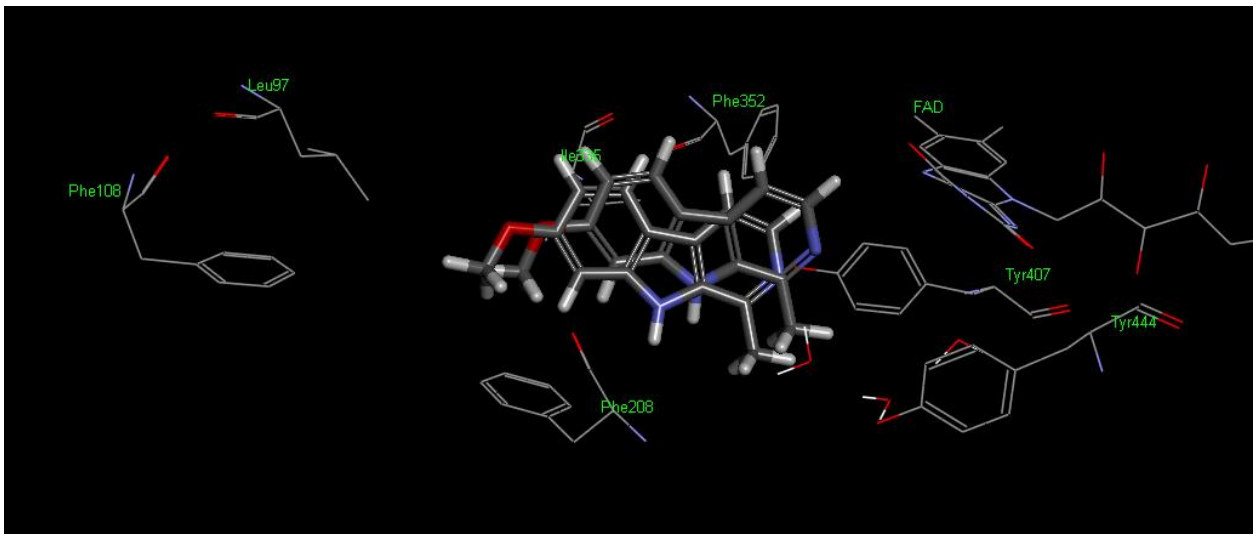

Figure 4.11 The docked binding orientation of harmine in MAO-A compared to the orientation of harmine in the X-ray crystal structure.

Safinamide docked into MAO-B

As shown in fig. 4.12, the orientation by which safinamide docks into the MAO-B active site is almost identical to the orientation observed in the X-ray crystal structure. The docked orientation of safinamide exhibits a RMSD value of only 0.44 Å from the orientation of the co-crystallised ligand. Based on the small RMSD, it may be concluded that the docking protocol is suitable for docking ligands into an active site model of MAO-B.

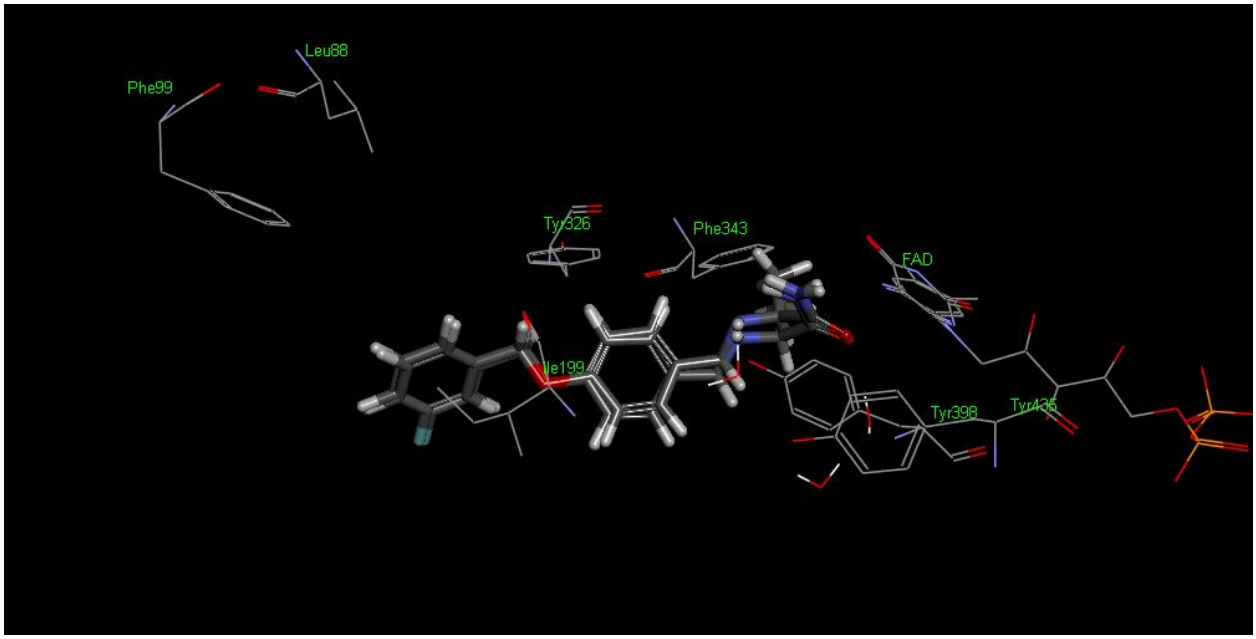

Figure 4.12 The docked binding orientation of safinamide in MAO-B compared to the orientation of safinamide in the X-ray crystal structure.

*Compounds **1e** and **1m** docked into the active site of MAO-A*:

The docking results show that 1-tetralone **1e** and the alcohol derivative **1m** exhibit similar binding orientations for the MAO-A active site. In this respect, the tetralone and tetralol moieties are directed towards the FAD cofactor while the C6 side chain projects towards the entrance of the MAO-A active site. For **1e**, the carbonyl oxygen is directed to the bottom of the active site cavity and forms a hydrogen bond to a water molecule. For the (R)-enantiomer of **1m**, the hydroxyl group is also directed towards the bottom of the active site and establishes hydrogen bonding to Tyr444 and a water molecule. The phenyl ring of the C6 side chain is stabilised by a pi-pi interaction with Phe208. Interestingly, for (S)-**1m**, the hydroxyl group is directed towards the top of the active site, with the resulting loss in hydrogen bonding as observed for (S)-**1m**. Based on the results it may be postulated that the (S)-enantiomer of **1m** should potentially exhibit weaker interaction and subsequently inhibition of MAO-A compared to the (R)-enantiomer. These observations show that the inhibitors are able to bind and interact with the MAO-A active site. The MAO inhibition data, however, shows that **1e** is a MAO-B inhibitor while **1m** does not inhibit MAO-A. A molecular explanation for the lack of MAO-A inhibition by **1m** is therefore not apparent. The orientations and interactions of **1e**, (R)-**1m** and (S)-**1m** are presented in the figures below.

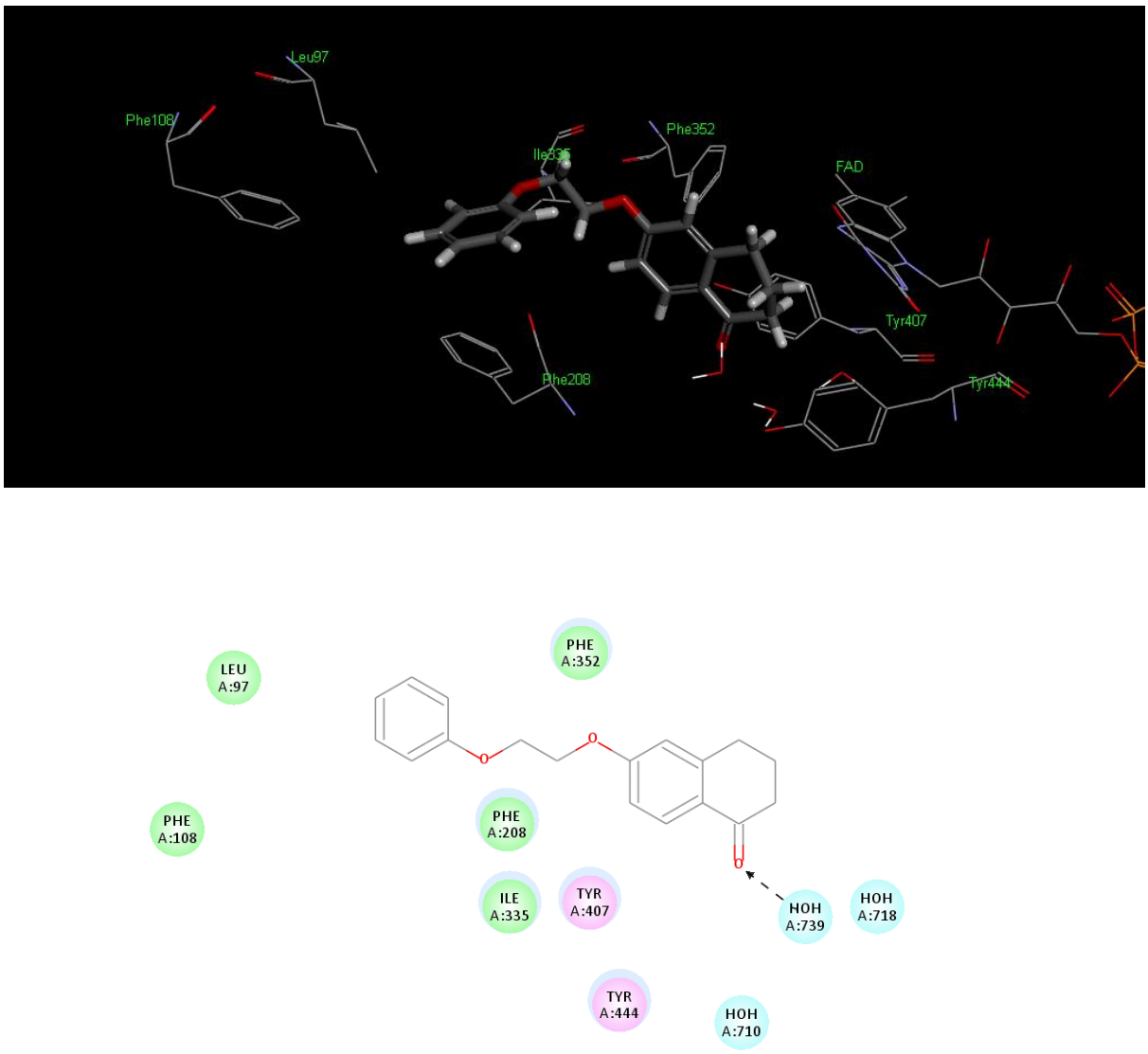

Figure 4.13 The docked binding orientation of 1e in MAO-A (top) with a 2D-diagram showing the key interactions (bottom). The dash line indicates hydrogen bonding while the blue shadow depicts van der Waals interactions.

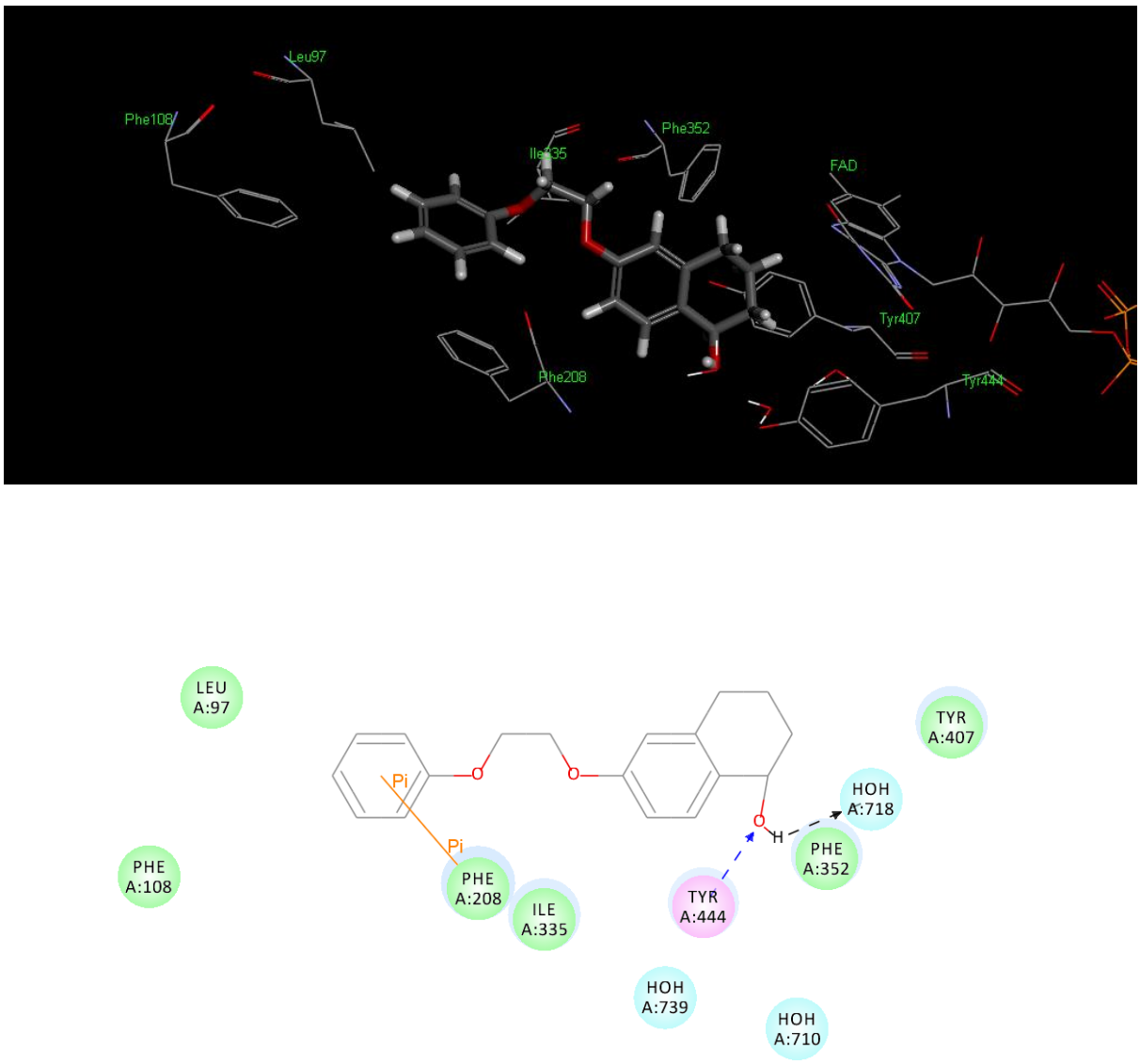

Figure 4.14 The docked binding orientation of (R)-1m in MAO-A (top) with a 2D-diagram showing the key interactions (bottom). The dash line indicates hydrogen bonding while the blue shadow depicts van der Waals interactions.

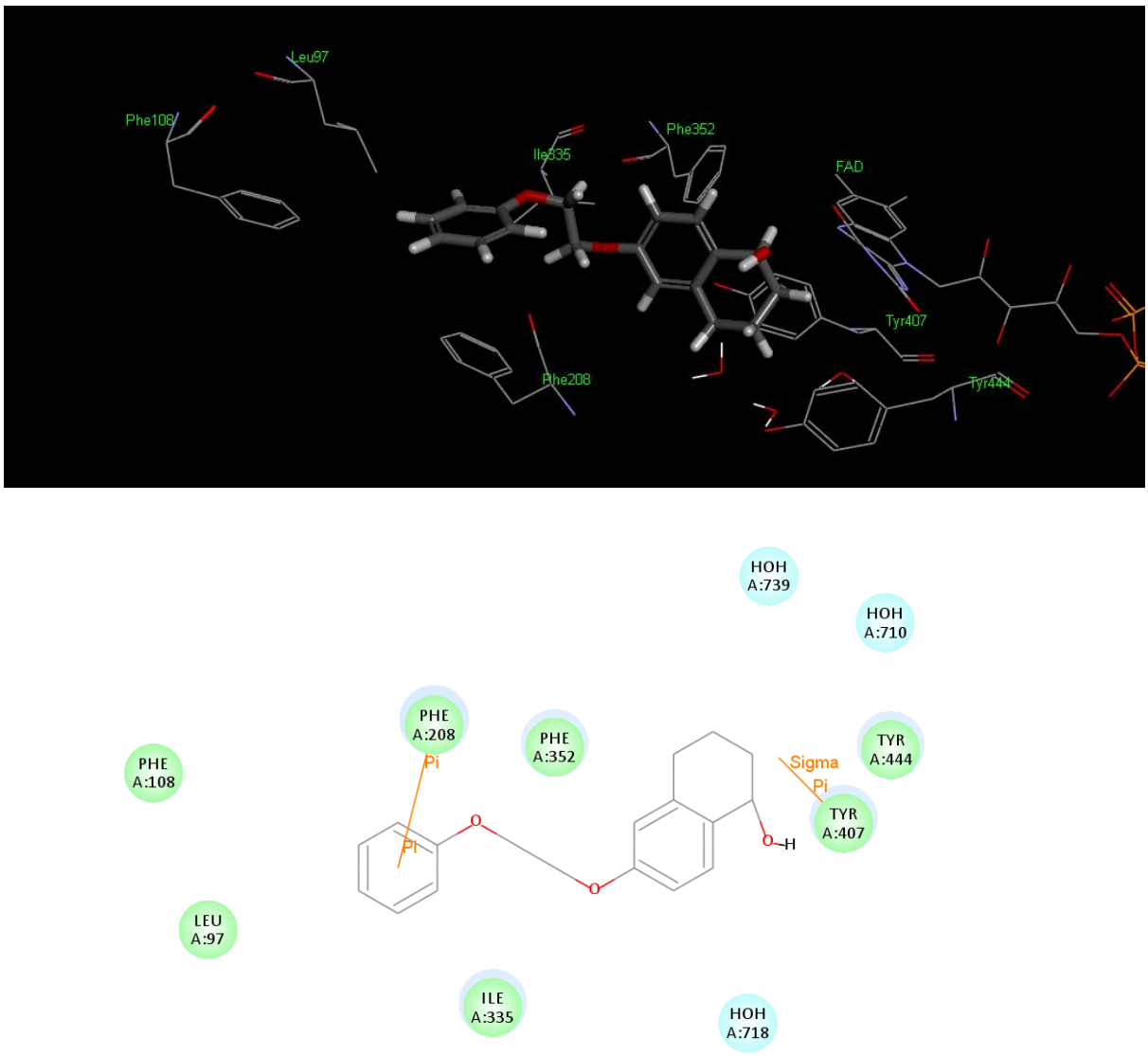

Figure 4.15 The docked binding orientation of (S)-1m in MAO-A (top) with a 2D-diagram showing the key interactions (bottom). The dash line indicates hydrogen bonding while the blue shadow depicts van der Waals interactions.

*Compounds **1e** and **1m** docked into the active site of MAO-B*:

In MAO-B, 1-tetralone **1e** and the alcohol derivative **1m** also exhibit similar binding orientations. As with MAO-A, the tetralone and tetralol moieties are directed towards the FAD cofactor while the C6 side chain projects into the entrance cavity of MAO-B. These inhibitors are therefore cavity spanning inhibitors, which may, in part, explain their high inhibition potencies towards MAO-B. Literature reports that cavity spanning inhibitors are in general more potent compared to inhibitors that only bind to the MAO-B substrate cavity (Hubálek *et al.*, 2004). For **1e**, the carbonyl oxygen is directed to the bottom of the active site cavity and forms a hydrogen bond with Tyr435 as well as a pi-pi interaction with Tyr398. For the (R)-and (S)-enantiomers of **1m**,

the hydroxyl group is also directed towards the bottom of the active site. The (R)-enantiomer forms a pi-pi interaction with Tyr398, while this interaction is absent for the (S)-enantiomer. The (S)-enantiomer, in turn, is hydrogen bonded to Tyr398. It is clear that the interactions that 1-tetralone **1e** and the alcohol derivative **1m** form with MAO-B are very similar. It may, however, be postulated that **1e** is stabilised by both pi-pi and hydrogen bond interactions while either enantiomer of **1m** is stabilised only by pi-pi or hydrogen bond interactions. This may explain the slightly higher potency MAO-B inhibition of **1e** compared to **1m**. The orientations and interactions of **1e**, (R)-**1m** and (S)-**1m** are presented in the figures below.

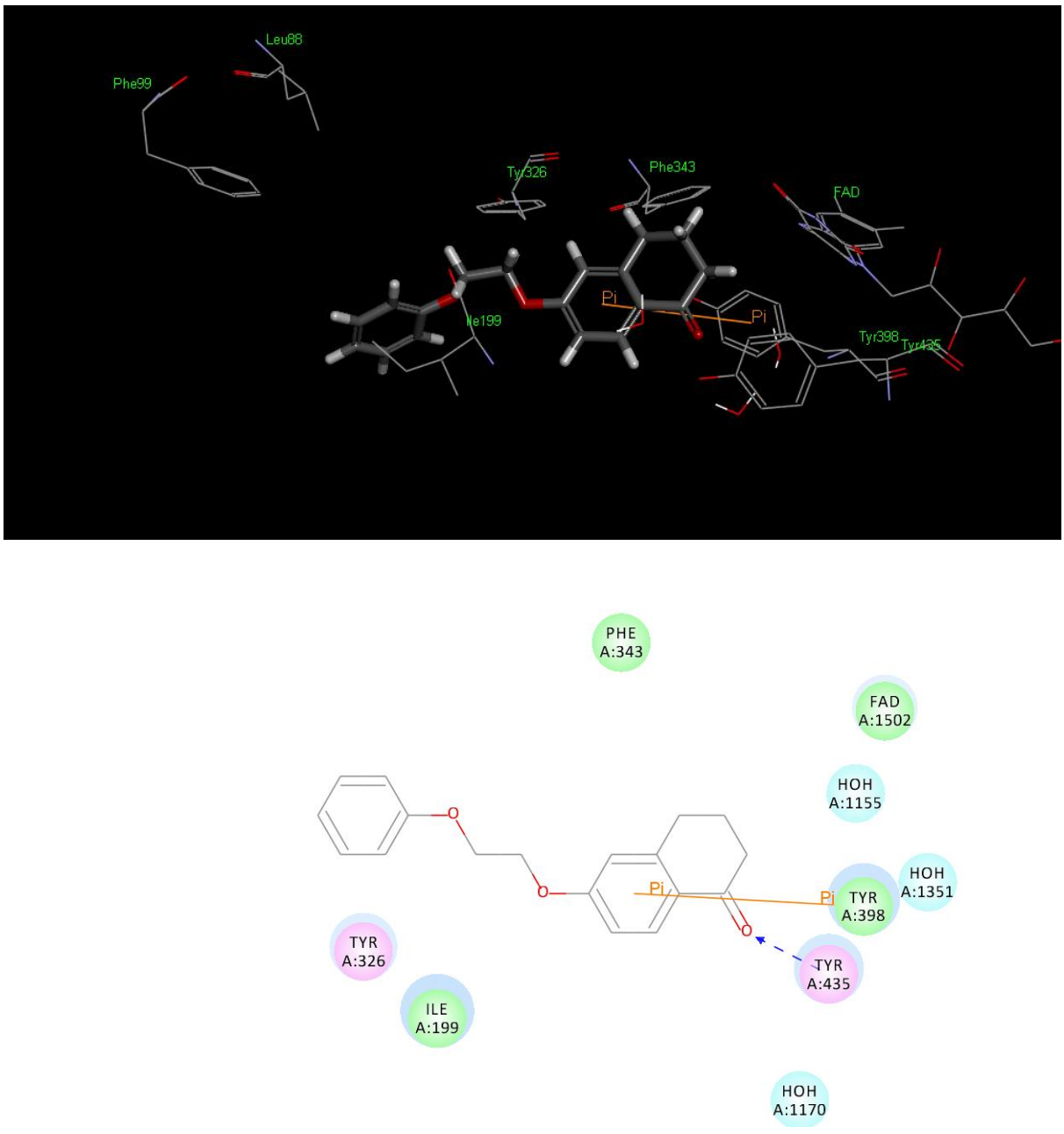

Figure 4.16 The docked binding orientation of (S)-1m in MAO-A (top) with a 2D-diagram showing the key interactions (bottom). The dash line indicates hydrogen bonding while the blue shadow depicts van der Waals interactions.

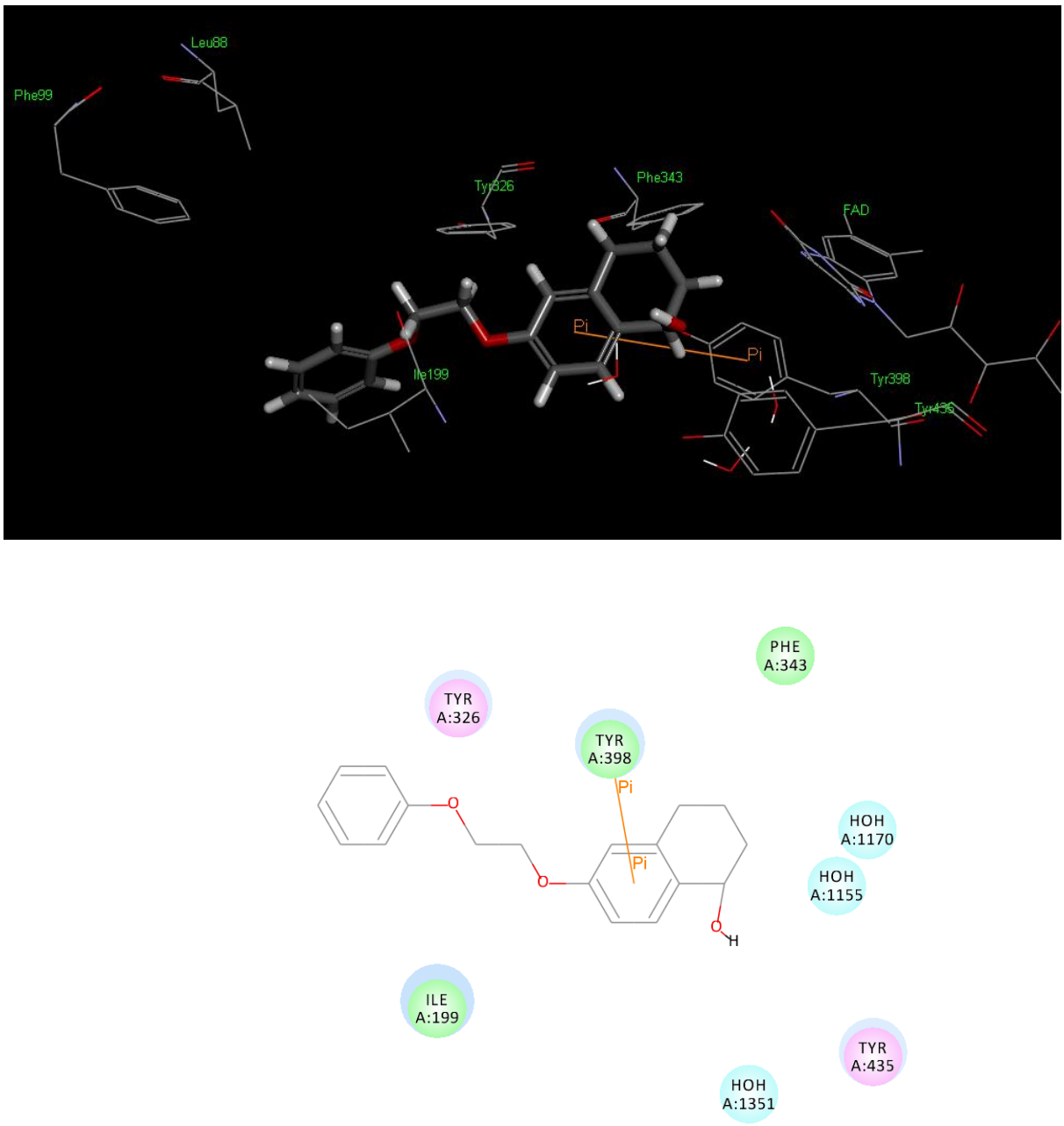

Figure 4.17 The docked binding orientation of (R)-1m in MAO-B (top) with a 2D-diagram showing the key interactions (bottom). The dash line indicates hydrogen bonding while the blue shadow depicts van der Waals interactions.

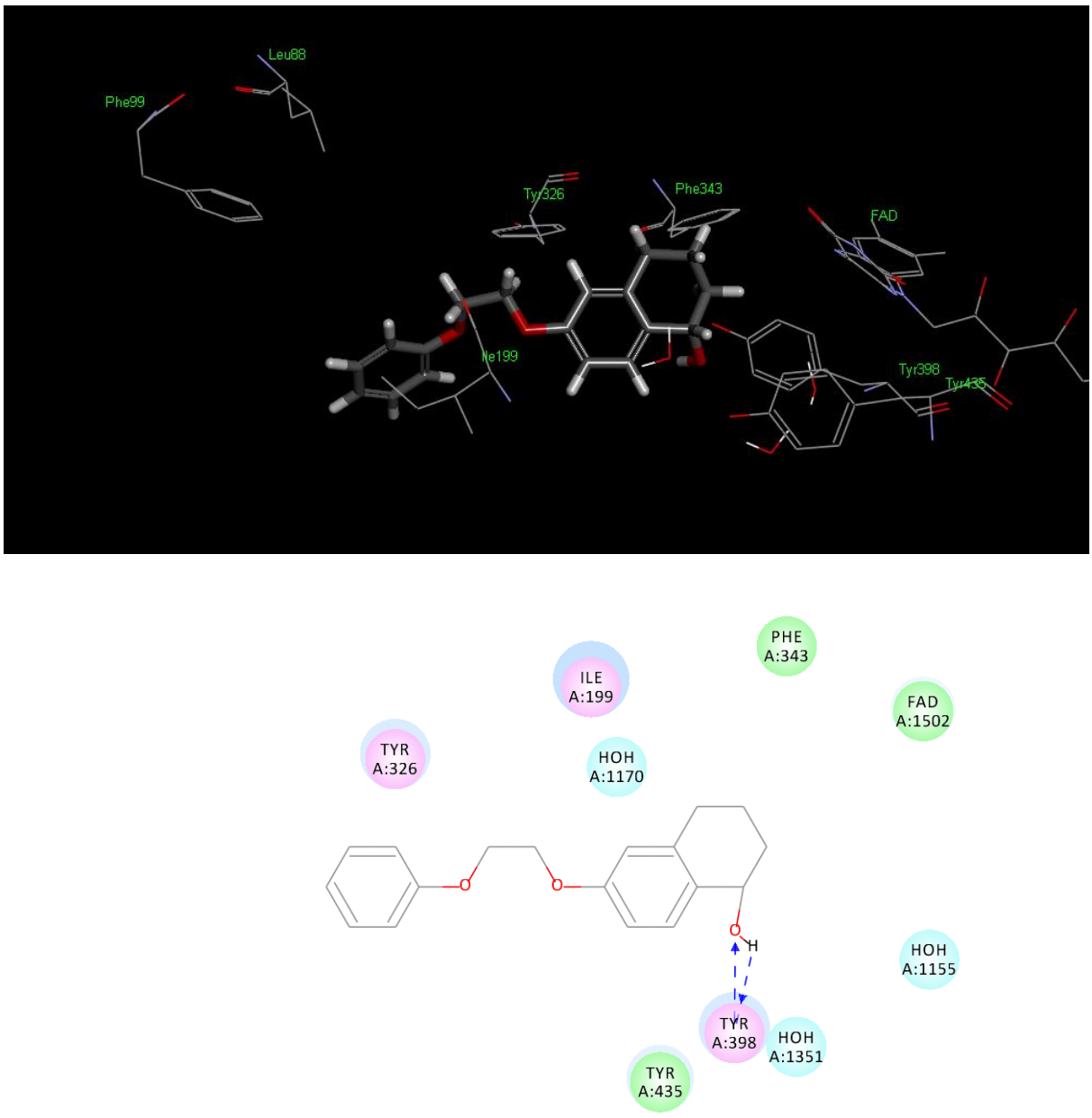

Figure 4.18 The docked binding orientation of (S)-1m in MAO-B (top) with a 2D-diagram showing the key interactions (bottom). The dash line indicates hydrogen bonding while the blue shadow depicts van der Waals interactions.

4.8 Conclusion

In this chapter the synthesised compounds were evaluated as MAO-A and MAO-B inhibitors. Their inhibition potencies were expressed as IC_{50} values, and the compound with the lowest value is the most potent inhibitor. Kynuramine was used as the enzyme substrate. Kynuramine is oxidised by MAO-A and MAO-B to yield 4-hydroxyquinoline which is a fluorescent product. The catalytic rates of MAO-A or MAO-B can thus be determined by measuring the amount of 4-hydroxyquinoline formed by fluorescence spectroscopy.

This study finds that compound **1h** is the most potent inhibitor with IC_{50} values for MAO-A and MAO-B of 0.036 µM and 0.0011 µM, respectively. The most potent inhibitors among the alcohol derivatives were **1p** and **1o** with IC_{50} values of 0.039 µM and 0.0075 µM, respectively, for the inhibition of MAO-A and MAO-B. The reversibility of MAO-A and MAO-B inhibition was evaluated by dialysis for **1p** and **1o**, respectively. It was found that inhibition could be reversed by dialysis which indicates that these inhibitors are reversible MAO inhibitors. Reversible MAO inhibitors have a low risk of causing the cheese reaction. The modes of inhibition of MAO-A and MAO-B were also evaluated for **1p** and **1o**. Lineweaver-Burk plots were constructed and showed that **1p** and **1o** are competitive inhibitors of MAO-A and MAO-B, respectively. K_i values of 1.0 µM and 0.0065 µM are estimated for the inhibition of MAO-A and MAO-B by **1o** and **1p**, respectively.

CHAPTER 5

CONCLUSION

5.1 Conclusion

Parkinson's disease is a disorder of which the pathogenesis is not completely understood. Parkinson's disease is characterised by the death of dopaminergic neurons in the substantia nigra in the brain. This causes a dopamine deficiency in the striatum, the point of projection of the nigrostriatal neurons. Symptoms such as tremors, stiffness, imbalance and shuffling can occur in patients with Parkinson's disease. The cornerstone of Parkinson's disease therapy is *L*-dopa, the metabolic precursor of dopamine. *L*-Dopa elevates the levels of dopamine in the striatum, although highly effective in the early stages of the disease it may cause dyskinesia with long-term treatment. Furthermore, *L*-dopa does not stop the progression of Parkinson's disease. MAO-B is the primary enzyme that metabolises dopamine in the brain. Studies have shown that inhibitors of MAO-B may potentially slow the progression of the disease, and also may delay disability that requires the initiation of *L*-dopa therapy. MAO-B inhibitors also may reduce the dose of *L*-dopa that is required for the treatment of the motor symptoms. Thus MAO-B inhibitors have clear clinical value, particularly as adjuvants to *L*-dopa. Furthermore, MAO-B inhibitors have an excellent safety profile.

In this study we synthesised and evaluated a series of 1-tetralone derivatives as MAO inhibitors in an attempt to discover novel MAO-B inhibitors. 1-Tetralone derivatives have already been shown in literature to act as potent and specific inhibitors of MAO-B, especially when substituted on C6 and C7. In this study, the 1-tetralone derivatives were thus substituted on C5, C6 and C7 with the benzyloxy, 4-chlorobenzyloxy and 2-phenoxyethoxy moieties. The 1-tetralone compounds thus obtained (**1a-h**) were subsequently reduced to their corresponding 1-tetralol derivatives (**1i-p**). This study is the first investigation of the MAO inhibition properties of 1-tetralol derivatives. Both the 1-tetralone and 1-tetralol derivatives of this study are expected to be potent inhibitors of MAO-B since these compounds have the ability to span both the substrate and entrance cavities of the MAO-B active site. Such cavity spanning inhibitors are in general potent and highly specific inhibitors of MAO-B, and thus will possess a low probability of causing the cheese reaction. Further this study also evaluated the reversibility of MAO inhibition, since reversible inhibitors also do not cause the cheese reaction, even when MAO-A is also inhibited.

Table 5.1 The synthesised 1-tetralone derivatives and their IC_{50} values for the inhibition of the MAOs.

Compound	IC_{50} (μM) – MAO-A	IC_{50} (μM) – MAO-B
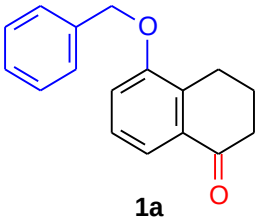 **1a**	53.9 ± 7.02	3.62 ± 0.34
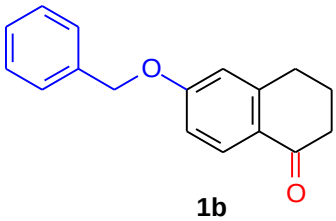 **1b**	1.39 ± 0.30	0.025 ± 0.0029
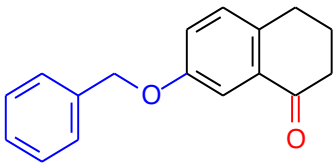 **1c**	0.623 ± 0.021	0.0024 ± 0.0004
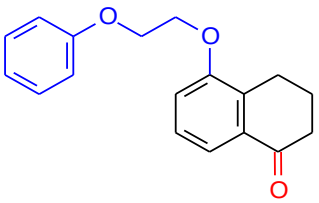 **1d**	No inhibition	3.26 ± 1.86
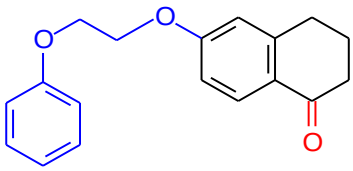 **1e**	2.58 ± 0.30	0.033 ± 0.0053

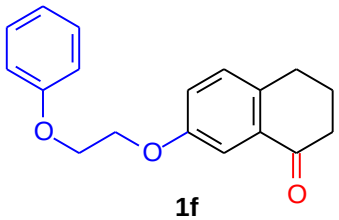 **1f**	1.91 ± 0.37	0.0012 ± 0.0003
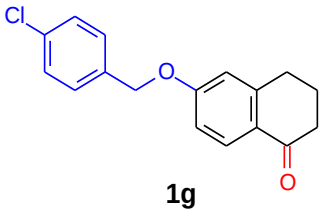 **1g**	0.575 ± 0.018	0.0055 ± 0.0006
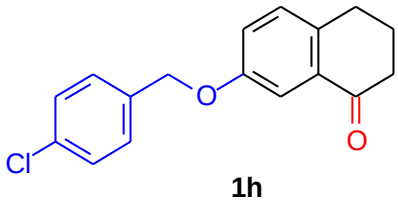 **1h**	0.036 ± 0.0059	0.0011 ± 0.0002

Table 5.2 The synthesised 1-tetralol derivatives and their IC_{50} values for the inhibition of the MAOs.

Compound	**IC_{50} (μM) – MAO-A**	**IC_{50} (μM) – MAO-B**
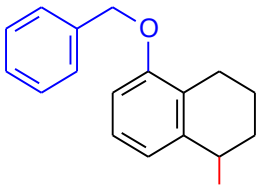 **1i**	9.27 ± 0.83	5.05 ± 0.42
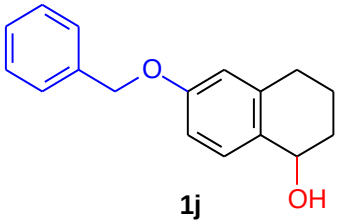 **1j**	35.5 ± 5.60	0.079 ± 0.012

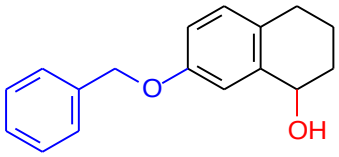 **1k**	34.6 ± 3.80	0.249 ± 0.061
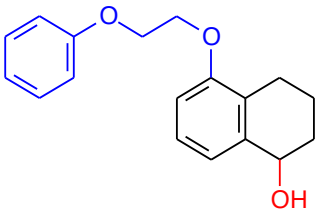 **1l**	No inhibition	1.66 ± 0.14
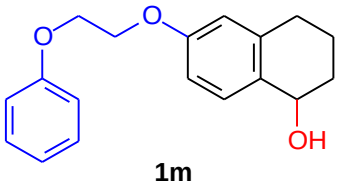 **1m**	No inhibition	0.068 ±0.0034
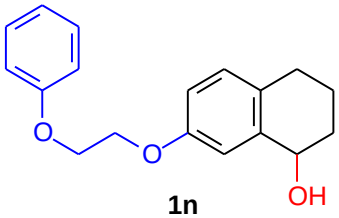 **1n**	No inhibition	0.189 ± 0.013
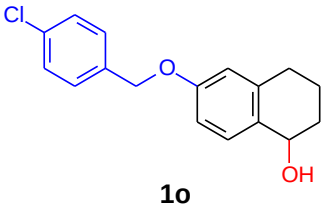 **1o**	1.086 ± 0.12	0.0075 ± 0.0011
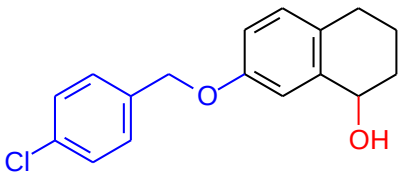 **1p**	0.785 ± 0.047	0.039 ± 0.013

The starting materials for the synthesis of the 1-tetralone derivatives, 5-, 6- and 7-hydroxy-1-tetralone were synthesised by heating (under reflux) the corresponding methoxy-1-tetralone derivative with aluminium chloride and toluene, and then extracting the product with ethyl acetate. Hydroxy-1-tetralone and the appropriate substituted alkyl bromide were then heated

under reflux with anhydrous potassium carbonate to produce compounds **1a-h**. To reduce the 1-tetralone derivatives to their corresponding 1-tetralol derivatives (**1i-p**), the 1-tetralone derivatives were heated under reflux in the presence of sodium borohydride with ethanol as solvent. The products were subsequently extracted with dichloromethane. NMR, MS and HPLC were employed to determine the structures and the purities of the synthesised compounds. All the compounds were found to be the desired products, and the purities were acceptable.

Both the 1-tetralone and 1-tetralol derivatives were evaluated as inhibitors of MAO using recombinant human MAO-A and MAO-B as enzyme sources and kynuramine as the substrate. Kynuramine is metabolised by MAO-A and MAO-B to yield 4-hydroxyquinoline which is a fluorescent product. By measuring the fluorescence of incubations containing MAO and kynuramine, the concentration of 4-hydroxyquinoline can be determined and the MAO activity can be calculated. Sigmoidal plots of enzyme catalytic rate versus the logarithm of the inhibitor concentration were constructed, and the IC_{50} values for the inhibition of MAO were determined from these plots. These results showed that both the 1-tetralone and 1-tetralol derivatives are specific inhibitors of MAO-B. Overall the 1-tetralone derivatives were more potent MAO-B inhibitors compared to the 1-tetralol derivatives, with the most potent MAO-B inhibitor being **1h**. The results also showed that substitution on C6 and C7 yields compounds that are much more potent inhibitors compared to compounds substituted on C5. Also larger substituents yielded derivatives that are more selective for MAO-B, while halogen substitution (with Cl) on the phenyl ring of the side chain increased inhibition potency.

The reversibility of MAO-A and MAO-B inhibition by the tetralol derivatives were evaluated with **1p** and **1o**, respectively, as representative compounds. The reversibility was determined by recording the degree of recovery of enzyme activity after dialysis of mixtures containing the enzyme and test inhibitor. After dialysis of mixtures containing MAO-A and **1p**, catalytic activity recovered to 81%, showing that **1p** is a reversible MAO-A inhibitor. After dialysis of mixtures containing MAO-B and **1o**, catalytic activity recovered to 76%, showing that **1o** is a reversible MAO-B inhibitor. The conclusion can be made that the 1-tetralol derivatives of this study are reversible inhibitors of human MAO-A and MAO-B. Sets of Lineweaver-Burk plots were also constructed for the inhibition of MAO-A and MAO-B by compounds **1p** and **1o**, respectively, in order to determine the mode of inhibition. The Lineweaver-Burk plots intersected on the y-axis, which indicates that both compounds are competitive inhibitors of MAO. It may thus be concluded that all the 1-tetralol derivatives of this study are competitive and reversible inhibitors of human MAO-A and MAO-B. Since the 1-tetralol derivatives (particularly **1m**) are specific and reversible MAO inhibitors, they possess a low probability of causing the cheese effect.

The possible binding orientations of **1m** and **1e** were also evaluated with molecular docking in an attempt to provide an explanation for their different inhibition potencies towards MAO-A and

MAO-B. It was however found, contrary to experimental results, that both the 1-tetralone and 1-tetralol derivatives bind to the active site of MAO-A. An explanation for this phenomenon is therefore not apparent. The difference in MAO-B inhibition potencies of **1e** and **1m** may be due to the possibility that the enantiomers of the alcohol derivative, (R)-**1m** and (S)-**1m**, exhibit differing binding modes to MAO-B.

This study has shown that both the 1-tetralone and 1-tetralol derivatives are highly potent inhibitors of human MAO-A and MAO-B. They are also reversible in their mode of inhibition. These are desirable attributes for the design of MAO inhibitors for the treatment of Parkinson's disease and specifically Parkinson's disease which presents with depression as comorbidity. The hypothesis of this study which states that the 1-tetralone and 1-tetralol derivatives of this study will act as high potency and specific MAO-B inhibitors has thus been proven.

5.1.1 Future recommendations

From the results of this study, the following recommendations can be made:

1) The study showed that the 1-tetralone and 1-tetralol structure serves as excellent scaffolds for designing drugs that inhibit MAO-B, and sometimes MAO-A. Both of these pathways may be expanded in the future with different substituents on the C6 and C7 positions.

2) Compound **1h** was the strongest MAO-B inhibitor among the tetralones and **1o** among the tetralol derivatives. Both of these can be lead compounds in future studies where other halogens can be added to the benzyloxy phenyl rings to further increase MAO-B inhibition.

3) Since the tetralol derivatives are more specific towards MAO-B in their inhibition, this scaffold can be further researched to find a novel, stronger and more specific inhibitor of MAO-B.

4) Halogen substituted tetralones, such as **1h** can be further studied to discover a novel reversible inhibitor for MAO-A and MAO-B which will serve as a dual-acting drug for Parkinson's disease and depression.

5) The different enantiomers of the tetralol derivatives can be studies to discover their different inhibition properties towards MAO-A and MAO-B.

BIBLIOGRAPHY

Aluf, Y., Vaya, J., Khatib, S., Loboda, Y. & Finberg, J.P. 2013. Selective inhibition of monoamine oxidase A or B reduces striatal oxidative stress in rats with partial depletion of the nigro-striatal dopaminergic pathway. *Neuropharmacology*. 65:48-57.

Alves, G., Forsaa, E.B., Pedersen, K.F., Gjerstad, M.D. & Larsen, J.P. 2008. Epidemiology of Parkinson's disease. *Journal of Neurology*. 255(S5):18-32.

Arai, R., Horiike, K. & Hasegawa, Y. 1998. Dopamine-degrading activity of monoamine oxidase is not detected by histochemistry in neurons of the substantia nigra pars compacta of the rat. *Brain Research*. 812(1-2):275-278.

Ascherio, A., Chen, H., Schwarzschild, M.A., Zhang, S.M., Colditz, G.A. & Speizer, F.E. 2003. Caffeine, postmenopausal estrogen, and risk of Parkinson's disease. *Neurology*. 60(5):790-795.

Ascherio, A., Weisskopf, M.G., O'Reilly, E.J., McCullough, M.L., Calle, E.E., Rodriguez, C. & Thun, M.J. 2004. Coffee consumption, gender, and Parkinson's disease mortality in the cancer prevention study II cohort: the modifying effects of estrogen. *American Journal of Epidemiology*. 160(10):977-984.

Azzaro, A.J., King, J., Kotzuky, J., Schoepp, D.D., Frost, J. & Schochet, S. 1985. Guinea pig striatum as a model of human dopamine deamination: the role of monoamine oxidase isoenzyme ratio, localization, and affinity for substrate in synaptic dopamine metabolism. *Journal of Neurochemistry*. 45(3):949–956.

Bach, A.W., Lan, N.C., Johnson, D.L., Abell, C.W., Bembenek, M.E., Kwan, S.W., Seeburg, P.H. & Shih, J.C. 1988. cDNA cloning of human liver monoamine oxidase A and B: molecular basis of differences in enzymatic properties. *Proceedings of the National Academy of Sciences of the United States of America*. 85(13):4934-4938.

Barton, D.A., Esler, M.D., Dawood, T., Lambert, E.A., Haikerwal, D., Brenchley, C., Socratous, F., Hastings, J., Guo, L., Wiesner, G., Kaye, D.M., Bayles, R., Schlaich, M.P. & Lambert, G.W. 2008. Elevated brain serotonin turnover in patients with depression: effect of genotype and therapy. *Archives of General Psychiatry*. 65(1):38-46.

Bar-Am, O., Amit, T., Youdim, M.B. & Weinreb, O. 2016. Neuroprotective and neurorestorative potential of propargylamine derivatives in ageing: focus on mitochondrial targets. *Journal of neural transmission*. 123(2):125-135.

Beckman, K.B. & Ames, B.N. 1998. The free radical theory of aging matures. *Physiological Reviews*. 78(2):547-581.

Benedetti, M.S., Boucher, T. & Fowler, C.J. 1983. The deamination of noradrenaline and 5-hydroxytryptamine by rat brain and heart monoamine oxidase and their inhibition by cimoxatone, toloxatone and MD 770222. *Naunyn-Schmiedeberg's Archives of Pharmacology*. 323(4):315–320.

Benedetti, M.S., Rovei, V., Dencker, S.J., Nagy, A. & Johansson, R. 1982. Pharmacokinetics of toloxatone in man following intravenous and oral administrations. *Arzneimittel-Forschung*. 32(3):276-280.

Berlin, I., Aubin, H.J., Pedarriosse, A.M., Rames, A., Lancrenon, S., Lagrue, G. & Lazabemide in Smoking Cessation Study Investigators. 2002. Lazabemide, a selective, reversible monoamine oxidase B inhibitor, as an aid to smoking cessation. *Addiction*. 97(10):1347-1354.

Berlin, I., Saïd, S., Spreux-Varoquaux, O., Launay, J.M., Olivares, R., Millet, V., Lecrubier, Y. & Puech, A.J. 1995. A reversible monoamine oxidase A inhibitor (moclobemide) facilitates smoking cessation and abstinence in heavy, dependent smokers. *Clinical Pharmacology and Therapeutics*. 58(4):444-452.

Berlin, I., Zimmer, R., Cournot, A., Payan, C., Pedarriosse, A.M. & Puech, A.J. 1989. Determination and comparison of the pressor effect of tyramine during long-term moclobemide and tranylcypromine treatment in healthy volunteers. *Clinical Pharmacology & Therapeutics*. 46(3):344-351.

Bhattacharya, S.K., Mitra, S.K. & Acharya, S.B. 1991. Anxiogenic activity of isatin, a putative biological factor, in rodents. *Journal of Psychopharmacology*. 5(3):202-206.

Birkmayer, W., Knoll, J., Riederer, P., Youdim, M.B., Hars, V. & Marton, J. 1985. Increased life expectancy resulting from addition of L-deprenyl to Madopar treatment in Parkinson's disease: a long-term study. *Journal of Neural Transmission*. 64(2):113-127.

Birkmayer, W., Riederer, P., Youdim, M.B. & Linauer, W. 1975. The potentiation of the anti-akinetic effect after L-dopa treatment by an inhibitor of MAO-B, Deprenil. *Journal of Neural Transmission*. 36(3-4):303-326.

Bieck, P.R., Firkusny, L., Schick, C., Antonin, K.H., Nilsson, E., Schulz, R., Schwenk, M. & Wollmann, H. 1989, Monoamine oxidase inhibition by phenelzine and brofaromine in healthy volunteers. *Clinical Pharmacology & Therapeutics*. 45(3):260-269.

Binda, C., Li, M., Hubálek, F., Restelli, N., Edmondson, D.E. & Mattevi, A. 2003. Insights into the mode of inhibition of human mitochondrial monoamine oxidase B from high resolution crystal structures. *Proceedings of the National Academy of Sciences of the United States of America*. 100(17):9750–9755.

Binda, C., Wang, J., Pisani, L., Caccia, C., Carotti, A., Salvati, P., Edmondson, D.E. & Mattevi, A. 2007. Structures of human monoamine oxidase B complexes with selective noncovalent inhibators: safinamide and coumarin Analogs. *Journal of Medicinal Chemistry*. 50(23):5848–5852.

Borštnar, R., Repič, M., Kržan, M., Mavri, J. & Vianello, R. 2011. Irreversible inhibition of monoamine oxidase B by the antiparkinsonian medicines rasagiline and selegiline: a computational study. *European Journal of Organic Chemistry*. 2011(32):6419–6433.

Bower, J.H., Maraganore, D.M., McDonnell, S.K. & Rocca W.A. 1999. Incidence and distribution of parkinsonism in Olmsted County, Minnesota, 1976-1990. *Neurology*. 52(6):1214-1220.

Buccafusco, J.J., Terry, A.V. Jr, Goren, T. & Blaugrun, E. 2003. Potential cognitive actions of (n-propargly-(3r)-aminoindan-5-yl)-ethyl, methyl carbamate (tv3326), a novel neuroprotective agent, as assessed in old rhesus monkeys in their performance of versions of a delayed matching task. *Neuroscience*. 119(3):669-678.

Bussell, R. Jr. & Eliezer, D. 2001. Residual structure and dynamics in Parkinson's disease-associated mutants of alpha-synuclein. *The Journal of Biological Chemistry*. 276(49):45996-46003.

Caccia, C., Maj, R., Calabresi, M., Maestroni, S., Faravelli, L., Curatolo, L., Salvati, P. & Fariello, R.G. 2006. Safinamide: from molecular targets to a new anti-Parkinson drug. *Neurology*. 67(7S2):S18-S23.

Caille, D., Bergis, O.E., Frankhauser, C., Gardes, A., Adam, R., Charieraas, T., Grosset, A., Rovei, V. & Jarreau, F.X. 1996. Befloxatone, a new reversible and selective monoamine oxidase-A inhibitor. II. Pharmacological profile. *The Journal of Pharmacology and Experimental Therapeutics*. 277(1):265-277.

Cao Danh, H., Strolin Benedetti, M. & Dostert, P. 1984. Differential changes in monoamine oxidase A and B activity in aging rat tissues (*In* Tripton, K.F., Dostert, P. & Benedetti, M.S. *ed.* Monoamine oxidase and disease. Prospects for therapy with reversible inhibitors. London: Academic Press. p. 301-317.)

Caslake, R., Macleod, A., Ives, N., Stowe, R. & Counsell, C. 2009. Monoamine oxidase B inhibitors versus other dopaminergic agents in early Parkinson's disease. *Cochrane Database of Systematic Reviews*. 7(4):1-27.

Cattaneo, C., Caccia, C., Marzo, A., Maj, R. & Fariello, R.G. 2003. Pressor response to intravenous tyramine in healthy subjects after safinamide, a novel neuroprotectant with selective, reversible monoamine oxidase B inhibition. *Clinical Neuropharmacology*. 26(4):213-217.

Cesura, A. M., Borroni, E., Gottowik, J., Kuhn, C., Malherbe, P., Martin, J. & Richards, J.G. 1999. Lazabemide for the treatment of Alzheimer's disease: rationale and therapeutic perspectives. *Advances in Neurology*. 80:521-528.

Cesura, A.M., Galva, M.D., Imhof, R., Kyburz, E., Picotti, G.B. & Da Prada, M. 1989. [^{3}H]Ro 19-6327: a reversible ligand and affinity labelling probe for monoamine oxidase-B. *European Journal of Pharmacology*. 162(3):457-465.

Chen, J.J. & Wilkinson, J.R. 2012. The monoamine oxidase type B inhibitor rasagiline in the treatment of Parkinson disease: is tyramine a challenge? *The Journal of Clinical Pharmacology.* 52(5):620-628.

Chen, K., Wu, H.F. & Shih, J.C. 1996. Influence of C terminus on monoamine oxidase A and B catalytic activity. *Journal of Neurochemistry*. 66(2):797-803.

Chiuccariello, L., Houle, S., Miler, L., Cooke, R.G., Rusjan, P.M., Rajkowska, G., Levitan, R.D., Kish, S.J., Kolla, N.J., Ou, X., Wilson, A.A. & Meyer, J.H. 2014. Elevated monoamine oxidase A binding during major depressive episodes is associated with greater severity and reversed neurovegetative symptoms. *Neuropsychopharmacology*. 39(4): 973-980.

Cohen, G. 2000. Oxidative stress, mitochondrial respiration, and Parkinson's disease. *Annals of the New York Academy of Sciences*. 899:112-120.

Curet, O., Damoiseau, G., Aubin, N., Sontag, N., Rovei, V. & Jarreau, F.X. 1996. Befloxatone, a new reversible and selective monoamine oxidase-A inhibitor. I. Biochemical profile. *Journal of Pharmacology and Experimental Therapeutics*. 277(1):253-264.

Da Prada, M., Kettler, R., Keller, H.H., Burkard, W.P., Muggli-Maniglio, D. & Haefely, W.E. 1989. Neurochemical profile of moclobemide, a short-acting and reversible inhibitor of monoamine oxidase type A. *Journal of Pharmacology and Experimental Therapeutics*. 248(1):400-414.

Da Prada, M., Pieri, L., Cesura, A.M. & Kettler, R. 1994. The pharmacology of moclobemide. *Reviews in Contemporary Pharmacotherapy.* 5:1-18.

Dauer, W. & Przedborski, S. 2003. Parkinson's disease: mechanisms and models. *Neuron*. 39(6):889-909.

De Colibus, L., Li, M., Binda, C., Lustig, A., Edmondson, D.E. & Mattevi, A. 2005. Three-dimensional structure of human monoamine oxidase A (MAO A): relation to the structures of rat MAO A and human MAOB. *Proceedings of the National Academy of Sciences of the United States of America*. 102(36):12684–12689.

De Rijk, M.C., Breteler, M.M., Graveland, G.A., Ott, A., Grobbee, D.E., van der Meché, F.G. & Hofman, A. 1995. Prevalence of Parkinson's disease in the elderly: the Rotterdam Study. *Neurology*. 45(12):2143-2146.

Deftereos, S.N., Dodou, E., Andronis, C. & Persidis, A. 2012. From depression to neurodegeneration and heart failure: re-examining the potential of MAO inhibitors. *Expert Review of Clinical Pharmacology*. 5(4):413-425.

Degkwitz, R., Frowin, R., Kulenkampff, C., & Mohs, U. 1960. Über die Wirkungen des L-DOPA beim Menschen und deren Beeinflussung durch Reserpin, Iproniazid und Vitamin B6. *Klinische Wochenschrift*. 38(3):120-123.

Dexter, D.T., Wells, F.R., Agid, F., Agid, Y., Lees, A.J., Jenner, P. & Marsden, C.D. 1987. Increased nigral iron content in post-mortem parkinsonian brain. *Lancet*. 2(8569):1219-1220.

Dingemanse, J., Wood, N., Guentert, T., Oie, S., Ouwerkerk, M. & Amrein, R. 1998. Clinical pharmacology of moclobemide during chronic administration of high doses to healthy subjects. *Psychopharmacology*. 140(2):164-172.

Edmondson, D.E., Binda, C., Wang, J., Upadhyay, A.K. & Mattevi, A. 2009. Molecular and mechanistic properties of the membrane-bound mitochondrial monoamine oxidases. *Biochemistry*. 48(20):4220-4230.

Elbaz, A. & Tranchant, C. 2007. Epidemiologic studies of environmental exposures in Parkinson's disease. *Journal of the Neurological Sciences*. 262(1-2):37-44.

Fassone, E. & Rahman, S. 2012. Complex I deficiency: clinical features, biochemistry and molecular genetics. *Journal of Medical Genetics*. 49(9):578-590.

Filipenko, M.L., Beilina, A.G., Alekseyenko, O.V., Dolgov, V.V. & Kudryavtseva, N.N. 2002. Repeated experience of social defeats increases serotonin transporter and monoamine oxidase A mRNA levels in raphe nuclei of male mice. *Neuroscience Letters*. 321(1-2):25-28.

Finberg, J.P. 2014. Update on the pharmacology of selective inhibitors of MAO-A and MAO-B: focus on modulation of CNS monoamine neurotransmitter release. *Pharmacology & Therapeutics*. 143(2):133-152.

Finberg, J.P. & Tenne, M. 1982. Relationship between tyramine potentiation and selective inhibition of monoamine oxidase types A and B in the rat vas deferens. *British Journal of Pharmacology*. 77(1):13-21.

Fitzgerald, L.W., Kaplinsky, L. & Kimelberg, H.K. 1990. Serotonin metabolism by monoamine oxidase in rat primary astrocyte cultures. *Journal of Neurochemistry*. 55(6):2008-2014.

Flamand, V., Zhao, H. & Peehl, D.M. 2010. Targeting monoamine oxidase A in advanced prostate cancer. *Journal of Cancer Research and Clinical Oncology*. 136(11):1761-1771.

Foley, P., Gerlach, M., Youdim, M.B.H. & Riederer, P. 2000. MAO-B inhibitors: multiple roles in the therapy of neurodegenerative disorders? *Parkinsonism and Related Disorders*. 6(1):25-47.

Fowler, C.J., Callingham, B.A., Mantle, T.J., Tipton, K.F. 1980. The effect of lipophilic compounds upon the activity of rat liver mitochondrial monoamine oxidase-A and -B. *Biochemical Pharmacology*. 29(8):1177-1183.

Fowler, J.S., Logan, J., Wang, G.J., Volkow, N.D., Telang, F., Zhu, W., Franceschi, D., Pappas, N., Ferrieri, R., Shea, C., Garza, V., Xu, Y., Schlyer, D., Gatley, S.J., Ding, Y.S., Alexoff, D., Warner, D., Netusil, N., Carter, P., Jayne, M., King, P. & Vaska, P. 2003. Low monoamine oxidase B in peripheral organs in smokers. *Proceedings of the National Academy of Sciences of the United States of America*. 100(20):11600-11605.

Fowler, J.S., Volkow, N.D., Wang, G.J., Logan, J., Pappas, N., Shea, C. & MacGregor, R. 1997. Age-related increases in brain monoamine oxidase B in living healthy human subjects. *Neurobiology of Aging*. 18(4):431-435.

Fowler, J.S., Volkow, N.D., Wang, G.J., Pappas, N., Logan, J., Shea, C., Alexoff, D., MacGregor, R.R., Schlyer, D.J., Zezulkova, I. & Wolf, A.P. 1996. Brain monoamine oxidase A inhibition in cigarette smokers. *Proceedings of the National Academy of Sciences of the United States of America*. 93(24):14065-14069.

Giasson, B.I., Duda, J.E., Murray, I.V., Chen, Q., Souza, J.M., Hurtig, H.I., Ischiropoulos, H., Trojanowski, J.Q. & Lee, V.M. 2000. Oxidative damage linked to neurodegeneration by selective alpha-synuclein nitration in synucleinopathy lesions. *Science.* 290(5493):985-989.

Glover, V., Bhattacharya, S.K. & Sandler, M. 1991. Isatin - a new biological factor. *Indian Journal of Experimental Biology*. 29(1):1-5.

Glover, V., Halket, J.M., Watkins, P.J., Clow, A., Goodwin, B.L. & Sandler, M. 1988. Isatin: identity with the purified endogenous monoamine oxidase inhibitor tribulin. *Journal of Neurochemistry*. 51(2):656-659.

Gottowik, J., Malherbe, P., Lang, G., Da Prada, M. & Cesura, A.M. 1995. Structure/function relationships of mitochondrial monoamine oxidase A and B chimeric forms. *The FEBS Journal*. 230(3):934-942.

Graham, D.G. 1978. Oxidative pathways for catecholamines in the genesis of neuromelanin and cytotoxic quinones. *Molecular Pharmacology*. 14(4):633-643.

Greenamyre, J.T., Sherer, T.B., Betarbet, R. & Panov, A.V. 2001. Complex I and Parkinson's disease. *IUBMB Life*. 52(3-5):135-141.

Grimsby, J., Chen, K., Wang, L.J., Lan, N.C. & Shih, J.C. 1991. Human monoamine oxidase A and B genes exhibit identical exon-intron organization. *Proceedings of the National Academy of Sciences of the United States of America*. 88(9):3637-3641.

Grosset, D., Taurah, L., Burn, D.J., MacMahon, D., Forbes, A., Turner, K., Bowron, A., Walker, R., Findley, L., Foster, O., Patel, K., Clough, C., Castleton, B., Smith, S., Carey, G., Murphy, T., Hill, J., Brechany, U., McGee, P., Reading, S., Brand, G., Kelly, L., Breen, K., Ford, S., Baker, M., Williams, A., Hearne, J., Qizilbash, N. & Chaudhuri, K.R. 2007. A multicentre longitudinal observational study of changes in self reported health status in people with Parkinson's disease left untreated at diagnosis. *Journal of Neurology, Neurosurgery, and Psychiatry*. 78(5):465-469.

Haefely, W.E., Kettler, R., Keller, H.H. & Da Prada, M. 1990. Ro 19-6327, a reversible and highly selective monoamine, oxidase B inhibitor: a novel tool to explore the MAO-B function in humans. *Advances in Neurology*. 53:505-512.

Hauptmann, N., Grimsby, J., Shih, J.C. & Cadenas, E. 1996. The metabolism of tyramine by monoamine oxidase A/B causes oxidative damage to mitochondrial DNA. *Archives of Biochemistry and Biophysics*. 335(2):295-304.

Hernán, M.A., Zhang, S.M., Rueda-deCastro, A.M., Colditz, G.A., Speizer, F.E. & Ascherio, A. 2001. Cigarette smoking and the incidence of Parkinson's disease in two prospective studies. *Annals of Neurology*. 50(6):780-786.

Herraiz, T. & Brandt, S.D. 2014. 5-(2-Aminopropyl)indole (5-IT): a psychoactive substance used for recreational purposes is an inhibitor of human monoamine oxidase (MAO). *Drug Testing and Analysis*. 6(7-8):607-613.

Herraiz, T. & Chaparro, C. 2005. Human monoamine oxidase is inhibited by tobacco smoke: beta-carboline alkaloids act as potent and reversible inhibitors. *Biochemical and Biophysical Research Communications*. 326(2):378-386.

Holloway, R.G., Shoulson, I., Fahn, S., Kieburtz, K., Lang, A., Marek, K., McDermott, M., Seibyl, J., Weiner, W., Musch, B., Kamp, C., Welsh, M., Shinaman, A., Pahwa, R., Barclay, L., Hubble, J., LeWitt, P., Miyasaki, J., Suchowersky, O., Stacy, M., Russell, D.S., Ford, B.,Hammerstad, J., Riley, D., Standaert, D., Wooten, F., Factor, S., Jankovic, J., Atassi, F., Kurlan, R., Panisset, M., Rajput, A., Rodnitzky, R., Shults, C., Petsinger, G., Waters, C., Pfeiffer, R., Biglan, K., Borchert, L., Montgomery, A., Sutherland, L., Weeks, C., DeAngelis, M., Sime, E., Wood, S., Pantella, C., Harrigan, M., Fussell, B., Dillon, S., Alexander-Brown, B., Rainey, P., Tennis, M., Rost-Ruffner, E., Brown, D., Evans, S., Berry, D., Hall, J., Shirley, T., Dobson, J., Fontaine, D., Pfeiffer, B., Brocht, A., Bennett, S., Daigneault, S., Hodgeman, K., O'Connell, C., Ross, T., Richard, K., Watts, A. & Parkinson Study Group. 2004. Pramipexole vs levodopa as initial treatment for Parkinson disease: a 4-year randomized controlled trial. *Archives of Neurology*. 61(7):1044-1053.

Hornykiewicz, O. 2001. Dopamine and Parkinson's disease. A personal view of the past, the present, and the future. *Advances in Neurology*. 86:1-11.

Hornykiewicz, O. 2002. Dopamine miracle: from brain homogenate to dopamine replacement. *Movement Disorders*. 17(3):501-508.

Houtsmuller, E.J., Thornton, J.A. & Stitzer, M.L. 2002. Effects of selegiline (L-deprenyl) during smoking and short-term abstinence. *Psychopharmacology*. 163(2):213-220.

Hoy, S.M. & Keating, G.M. 2012. Rasagiline: a review of its use in the treatment of idiopathic Parkinson’s disease. *Drugs*. 72(5):643-669.

Hubálek, F., Binda, C., Li, M., Herzig, Y., Sterling, J., Youdim, M.B., Mattevi, A. & Edmondson, D.E. 2004. Inactivation of purified human recombinant monoamine oxidases A and B by rasagiline and its analogues. *Journal of Medicinal Chemistry*. 47(7):1760-1766.

Hubálek, F., Pohl, J. & Edmondson D.E. 2003. Structural comparison of human monoamine oxidases A and B: mass spectrometry monitoring of cysteine reactivities. *The Journal of Biological Chemistry*. 278(31):28612-28618.

Ives, N.J., Stowe, R.L., Marro, J., Counsell, C., Macleod, A., Clarke, C.E., Gray, R. & Wheatley, K. 2004. Monoamine oxidase type B inhibitors in early Parkinson's disease: meta-analysis of 17 randomised trials involving 3525 patients. *British Medical Journal*. 329(7466):593.

Jankovic, J. 2008. Are adenosine antagonists, such as istradefylline, caffeine, and chocolate, useful in the treatment of Parkinson's disease? *Annals of Neurology*. 63(3):267-269.

Jenner, P. & Marsden, C.D. 1988. MPTP-induced Parkinsonism as an experimental model of Parkinson's Disease. (*In* Jankovic, J. & Tolosa, E. *ed.* Parkinson's Disease and Movement Disorders. Baltimore-Munich: Urban & Schwarzenberg. p.37-48.)

Jenner, P. & Olanow, C.W. 1998. Understanding cell death in Parkinson's disease. *Annals of Neurology*. 44(3S1):S72-S84.

Johnson, S., Stockmeier, C.A., Meyer, J.H., Austin, M.C., Albert, P.R., Wang, J., May, W.L., Rajkowska, G., Overholser, J.C., Jurjus, G., Dieter, L., Johnson, C., Sittman, D.B. & Ou, X.M. 2011. The reduction of R1, a novel repressor protein for monoamine oxidase A, in major depressive disorder. *Neuropsychopharmacology*. 36(10):2139-2148.

Johnston, J.P. 1968. Some observations upon a new inhibitor of monoamine oxidase in brain tissue. *Biochemical Pharmacology*. 17(7):1285-1297.

Kaakkola, S., Mannisto, P.T. & Nissinen, E. 1987. Striatal membrane-bound and soluble catechol-O-methyl-transferase after selective neuronal lesions in the rat. *Journal of Neural Transmission*. 69(3-4):221-228.

Kalgutkar, A.S., Dalvie, D.K., Castagnoli, N. Jr. & Taylor, T.J. 2001. Interactions of nitrogen-containing xenobiotics with monoamine oxidase (MAO) isozymes A and B: SAR studies on MAO substrates and inhibitors. *Chemical Research in Toxicology*. 14(9):1139-1162.

Kalir, A., Sabbagh, A. & Youdim, M.B.H. 1981. Selective acetylenic 'suicide' and reversible inhibitors of monoamine oxidase types A and B. *British Journal of Pharmacology*. 73(1):55-64.

Kaludercic, N., Deshwal, S. & Di Lisa, D. 2014. Reactive oxygen species and redox compartmentalization. *Frontiers in Physiology*. 5:1-15.

Katzenschlager, R., Head, J., Schrag, A., Ben-Shlomo, Y., Evans, A., Lees, A.J. & Parkinson's Disease Research Group of the United Kingdom. 2008. Fourteen-year final report of the randomized PDRG-UK trial comparing three initial treatments in PD. *Neurology*. 71(7):474-480.

Kaur, D., Yantiri, F., Rajagopalan, S., Kumar, J., Mo, J.Q., Boonplueang, R., Viswanath, V., Jacobs, R., Yang, L., Beal, M.F., DiMonte, D., Volitaskis, I., Ellerby, L., Cherny, R.A., Bush, A.I. & Andersen, J.K. 2003. Genetic or pharmacological iron chelation prevents MPTP-induced neurotoxicity in vivo: a novel therapy for Parkinson's disease. *Neuron*. 37(6):899-909.

Kempster, P.A., Hurwitz, B. & Lees, A.J. 2007. A new look at James Parkinson's essay on the shaking palsy. *Neurology*. 69(5):482-485.

Kennedy, B.P., Ziegler, M.G., Alford, M., Hansen, L.A., Thal, L.J. & Masliah E. 2003. Early and persistent alterations in prefrontal cortex MAO A and B in Alzheimer's disease. *Journal of Neural Transmission*. 110(7):789-801.

Kettler, R., Da Prada, M. & Burkard, W.P. 1990. Comparison of monoamine oxidase-A inhibition by moclobemide *in vitro* and *ex vivo* in rats. *Acta Psychiatrica Scandinavica*. 360:101-102.

Knoll, J. 1988. The striatal dopamine dependency of life span in male rats. Longevity study with (-)-deprenyl. *Mechanisms of Ageing and Development*. 46(1-3):237-262.

Kochersperger, L.M., Parker, E.L., Siciliano, M., Darlington, G.J. & Denney, R.M. 1986. Assignment of genes for human monoamine oxidases A and B to the X chromosome. *Journal of Neuroscience Research*. 16(4):601-616.

Kunduzova, O.R., Bianchi, P., Parini, A. & Cambon, C. 2002. Hydrogen peroxide production by monoamine oxidase during ischemia/reperfusion. *European Journal of Pharmacology.* 448(2-3):225-230.

Lange, D.J., Murphy, P.L., Diamond, B., Appel, V., Lai, E.C., Younger, D.S. & Appel, S.H. 1998. Selegiline is ineffective in a collaborative double-blind, placebo-controlled trial for treatment of amyotrophic lateral sclerosis. *Archives of Neurology*. 55(1):93-96.

Lees, A.J. 1995. Comparison of therapeutic effects and mortality data of levodopa and levodopa combined with selegiline in patients with early, mild Parkinson's disease. *British Medical Journal*. 311(7020):1602-1607.

Lees, A.J., Hardy, J. & Revesz, T. 2009. Parkinson's disease. *Lancet*. 373(9680):2055-2066.

Legoabe, L.J., Petzer, A. & Petzer, J.P. 2015. The synthesis and evaluation of C7-substituted α-tetralone derivatives as inhibitors of monoamine oxidase. *Chemical Biology & Drug Design*. 86(4):895-904.

Legoabe, L.J., Petzer, A. & Petzer, J.P. 2014. α-Tetralone derivatives as inhibitors of monoamine oxidase. *Bioorganic & Medicinal Chemistry Letters*. 24(12):2758-2763.

LeWitt, P.A. & Taylor, D.C. 2008. Protection against Parkinson's disease progression: Clinical experience. *Neurotherapeutics*. 5(2):210-225.

Liotti, M., Mayberg, H.S., McGinnis, S., Brannan, S.L. & Jerabek, P. 2002. Unmasking disease-specific cerebral blood flow abnormalities: mood challenge in patients with remitted unipolar depression. *The American Journal of Psychiatry*. 159(11):1830-1840.

Lum, C.T. & Stahl, S.M. 2012. Opportunities for reversible inhibitors of monoamine oxidase-A (RIMAs) in the treatment of depression. *CNS Spectrums*. 17(3):107-120.

Magyar, L. 1993. Pharmacology of monoamine oxidase type-B inhibitors. (*In* Szelényi, I. *ed*. Inhibitors of Monoamine Oxidase B, Pharmacology and Clinical Use in Neurodegenerative Disorders. Birkhauser Verlag: Basel. p.125-143.)

Malnoë, A. & Benedetti, M.S. 1979. Metabolic fate of 3-(3-methylphenyl)-5-hydroxymethyl-2-oxazolidinone (toloxatone), a new antidepressant agent, in man. *Xenobiotica*. 9(5):281-288.

Mann, J.J., Aarons, S.F., Frances, A.J. & Brown, R.D. 1984. Studies of selective and reversible monoamine oxidase inhibitors. *Journal of Clinical Psychiatry*. 45(7P2):62-66.

Mann, J.J., Aarons, S.F., Wilner, P.J., Keilp, J.G., Sweeney, J.A., Pearlstein, T., Frances, A.J., Kocsis, J.H. & Brown, R.P. 1989. A controlled study of the antidepressant efficacy and side effects of (-)-deprenyl. A selective monoamine oxidase inhibitor. *Archives of General Psychiatry*. 46(1):45-50.

Marin, D.B., Bierer, L.M., Lawlor, B.A., Ryan, T.M., Jacobson, R., Schmeidler, J., Mohs, R.C. & Davis, K.L. 1995. L-Deprenyl and physostigmine for the treatment of Alzheimer's disease. *Psychiatry Research*. 58(3):181-189.

Maurel, A., Hernanded, C., Kunduzova, O., Bompart, G., Cambon, C., Parini, A. & Francés, B. 2003. Age-dependent increase in hydrogen peroxide production by cardiac monoamine oxidase A in rats. *American Journal of Physiology Heart and Circulatory Physiology*. 284(4):H1460-H1467.

Medvedev, A.E., Goodwin, B., Clow, A., Halket, J., Glover, V. & Sandler, M. 1992. Inhibitory potency of some isatin analogues on human monoamine oxidase A and B. *Biochemical Pharmacology*. 44(3):590-592.

Medvedev, A.E., Ivanov, A.S., Kamyshanskaya, N.S., Kirkel, A.Z., Moskvitina, T.A., Gorkin, V.Z., Li, N.Y. & Marshakov, V.Y. 1995. Interaction of indole derivatives with monoamine oxidase A and B. Studies on the structure-inhibitory activity relationship. *Biochemistry and Molecular Biology International*. 36(1):113-122.

Meyer, J.H. 2012. Neuroimaging markers of cellular function in major depressive disorder: implications for therapeutics, personalized medicine, and prevention. *Clinical Pharmacology and Therapeutics*. 91(2):201-14.

Meyer, J.H., Ginovart, N., Boovariwala, A., Sagrati, S., Hussey, D., Garcia, A., Young, T., Praschak-Rieder, N., Wilson, A.A. & Houle, S. 2006. Elevated monoamine oxidase a levels in the brain: an explanation for the monoamine imbalance of major depression. *Archives of General Psychiatry*. 63(11):1209-1216.

Meyer, J.H., Wilson, A.A., Sagrati, S., Miler, L., Rusjan, P., Bloomfield, P.M., Clark, M., Sacher, J., Voineskos, A.N. & Houle, S. 2009. Brain monoamine oxidase A binding in major depressive disorder: relationship to selective serotonin reuptake inhibitor treatment, recovery, and recurrence. *Archives of General Psychiatry.* 66(12):1304-1312.

Mitoma, J. & Ito, A. 1992. Mitochondrial targeting signal of rat liver monoamine oxidase B is located at its carboxy terminus. *The Journal of Biochemistry*. 111(1):20-24.

Mounsey, R.B. & Teismann, P. 2012. Chelators in the treatment of iron accumulation in Parkinson's disease. *International Journal of Cell Biology*. 2012:1-12.

Naoi, M., Maruyama, W. & Inaba-Hasegawa, K. 2013. Revelation in the neuroprotective functions of rasagiline and selegiline: the induction of distinct genes by different mechanisms. *Expert Review of Neurotherapeutics*. 13(6):671-684.

Narendra, D., Tanaka, A., Suen, D.F. & Youle, R.J. 2008. Parkin is recruited selectively to impaired mitochondria and promotes their autophagy. *Journal of Cell Biology*. 183(5):795-803.

Neuvonen, P.J., Pohjola-Sintonen, S., Tacke, U. & Vuori, E. 1993. Five fatal cases of serotonin syndrome after moclobemide-citalopram or moclobemide-clomipramine overdoses. *Lancet*. 342(8884):1419.

Nicklas, W.J., Youngster, S.K., Kindt, M.V. & Heikkila, R.E. 1987. MPTP, MPP^+ and mitochondrial function. *Life Sciences*. 40(8):721-729.

Olanow, C.W. &, McNaught, K.S. 2006. Ubiquitin-proteasome system and Parkinson's disease. *Movement Disorders*. 21(11):1806-1823.

Olanow, C.W., Hauser, R.A., Jankovic, J., Langston, W., Lang, A., Poewe, W., Tolosa, E., Stocchi, F., Melamed, E., Eyal, E. & Rascol O. 2008. A randomized, double-blind, placebo-controlled, delayed start study to assess rasagiline as a disease modifying therapy in Parkinson's disease (the ADAGIO study): rationale, design, and baseline characteristics. *Movement Disorders*. 23(15):2194-2201.

Olanow, C.W., Rascol, O., Hauser, R., Feigin, P.D., Jankovic, J., Lang, A., Langston, W., Melamed, E., Poewe, W., Stocchi, F., Tolosa, E & ADAGIO Study Investigators. 2009. A double-blind, delayed-start trial of rasagiline in Parkinson's disease. *The New England Journal of Medicine*. 361(13):1268-1278.

Oreland, L., Arai, Y., Strenström, A. & Fowler, C.J. 1983. Monoamine oxidase activity and localization in the brain and the activity in relation to psychiatric disorders1. (*In* Beckmann, A. & Riederer, P. *ed*. Monoamine oxidase and its selective inhibitors. Basel: Karger. p.246-254.)

Ou, X.M., Chen, K. & Shih, J.C. 2006. Glucocorticoid and androgen activation of monoamine oxidase A is regulated differently by R1 and Sp1. *The Journal of Biological Chemistry*. 281(30):21512-21525.

Pålhagen, S., Heinonen, E., Hägglund, J., Kaugesaar, T., Mäki-Ikola, O., Palm, R. & Swedish Parkinson Study Group. 2006. Selegiline slows the progression of the symptoms of Parkinson disease. *Neurology*. 66(8):1200-1206.

Pålhagen, S., Heinonen, E.H., Hägglund, J., Kaugesaar, T., Kontants, H., Mäki-Ikola, O., Palm, R. & Turunen, J. 1998. Selegiline delays the onset of disability in de novo parkinsonian patients. Swedish Parkinson Study Group. *Neurology*. 51(2):520-525.

Palmer, T. & Bonner, P. 2007. Principles of Biochemistry with a human focus. 1st *ed*. Toronto, Canada: Brooks/Cole Thomson Learning. p.62-70.

Panisset, M., Chen, J.J., Rhyee, S.H., Conner, J., Mathena, J. & STACCATO study investigators. 2014. Serotonin toxicity association with concomitant antidepressants and rasagiline treatment: retrospective study (STACCATO). *Pharmacotherapy*. 34(12):1250-1258.

Parkinson, J. 2002. An essay on the shaking palsy. 1817. *The Journal of Neuropsychiatry and Clinical Neurosciences*. 14(2):223-236.

Parkinson Study Group. 1993. Effects of tocopherol and deprenyl on the progression of disability in early Parkinson's disease. *The New England Journal of Medicine*. 328(3):176-183.

Parkinson Study Group. 2002. A controlled trial of rasagiline in early Parkinson disease: the TEMPO Study. *Archives of Neurology*. 59(12):1937-1943.

Parkinson Study Group. 2004. A controlled, randomized, delayed-start study of rasagiline in early Parkinson disease. *Archives of Neurology*. 61(4):561-566.

Parkinson Study Group. 2005. A randomized placebo-controlled trial of rasagiline in levodopa-treated patients with Parkinson disease and motor fluctuations: the PRESTO study. *Archives of Neurology*. 62(2):241-248.

Patel, S.V., Tariot, P.N. & Asnis, J. 1996. L-Deprenyl augmentation of fluoxetine in a patient with Huntington's disease. *Annals of Clinical Psychiatry*. 8(1):23-26.

Petzer, A., Pienaar, A. & Petzer, J.P. 2013. The inhibition of monoamine oxidase by esomeprazole. *Drug Research*. 63(9):462-467.

Poltyrev, T., Gorodetsky, E., Bejar, C., Schorer-Apelbaum, D. & Weinstock, M. 2005. Effect of chronic treatment with ladostigil (TV-3326) on anxiogenic and depressive-like behaviour and on activity of the hypothalamic-pituitary-adrenal axis in male and female prenatally stressed rats. *Psychopharmacology*. 181(1):118-125.

Rajkowska, G. & Stockmeier, C.A. 2013. Astrocyte pathology in major depressive disorder: insights from human postmortem brain tissue. *Current Drug Targets*. 14(11):1225-1236.

Rascol, O., Brooks, D.J., Korczyn, A.D., De, D.P.P., Clarke, C.E. & Lang, A.E. 2000. A five-year study of the incidence of dyskinesia in patients with early Parkinson’s disease who were treated with ropinirole or levodopa. *The New England Journal of Medicine*. 342(20):1484-1491.

Rascol, O., Brooks, D.J., Melamed, E., Oertel, W., Poewe, W., Stocchi, F., Tolosa, E. & LARGO study group. 2005. Rasagiline as an adjunct to levodopa in patients with Parkinson's disease and motor fluctuations (LARGO, Lasting effect in Adjunct therapy with Rasagiline Given Once daily, study): a randomised, double-blind, parallel-group trial. *Lancet.* 365(9463):947-954.

Reijnders, J.S., Ehrt, U., Weber, W.E., Aarsland, D. & Leentjens, A.F. 2008. A systematic review of prevalence studies of depression in Parkinson's disease. *Movement Disorders*. 23(2):183-189.

Ressler, K.J. & Mayberg, H.S. 2007. Targeting abnormal neural circuits in mood and anxiety disorders: from the laboratory to the clinic. *Nature Neuroscience*. 10(9):1116-1124.

Richard, I.H., McDermott, M.P., Kurlan, R., Lyness, J.M., Como, P.G., Pearson, N., Factor, S.A., Juncos, J., Serrano Ramos, C., Brodsky, M., Manning, C., Marsh, L., Shulman, L., Fernandez, H.H., Black, K.J., Panisset, M., Christine, C.W., Jiang, W., Singer, C., Horn, S., Pfeiffer, R., Rottenberg, D., Slevin, J., Elmer, L., Press, D., Hyson, H.C., McDonald, W. & SAD-PD Study Group. 2012. A randomized, double-blind, placebo-controlled trial of antidepressants in Parkinson disease. *Neurology*. 78(16):1229-1236.

Riederer, P. & Müller, T. 2017. Use of monoamine oxidase inhibitors in chronic neurodegeneration. *Expert Opinion on Drug Metabolism & Toxicology*. 13(2):233-240.

Riederer, P., Youdim, M.B., Rausch, W.D., Birkmayer, W., Jellinger, K. & Seemann, D. 1978. On the mode of action of L-deprenyl in the human central nervous system. *Journal of Neural Transmission*. 43(3-4):217-226.

Ross, S.B. 1987. Distribution of the two forms of monoamine oxidase within monoaminergic neurons of the guinea pig brain. *Journal of Neurochemistry*. 48(2):609-614.

Sagot, Y., Toni, N., Perrelet, D., Lurot, S., King, B., Rixner, H., Mattenberger, L., Waldmeier, P.C. & Kato, A.C. 2000. An orally active anti-apoptotic molecule (CGP 3466B) preserves mitochondria and enhances survival in an animal model of motoneuron disease. *British Journal of Pharmacology*. 131(4):721-728.

Samii, A., Nutt, J.G. & Ransom, B.R. 2004. Parkinson's disease. *Lancet*. 363(9423):1783-1793.

Sano, H. 2000. Biochemistry of the extrapyramidal system. *Parkinsonism and Related Disorders*. 6(1):3-6.

Sareen, K., Kohli, R.P., Amma, M.K.P. & Gujral, M.L. 1962. Anticonvulsant drugs based on the neurochemistry of seizures. *Indian Journal of Physiology and Pharmacology*. 6:87-94.

Saura, J., Bleuel, Z., Ulrich, J., Mendelowitsch, A., Chen, K., Shih, J.C., Malherbe, P., Da Prada, M. & Richards, J.G. 1996. Molecular neuroanatomy of human monoamine oxidases A and B revealed by quantitative enzyme radioautography and in situ hybridization histochemistry. *Neuroscience*. 70(3):755-774.

Saura, J., Kettler, R., Da Prada, M. & Richards, J.G. 1992. Quantitative enzyme radioautography with H-Ro 41-1049 and H-Ro 19-6327 *in vitro*: localization and abundance of MAO-A and MAO-B in rat CNS, peripheral organs, and human brain. *The Journal of Neuroscience*. 12(5):1977-1999.

Saura Marti, J., Kettler, R., Da Prada, M. & Richards, J.G. 1990. Molecular neuroanatomy of MAO-A and MAO-B. *Journal of Neural Transmission*. 32:49-53.

Schmidt, H.D., Shelton, R.C. & Duman, R.S. 2011. Functional biomarkers of depression: diagnosis, treatment, and pathophysiology. *Neuropsychopharmacology*. 36(12):2375-2394.

Seidel, J. & Wenzel, J. 1979. Some histochemical and electrophysiological effects of isatin. *Polish Journal of Pharmacology and Pharmacy*. 31(4):407-412.

Sherman, M.Y. & Goldberg, A.L. 2001. Cellular defences against unfolded proteins: a cell biologist thinks about neurodegenerative diseases. *Neuron*. 29(1):15-32.

Shi, Z.H., Nie, G., Duan, X.L., Rouault, T., Wu, W.S., Ning, B., Zhang, N., Chang, Y.Z. & Zhao, B.L. 2010. Neuroprotective mechanism of mitochondrial ferritin on 6-hydroxydopamine-induced dopaminergic cell damage: implication for neuroprotection in Parkinson's disease. *Antioxidants and Redox Signaling*. 13(6):783-796.

Shih, J.C., Chen, K. & Geha, R.M. 1998. Determination of regions important for monoamine oxidase (MAO) A and B substrate and inhibitor sensitivities. *Journal of Neural Transmission*. 52:1-8.

Shih, J.C., Chen, K. & Ridd, M.J. 1999. Monoamine oxidase: rrom genes to behavior. *Annual Review of Neuroscience*. 22:197-217.

Sivenius, J., Sarasoja, T., Aaltonen, H., Heinonen, E., Kilkku, O. & Reinikainen, K. 2001. Selegiline treatment facilitates recovery after stroke. *Neurorehabilitation and Neural Repair*. 15(3):183-190.

Slotkin, T.A., Seidler, F.J. & Ritchie, J.C. 1998. Effects of aging and glucocorticoid treatment on monoamine oxidase subtypes in rat cerebral cortex: therapeutic implications. *Brain Research Bulletin*. 47(4):345-348.

Sofic, E., Riederer, P., Heinsen, H., Beckmann, H., Reynolds, G.P., Hebenstreit, G. & Youdim, M.B. 1988. Increased iron (III) and total iron content in post mortem substantia nigra of parkinsonian brain. *Journal of Neural Transmission*. 74(3):199-205.

Son, S.Y., Ma, J., Kondou, Y., Yoshimura, M., Yamashita, E. & Tsukihara, T. 2008. Structure of human monoamine oxidase A at 2.2-Å resolution: the control of opening the entry for substrates/inhibitors. *Proceedings of the National Academy of the Sciences of the United States of America*. 105(15):5739–5744.

Squires, R.F. 1972. Multiple forms of monoamine oxidase in intact mitochondria as characterized by selective inhibitors and thermal stability: a comparison of eight mammalian species. *Advances in Biochemical Psychopharmacology*. 5:355-370.

Steinberg, M. & Morin, A.K. 2007. Mild serotonin syndrome associated with concurrent linezolid and fluoxetine. *American Journal of Health-System Pharmacy*. 64(1):59-62.

Strydom, B., Malan, S.F., Castagnoli, N. Jr., Bergh, J.J. & Petzer, J.P. 2010. Inhibition of monoamine oxidase B by 8-benzyloxycaffeine analogues. *Bioorganic & medicinal chemistry*. 18(3):1018-1028.

Strydom, B., Bergh, J.J. & Petzer, J.P. 2012. The inhibition of monoamine oxidase by 8-(2-phenoxyethoxy) caffeine analogues. *Arzneimittelforschung*. *62*(11):513-518.

Sternbach, H. 1991. The serotonin syndrome. *The American Journal of Psychiatry*. 148(6):705-713.

Stocchi, F., Arnold, G., Onofrj, M., Kwiecinski, H., Szczudlik, A., Thomas, A., Bonuccelli, U., Van Dijk, A., Cattaneo, C., Sala, P., Fariello, R.G. & Safinamide Parkinson's Study Group. 2004. Improvement of motor function in early Parkinson disease by safinamide. *Neurology*. 63(4):746-748.

Stowe, R., Ives, N., Clarke, C.E., Handley, K., Furmston, A., Deane, K., van Hilten, J.J., Wheatley, K. & Gray, R. 2011. Meta-analysis of the comparative efficacy and safety of adjuvant treatment to levodopa in later Parkinson's disease. *Movement Disorders*. 26(4):587-598.

Sturza, A., Duicu, O.M., Vaduva, A., Dănilă, M.D., Noveanu, L., Varró, A. & Muntean, D.M. 2015. Monoamine oxidases are novel sources of cardiovascular oxidative stress in experimental diabetes. *Canadian Journal of Physiology and Pharmacology*. 93(7):555-561.

Tanner, C.M. 2003. Is the cause of Parkinson's disease environmental or hereditary? Evidence from twin studies. *Therapeutic Advances in Neurological Disorders*. 91:133-142.

Taylor, K.S., Counsell, C.E., Gordon, J.C. & Harris, C.E. 2005. Screening for undiagnosed parkinsonism among older people in general practice. *Age and Ageing*. 34:501-504.

Thacker, E.L., Chen, H., Patel, A.V., McCullough, M.L., Calle, E.E., Thun, M.J., Schwarzschild, M.A. & Ascherio, A. 2008. Recreational physical activity and risk of Parkinson's disease. *Movement Disorders*. 23(1):69-74.

Tipton, K.F., Boyce, S., O'Sullivan, J., Davey, G.P. & Healy, J. 2004. Monoamine oxidases: certainties and uncertainties. *Current Medicinal Chemistry*. 11(15):1965-1982.

Trivedi, M.H., Rush, A.J.,Wisniewski, S.R., Nierenberg, A.A., Warden, D., Ritz, L., Norquist, G., Howland, R.H., Lebowitz, B., McGrath, P.J., Shores-Wilson, K., Biggs, M.M., Balasubramani, G.K., Fava, M. & STAR*D Study Team. 2006. Evaluation of outcomes with citalopram for depression using measurement-based care in STAR*D: implications for clinical practice. *The American Journal of Psychiatry*. 163(1):28-40.

Twelves, D., Perkins, K.S. & Counsell, C. 2003. Systematic review of incidence studies of Parkinson's disease. *Movement Disorders*. 18(1):19-31.

Umbarkar, P., Singh, S., Arkat, S., Bodhankar, S.L., Lohidasan, S. & Sitasawad, S.L. 2015. Monoamine oxidase-A is an important source of oxidative stress and promotes cardiac dysfunction, apoptosis, and fibrosis in diabetic cardiomyopathy. *Free Radical Biology and Medicine*. 87:263-273.

Van Gelder, W., Huijskes-Heins, M.I., Cleton-Soeteman, M.I., van Dijk, J.P. & van Eijk, H.G. 1998. Iron uptake in blood–brain barrier endothelial cells cultured in iron-depleted and iron-enriched media. *Journal of Neurochemistry*. 71(3):1134–1140.

Vistelle, R., Lamiable, D., Zinsou, M., Leon, A. & Wiczewski, M. 1992. Toloxatone pharmacokinetics in the plasma and cerebrospinal fluid of the rabbit. *Journal of Pharmacy and Pharmacology*. 44(2):124-126.

Von Korff, R.W. 1979. Monoamine oxidase: unanswered questions. (*In* Singer, T.P., von Korff, R.W. & Murphy, D.L., *ed*. Monoamine oxidase: structure, function and altered functions. New York: Academic Press. p.1-7.)

Vondriska, T.M., Klein, J.B. & Ping, P. 2001. Use of functional proteomics to investigate PKC epsilon-mediated cardioprotection: the signaling module hypothesis. *The American Journal of Physiology-Heart and Circulatory Physiology*. 280(4):H1434-H1441.

Waibel, S., Reuter, A., Malessa, S., Blaugrund, E. & Ludolph, A.C. 2004. Rasagiline alone and in combination with riluzole prolongs survival in an ALS mouse model. *Journal of Neurology*. 251(9):1080-1084.

Watkins, P., Clow, A., Glover, V., Halket, J., Przyborowska, A. & Sandler, M. 1990. Isatin, regional distribution in rat brain and tissues. *Neurochemistry International*. 17(2):321-323.

Weinreb, O., Amit, T., Riederer, P., Youdim, M.B. & Mandel, S.A. 2011. Neuroprotective profile of the multitarget drug rasagiline in Parkinson's disease. *International Review of Neurobiology*. 100:127-149.

Weinreb, O., Badinter, F., Amit, T., Bar-Am, O. & Youdim, M.B. 2015. Effect of long-term treatment with rasagiline on cognitive deficits and related molecular cascades in aged mice. *Neurobiology of Aging*. 36(9):2628-2636.

Weinreb, O., Bar-Am, O., Amit, T., Chillag-Talmor, O. & Youdim M.B. 2004. Neuroprotection via pro-survival protein kinase C isoforms associated with Bcl-2 family members. *FASEB Journal*. 18(12):1471-1473.

Weinstock, M., Gorodetsky, E., Poltyrev, T., Gross, A., Sagi, Y. & Youdim, M.B. 2003. A novel cholinesterase and brain-selective monoamine oxidase inhibitor for the treatment of dementia comorbid with depression and Parkinson's disease. *Progress in Neuro-Psychopharmacology and Biological Psychiatry*. 27(4): 555-561.

Weintraub, D., Moberg, P.J., Duda, J.E., Katz, I.R. & Stern, M.B. 2003. Recognition and treatment of depression in Parkinson's disease. *Journal of Geriatric Psychiatry and Neurology*. 16(3):178-183.

Westlund, K.N., Denney, R.M., Rose, R.M. & Abell, C.W. 1988. Localization of distinct monoamine oxidase A and monoamine oxidase B cell populations in human brainstem. *Neuroscience*. 25(2):439-456.

Westlund, K.N., Denney, R.M., Kochersperger, L.M., Rose, R.M. & Abell, C.W. 1985. Distinct monoamine oxidase A and B populations in primate brain. *Science*. 230(4722):181-183.

World Health Organization. 2008: The Global Burden of Disease: 2004 update World Health Organization, Geneva.

Wu, H., Luo, J., Yu, H., Rattner, A., Mo, A., Wang, Y., Smallwood, P.M., Erlanger, B., Wheelan, S.J. & Nathans, J. 2014. Cellular resolution maps of X-chromosome inactivation: implications for neural development, function, and disease. *Neuron*. 81(1):103-119.

Xu, H., Xiao, T., Chen, C.H., Li, W., Meyer, C.A., Wu, Q., Wu, D., Cong, L., Zhang, F., Liu, J.S., Brown, M. & Liu, X.S. 2015. Sequence determinants of improved CRISPR sgRNA design. *Genome Research*. 25(8):1147-1157.

You, L.H., Li, F., Wang, L., Zhao, S.E., Wang, S.M., Zhang, L.L., Zhang, L.H., Duan, X.L., Yu, P. & Chang, Y.Z. 2015. Brain iron accumulation exacerbates the pathogenesis of MPTP-induced Parkinson's Disease. *Neuroscience*. 284:234-246.

Youdim, M.B. & Bakhle, Y.S. 2006. Monoamine oxidase: isoforms and inhibitors in Parkinson's disease. *British Journal of Pharmacology*. 147(S1):S287-S296.

Youdim, M.B., Edmondson, D. & Tipton, K.F. 2006. The therapeutic potential of monoamine oxidase inhibitors. *Nature Reviews Neuroscience*. 7(4):295-309.

Youdim, M.B., Gross, A. & Finberg, J.P. 2001. Rasagiline [N-propargyl-1R(+)-aminoindan], a selective and potent inhibitor of mitochondrial monoamine oxidase B. *British Journal of Pharmacology*. 132(2):500-506.

Youdim, M.B., Kupershmidt, L., Amit, T. & Weinreb, O. 2014. Promises of novel multi-target neuroprotective and neurorestorative drugs for Parkinson's disease. *Parkinsonism and Related Disorders*. 20(S1):S132-S136.

Youdim, M.B. & Weinstock, M. 2001. Molecular basis of neuroprotective activities of rasagiline and the anti-Alzheimer drug TV3326 [(N-propargyl-(3R)aminoindan-5-YL)-ethyl methyl carbamate]. *Cellular and Molecular Neurobiology*. 21(6):555-573.

Zagmutt, F.J. & Tarrants, M.L. 2012. Indirect comparisons of adverse events and dropout rates in early Parkinson's disease trials of pramipexole, ropinirole, and rasagiline. *Journal of Neuroscience*. 122(7):345-353.

Zisook, S. 1985. A clinical overview of monoamine oxidase inhibitors. *Psychosomatics*. 26(3):240-246.

ANNEXURES

Compound 1a - ^{13}C NMR spectrum:

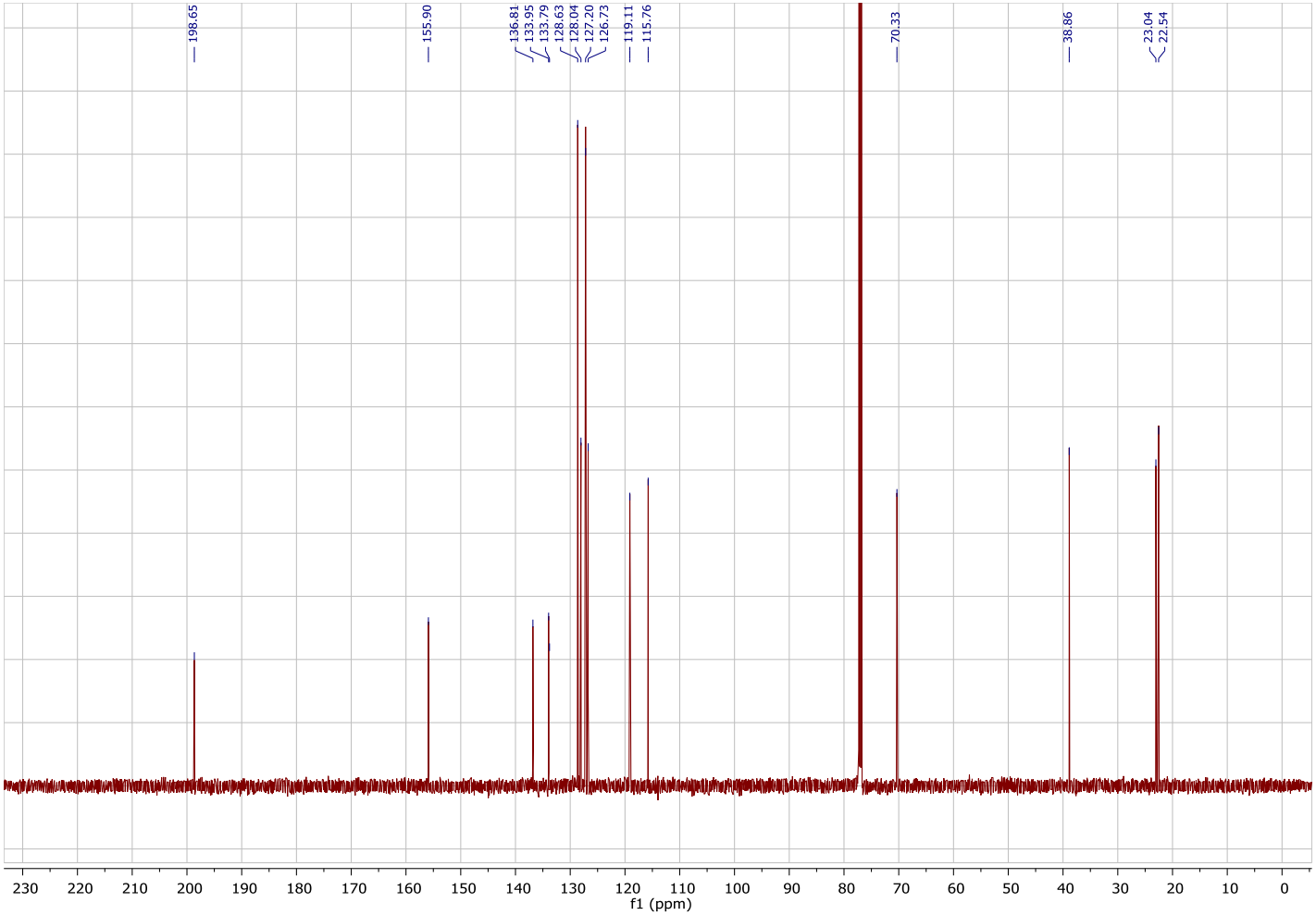

Compound 1a - ^{1}H NMR spectrum:

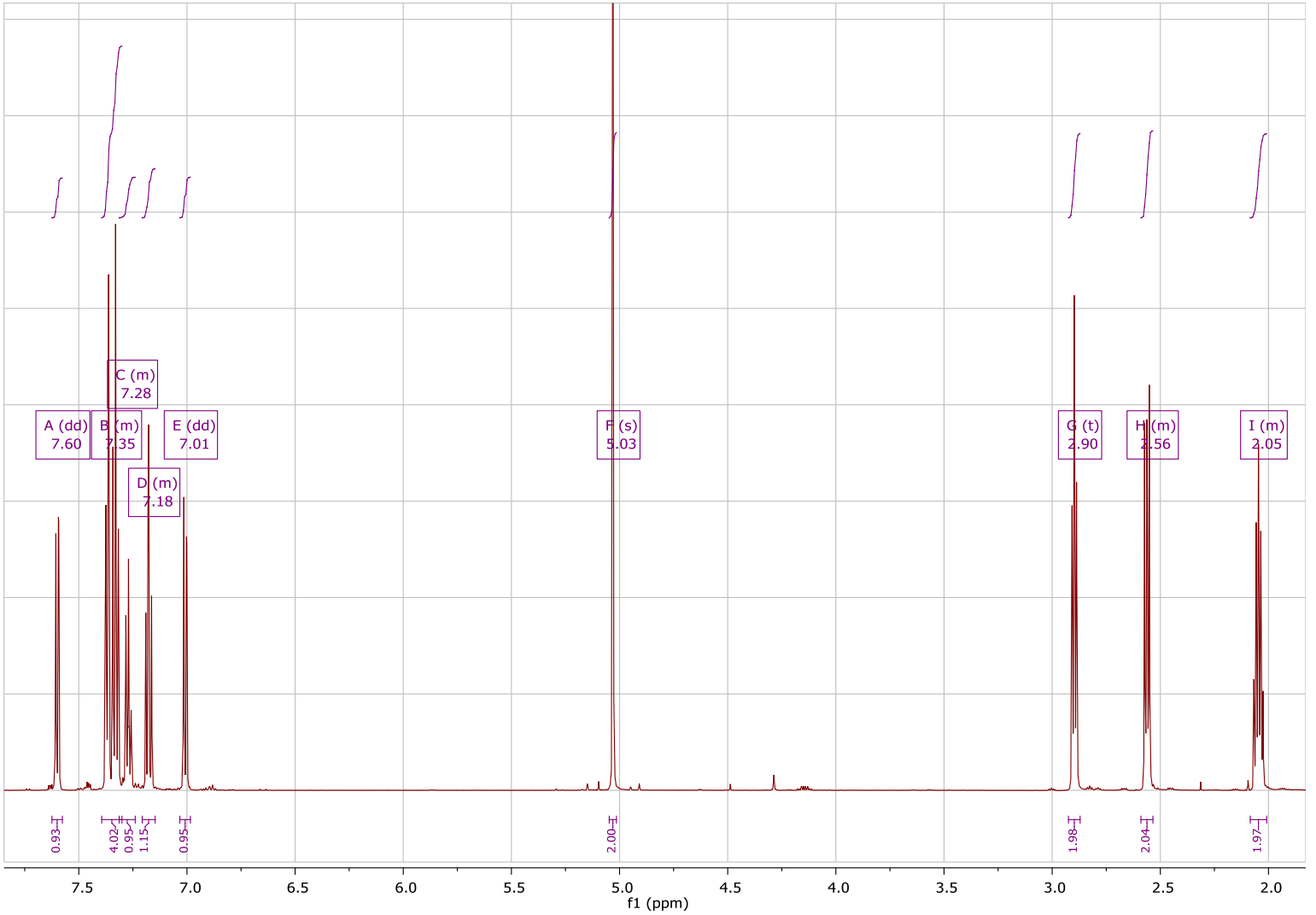

Compound 1b – ^{13}C NMR spectrum:

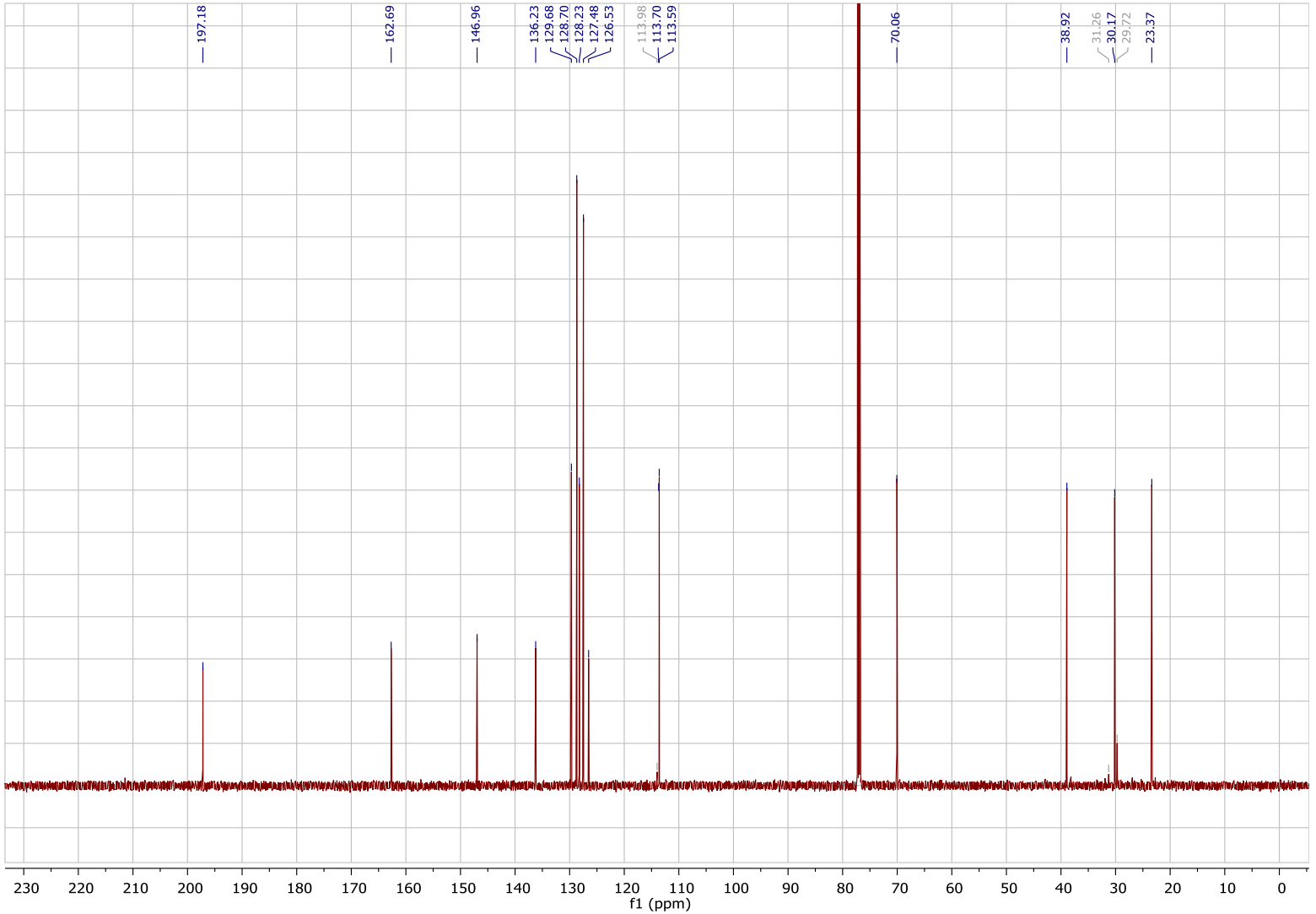

Compoud 1b – ^{1}H NMR spectrum:

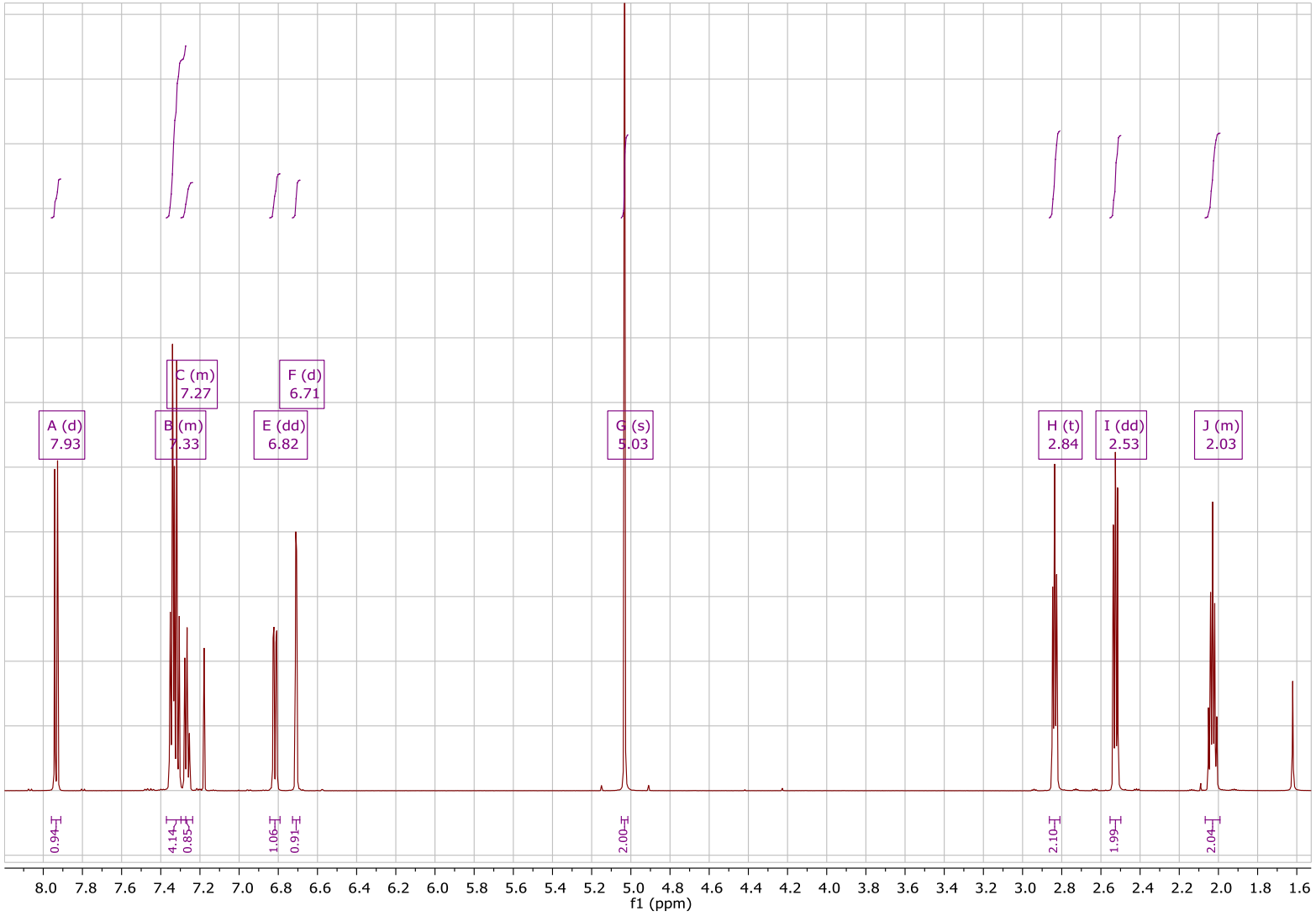

Compound 1c - ^{13}C NMR spectrum:

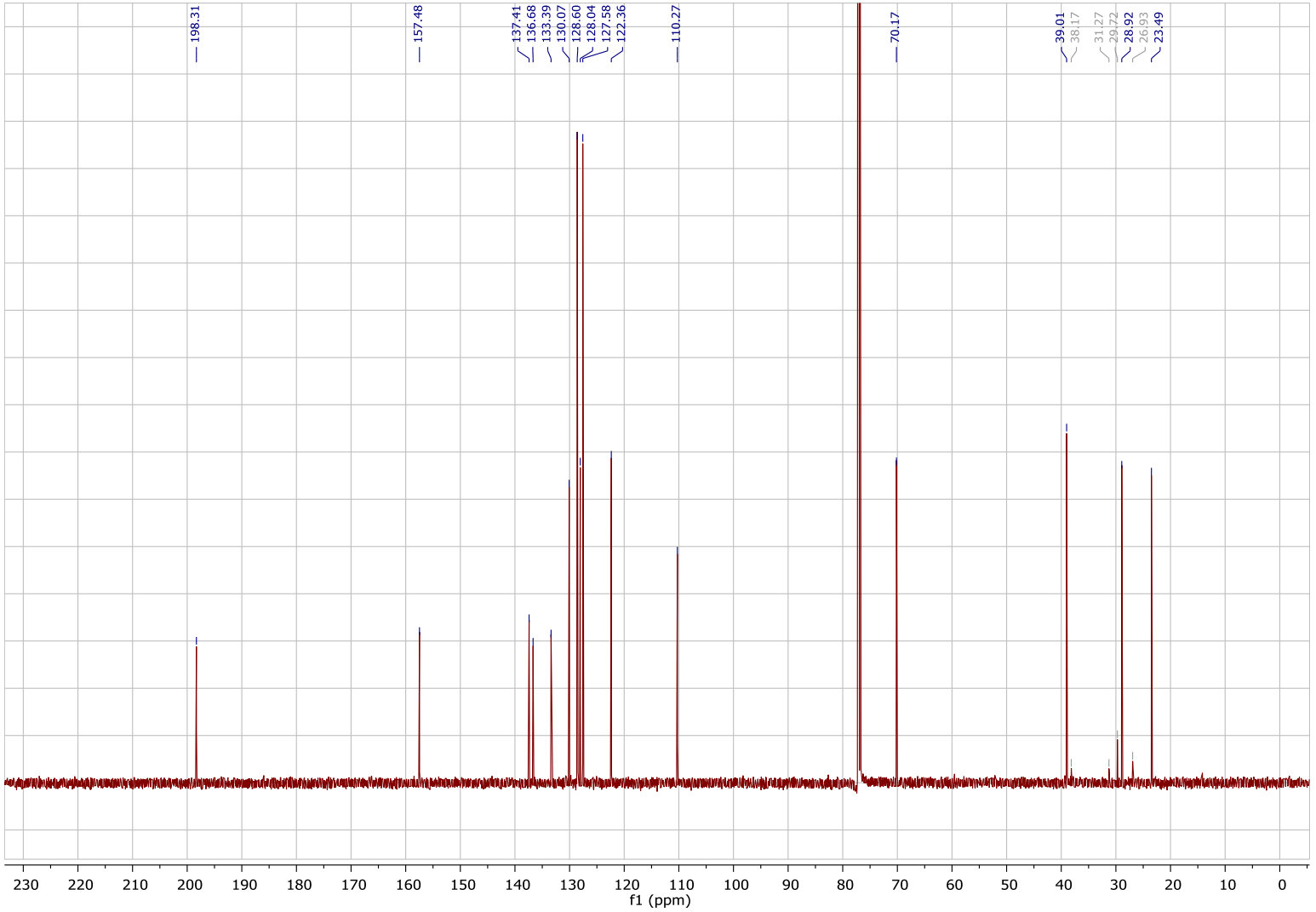

Compound 1c – ^{1}H NMR spectrum:

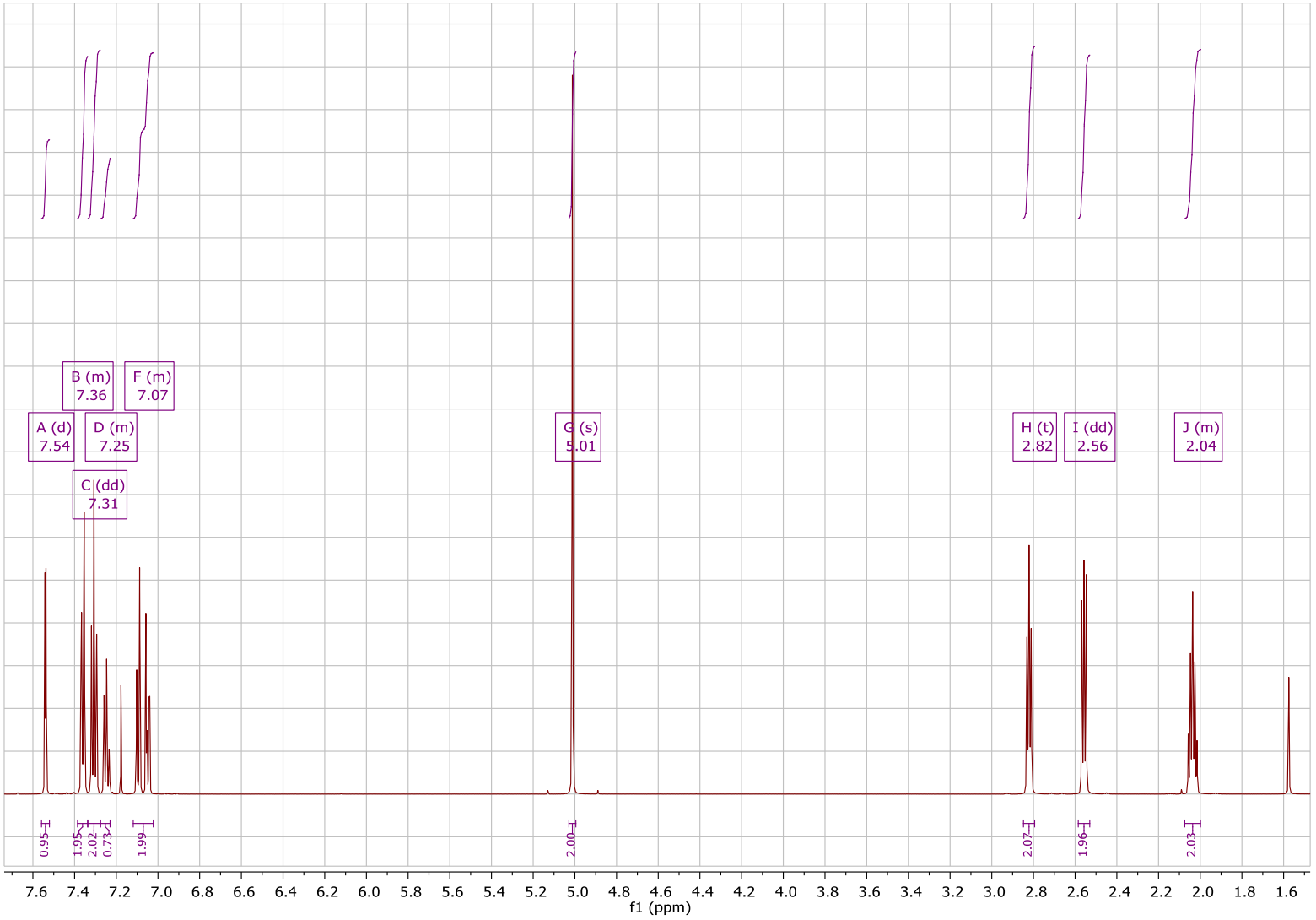

Compound 1d - ^{13}C NMR spectrum:

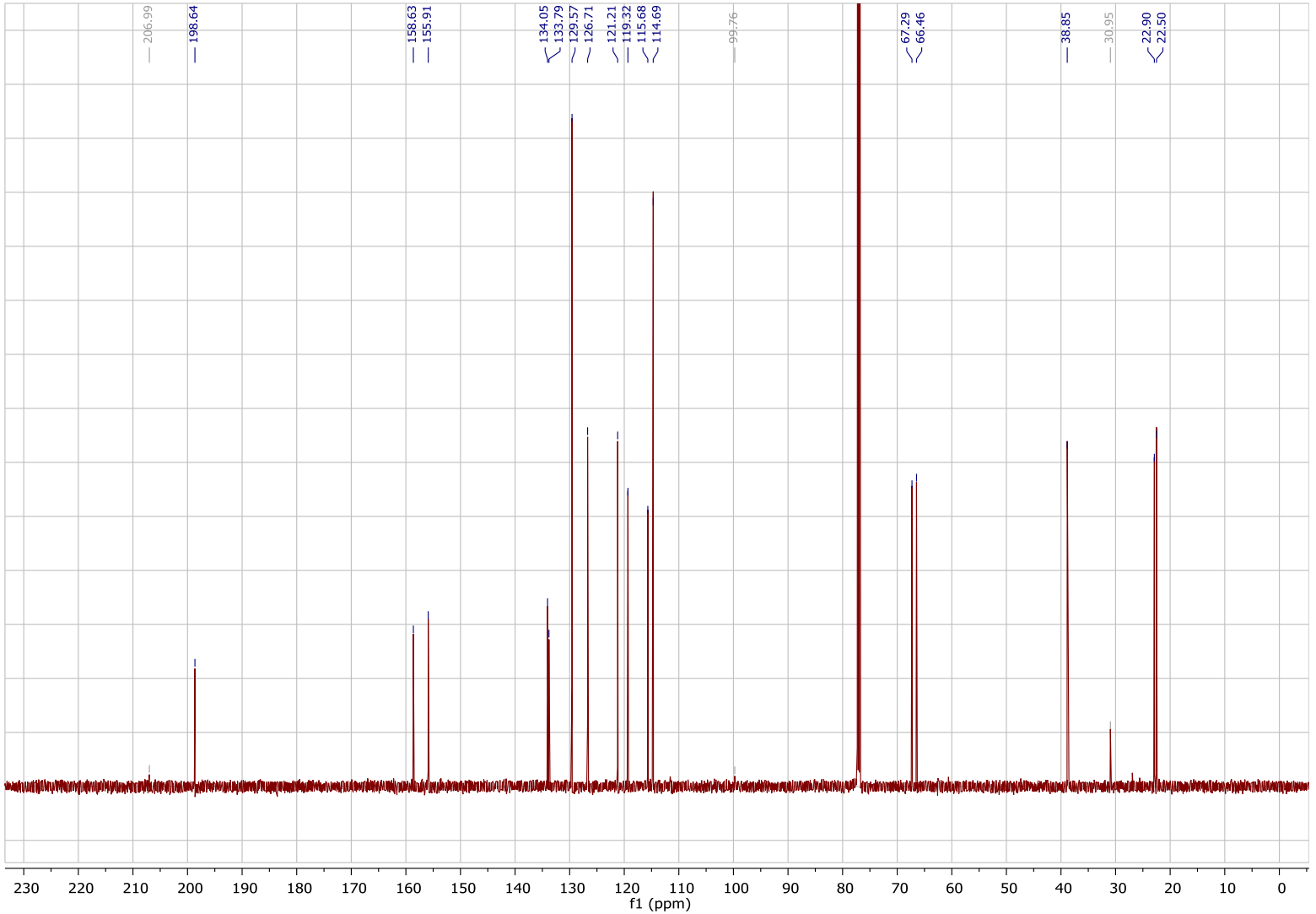

Compound 1d – ^{1}H NMR spectrum:

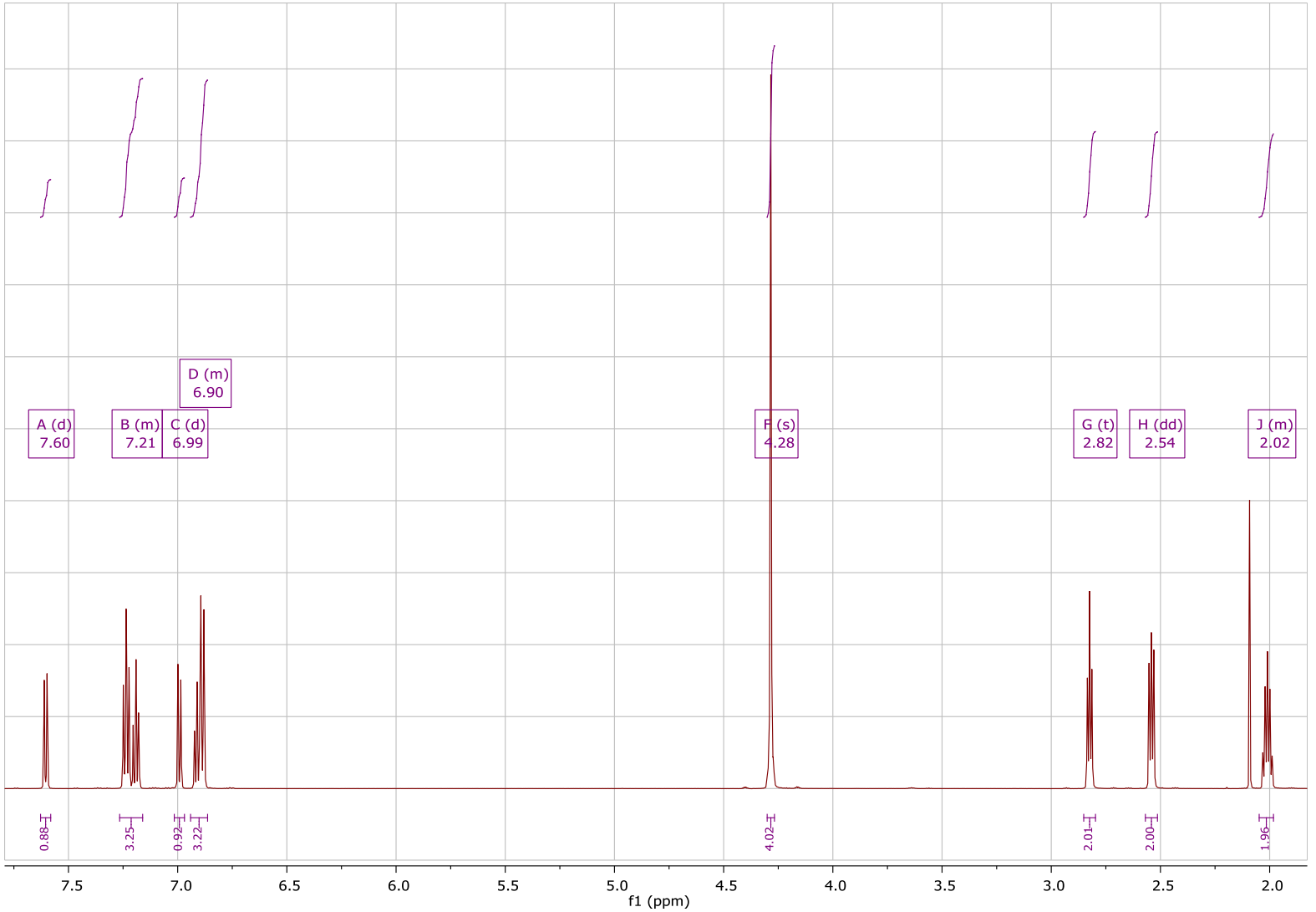

Compound 1e - ^{13}C NMR spectrum:

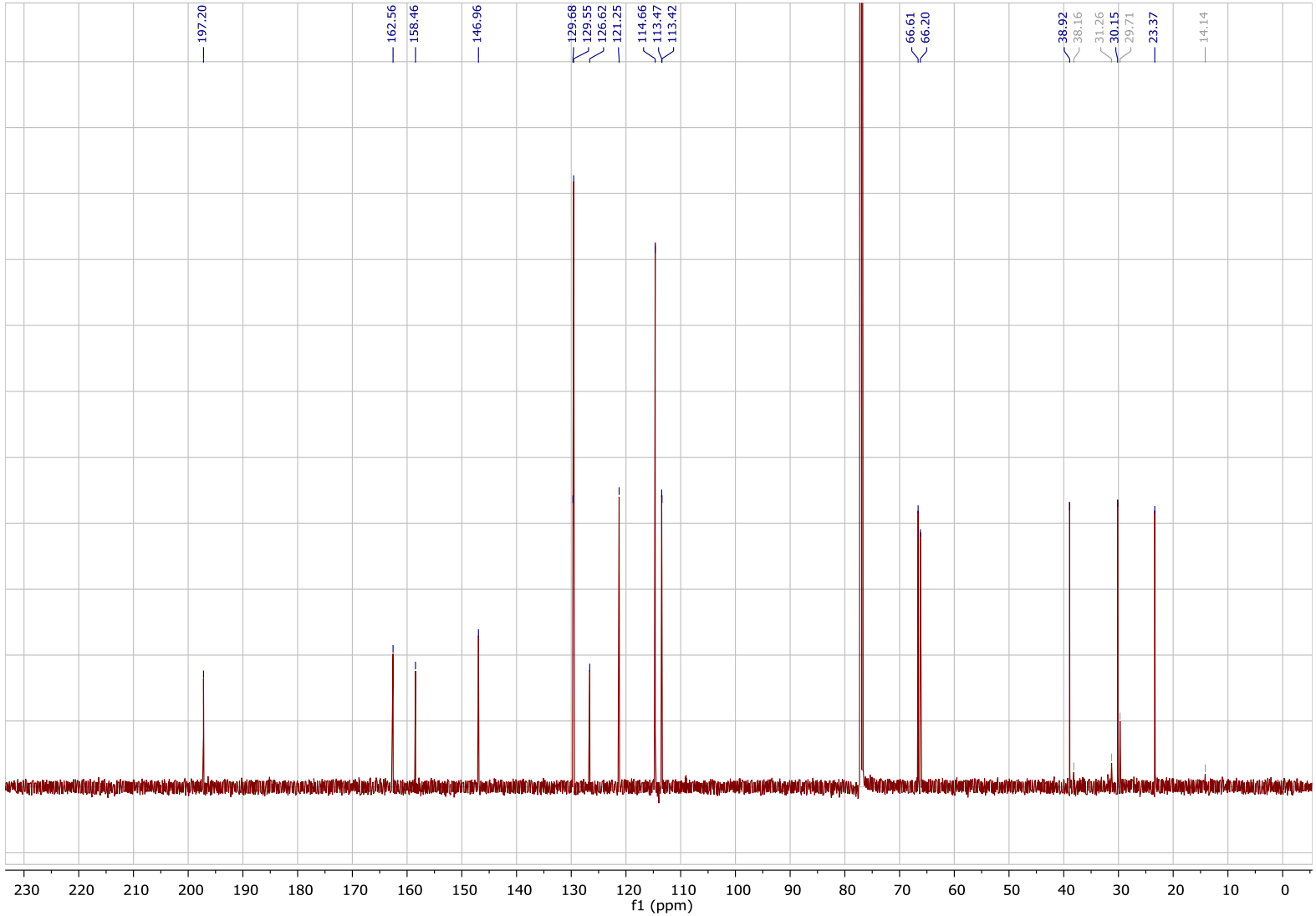

Compound 1e – ^{1}H NMR spectrum:

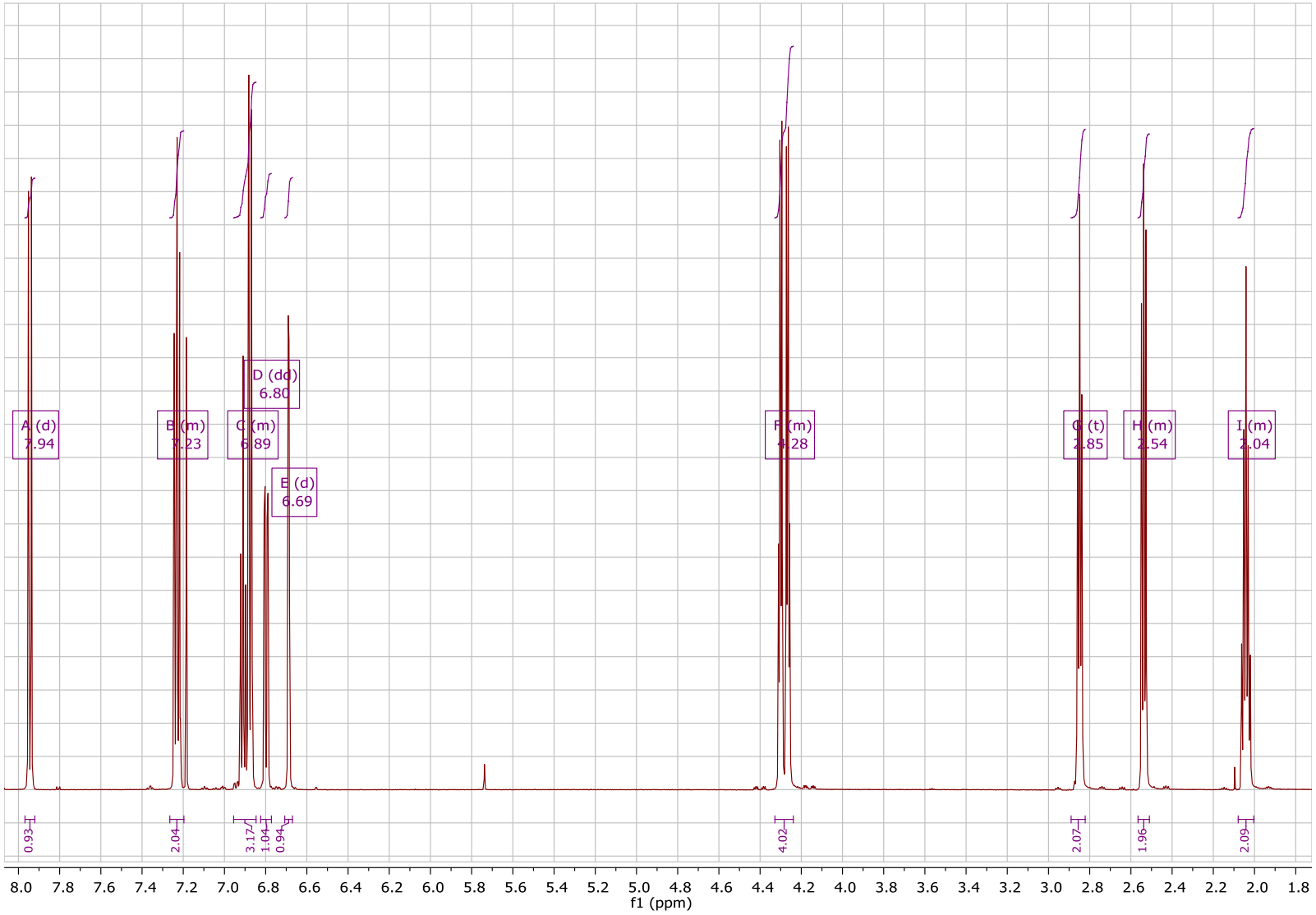

Compound 1f - ^{13}C NMR spectrum:

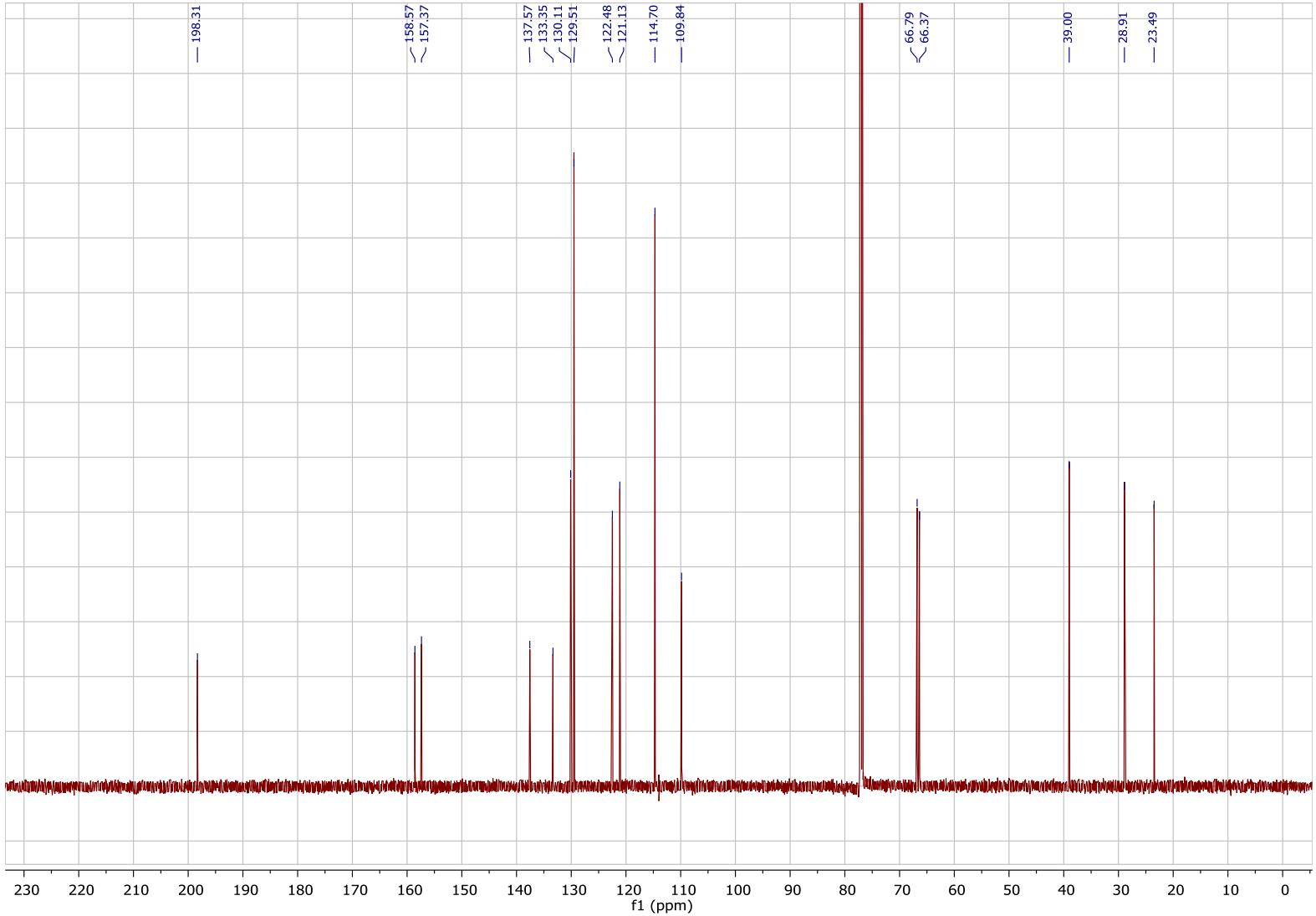

Compound 1f – ^{1}H NMR spectrum:

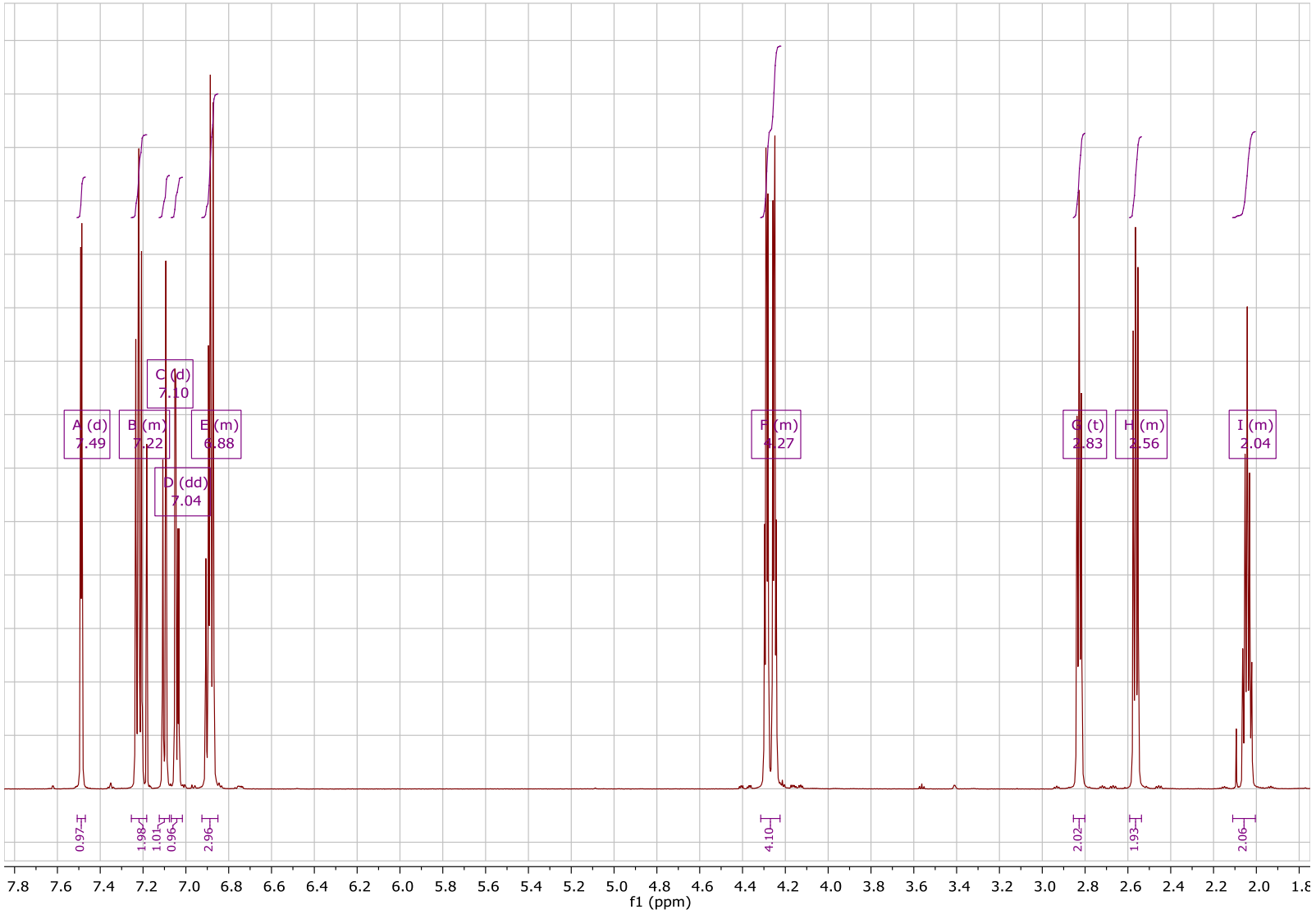

Compound 1g - ^{13}C NMR spectrum:

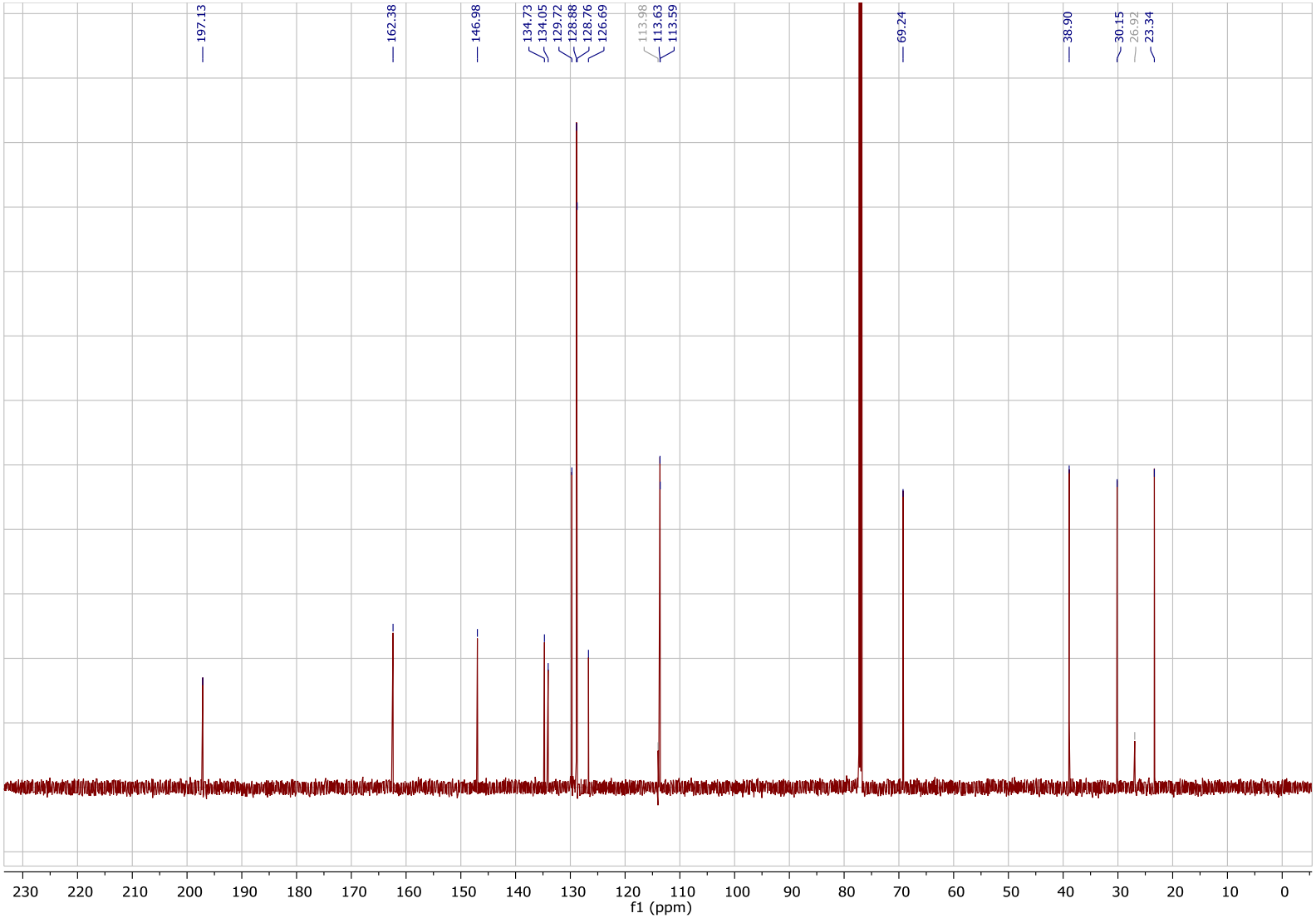

Compound 1g – ^{1}H NMR spectrum:

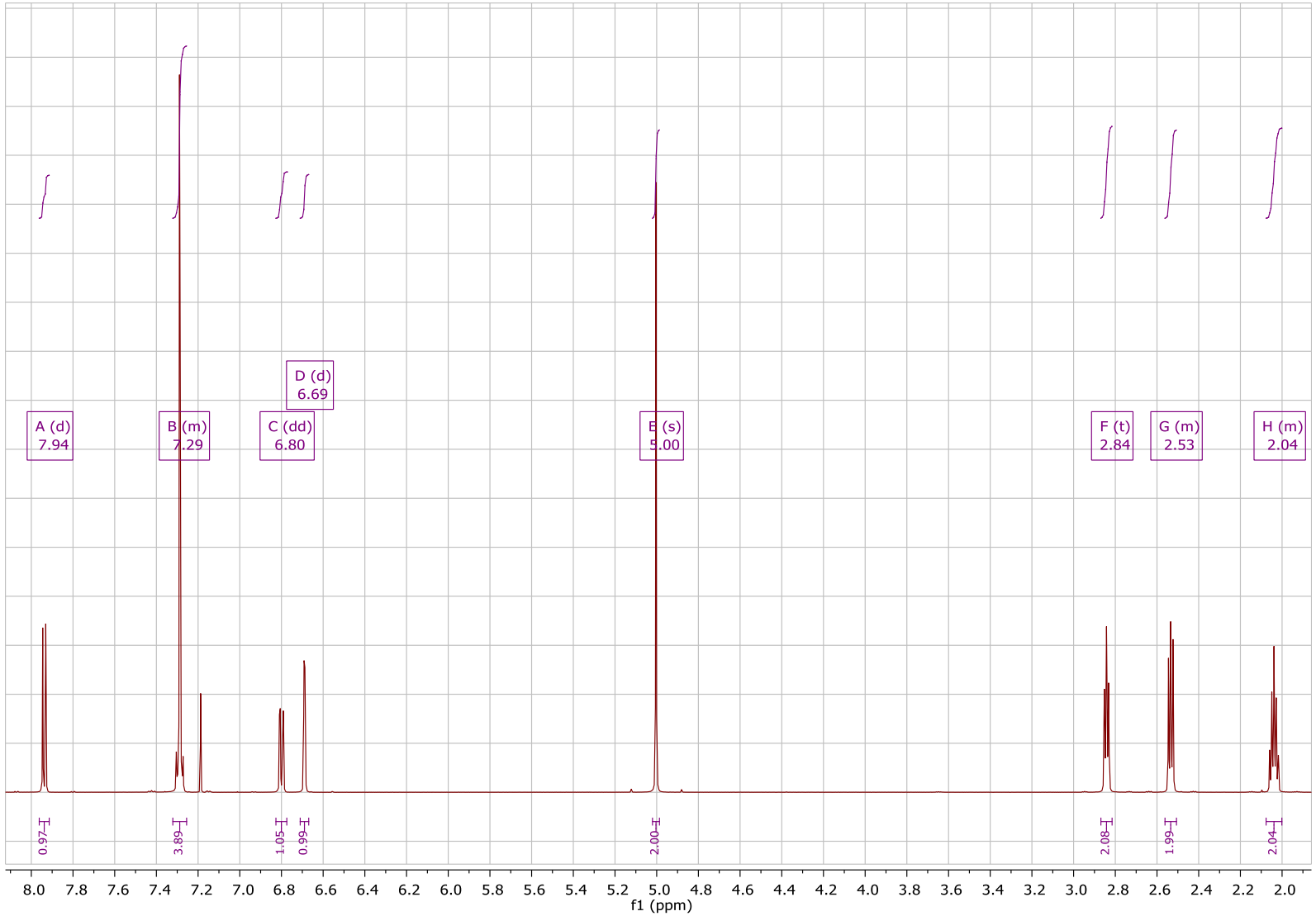

Compound 1h - ^{13}C NMR spectrum:

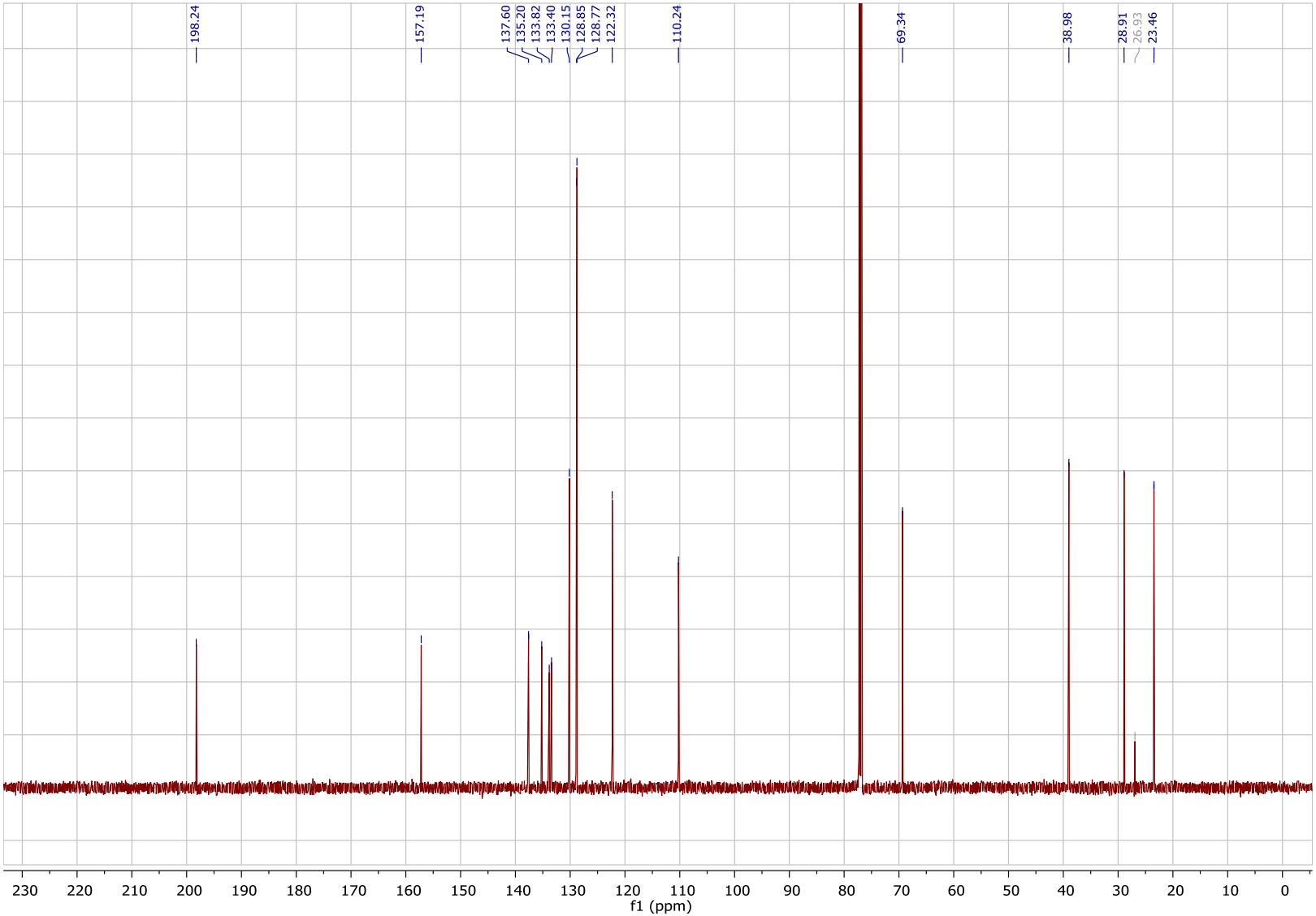

Compound 1h – ^{1}H NMR spectrum:

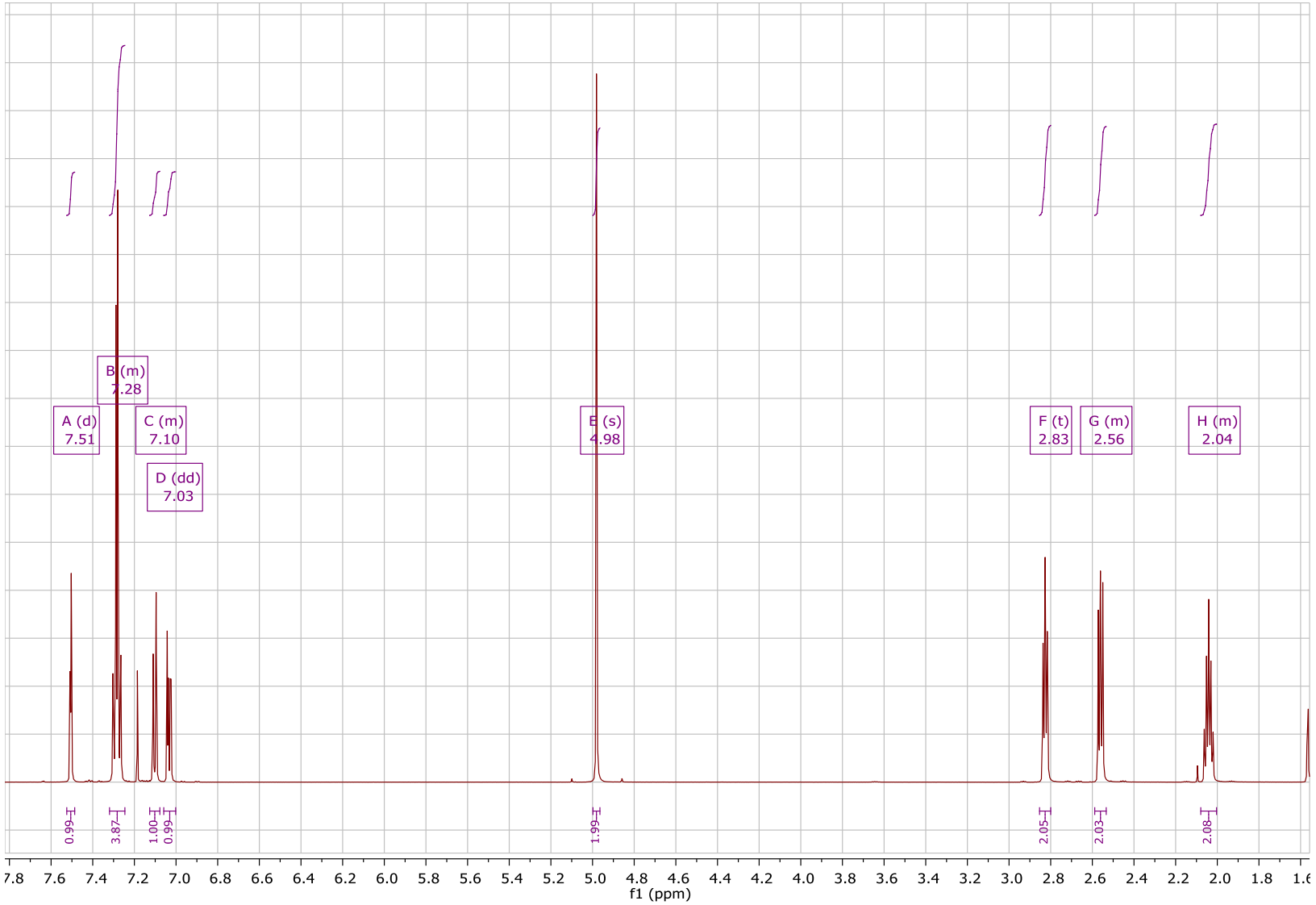

Compound 1i - ^{13}C NMR spectrum:

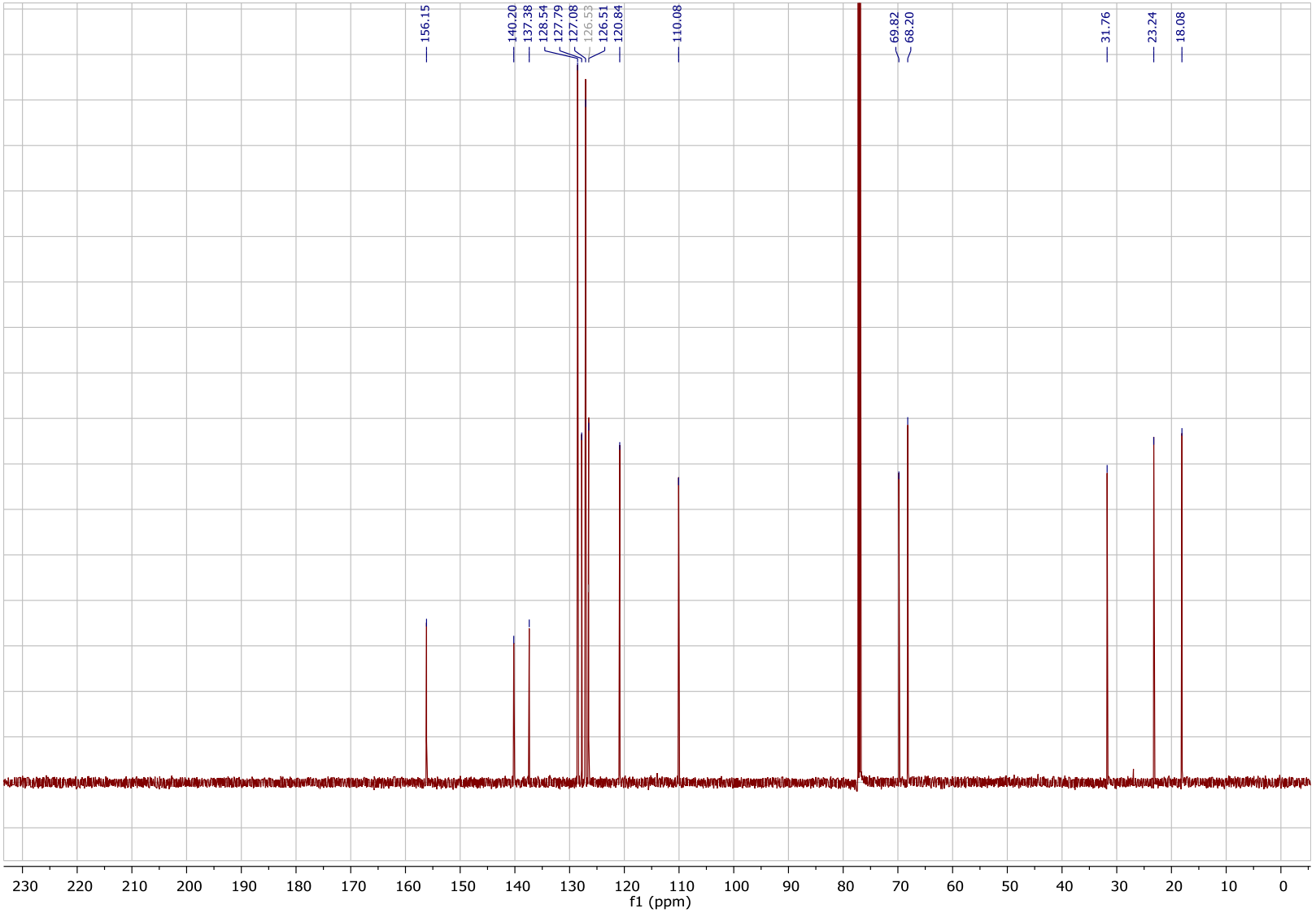

Compound 1i – ^{1}H NMR spectrum:

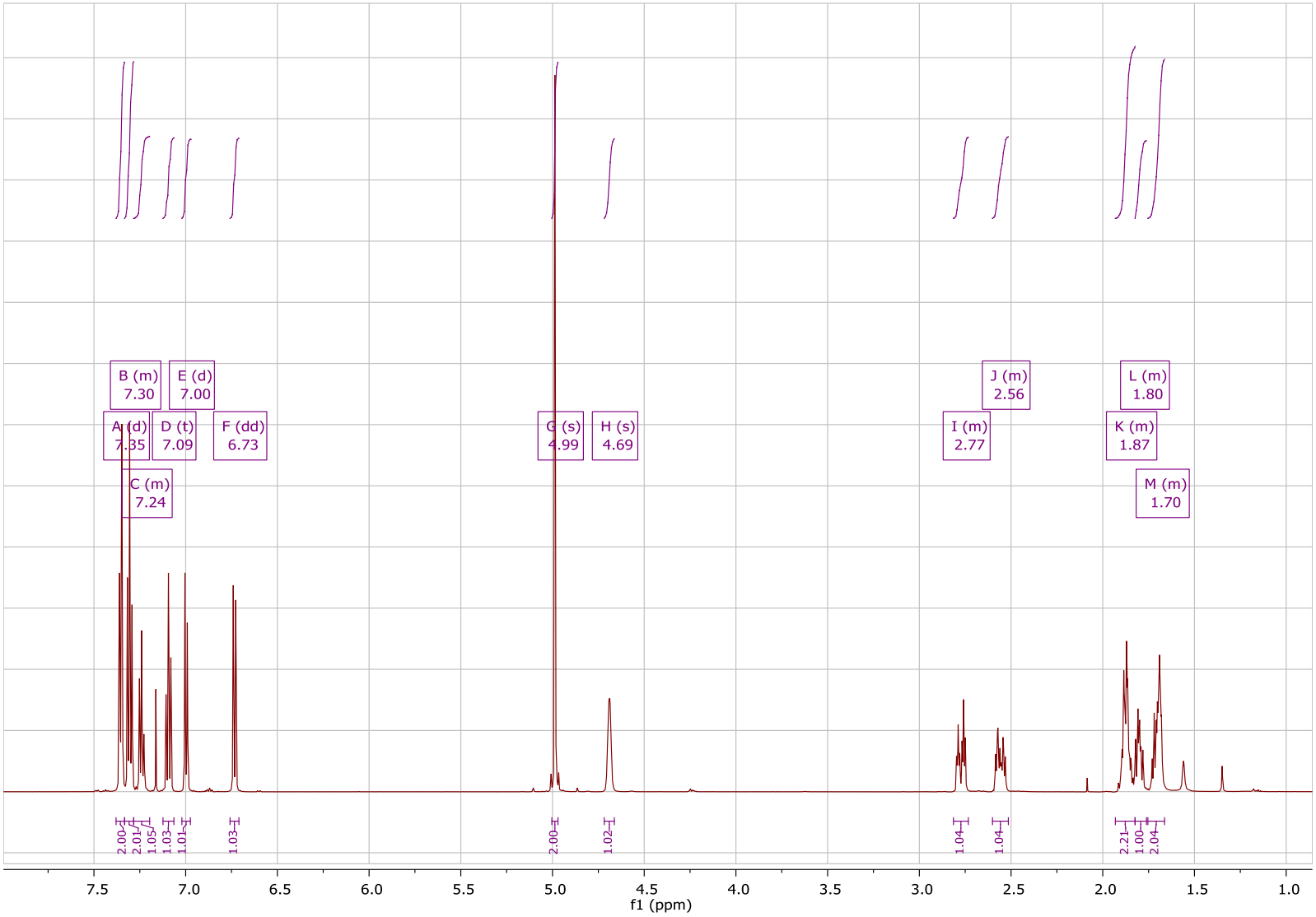

Compound 1j - ^{13}C NMR spectrum:

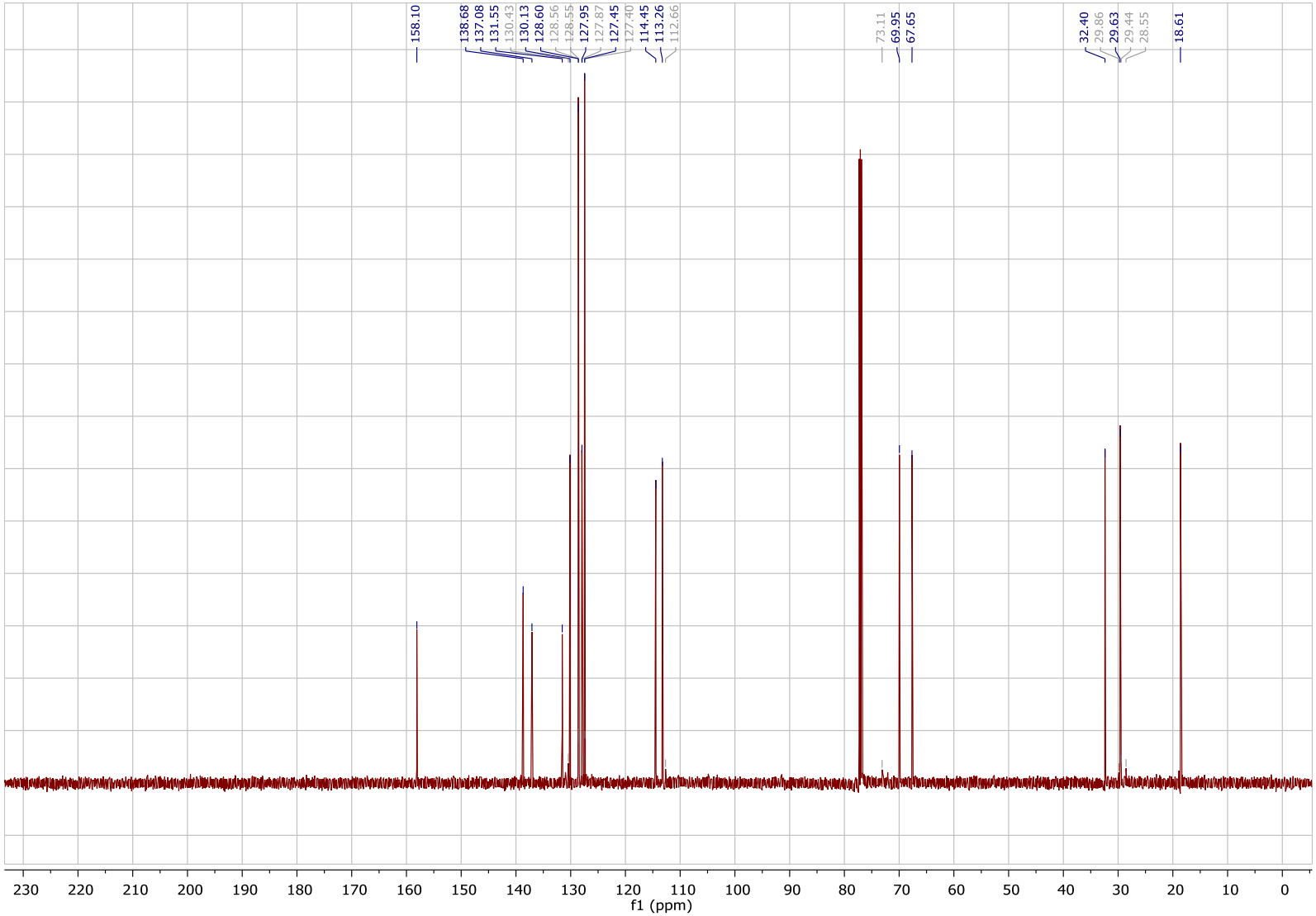

Compound 1j – ^{1}H NMR spectrum:

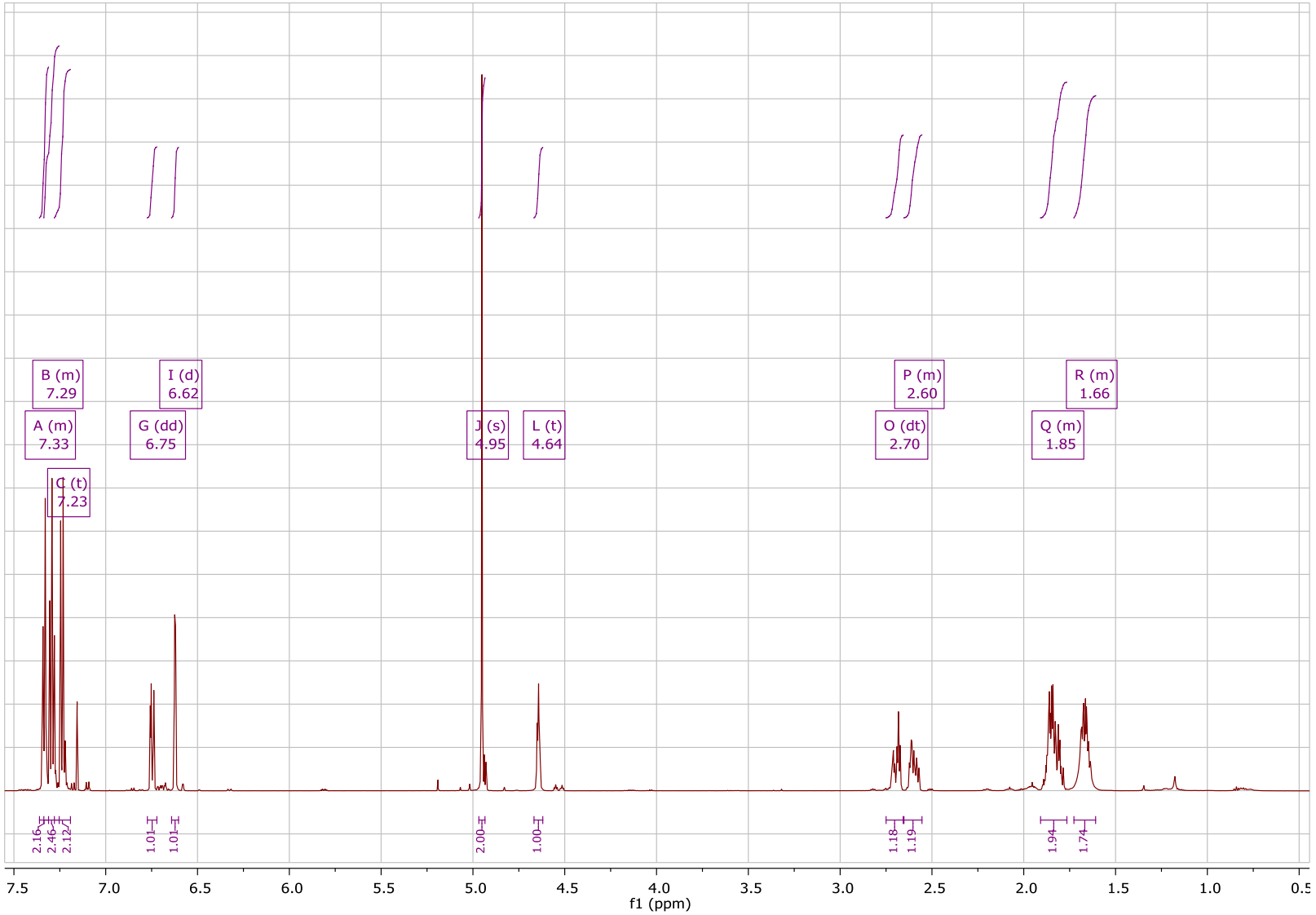

Compound 1k - ^{13}C NMR spectrum:

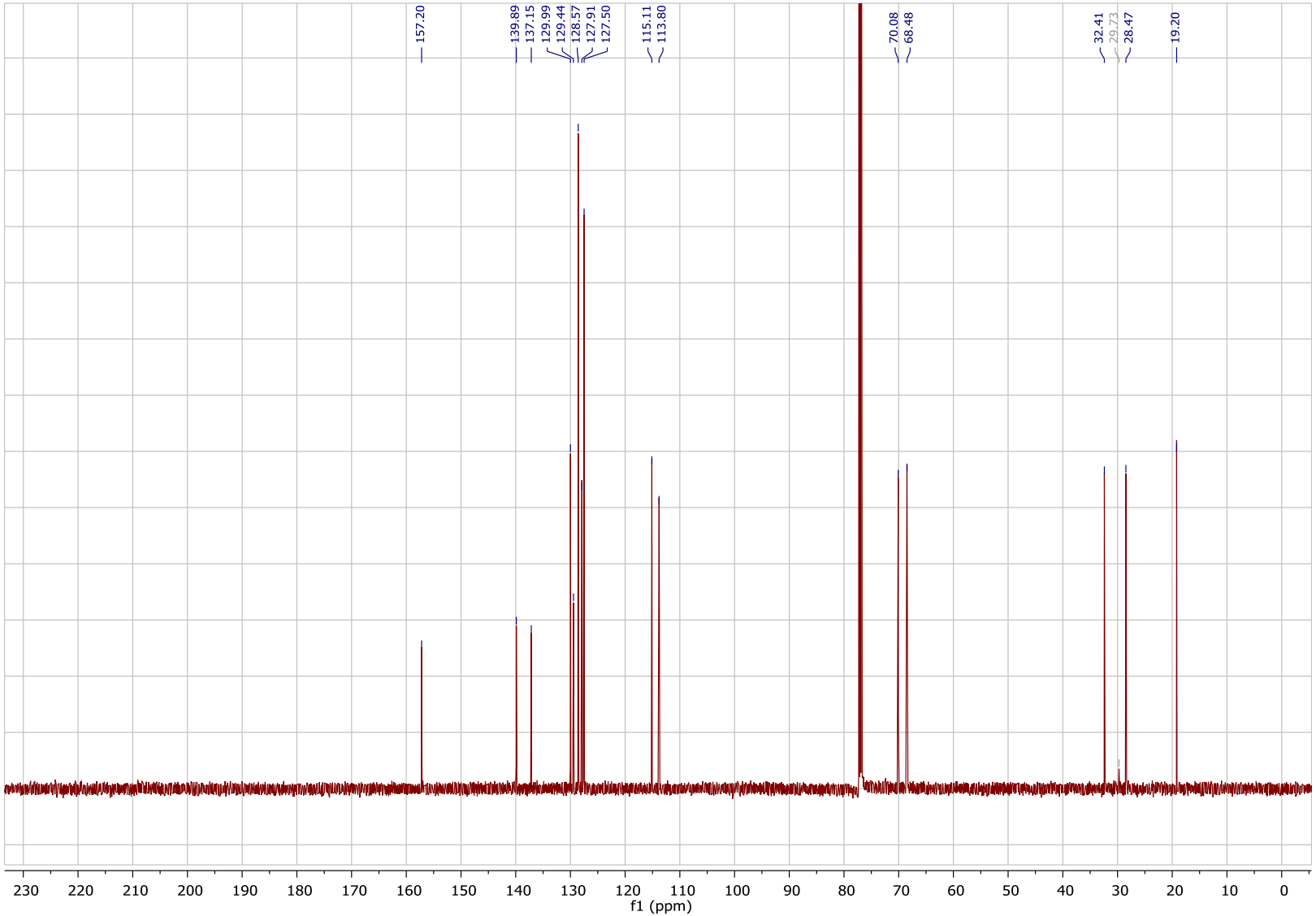

Compound 1k – ^{1}H NMR spectrum:

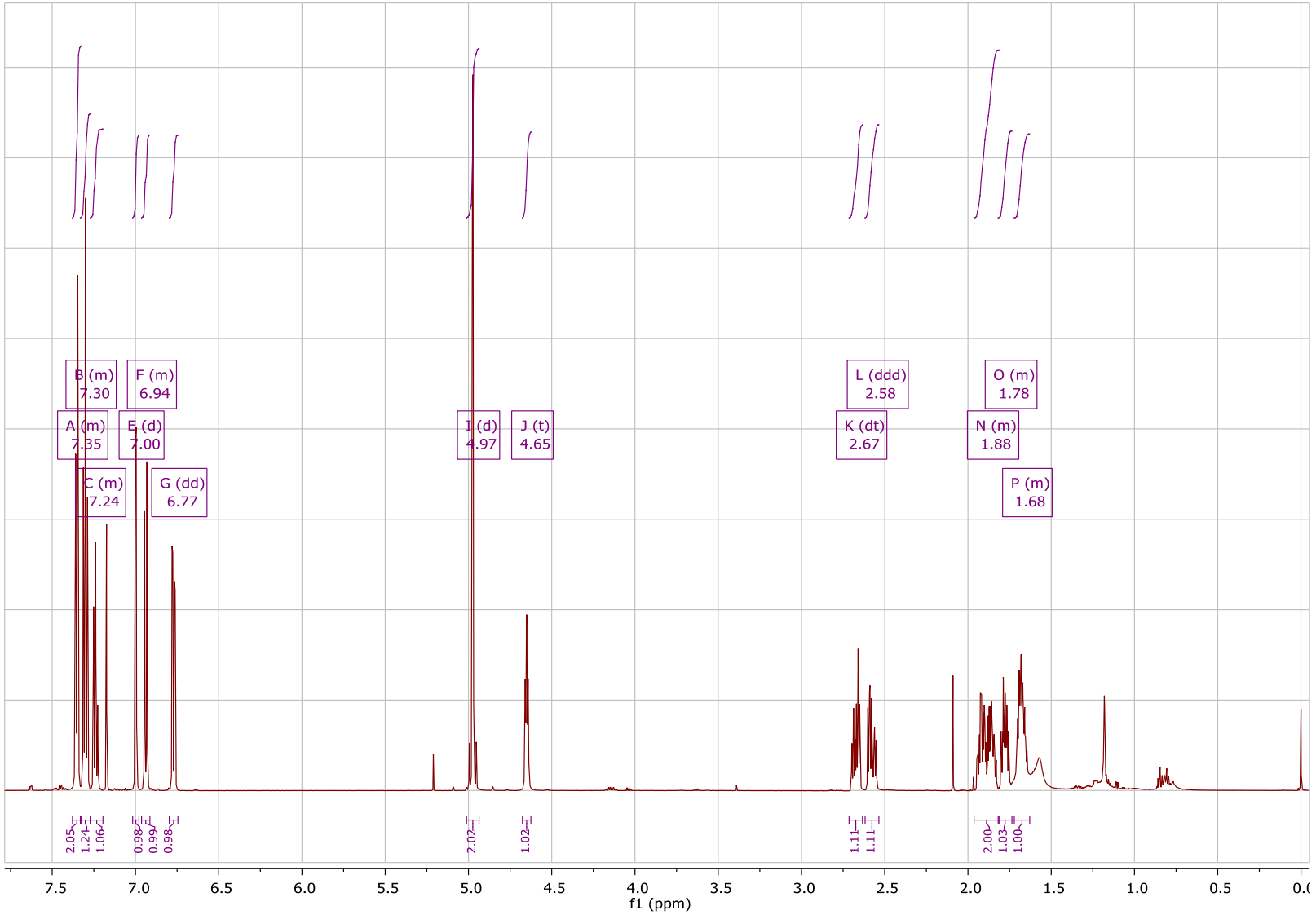

Compound 1l - ^{13}C NMR spectrum:

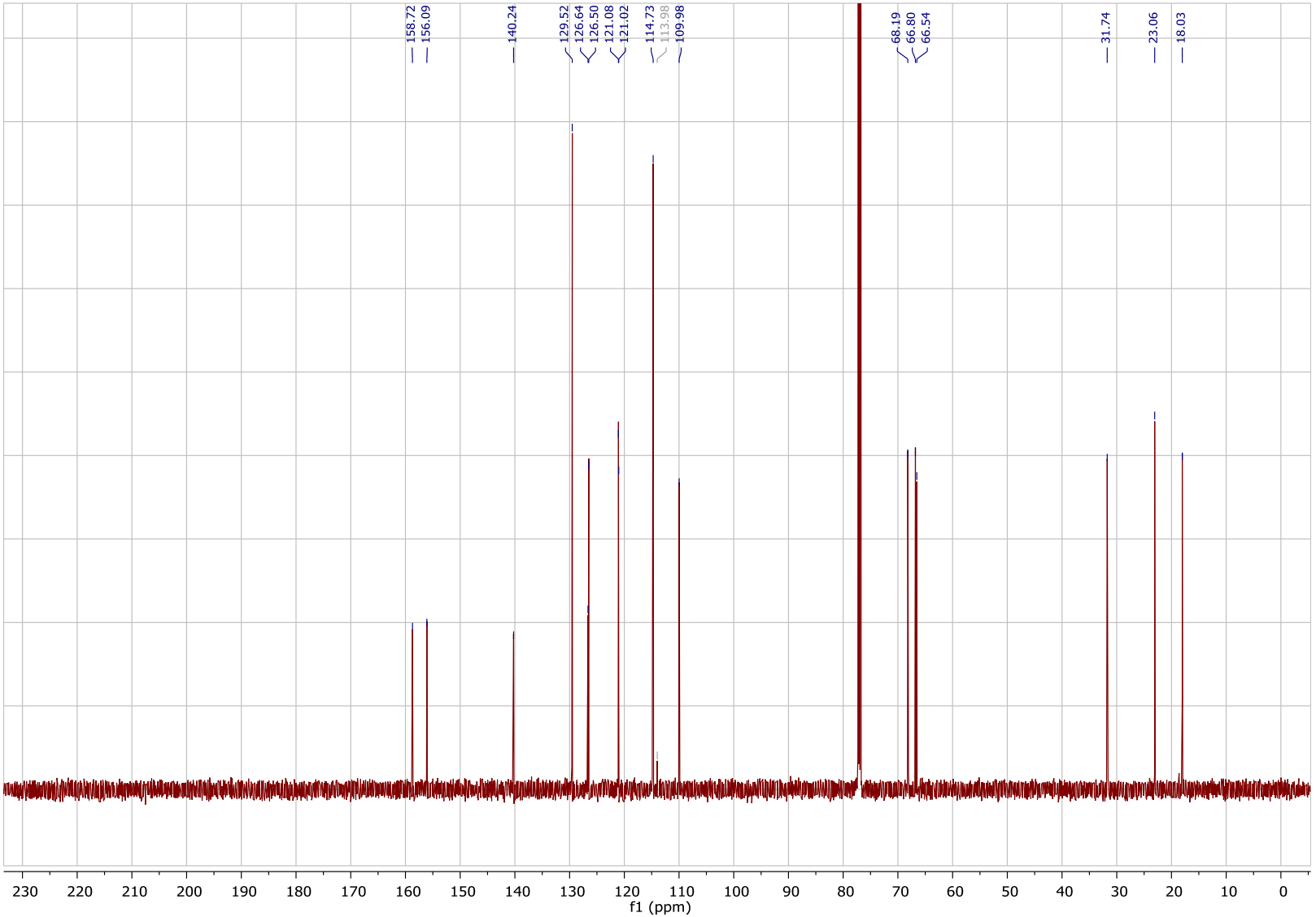

Compound 1l – ^{1}H NMR spectrum:

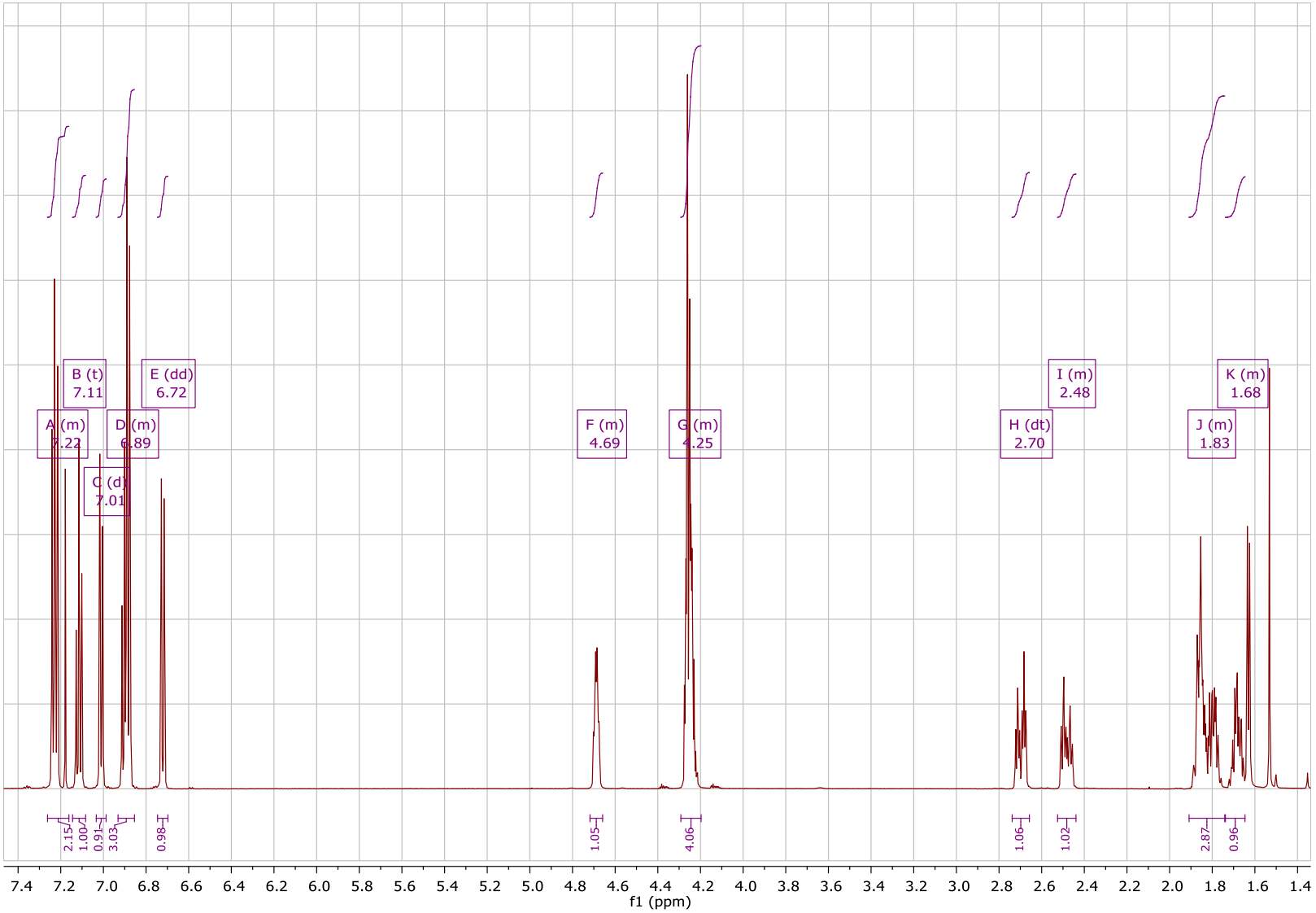

Compound 1m - ^{13}C NMR spectrum:

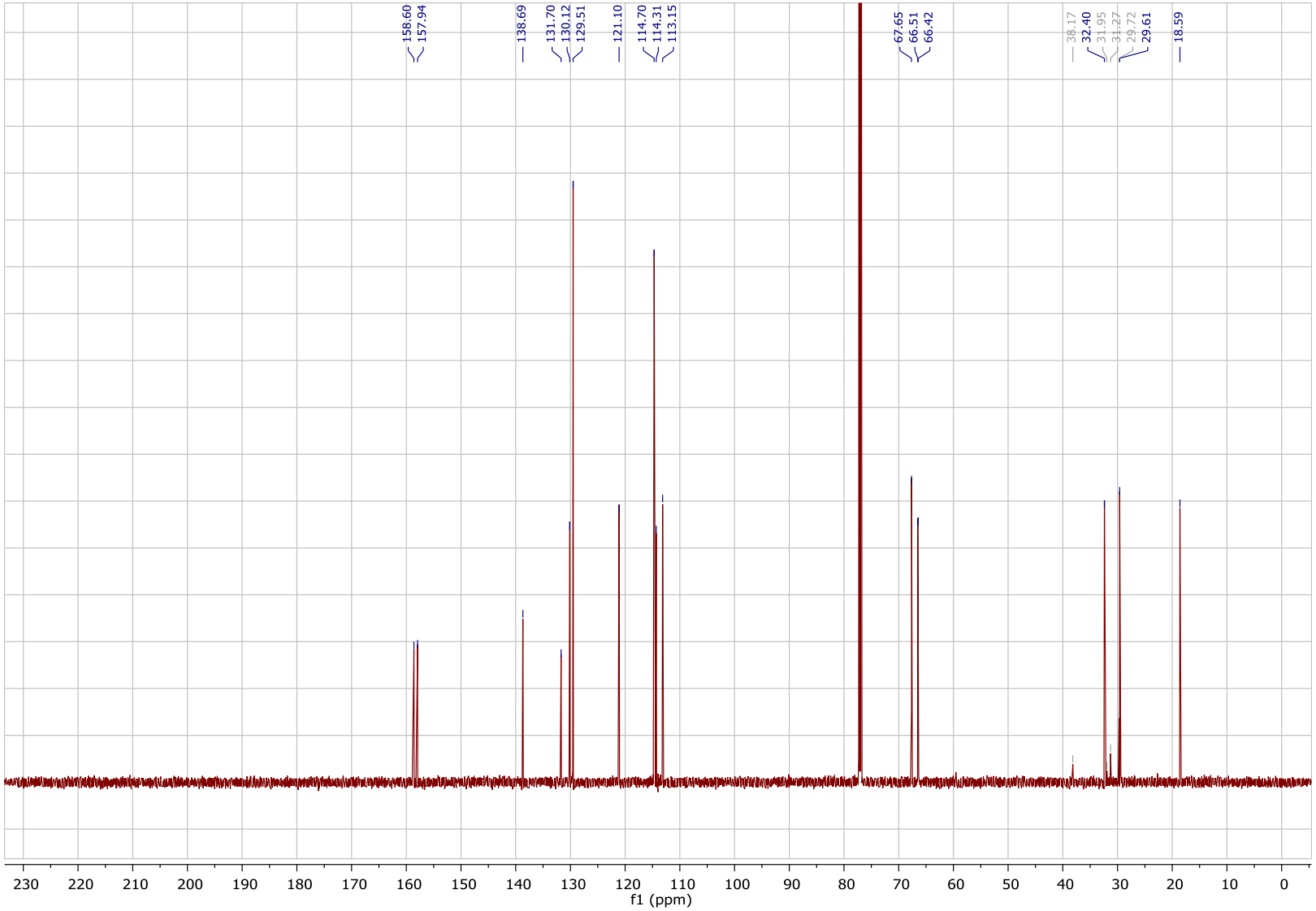

Compound 1m – ^{1}H NMR spectrum:

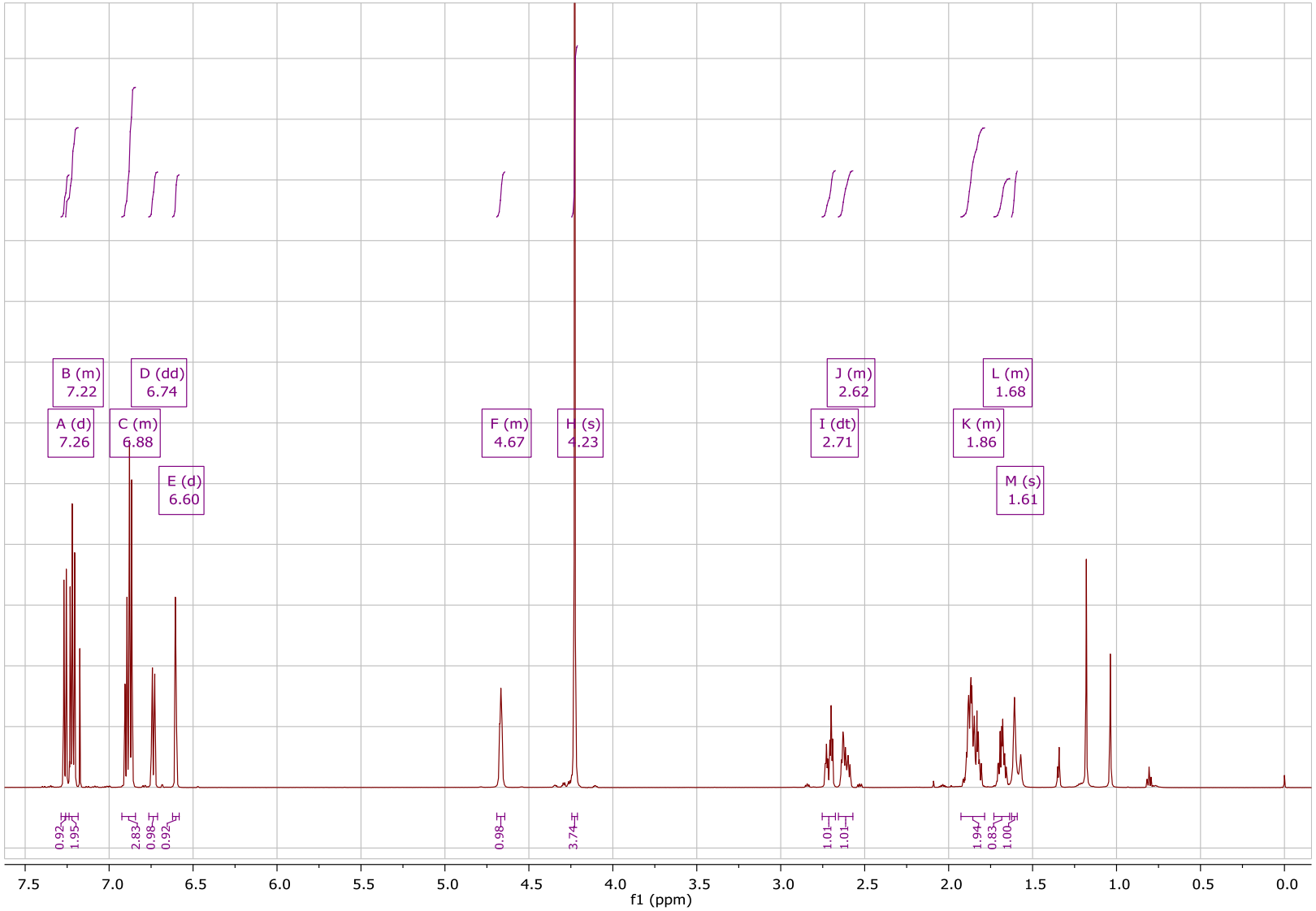

Compound 1n - ^{13}C NMR spectrum:

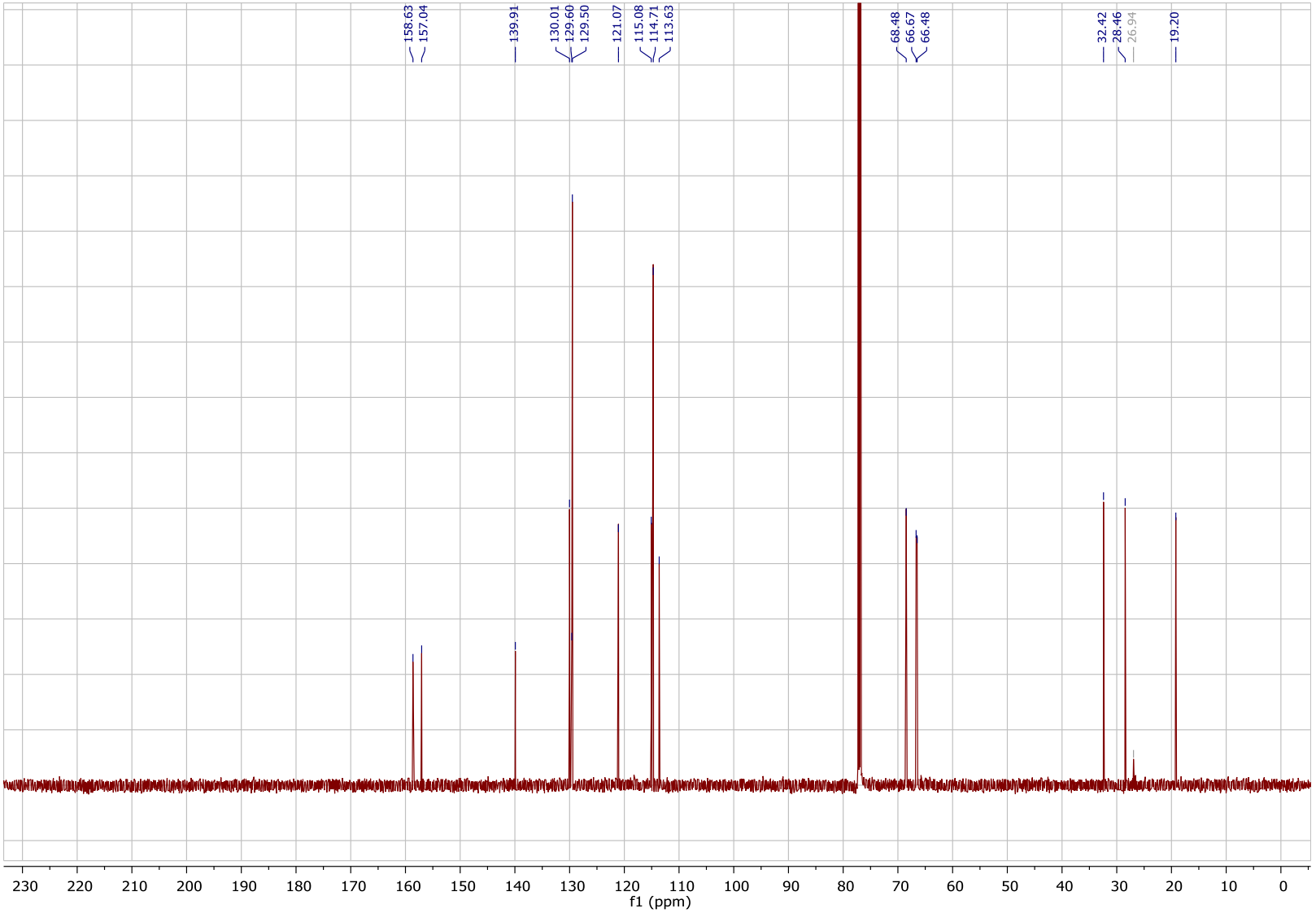

Compound 1n – ^{1}H NMR spectrum:

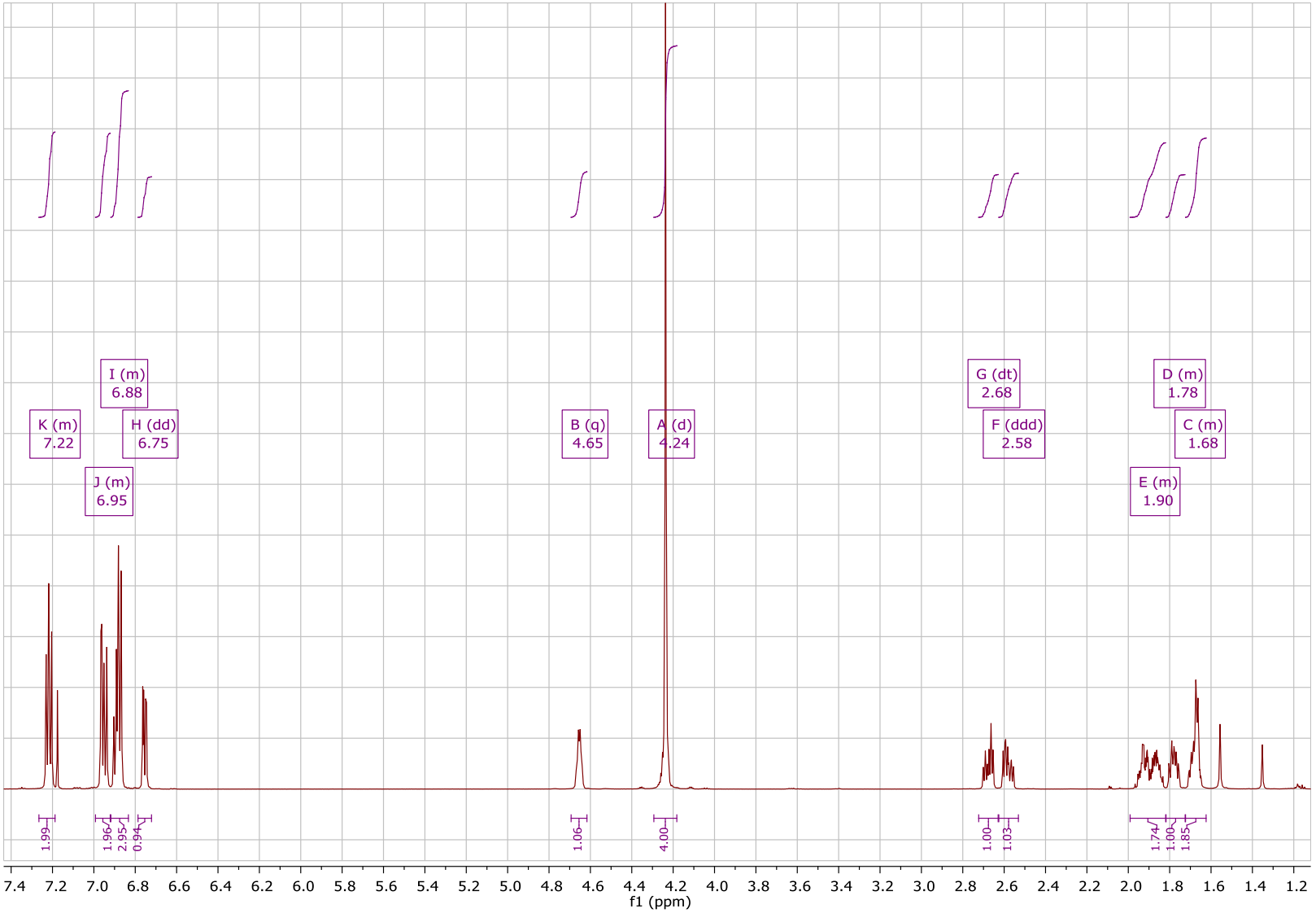

Compound 1o - ^{13}C NMR spectrum:

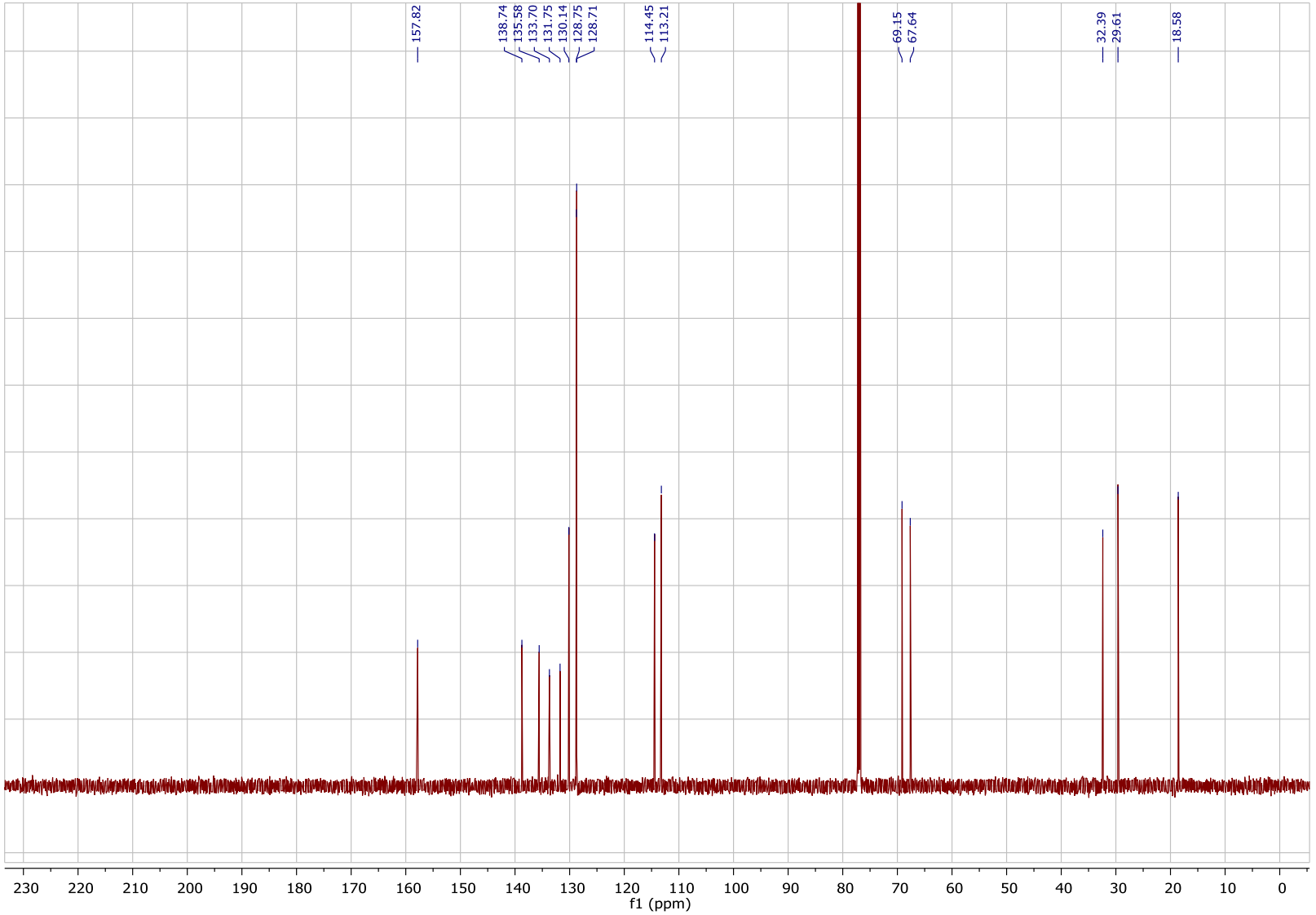

Compound 1o – ^{1}H NMR spectrum:

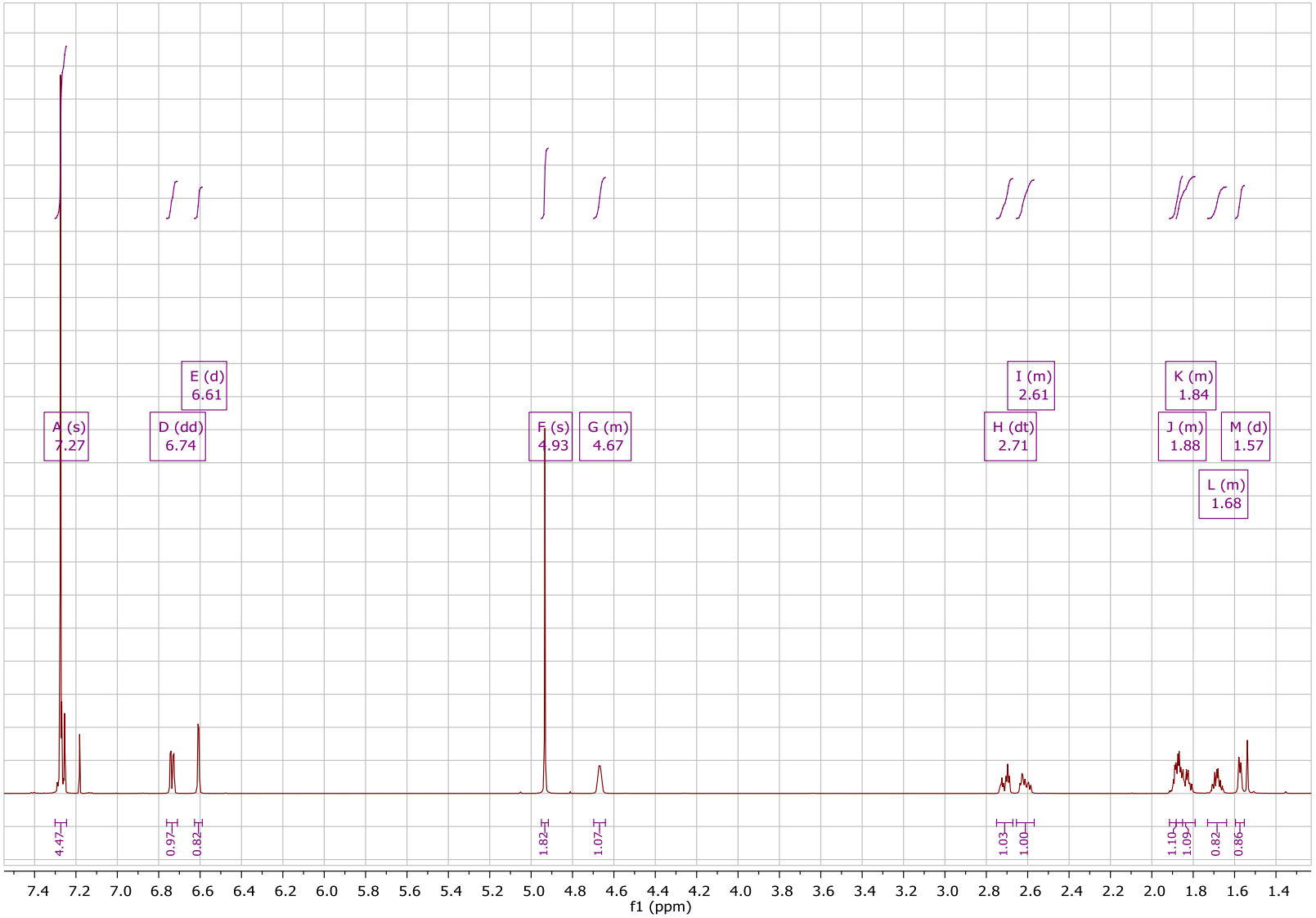

Compound 1p - ^{13}C NMR spectrum:

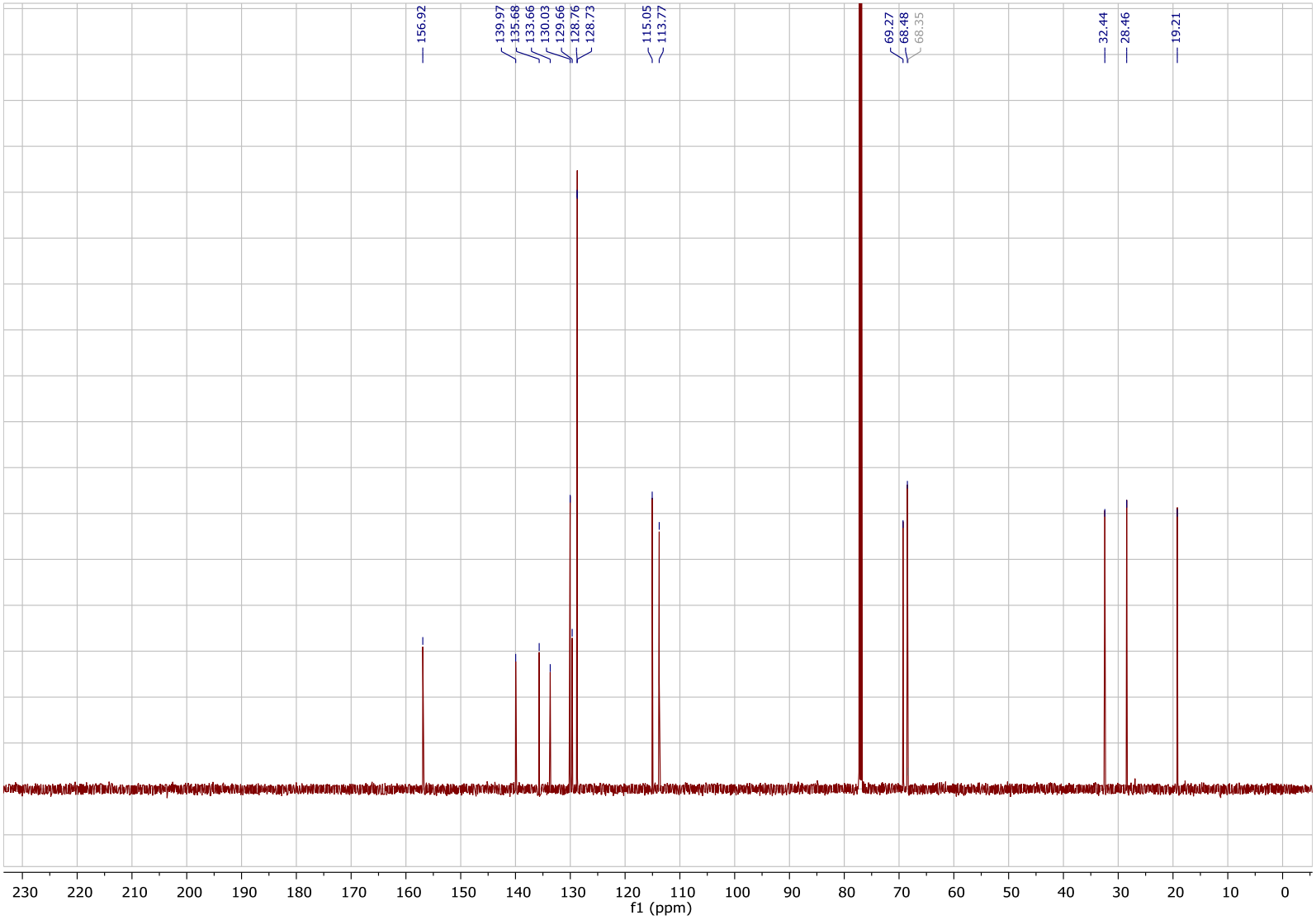

Compound 1p – ^{1}H NMR spectrum:

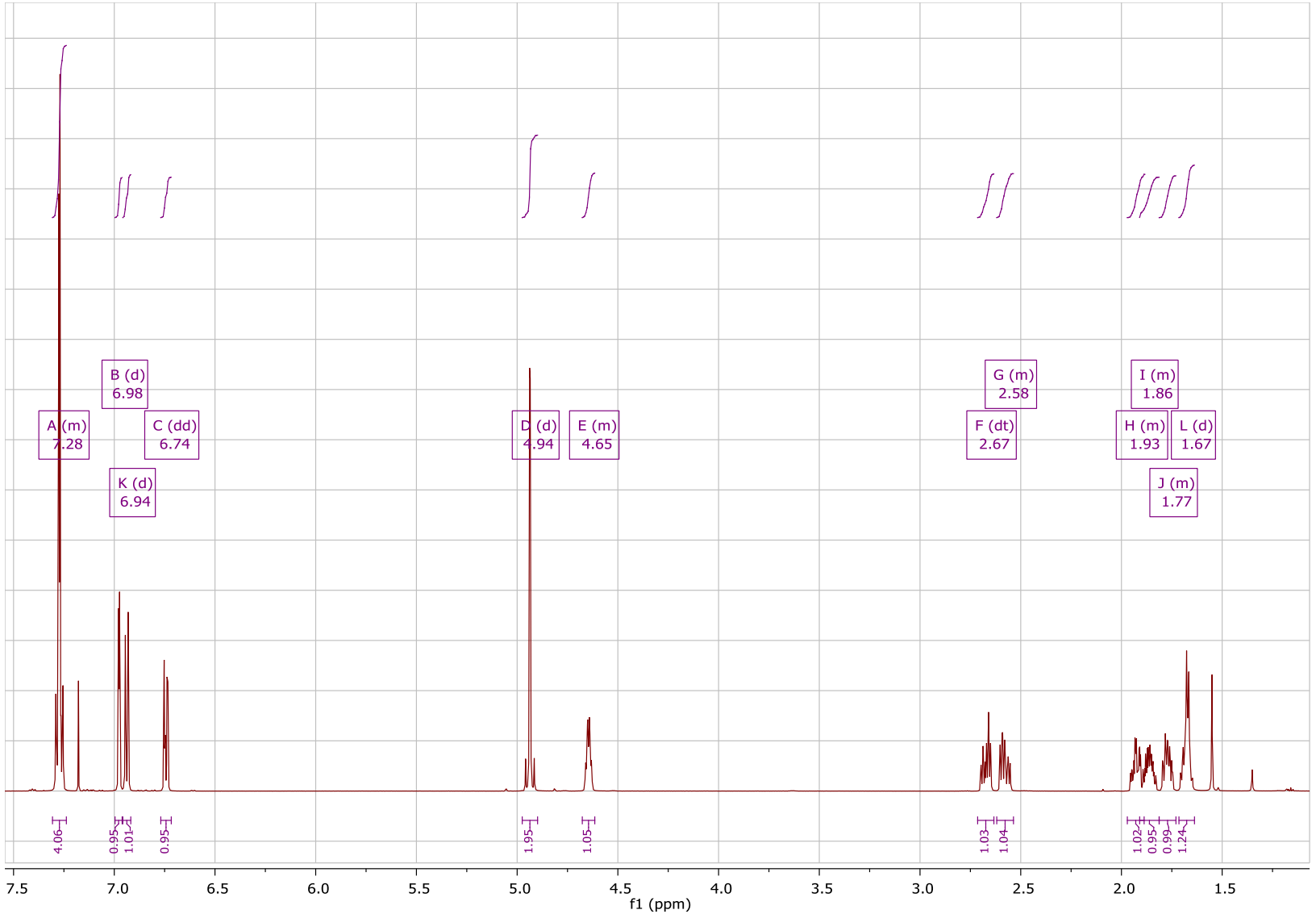

Compound 1a – MS:

Mass Spectrum SmartFormula Report

Analysis Info

Analysis Name	D:\Data\19092017\LADMS000014.d	Acquisition Date	9/19/2017 11:12:06 AM
Method	tune_low11092017.m	Laboratory	Laboratory for Analytical Services
Sample Name	R2-S2-1A	Operator	JHL Jordaan
Comment		Instrument / Ser#	micrOTOF-Q II 2010390

Acquisition Parameter

Source Type	APCI	Ion Polarity	Positive	Set Nebulizer	1.6 Bar
Focus	Not active	Set Capillary	4500 V	Set Dry Heater	200 °C
Scan Begin	50 m/z	Set End Plate Offset	-500 V	Set Dry Gas	8.0 l/min
Scan End	1500 m/z	Set Collision Cell RF	100.0 Vpp	Set Divert Valve	Waste

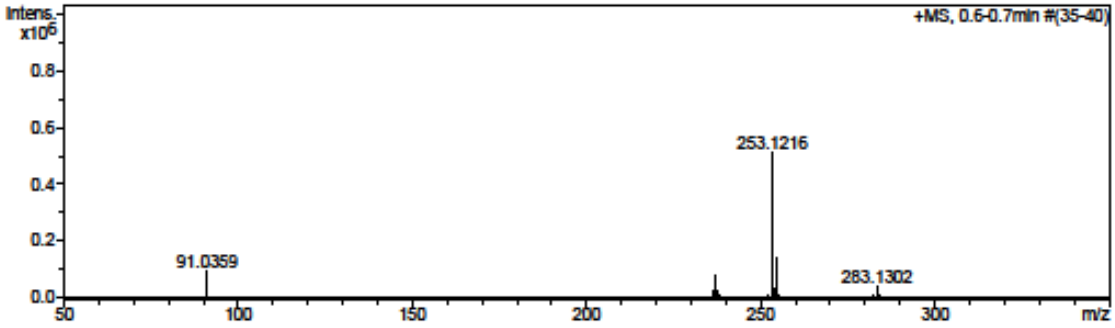

Meas. m/z	#	Formula	Score	m/z	err [mDa]	err [ppm]	mSigma	rdb	N-Rule	e⁻ Conf
253.1216	1	C 17 H 17 O 2	100.00	253.1223	0.7	2.8	54.8	9.5	ok	even

Compound 1b – MS:

Mass Spectrum SmartFormula Report

Analysis Info

Analysis Name	D:\Data\19092017\LADMS000013.d	Acquisition Date	9/19/2017 11:06:41 AM
Method	tune_low11092017.m	Laboratory	Laboratory for Analytical Services
Sample Name	R3-S2-1B	Operator	JHL Jordaan
Comment		Instrument / Ser#	micrOTOF-Q II 2010390

Acquisition Parameter

Source Type	APCI	Ion Polarity	Positive	Set Nebulizer	1.6 Bar
Focus	Not active	Set Capillary	4500 V	Set Dry Heater	200 °C
Scan Begin	50 m/z	Set End Plate Offset	-500 V	Set Dry Gas	8.0 l/min
Scan End	1500 m/z	Set Collision Cell RF	100.0 Vpp	Set Divert Valve	Waste

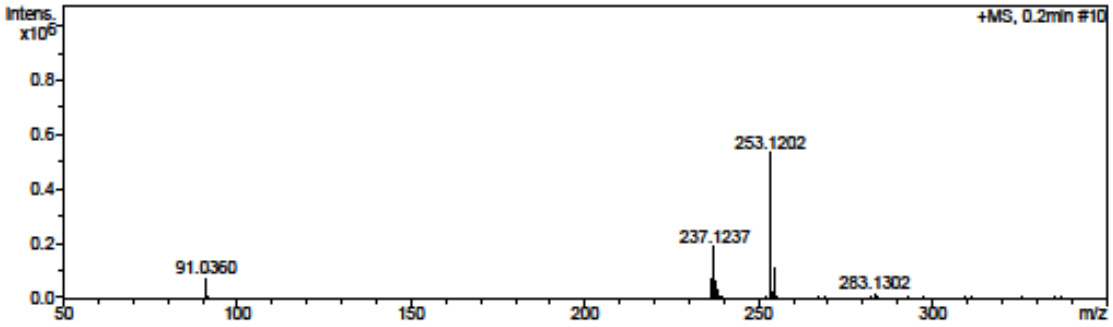

Meas. m/z	#	Formula	Score	m/z	err [mDa]	err [ppm]	mSigma	rdb	N-Rule	e⁻ Conf
253.1202	1	C 17 H 17 O 2	100.00	253.1223	2.1	8.4	15.4	9.5	ok	even

Compound 1c – MS:

Mass Spectrum SmartFormula Report

Analysis Info

Analysis Name	D:\Data\19092017\LADMS000016.d	Acquisition Date	9/19/2017 11:28:18 AM
Method	tune_low11092017.m	Laboratory	Laboratory for Analytical Services
Sample Name	R1-S2-1C	Operator	JHL Jordaan
Comment		Instrument / Ser#	micrOTOF-Q II 2010390

Acquisition Parameter

Source Type	APCI	Ion Polarity	Positive	Set Nebulizer	1.6 Bar
Focus	Not active	Set Capillary	4500 V	Set Dry Heater	200 °C
Scan Begin	50 m/z	Set End Plate Offset	-500 V	Set Dry Gas	8.0 l/min
Scan End	1500 m/z	Set Collision Cell RF	100.0 Vpp	Set Divert Valve	Waste

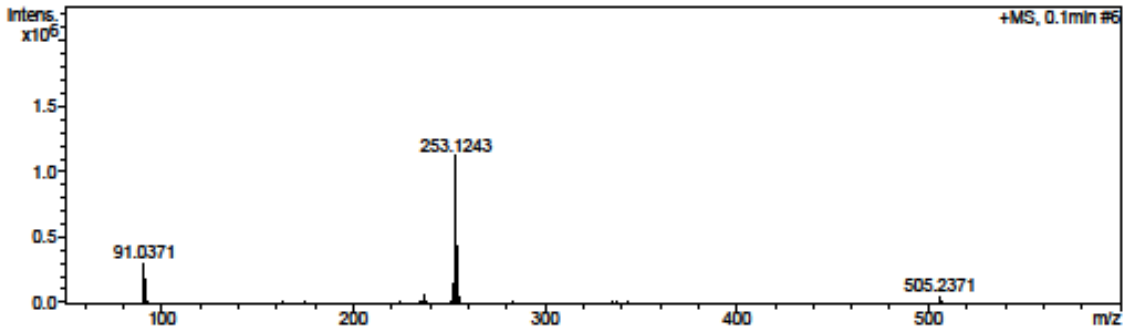

Meas. m/z	#	Formula	Score	m/z	err [mDa]	err [ppm]	mSigma	rdb	N-Rule	e⁻ Conf
253.1243	1	C 17 H 17 O 2	100.00	253.1223	-2.0	-7.9	120.7	9.5	ok	even

Compound 1d – MS:

Mass Spectrum SmartFormula Report

Analysis Info

Analysis Name	D:\Data\19092017\LADMS000007.d	Acquisition Date	9/19/2017 10:09:28 AM
Method	tune_low11092017.m	Laboratory	Laboratory for Analytical Services
Sample Name	R12-S1-1D	Operator	JHL Jordaan
Comment		Instrument / Ser#	micrOTOF-Q II 2010390

Acquisition Parameter

Source Type	APCI	Ion Polarity	Positive	Set Nebulizer	1.6 Bar
Focus	Not active	Set Capillary	4500 V	Set Dry Heater	200 °C
Scan Begin	50 m/z	Set End Plate Offset	-500 V	Set Dry Gas	8.0 l/min
Scan End	1500 m/z	Set Collision Cell RF	100.0 Vpp	Set Divert Valve	Waste

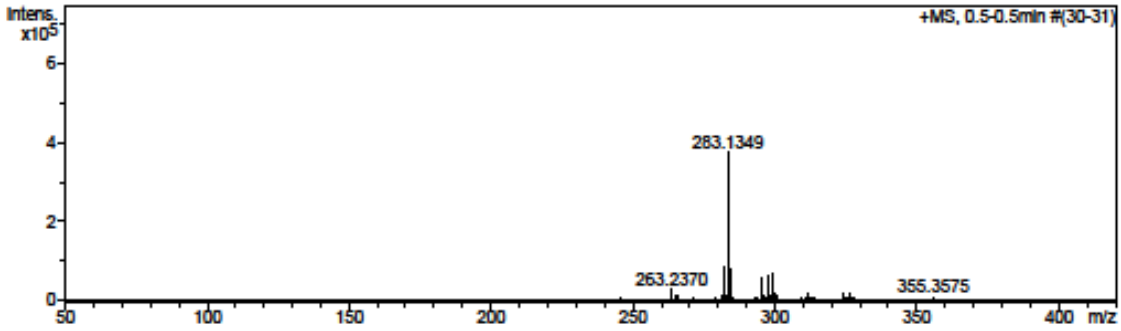

Meas. m/z	#	Formula	Score	m/z	err [mDa]	err [ppm]	mSigma	rdb	N-Rule	e⁻ Conf
283.1349	1	C 18 H 19 O 3	100.00	283.1329	-2.0	-7.0	20.7	9.5	ok	even
	2	C 16 H 17 N 3 O 2	25.93	283.1315	-3.3	-11.8	27.0	10.0	ok	odd

Compound 1e – MS:

Mass Spectrum SmartFormula Report

Analysis Info

Analysis Name	D:\Data\19092017\LADMS000011.d	Acquisition Date	9/19/2017 10:30:24 AM
Method	tune_low11092017.m	Laboratory	Laboratory for Analytical Services
Sample Name	R4-S1-1E	Operator	JHL Jordaan
Comment		Instrument / Ser#	micrOTOF-Q II 2010390

Acquisition Parameter

Source Type	APCI	Ion Polarity	Positive	Set Nebulizer	1.6 Bar
Focus	Not active	Set Capillary	4500 V	Set Dry Heater	200 °C
Scan Begin	50 m/z	Set End Plate Offset	-500 V	Set Dry Gas	8.0 l/min
Scan End	1500 m/z	Set Collision Cell RF	100.0 Vpp	Set Divert Valve	Waste

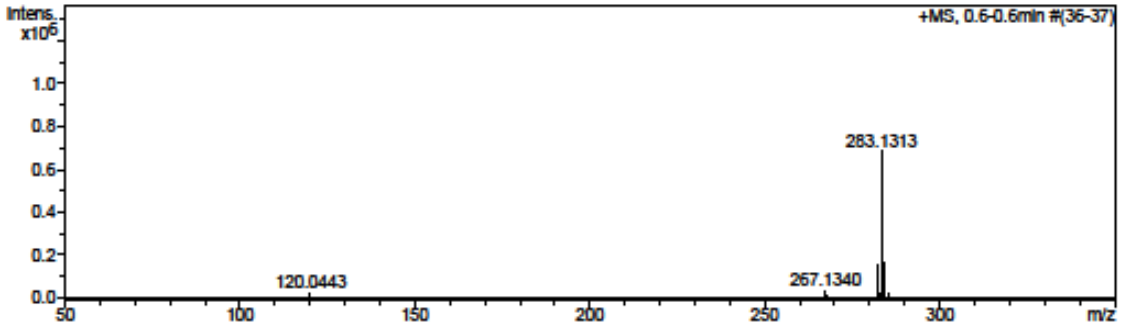

Meas. m/z	#	Formula	Score	m/z	err [mDa]	err [ppm]	mSigma	rdb	N-Rule	e⁻ Conf
283.1313	1	C 18 H 19 O 3	100.00	283.1329	1.6	5.7	31.3	9.5	ok	even

Compound 1f – MS:

Mass Spectrum SmartFormula Report

Analysis Info

Analysis Name	D:\Data\19092017\LADMS000009.d	Acquisition Date	9/19/2017 10:23:12 AM
Method	tune_low11092017.m	Laboratory	Laboratory for Analytical Services
Sample Name	R7-S1-1F	Operator	JHL Jordaan
Comment		Instrument / Ser#	micrOTOF-Q II 2010390

Acquisition Parameter

Source Type	APCI	Ion Polarity	Positive	Set Nebulizer	1.6 Bar
Focus	Not active	Set Capillary	4500 V	Set Dry Heater	200 °C
Scan Begin	50 m/z	Set End Plate Offset	-500 V	Set Dry Gas	8.0 l/min
Scan End	1500 m/z	Set Collision Cell RF	100.0 Vpp	Set Divert Valve	Waste

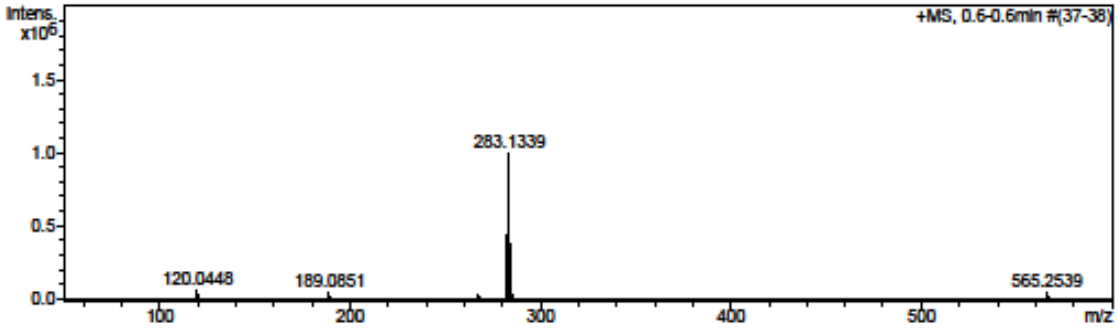

Meas. m/z	#	Formula	Score	m/z	err [mDa]	err [ppm]	mSigma	rdb	N-Rule	e⁻ Conf
283.1339	1	C 18 H 19 O 3	100.00	283.1329	-1.1	-3.8	112.1	9.5	ok	even

Compound 1g – MS:

Mass Spectrum SmartFormula Report

Analysis Info

Analysis Name	D:\Data\21062017\LADMS000020.d	Acquisition Date	6/21/2017 1:15:23 PM
Method	tune_low08062017.m	Laboratory	Laboratory for Analytical Services
Sample Name	R14 S1	Operator	JHL Jordaan
Comment		Instrument / Ser#	micrOTOF-Q II 2010390

Acquisition Parameter

Source Type	APCI	Ion Polarity	Positive	Set Nebulizer	1.6 Bar
Focus	Not active	Set Capillary	4500 V	Set Dry Heater	200 °C
Scan Begin	50 m/z	Set End Plate Offset	-500 V	Set Dry Gas	8.0 l/min
Scan End	1500 m/z	Set Collision Cell RF	100.0 Vpp	Set Divert Valve	Waste

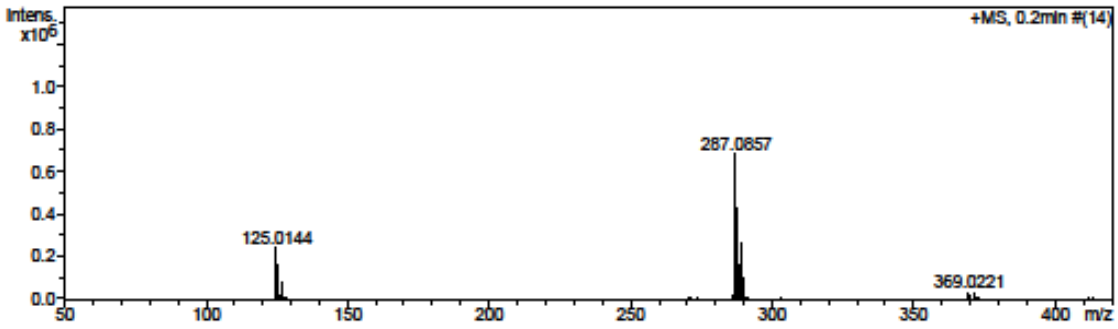

Meas. m/z	#	Formula	Score	m/z	err [mDa]	err [ppm]	mSigma	rdb	N-Rule	e⁻ Conf
125.0144	1	C 7 H 6 Cl	100.00	125.0153	0.8	6.5	0.6	4.5	ok	even
287.0857	1	C 17 H 16 Cl O 2	100.00	287.0833	-2.3	-8.2	37.4	9.5	ok	even
	2	C 23 H 11	0.02	287.0855	-0.1	-0.5	212.9	18.5	ok	even

Compound 1h – MS:

Mass Spectrum SmartFormula Report

Analysis Info

Analysis Name	D:\Data\21062017\LADMS000022.d	Acquisition Date	6/21/2017 1:20:43 PM
Method	tune_low08062017.m	Laboratory	Laboratory for Analytical Services
Sample Name	R13 S1	Operator	JHL Jordaan
Comment		Instrument / Ser#	micrOTOF-Q II 2010390

Acquisition Parameter

Source Type	APCI	Ion Polarity	Positive	Set Nebulizer	1.6 Bar
Focus	Not active	Set Capillary	4500 V	Set Dry Heater	200 °C
Scan Begin	50 m/z	Set End Plate Offset	-500 V	Set Dry Gas	8.0 l/min
Scan End	1500 m/z	Set Collision Cell RF	100.0 Vpp	Set Divert Valve	Waste

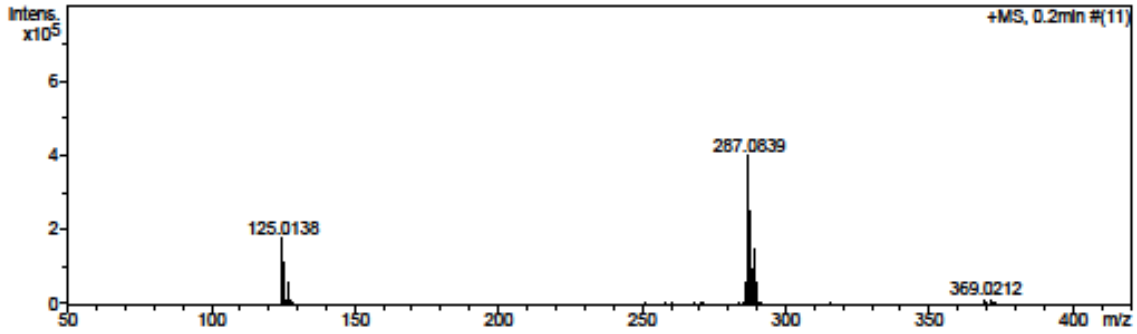

Meas. m/z	#	Formula	Score	m/z	err [mDa]	err [ppm]	mSigma	rdb	N-Rule	e⁻ Conf
125.0138	1	C 7 H 6 Cl	100.00	125.0153	1.5	11.8	1.3	4.5	ok	even
287.0839	1	C 17 H 16 Cl O 2	100.00	287.0833	-0.5	-1.8	35.5	9.5	ok	even
	2	C 23 H 11	0.00	287.0855	1.7	5.8	205.5	18.5	ok	even

Compound 1i – MS:

Mass Spectrum SmartFormula Report

Analysis Info

Analysis Name	D:\Data\21062017\LADMS000021.d	Acquisition Date	6/21/2017 1:17:35 PM
Method	tune_low08062017.m	Laboratory	Laboratory for Analytical Services
Sample Name	R2 S3	Operator	JHL Jordaan
Comment		Instrument / Ser#	micrOTOF-Q II 2010390

Acquisition Parameter

Source Type	APCI	Ion Polarity	Positive	Set Nebulizer	1.6 Bar
Focus	Not active	Set Capillary	4500 V	Set Dry Heater	200 °C
Scan Begin	50 m/z	Set End Plate Offset	-500 V	Set Dry Gas	8.0 l/min
Scan End	1500 m/z	Set Collision Cell RF	100.0 Vpp	Set Divert Valve	Waste

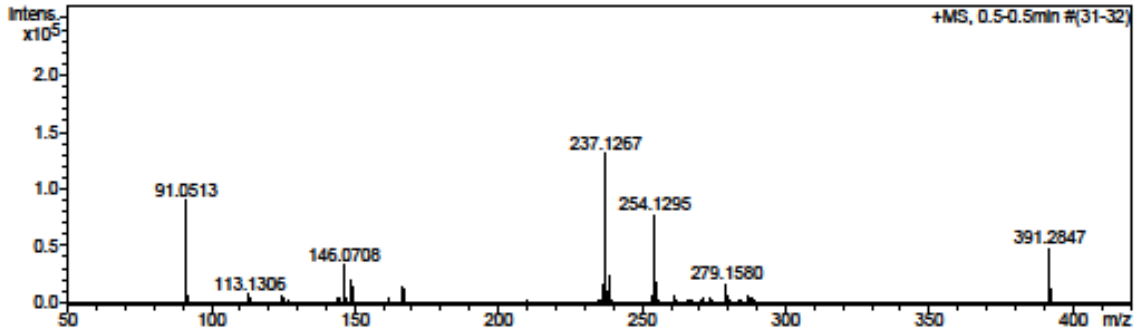

Meas. m/z	#	Formula	Score	m/z	err [mDa]	err [ppm]	mSigma	rdb	N-Rule	e⁻ Conf
91.0513	1	C 7 H 7	100.00	91.0542	2.9	32.1	2.0	4.5	ok	even
237.1267	1	C 17 H 17 O	100.00	237.1274	0.7	2.9	8.8	9.5	ok	even
254.1295	1	C 17 H 18 O 2	100.00	254.1301	0.6	2.5	4.4	9.0	ok	odd
391.2847	1	C 24 H 39 O 4	100.00	391.2843	-0.4	-1.1	3.0	5.5	ok	even

Compound 1j – MS:

Mass Spectrum SmartFormula Report

Analysis Info

Analysis Name	D:\Data\19092017\LADMS000012.d	Acquisition Date	9/19/2017 11:01:41 AM
Method	tune_low11092017.m	Laboratory	Laboratory for Analytical Services
Sample Name	R3-S3-1J	Operator	JHL Jordaan
Comment		Instrument / Ser#	micrOTOF-Q II 2010390

Acquisition Parameter

Source Type	APCI	Ion Polarity	Positive	Set Nebulizer	1.6 Bar
Focus	Not active	Set Capillary	4500 V	Set Dry Heater	200 °C
Scan Begin	50 m/z	Set End Plate Offset	-500 V	Set Dry Gas	8.0 l/min
Scan End	1500 m/z	Set Collision Cell RF	100.0 Vpp	Set Divert Valve	Waste

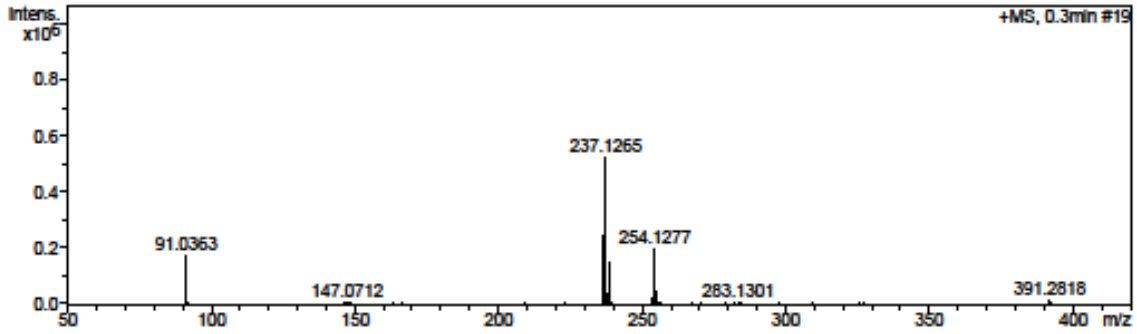

Meas. m/z	#	Formula	Score	m/z	err [mDa]	err [ppm]	mSigma	rdb	N-Rule	e⁻ Conf
237.1265	1	C 17 H 17 O	100.00	237.1274	0.9	3.8	56.4	9.5	ok	even
254.1277	1	C 17 H 18 O 2	100.00	254.1301	2.4	9.6	23.3	9.0	ok	odd

Compound 1k – MS:

Mass Spectrum SmartFormula Report

Analysis Info

Analysis Name	D:\Data\19092017\LADMS000015.d	Acquisition Date	9/19/2017 11:24:11 AM
Method	tune_low11092017.m	Laboratory	Laboratory for Analytical Services
Sample Name	R1-S3-1K	Operator	JHL Jordaan
Comment		Instrument / Ser#	micrOTOF-Q II 2010390

Acquisition Parameter

Source Type	APCI	Ion Polarity	Positive	Set Nebulizer	1.6 Bar
Focus	Not active	Set Capillary	4500 V	Set Dry Heater	200 °C
Scan Begin	50 m/z	Set End Plate Offset	-500 V	Set Dry Gas	8.0 l/min
Scan End	1500 m/z	Set Collision Cell RF	100.0 Vpp	Set Divert Valve	Waste

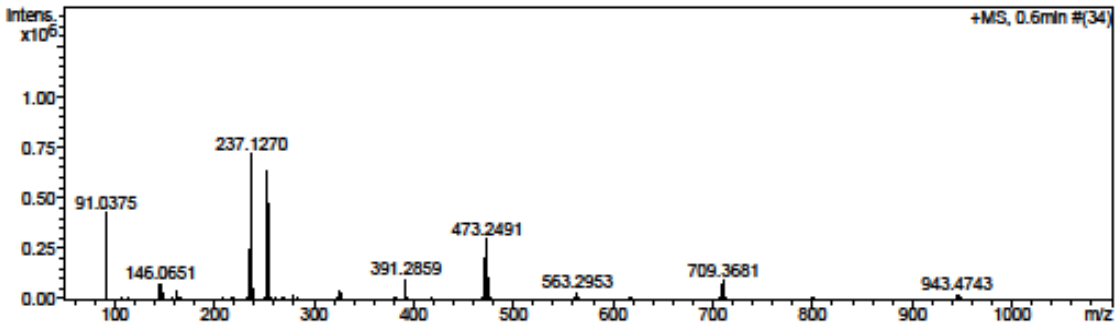

Meas. m/z	#	Formula	Score	m/z	err [mDa]	err [ppm]	mSigma	rdb	N-Rule	e⁻ Conf
237.1270	1	C 17 H 17 O	100.00	237.1274	0.4	1.7	15.0	9.5	ok	even
254.1305	1	C 17 H 18 O 2	100.00	254.1301	-0.4	-1.4	3.9	9.0	ok	odd

Compound 1l – MS:

Mass Spectrum SmartFormula Report

Analysis Info

Analysis Name	D:\Data\21062017\LADMS000016.d	Acquisition Date	6/21/2017 12:30:27 PM
Method	tune_low08062017.m	Laboratory	Laboratory for Analytical Services
Sample Name	R12 S2	Operator	JHL Jordaan
Comment		Instrument / Ser#	micrOTOF-Q II 2010390

Acquisition Parameter

Source Type	APCI	Ion Polarity	Positive	Set Nebulizer	1.6 Bar
Focus	Not active	Set Capillary	4500 V	Set Dry Heater	200 °C
Scan Begin	50 m/z	Set End Plate Offset	-500 V	Set Dry Gas	8.0 l/min
Scan End	1500 m/z	Set Collision Cell RF	100.0 Vpp	Set Divert Valve	Waste

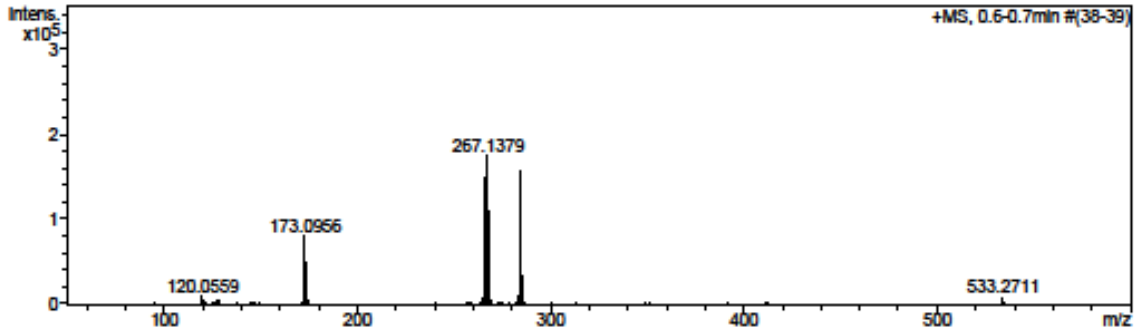

Meas. m/z	#	Formula	Score	m/z	err [mDa]	err [ppm]	mSigma	rdb	N-Rule	e⁻ Conf
173.0956	1	C 12 H 13 O	100.00	173.0961	0.5	2.7	4.5	6.5	ok	even
266.1305	1	C 18 H 18 O 2	100.00	266.1301	-0.4	-1.5	481.6	10.0	ok	odd
267.1379	1	C 18 H 19 O 2	100.00	267.1380	0.0	0.2	11.2	9.5	ok	even
284.1416	1	C 18 H 20 O 3	100.00	284.1407	-0.9	-3.2	7.2	9.0	ok	odd

Compound 1m – MS:

Mass Spectrum SmartFormula Report

Analysis Info

Analysis Name	D:\Data\19092017\LADMS000010.d	Acquisition Date	9/19/2017 10:26:48 AM
Method	tune_low11092017.m	Laboratory	Laboratory for Analytical Services
Sample Name	R4-S2-1M	Operator	JHL Jordaan
Comment		Instrument / Ser#	micrOTOF-Q II 2010390

Acquisition Parameter

Source Type	APCI	Ion Polarity	Positive	Set Nebulizer	1.6 Bar
Focus	Not active	Set Capillary	4500 V	Set Dry Heater	200 °C
Scan Begin	50 m/z	Set End Plate Offset	-500 V	Set Dry Gas	8.0 l/min
Scan End	1500 m/z	Set Collision Cell RF	100.0 Vpp	Set Divert Valve	Waste

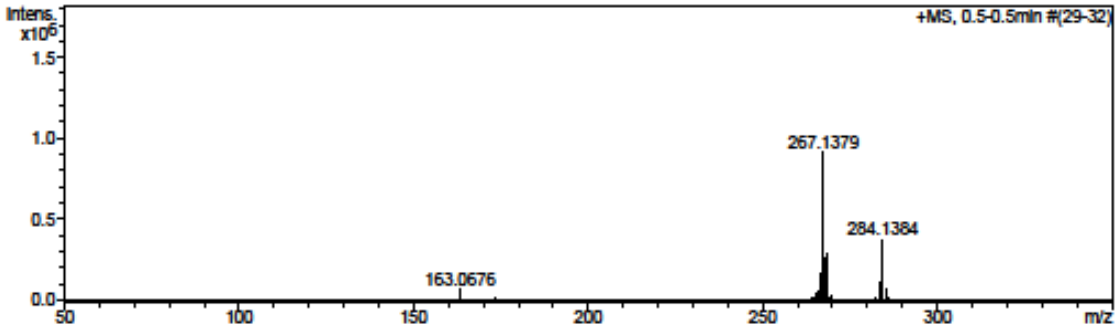

Meas. m/z	#	Formula	Score	m/z	err [mDa]	err [ppm]	mSigma	rdb	N-Rule	e⁻ Conf
267.1379	1	C 18 H 19 O 2	100.00	267.1380	0.0	0.1	68.1	9.5	ok	even
284.1384	1	C 18 H 20 O 3	100.00	284.1407	2.3	8.2	18.3	9.0	ok	odd

Compound 1n – MS:

Mass Spectrum SmartFormula Report

Analysis Info

Analysis Name	D:\Data\19092017\LADMS000008.d	Acquisition Date	9/19/2017 10:14:46 AM
Method	tune_low11092017.m	Laboratory	Laboratory for Analytical Services
Sample Name	R7-S2-1N	Operator	JHL Jordaan
Comment		Instrument / Ser#	micrOTOF-Q II 2010390

Acquisition Parameter

Source Type	APCI	Ion Polarity	Positive	Set Nebulizer	1.6 Bar
Focus	Not active	Set Capillary	4500 V	Set Dry Heater	200 °C
Scan Begin	50 m/z	Set End Plate Offset	-500 V	Set Dry Gas	8.0 l/min
Scan End	1500 m/z	Set Collision Cell RF	100.0 Vpp	Set Divert Valve	Waste

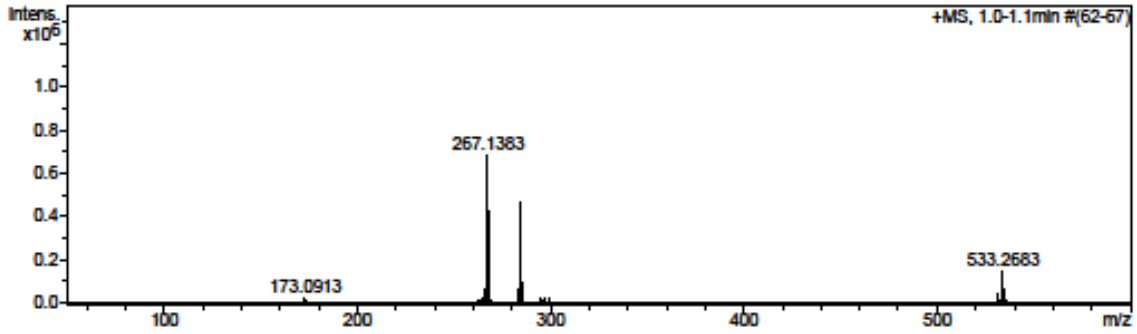

Meas. m/z	#	Formula	Score	m/z	err [mDa]	err [ppm]	mSigma	rdb	N-Rule	e⁻ Conf
284.1410	1	C 18 H 20 O 3	100.00	284.1407	-0.3	-1.0	6.7	9.0	ok	odd

Compound 1o – MS:

Mass Spectrum SmartFormula Report

Analysis Info

Analysis Name	D:\Data\21062017\LADMS000019.d	Acquisition Date	6/21/2017 1:11:51 PM
Method	tune_low08062017.m	Laboratory	Laboratory for Analytical Services
Sample Name	R14 S2	Operator	JHL Jordaan
Comment		Instrument / Ser#	micrOTOF-Q II 2010390

Acquisition Parameter

Source Type	APCI	Ion Polarity	Positive	Set Nebulizer	1.6 Bar
Focus	Not active	Set Capillary	4500 V	Set Dry Heater	200 °C
Scan Begin	50 m/z	Set End Plate Offset	-500 V	Set Dry Gas	8.0 l/min
Scan End	1500 m/z	Set Collision Cell RF	100.0 Vpp	Set Divert Valve	Waste

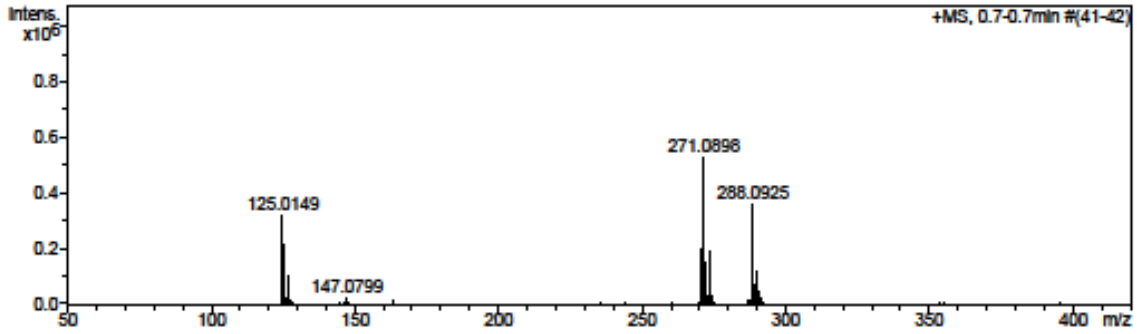

Meas. m/z	#	Formula	Score	m/z	err [mDa]	err [ppm]	mSigma	rdb	N-Rule	e⁻ Conf
125.0149	1	C 7 H 6 Cl	100.00	125.0153	0.4	2.8	2.6	4.5	ok	even
271.0898	1	C 17 H 16 Cl O	100.00	271.0884	-1.4	-5.0	50.6	9.5	ok	even
288.0925	1	C 17 H 17 Cl O 2	100.00	288.0912	-1.4	-4.8	7.6	9.0	ok	odd
	2	C 23 H 12	0.03	288.0934	0.8	2.8	185.9	18.0	ok	odd

Compound 1p – MS:

Mass Spectrum SmartFormula Report

Analysis Info

Analysis Name	D:\Data\21062017\LADMS000018.d	Acquisition Date	6/21/2017 1:08:42 PM
Method	tune_low08062017.m	Laboratory	Laboratory for Analytical Services
Sample Name	R13 S2	Operator	JHL Jordaan
Comment		Instrument / Ser#	micrOTOF-Q II 2010390

Acquisition Parameter

Source Type	APCI	Ion Polarity	Positive	Set Nebulizer	1.6 Bar
Focus	Not active	Set Capillary	4500 V	Set Dry Heater	200 °C
Scan Begin	50 m/z	Set End Plate Offset	-500 V	Set Dry Gas	8.0 l/min
Scan End	1500 m/z	Set Collision Cell RF	100.0 Vpp	Set Divert Valve	Waste

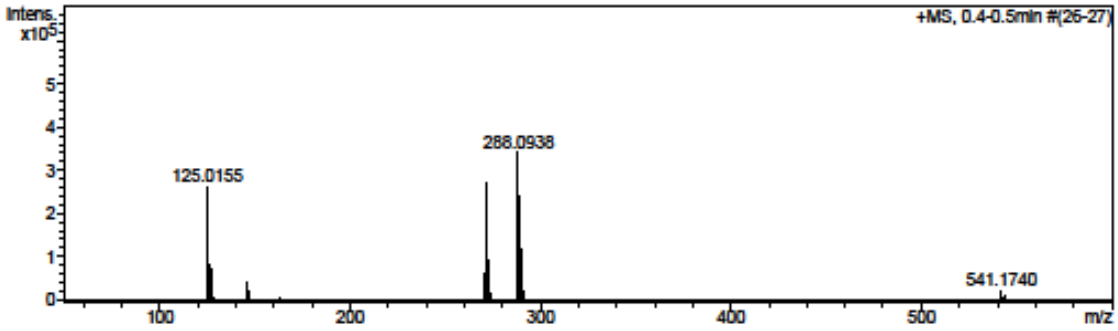

Meas. m/z	#	Formula	Score	m/z	err [mDa]	err [ppm]	mSigma	rdb	N-Rule	e⁻ Conf
125.0155	1	C 7 H 6 Cl	100.00	125.0153	-0.2	-1.9	5.7	4.5	ok	even
271.0905	1	C 17 H 16 Cl O	100.00	271.0884	-2.1	-7.8	35.1	9.5	ok	even
288.0938	1	C 17 H 17 Cl O 2	100.00	288.0912	-2.6	-9.0	9.2	9.0	ok	odd
	2	C 23 H 12	0.14	288.0934	-0.4	-1.4	182.1	18.0	ok	odd

Bruker Compass DataAnalysis 4.0 printed: 6/21/2017 1:10:23 PM Page 1 of 1

Compound 1a – HPLC trace:

```
Data File C:\CHEM32\1\DATA\PURITY\PUR2AUG 2017-08-02 09-34-03\Pur2Aug0000013.D
Sample Name: R2S2 1mM

=====================================================================
Acq. Operator   : SYSTEM                        Seq. Line :  13
Acq. Instrument : H1                            Location :   13
Injection Date  : 8/2/2017 12:51:01 PM               Inj :   1
                                               Inj Volume : 10.000 µl
Acq. Method     : C:\Chem32\1\Data\PURITY\Pur2Aug 2017-08-02 09-34-03\Purity.M
Last changed    : 7/31/2017 1:40:47 PM by SYSTEM
Analysis Method : C:\CHEM32\1\METHODS\Purity.M
Last changed    : 8/7/2017 9:01:46 AM by SYSTEM
                  (modified after loading)
Method Info     : Purity Test
                  Venusil XBP C18(2) 150 x 4.6 mm
                  acn/water  30/70,   85% after 5 min, to 15 min, stop 20 min.
                  wavelength  210, 230,  254, 280, 300 nm, 4 nm BW
                  1 ml/min,
```

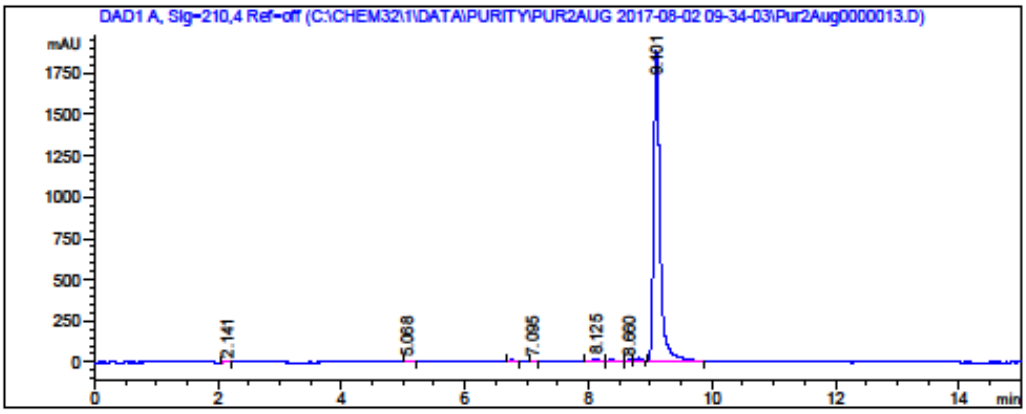


```
=====================================================================
                        Area Percent Report
=====================================================================

Sorted By             :      Signal
Multiplier            :      1.0000
Dilution              :      1.0000
Do not use Multiplier & Dilution Factor with ISTDs


Signal 1: DAD1 A, Sig=210,4 Ref=off

Peak RetTime Type  Width     Area      Height     Area
  #   [min]        [min]   [mAU*s]     [mAU]       %
----|-------|----|-------|----------|----------|--------|
   1   2.141 BB    0.0832   10.58801    1.59988   0.0771
   2   5.068 BB    0.0578    8.28389    2.20830   0.0603
   3   6.767 BB    0.0702   24.24506    5.21400   0.1764
   4   7.095 BB    0.0640    5.09079    1.29134   0.0370
   5   8.125 BB    0.0859   42.06221    7.01606   0.3061
   6   8.377 BB    0.0869   26.90502    4.83848   0.1958
   7   8.660 BB    0.0672   12.09456    2.86653   0.0880
   8   8.816 BB    0.0819   79.80678   15.03666   0.5808
   9   9.101 BB    0.1099 1.35315e4  1881.11780  98.4784

H1 8/7/2017 9:14:58 AM SYSTEM                          Page   1 of 2
```

Compound 1b – HPLC trace:

Data File C:\CHEM32\1\DATA\PURITY\PUR2AUG 2017-08-02 09-34-03\Pur2Aug0000017.D
Sample Name: R3S2 1mM

```
======================================================================
Acq. Operator   : SYSTEM                       Seq. Line :  17
Acq. Instrument : H1                            Location :   17
Injection Date  : 8/2/2017 1:56:19 PM                Inj :   1
                                               Inj Volume : 10.000 µl
Acq. Method     : C:\Chem32\1\Data\PURITY\Pur2Aug 2017-08-02 09-34-03\Purity.M
Last changed    : 7/31/2017 1:40:47 PM by SYSTEM
Analysis Method : C:\CHEM32\1\METHODS\Purity.M
Last changed    : 8/7/2017 9:01:46 AM by SYSTEM
                  (modified after loading)
Method Info     : Purity Test
                  Venusil XBP C18(2) 150 x 4.6 mm
                  acn/water  30/70,   85% after 5 min, to 15 min, stop 20 min.
                  wavelength  210, 230,  254, 280, 300 nm, 4 nm BW
                  1 ml/min,
```

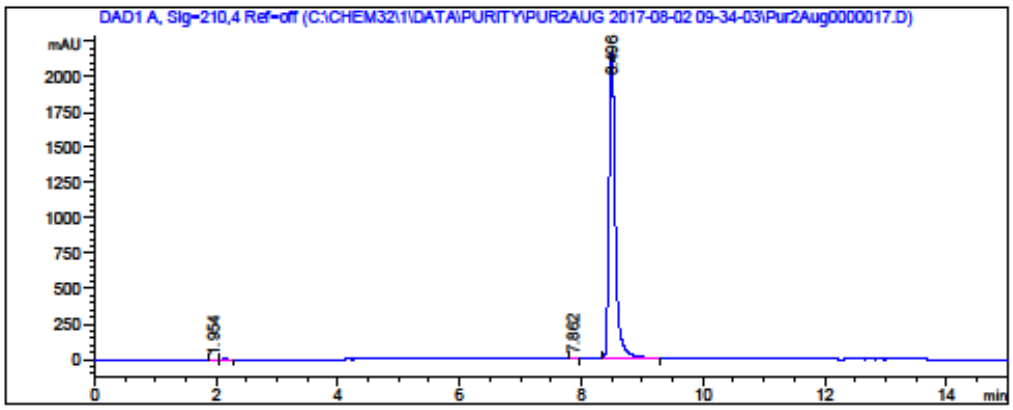


```
======================================================================
                        Area Percent Report
======================================================================

Sorted By             :      Signal
Multiplier            :      1.0000
Dilution              :      1.0000
Do not use Multiplier & Dilution Factor with ISTDs


Signal 1: DAD1 A, Sig=210,4 Ref=off

Peak RetTime Type  Width     Area      Height     Area
  #   [min]        [min]   [mAU*s]     [mAU]       %
----|-------|----|-------|----------|----------|--------|
   1   1.954 BB    0.0727    6.73913    1.21611   0.0435
   2   2.159 BB    0.1084   18.95153    2.39348   0.1223
   3   7.862 BB    0.0870    7.30777    1.20164   0.0472
   4   8.496 BB    0.1089 1.54621e4  2175.04321  99.7870

Totals :                  1.54951e4  2179.85444


======================================================================
                        *** End of Report ***

H1 8/7/2017 9:17:50 AM SYSTEM                          Page   1 of 1
```

Compound 1c – HPLC trace:

```
Data File C:\CHEM32\1\DATA\PURITY\PUR2AUG 2017-08-02 09-34-03\Pur2Aug0000009.D
Sample Name: R1S2 1mM

    ======================================================================
    Acq. Operator   : SYSTEM                        Seq. Line :   9
    Acq. Instrument : H1                            Location :   9
    Injection Date  : 8/2/2017 11:45:47 AM               Inj :   1
                                                  Inj Volume : 10.000 µl
    Acq. Method     : C:\Chem32\1\Data\PURITY\Pur2Aug 2017-08-02 09-34-03\Purity.M
    Last changed    : 7/31/2017 1:40:47 PM by SYSTEM
    Analysis Method : C:\CHEM32\1\METHODS\Purity.M
    Last changed    : 8/7/2017 9:01:46 AM by SYSTEM
                      (modified after loading)
    Method Info     : Purity Test
                      Venusil XBP C18(2) 150 x 4.6 mm
                      acn/water  30/70,   85% after 5 min, to 15 min, stop 20 min.
                      wavelength  210, 230,  254, 280, 300 nm, 4 nm BW
                      1 ml/min,
```

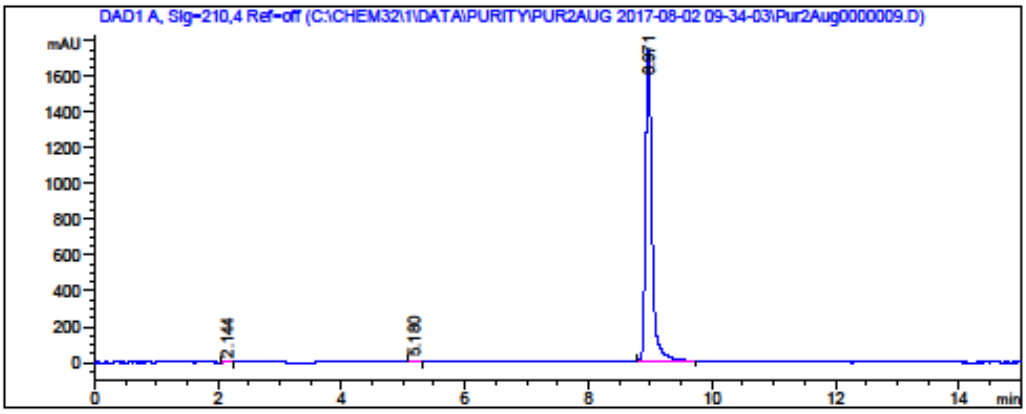


```
    ======================================================================
                            Area Percent Report
    ======================================================================

    Sorted By             :      Signal
    Multiplier            :      1.0000
    Dilution              :      1.0000
    Do not use Multiplier & Dilution Factor with ISTDs


    Signal 1: DAD1 A, Sig=210,4 Ref=off

    Peak RetTime Type  Width     Area      Height     Area
      #   [min]       [min]   [mAU*s]     [mAU]       %
    ----|-------|----|-------|----------|----------|--------|
       1   2.144 BB    0.1001   18.20947    2.46752   0.1500
       2   5.180 BB    0.0614   14.40610    3.54379   0.1187
       3   8.971 BB    0.1053 1.21083e4  1737.48145  99.7314

    Totals :                   1.21409e4  1743.49276


    ======================================================================
                            *** End of Report ***

H1 8/7/2017 9:12:55 AM SYSTEM                                  Page   1 of 1
```

Compound 1d – HPLC trace:

```
Data File C:\CHEM32\1\DATA\PURITY\PUR2AUG 2017-08-02 09-34-03\Pur2Aug0000029.D
Sample Name: R12S1 1mM

    ======================================================================
    Acq. Operator   : SYSTEM                        Seq. Line :  29
    Acq. Instrument : H1                             Location :   29
    Injection Date  : 8/2/2017 5:11:49 PM                 Inj :   1
                                                  Inj Volume : 10.000 µl
    Acq. Method     : C:\Chem32\1\Data\PURITY\Pur2Aug 2017-08-02 09-34-03\Purity.M
    Last changed    : 7/31/2017 1:40:47 PM by SYSTEM
    Analysis Method : C:\CHEM32\1\METHODS\Purity.M
    Last changed    : 8/7/2017 9:01:46 AM by SYSTEM
                      (modified after loading)
    Method Info     : Purity Test
                      Venusil XBP C18(2) 150 x 4.6 mm
                      acn/water  30/70,   85% after 5 min, to 15 min, stop 20 min.
                      wavelength  210, 230,  254, 280, 300 nm, 4 nm BW
                      1 ml/min,
```

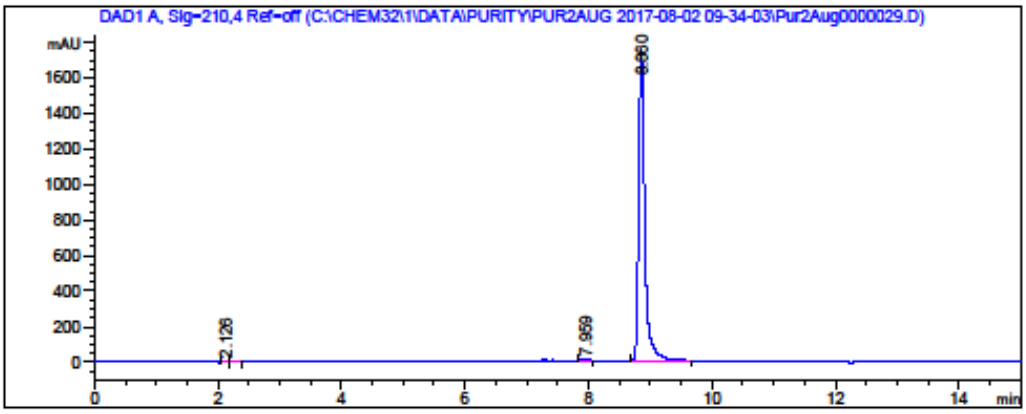


```
    ======================================================================
                            Area Percent Report
    ======================================================================

    Sorted By             :      Signal
    Multiplier            :      1.0000
    Dilution              :      1.0000
    Do not use Multiplier & Dilution Factor with ISTDs


    Signal 1: DAD1 A, Sig=210,4 Ref=off

    Peak RetTime Type  Width     Area      Height     Area
      #   [min]       [min]   [mAU*s]     [mAU]       %
    ----|-------|----|-------|----------|----------|--------|
       1   2.126 BB    0.0635    6.43440    1.45855   0.0535
       2   2.261 BB    0.0603    7.38851    1.86013   0.0614
       3   7.959 BB    0.0957   11.97286    1.55673   0.0995
       4   8.860 BB    0.1043 1.20053e4  1745.30847  99.7856

    Totals :                   1.20311e4  1750.18388


    ======================================================================
                            *** End of Report ***

H1 8/7/2017 9:23:48 AM SYSTEM                                  Page   1 of 1
```

Compound 1e – HPLC trace:

```
Data File C:\CHEM32\1\DATA\PURITY\PUR2AUG 2017-08-02 09-34-03\Pur2Aug0000021.D
Sample Name: R4S1 1mM

    ======================================================================
    Acq. Operator   : SYSTEM                        Seq. Line :  21
    Acq. Instrument : H1                             Location :   21
    Injection Date  : 8/2/2017 3:01:38 PM                 Inj :   1
                                                  Inj Volume : 10.000 µl
    Acq. Method     : C:\Chem32\1\Data\PURITY\Pur2Aug 2017-08-02 09-34-03\Purity.M
    Last changed    : 7/31/2017 1:40:47 PM by SYSTEM
    Analysis Method : C:\CHEM32\1\METHODS\Purity.M
    Last changed    : 8/7/2017 9:01:46 AM by SYSTEM
                      (modified after loading)
    Method Info     : Purity Test
                      Venusil XBP C18(2) 150 x 4.6 mm
                      acn/water  30/70,   85% after 5 min, to 15 min, stop 20 min.
                      wavelength  210, 230,  254, 280, 300 nm, 4 nm BW
                      1 ml/min,
```

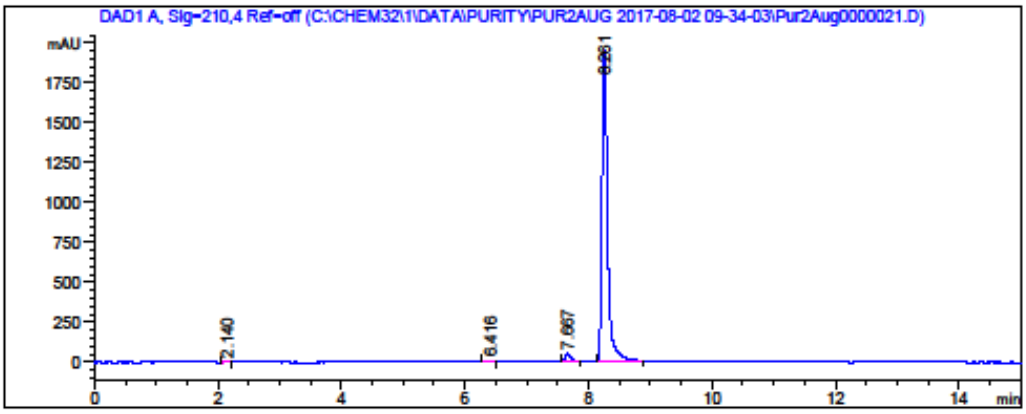


```
    ======================================================================
                              Area Percent Report
    ======================================================================

    Sorted By             :      Signal
    Multiplier            :      1.0000
    Dilution              :      1.0000
    Do not use Multiplier & Dilution Factor with ISTDs


    Signal 1: DAD1 A, Sig=210,4 Ref=off

    Peak RetTime Type  Width     Area      Height     Area
      #   [min]       [min]   [mAU*s]     [mAU]       %
    ----|-------|----|-------|----------|----------|--------|
       1   2.140 BB    0.0872   12.27768    2.26652   0.0983
       2   6.416 BB    0.0770    7.36044    1.28147   0.0589
       3   7.667 BB    0.0761  204.07788   40.96951   1.6343
       4   8.261 BB    0.0956 1.22636e4  1943.47266  98.2085

    Totals :                   1.24873e4  1987.99015


    ======================================================================
                              *** End of Report ***

H1 8/7/2017 9:20:13 AM SYSTEM                                  Page   1 of 1
```

Compound 1f – HPLC trace:

Data File C:\CHEM32\1\DATA\PURITY\PUR2AUG 2017-08-02 09-34-03\Pur2Aug0000025.D
Sample Name: R7S1 1mM

```
======================================================================
Acq. Operator   : SYSTEM                       Seq. Line :  25
Acq. Instrument : H1                            Location :   25
Injection Date  : 8/2/2017 4:06:40 PM                Inj :   1
                                               Inj Volume : 10.000 µl
Acq. Method     : C:\Chem32\1\Data\PURITY\Pur2Aug 2017-08-02 09-34-03\Purity.M
Last changed    : 7/31/2017 1:40:47 PM by SYSTEM
Analysis Method : C:\CHEM32\1\METHODS\Purity.M
Last changed    : 8/7/2017 9:01:46 AM by SYSTEM
                  (modified after loading)
Method Info     : Purity Test
                  Venusil XBP C18(2) 150 x 4.6 mm
                  acn/water  30/70,   85% after 5 min, to 15 min, stop 20 min.
                  wavelength  210, 230,  254, 280, 300 nm, 4 nm BW
                  1 ml/min,
```

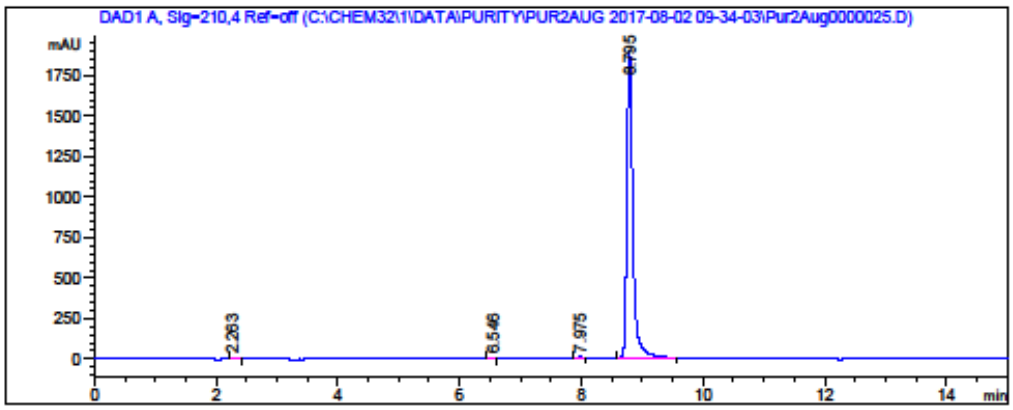


```
======================================================================
                        Area Percent Report
======================================================================

Sorted By             :      Signal
Multiplier            :      1.0000
Dilution              :      1.0000
Do not use Multiplier & Dilution Factor with ISTDs


Signal 1: DAD1 A, Sig=210,4 Ref=off

Peak RetTime Type  Width     Area      Height     Area
  #   [min]        [min]   [mAU*s]     [mAU]       %
----|-------|----|-------|----------|----------|--------|
   1   2.263 BB    0.0658   13.24446    2.98291   0.1020
   2   6.546 BB    0.0637    7.20709    1.69086   0.0555
   3   7.975 BB    0.0802   13.45632    2.37244   0.1037
   4   8.795 BB    0.1038 1.29469e4  1893.30151  99.7388

Totals :                   1.29808e4  1900.34773


======================================================================
                        *** End of Report ***

H1 8/7/2017 9:22:06 AM SYSTEM                          Page   1 of 1
```

Compound 1g – HPLC trace:

Data File C:\CHEM32\1\DATA\PURITY\PUR2AUG 2017-08-02 09-34-03\Pur2Aug0000037.D
Sample Name: R14S1 1mM

```
=====================================================================
Acq. Operator   : SYSTEM                       Seq. Line :  37
Acq. Instrument : H1                            Location :   37
Injection Date  : 8/2/2017 7:22:23 PM                Inj :   1
                                               Inj Volume : 10.000 µl
Acq. Method     : C:\Chem32\1\Data\PURITY\Pur2Aug 2017-08-02 09-34-03\Purity.M
Last changed    : 7/31/2017 1:40:47 PM by SYSTEM
Analysis Method : C:\CHEM32\1\METHODS\Purity.M
Last changed    : 8/7/2017 9:01:46 AM by SYSTEM
                  (modified after loading)
Method Info     : Purity Test
                  Venusil XBP C18(2) 150 x 4.6 mm
                  acn/water  30/70,   85% after 5 min, to 15 min, stop 20 min.
                  wavelength  210, 230,  254, 280, 300 nm, 4 nm BW
                  1 ml/min,
```

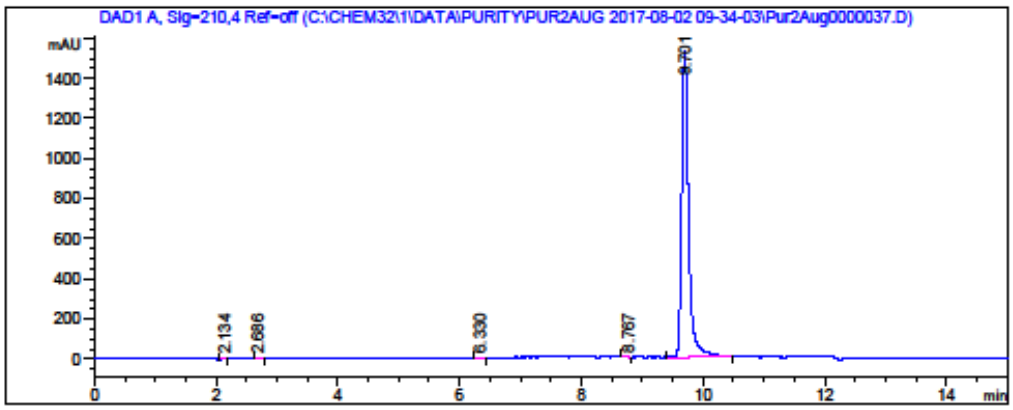


```
=====================================================================
                        Area Percent Report
=====================================================================

Sorted By             :      Signal
Multiplier            :      1.0000
Dilution              :      1.0000
Do not use Multiplier & Dilution Factor with ISTDs


Signal 1: DAD1 A, Sig=210,4 Ref=off

Peak RetTime Type  Width     Area      Height     Area
  #   [min]        [min]   [mAU*s]     [mAU]       %
----|-------|----|-------|----------|----------|--------|
   1   2.134 BB    0.0616    6.44322    1.58026   0.0527
   2   2.686 BB    0.0687    9.74176    2.00484   0.0797
   3   6.330 BB    0.0780    7.83669    1.38615   0.0641
   4   8.767 BB    0.0635    7.75223    1.69020   0.0634
   5   9.701 BB    0.1211 1.21909e4  1527.59033  99.7400

Totals :                   1.22227e4  1534.25178

=====================================================================
```

Compound 1h – HPLC trace:

Data File C:\CHEM32\1\DATA\PURITY\PUR2AUG 2017-08-02 09-34-03\Pur2Aug0000033.D
Sample Name: R13S1 1mM

```
=====================================================================
Acq. Operator   : SYSTEM                        Seq. Line :  33
Acq. Instrument : H1                             Location :  33
Injection Date  : 8/2/2017 6:17:05 PM                 Inj :  1
                                                Inj Volume : 10.000 µl
Acq. Method     : C:\Chem32\1\Data\PURITY\Pur2Aug 2017-08-02 09-34-03\Purity.M
Last changed    : 7/31/2017 1:40:47 PM by SYSTEM
Analysis Method : C:\CHEM32\1\METHODS\Purity.M
Last changed    : 8/7/2017 9:01:46 AM by SYSTEM
                  (modified after loading)
Method Info     : Purity Test
                  Venusil XBP C18(2) 150 x 4.6 mm
                  acn/water  30/70,   85% after 5 min, to 15 min, stop 20 min.
                  wavelength  210, 230,  254, 280, 300 nm, 4 nm BW
                  1 ml/min,
```

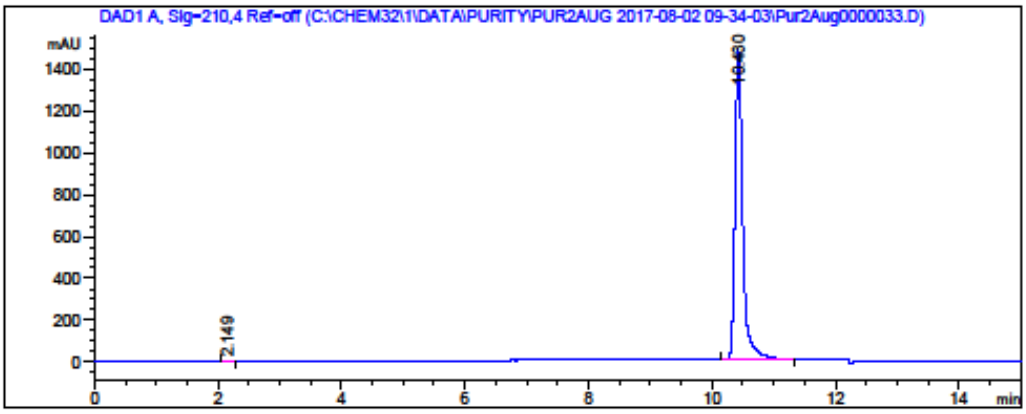


```
=====================================================================
                        Area Percent Report
=====================================================================

Sorted By             :      Signal
Multiplier            :      1.0000
Dilution              :      1.0000
Do not use Multiplier & Dilution Factor with ISTDs


Signal 1: DAD1 A, Sig=210,4 Ref=off

Peak RetTime Type  Width     Area      Height     Area
  #   [min]       [min]   [mAU*s]     [mAU]       %
----|-------|----|-------|----------|----------|--------|
   1   2.149 BB    0.0969   20.40456    2.73920   0.1558
   2  10.430 BB    0.1307 1.30748e4  1485.41333  99.8442

Totals :                  1.30952e4  1488.15253


=====================================================================
                        *** End of Report ***
```

Compound 1i – HPLC trace:

```
Data File C:\CHEM32\1\DATA\PURITY\PUR2AUG 2017-08-02 09-34-03\Pur2Aug0000015.D
Sample Name: R2S3 1mM

    ======================================================================
    Acq. Operator   : SYSTEM                        Seq. Line :  15
    Acq. Instrument : H1                             Location :   15
    Injection Date  : 8/2/2017 1:23:42 PM                 Inj :   1
                                                  Inj Volume : 10.000 µl
    Acq. Method     : C:\Chem32\1\Data\PURITY\Pur2Aug 2017-08-02 09-34-03\Purity.M
    Last changed    : 7/31/2017 1:40:47 PM by SYSTEM
    Analysis Method : C:\CHEM32\1\METHODS\Purity.M
    Last changed    : 8/7/2017 9:01:46 AM by SYSTEM
                      (modified after loading)
    Method Info     : Purity Test
                      Venusil XBP C18(2) 150 x 4.6 mm
                      acn/water  30/70,   85% after 5 min, to 15 min, stop 20 min.
                      wavelength  210, 230,  254, 280, 300 nm, 4 nm BW
                      1 ml/min,
```

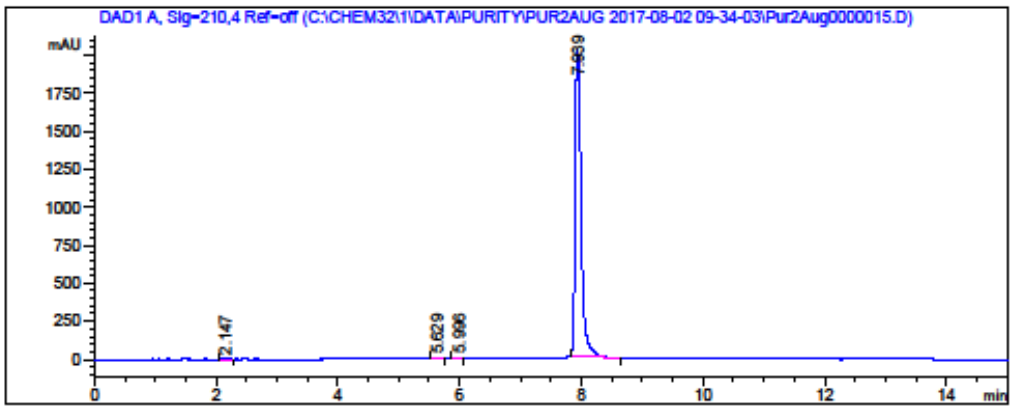


```
    ======================================================================
                            Area Percent Report
    ======================================================================

    Sorted By             :      Signal
    Multiplier            :      1.0000
    Dilution              :      1.0000
    Do not use Multiplier & Dilution Factor with ISTDs


    Signal 1: DAD1 A, Sig=210,4 Ref=off

    Peak RetTime Type  Width     Area      Height     Area
      #   [min]        [min]   [mAU*s]     [mAU]       %
    ----|-------|----|-------|----------|----------|--------|
       1   2.147 BB    0.1091   22.67553    2.78235   0.1658
       2   5.629 BB    0.0754   13.63547    2.67657   0.0997
       3   5.996 BB    0.0595   22.52045    6.03587   0.1647
       4   7.939 BB    0.1051 1.36184e4  2008.53052  99.5699

    Totals :                   1.36773e4  2020.02530


    ======================================================================
                            *** End of Report ***

H1 8/7/2017 9:17:07 AM SYSTEM                                  Page   1 of 1
```

Compound 1j – HPLC trace:

```
Data File C:\CHEM32\1\DATA\PURITY\PUR2AUG 2017-08-02 09-34-03\Pur2Aug0000019.D
Sample Name: R3S3 1mM

    ======================================================================
    Acq. Operator   : SYSTEM                        Seq. Line :  19
    Acq. Instrument : H1                             Location :   19
    Injection Date  : 8/2/2017 2:28:55 PM                 Inj :   1
                                                  Inj Volume : 10.000 µl
    Acq. Method     : C:\Chem32\1\Data\PURITY\Pur2Aug 2017-08-02 09-34-03\Purity.M
    Last changed    : 7/31/2017 1:40:47 PM by SYSTEM
    Analysis Method : C:\CHEM32\1\METHODS\Purity.M
    Last changed    : 8/7/2017 9:01:46 AM by SYSTEM
                      (modified after loading)
    Method Info     : Purity Test
                      Venusil XBP C18(2) 150 x 4.6 mm
                      acn/water  30/70,   85% after 5 min, to 15 min, stop 20 min.
                      wavelength  210, 230,  254, 280, 300 nm, 4 nm BW
                      1 ml/min,
```

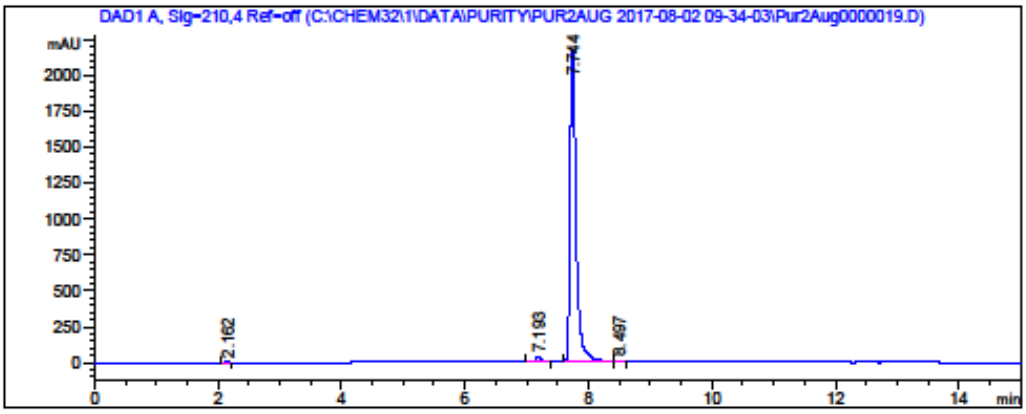


```
    ======================================================================
                              Area Percent Report
    ======================================================================

    Sorted By             :      Signal
    Multiplier            :      1.0000
    Dilution              :      1.0000
    Do not use Multiplier & Dilution Factor with ISTDs


    Signal 1: DAD1 A, Sig=210,4 Ref=off

    Peak RetTime Type  Width     Area      Height     Area
      #   [min]       [min]   [mAU*s]     [mAU]       %
    ----|-------|----|-------|----------|----------|--------|
       1   2.162 BB    0.0986   12.60917    1.62454   0.0843
       2   7.193 BB    0.0720  158.89876   33.08935   1.0617
       3   7.744 BB    0.1035 1.47822e4  2170.57983  98.7718
       4   8.497 BB    0.0744   12.30221    2.54433   0.0822

    Totals :                  1.49660e4  2207.83805

    ======================================================================
                              *** End of Report ***

H1 8/7/2017 9:19:30 AM SYSTEM                                  Page   1 of 1
```

Compound 1k – HPLC trace:

Data File C:\CHEM32\1\DATA\PURITY\PUR2AUG 2017-08-02 09-34-03\Pur2Aug0000011.D
Sample Name: R1S3 1mM

```
=====================================================================
Acq. Operator   : SYSTEM                        Seq. Line :  11
Acq. Instrument : H1                             Location :  11
Injection Date  : 8/2/2017 12:18:31 PM               Inj :  1
                                                Inj Volume : 10.000 µl
Acq. Method     : C:\Chem32\1\Data\PURITY\Pur2Aug 2017-08-02 09-34-03\Purity.M
Last changed    : 7/31/2017 1:40:47 PM by SYSTEM
Analysis Method : C:\CHEM32\1\METHODS\Purity.M
Last changed    : 8/7/2017 9:01:46 AM by SYSTEM
                  (modified after loading)
Method Info     : Purity Test
                  Venusil XBP C18(2) 150 x 4.6 mm
                  acn/water  30/70,   85% after 5 min, to 15 min, stop 20 min.
                  wavelength  210, 230,  254, 280, 300 nm, 4 nm BW
                  1 ml/min,
```

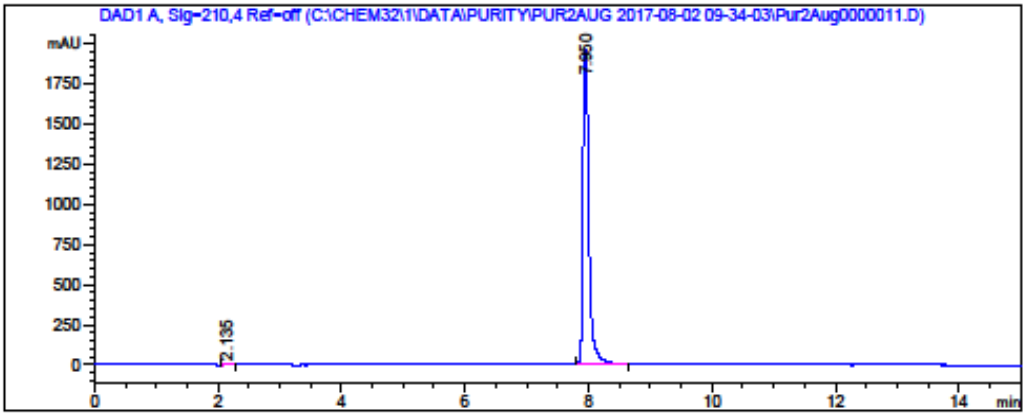


```
=====================================================================
                        Area Percent Report
=====================================================================

Sorted By             :      Signal
Multiplier            :      1.0000
Dilution              :      1.0000
Do not use Multiplier & Dilution Factor with ISTDs


Signal 1: DAD1 A, Sig=210,4 Ref=off

Peak RetTime Type  Width     Area      Height     Area
  #   [min]        [min]   [mAU*s]     [mAU]       %
----|-------|----|-------|----------|----------|--------|
   1   2.135 BB    0.0988   15.12149    2.18384   0.1202
   2   7.950 BB    0.0989 1.25651e4  1956.68799  99.8798

Totals :                  1.25802e4  1958.87182


=====================================================================
                        *** End of Report ***
```

H1 8/7/2017 9:14:12 AM SYSTEM Page 1 of 1

Compound 1l – HPLC trace:

```
Data File C:\CHEM32\1\DATA\PURITY\PUR2AUG 2017-08-02 09-34-03\Pur2Aug0000031.D
Sample Name: R12S2 1mM

=====================================================================
Acq. Operator   : SYSTEM                        Seq. Line :  31
Acq. Instrument : H1                            Location :   31
Injection Date  : 8/2/2017 5:44:35 PM                Inj :   1
                                               Inj Volume : 10.000 µl
Acq. Method     : C:\Chem32\1\Data\PURITY\Pur2Aug 2017-08-02 09-34-03\Purity.M
Last changed    : 7/31/2017 1:40:47 PM by SYSTEM
Analysis Method : C:\CHEM32\1\METHODS\Purity.M
Last changed    : 8/7/2017 9:01:46 AM by SYSTEM
                  (modified after loading)
Method Info     : Purity Test
                  Venusil XBP C18(2) 150 x 4.6 mm
                  acn/water  30/70,   85% after 5 min, to 15 min, stop 20 min.
                  wavelength  210, 230,  254, 280, 300 nm, 4 nm BW
                  1 ml/min,
```

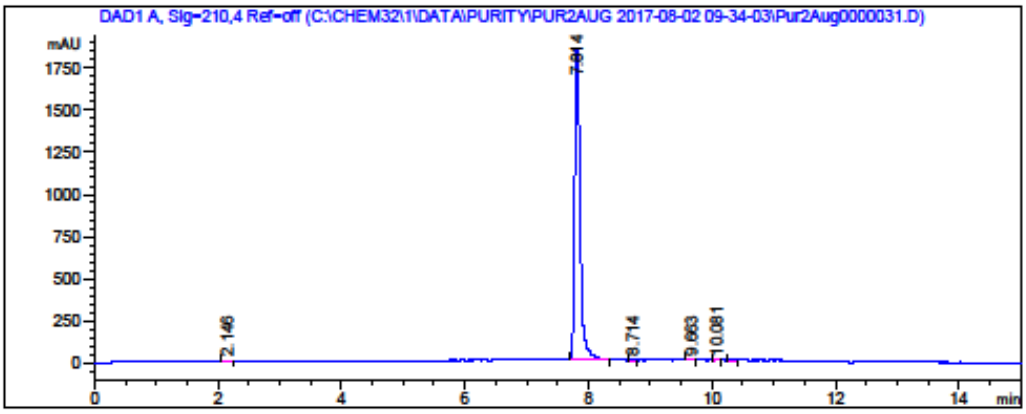


```
=====================================================================
                        Area Percent Report
=====================================================================

Sorted By             :      Signal
Multiplier            :      1.0000
Dilution              :      1.0000
Do not use Multiplier & Dilution Factor with ISTDs


Signal 1: DAD1 A, Sig=210,4 Ref=off

Peak RetTime Type  Width     Area      Height     Area
  #   [min]        [min]   [mAU*s]     [mAU]       %
----|-------|----|-------|----------|----------|--------|
   1   2.146 BB    0.0943   15.36826    2.03127   0.1410
   2   7.814 BB    0.0889 1.08525e4  1838.89758  99.5899
   3   8.714 BB    0.0632    6.31573    1.49627   0.0580
   4   9.663 BB    0.0554    5.86013    1.57620   0.0538
   5  10.081 BB    0.0548    5.29892    1.21788   0.0486
   6  10.348 BB    0.0709   11.84954    2.19772   0.1087

Totals :                  1.08972e4  1847.41691

H1 8/7/2017 9:24:43 AM SYSTEM                          Page   1 of 2
```

Compound 1m – HPLC trace:

```
Data File C:\CHEM32\1\DATA\PURITY\PUR2AUG 2017-08-02 09-34-03\Pur2Aug0000023.D
Sample Name: R4S2 1mM

    ======================================================================
    Acq. Operator   : SYSTEM                        Seq. Line :  23
    Acq. Instrument : H1                             Location :   23
    Injection Date  : 8/2/2017 3:34:12 PM                 Inj :   1
                                                  Inj Volume : 10.000 µl
    Acq. Method     : C:\Chem32\1\Data\PURITY\Pur2Aug 2017-08-02 09-34-03\Purity.M
    Last changed    : 7/31/2017 1:40:47 PM by SYSTEM
    Analysis Method : C:\CHEM32\1\METHODS\Purity.M
    Last changed    : 8/7/2017 9:01:46 AM by SYSTEM
                      (modified after loading)
    Method Info     : Purity Test
                      Venusil XBP C18(2) 150 x 4.6 mm
                      acn/water  30/70,   85% after 5 min, to 15 min, stop 20 min.
                      wavelength  210, 230,  254, 280, 300 nm, 4 nm BW
                      1 ml/min,
```

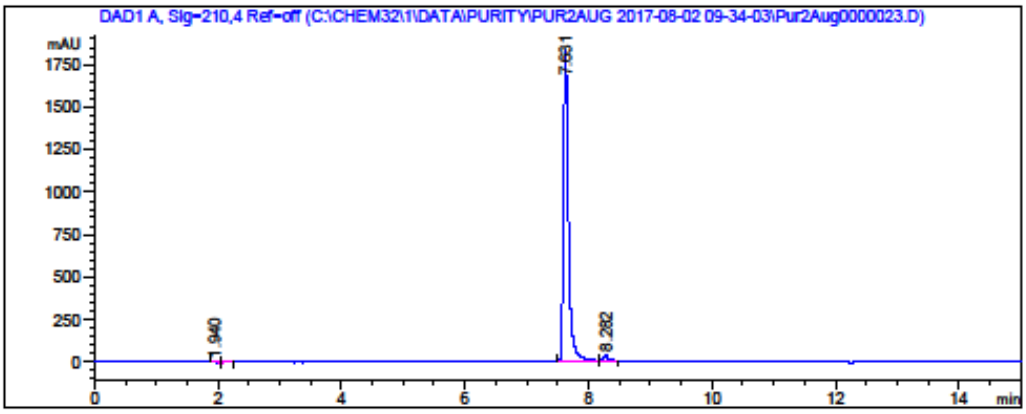


```
    ======================================================================
                            Area Percent Report
    ======================================================================

    Sorted By             :      Signal
    Multiplier            :      1.0000
    Dilution              :      1.0000
    Do not use Multiplier & Dilution Factor with ISTDs


    Signal 1: DAD1 A, Sig=210,4 Ref=off

    Peak RetTime Type  Width     Area      Height     Area
      #   [min]       [min]   [mAU*s]     [mAU]       %
    ----|-------|----|-------|----------|----------|--------|
       1   1.940 BB    0.0791    7.59756    1.24738   0.0723
       2   2.151 BB    0.1001   16.91989    2.29399   0.1610
       3   7.631 BB    0.0859 1.03355e4  1830.72900  98.3407
       4   8.282 BB    0.0818  149.87645   27.39572   1.4260

    Totals :                  1.05099e4  1861.66609


    ======================================================================
                            *** End of Report ***

H1 8/7/2017 9:21:06 AM SYSTEM                                  Page   1 of 1
```

Compound 1n – HPLC trace:

Data File C:\CHEM32\1\DATA\PURITY\PUR2AUG 2017-08-02 09-34-03\Pur2Aug0000027.D
Sample Name: R7S2 1mM

Acq. Operator	: SYSTEM	Seq. Line :	27
Acq. Instrument	: H1	Location :	27
Injection Date	: 8/2/2017 4:39:19 PM	Inj :	1
		Inj Volume :	10.000 µl
Acq. Method	: C:\Chem32\1\Data\PURITY\Pur2Aug 2017-08-02 09-34-03\Purity.M		
Last changed	: 7/31/2017 1:40:47 PM by SYSTEM		
Analysis Method	: C:\CHEM32\1\METHODS\Purity.M		
Last changed	: 8/7/2017 9:01:46 AM by SYSTEM (modified after loading)		
Method Info	: Purity Test Venusil XBP C18(2) 150 x 4.6 mm acn/water 30/70, 85% after 5 min, to 15 min, stop 20 min. wavelength 210, 230, 254, 280, 300 nm, 4 nm BW 1 ml/min,		

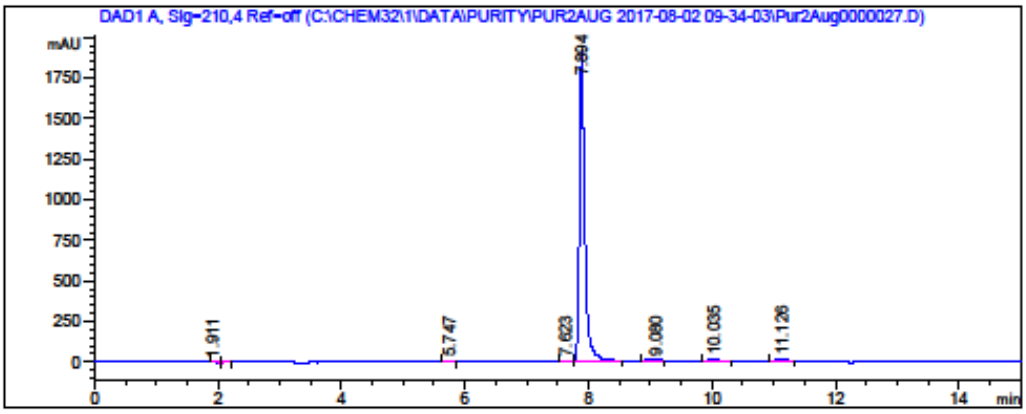

Area Percent Report

Sorted By : Signal
Multiplier : 1.0000
Dilution : 1.0000
Do not use Multiplier & Dilution Factor with ISTDs

Signal 1: DAD1 A, Sig=210,4 Ref=off

Peak #	RetTime [min]	Type	Width [min]	Area [mAU*s]	Height [mAU]	Area %
1	1.911	BB	0.0938	7.41619	1.05831	0.0635
2	2.156	BB	0.1034	14.66382	1.87224	0.1255
3	5.747	BB	0.0775	8.75485	1.60780	0.0749
4	7.623	BB	0.0744	7.22868	1.39625	0.0619
5	7.894	BB	0.0899	1.14655e4	1912.96326	98.1242
6	9.080	BB	0.1664	23.19009	1.70790	0.1985
7	10.035	BB	0.1268	92.84290	11.18803	0.7946
8	11.126	BB	0.1202	65.08799	7.28465	0.5570
Totals :				1.16846e4	1939.07843	

Compound 1o – HPLC trace:

```
Data File C:\CHEM32\1\DATA\PURITY\PUR2AUG 2017-08-02 09-34-03\Pur2Aug0000039.D
Sample Name: R14S2 1mM

    ======================================================================
    Acq. Operator   : SYSTEM                        Seq. Line :  39
    Acq. Instrument : H1                             Location :   39
    Injection Date  : 8/2/2017 7:54:53 PM                 Inj :   1
                                                  Inj Volume : 10.000 µl
    Acq. Method     : C:\Chem32\1\Data\PURITY\Pur2Aug 2017-08-02 09-34-03\Purity.M
    Last changed    : 7/31/2017 1:40:47 PM by SYSTEM
    Analysis Method : C:\CHEM32\1\METHODS\Purity.M
    Last changed    : 8/7/2017 9:01:46 AM by SYSTEM
                      (modified after loading)
    Method Info     : Purity Test
                      Venusil XBP C18(2) 150 x 4.6 mm
                      acn/water  30/70,   85% after 5 min, to 15 min, stop 20 min.
                      wavelength  210, 230,  254, 280, 300 nm, 4 nm BW
                      1 ml/min,
```

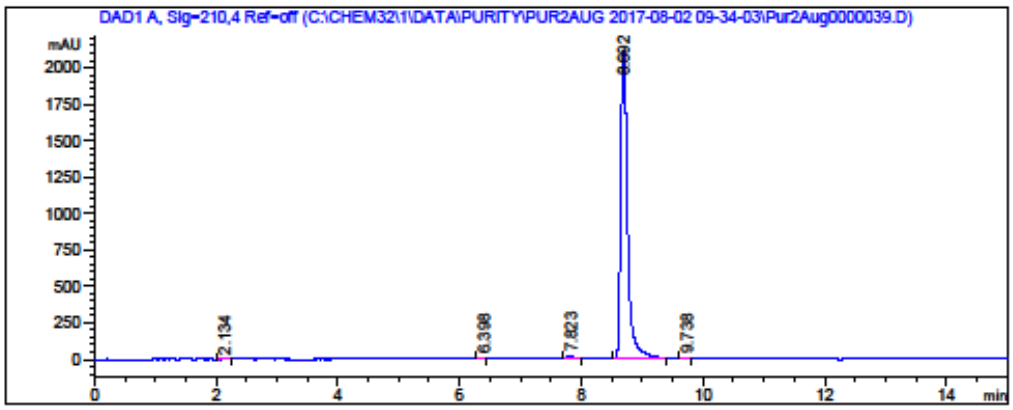


```
    ======================================================================
                            Area Percent Report
    ======================================================================

    Sorted By             :      Signal
    Multiplier            :      1.0000
    Dilution              :      1.0000
    Do not use Multiplier & Dilution Factor with ISTDs


    Signal 1: DAD1 A, Sig=210,4 Ref=off

    Peak RetTime Type  Width     Area      Height     Area
      #   [min]        [min]   [mAU*s]     [mAU]       %
    ----|-------|----|-------|----------|----------|--------|
       1   2.134 BB    0.0826   11.57382    1.85868   0.0686
       2   6.398 BB    0.0770    6.02087    1.27691   0.0357
       3   7.823 BB    0.0811   60.25361   11.50329   0.3573
       4   8.692 BB    0.1209 1.67757e4  2107.81445  99.4688
       5   9.738 BB    0.1037   11.73987    1.40130   0.0696

    Totals :                  1.68653e4  2123.85463

    ======================================================================

H1 8/7/2017 9:28:00 AM SYSTEM                                  Page   1 of 2
```

Compound 1p – HPLC trace:

Data File C:\CHEM32\1\DATA\PURITY\PUR2AUG 2017-08-02 09-34-03\Pur2Aug0000035.D
Sample Name: R13S2 1mM

```
======================================================================
Acq. Operator   : SYSTEM                       Seq. Line :  35
Acq. Instrument : H1                            Location :  35
Injection Date  : 8/2/2017 6:49:46 PM                Inj :  1
                                               Inj Volume : 10.000 µl
Acq. Method     : C:\Chem32\1\Data\PURITY\Pur2Aug 2017-08-02 09-34-03\Purity.M
Last changed    : 7/31/2017 1:40:47 PM by SYSTEM
Analysis Method : C:\CHEM32\1\METHODS\Purity.M
Last changed    : 8/7/2017 9:01:46 AM by SYSTEM
                  (modified after loading)
Method Info     : Purity Test
                  Venusil XBP C18(2) 150 x 4.6 mm
                  acn/water  30/70,   85% after 5 min, to 15 min, stop 20 min.
                  wavelength  210, 230,  254, 280, 300 nm, 4 nm BW
                  1 ml/min,
```

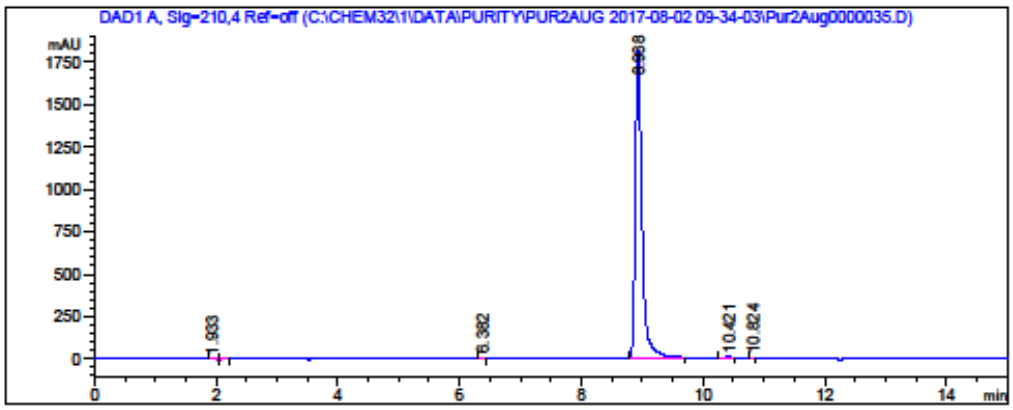


```
======================================================================
                        Area Percent Report
======================================================================

Sorted By             :      Signal
Multiplier            :      1.0000
Dilution              :      1.0000
Do not use Multiplier & Dilution Factor with ISTDs


Signal 1: DAD1 A, Sig=210,4 Ref=off

Peak RetTime Type  Width     Area      Height     Area
  #   [min]        [min]   [mAU*s]     [mAU]       %
----|-------|----|-------|----------|----------|--------|
   1   1.933 BB    0.0581    7.38694    1.65416   0.0545
   2   2.146 BB    0.0812   12.84182    2.29936   0.0948
   3   6.382 BB    0.0503    5.45204    1.50504   0.0402
   4   8.938 BB    0.1149 1.34949e4  1811.12878  99.6198
   5  10.421 BB    0.1009   20.75920    2.55115   0.1532
   6  10.824 BB    0.0561    5.06358    1.34007   0.0374

Totals :                  1.35464e4  1820.47858
```